NASA Conference Publication 3312

Thermal Barrier Coating Workshop

Proceedings of a conference held at
NASA Lewis Research Center
Cleveland, Ohio
March 27–29, 1995

NASA Conference Publication 3312

Thermal Barrier Coating Workshop

Proceedings of a Conference
held at and sponsored by NASA Lewis Research Center
and cosponsored by DOE and NIST
Cleveland, Ohio
March 27–29, 1995

National Aeronautics and
Space Administration

Office of Management

**Scientific and Technical
Information Program**

1995

Foreword

Thermal barrier coatings (TBCs) were first used in relatively minor roles in aircraft turbine engines over 30 years ago. The early success and high potential benefits of TBCs prompted continuing development for more challenging applications. Recent TBC successes in high pressure turbine blade applications has led to the recognition that TBC coated superalloys offer the most viable materials solution to both near term and longer term engine challenges. Consequently, there has been a tremendous recent increase in the research and development activities associated with TBC use in turbines. Research and development of TBCs for diesel engine applications was initiated relatively recently for development of a low heat rejection engine. While this concept has met with limited success, diesel engine TBC research has been redirected toward increasing the durability of critical components while continuing the use of low cost base materials.

The recent emphasis on TBCs has highlighted the fact that TBC behavior is not well understood. For instance, knowledge of the most important issues, durability and failure mechanisms, is primarily at an empirical level. Similarly, the physical, mechanical and thermal properties of TBCs have not been adequately characterized. Consequently, design tools for TBCs and the life prediction capabilities required for critical components tend to be empirical in nature and application specific, rather than comprehensive. Furthermore, the lack of solid information on TBC performance has led to a significant amount of TBC "folk lore" that can be misleading. The goals of the Thermal Barrier Coating Workshop were to assess the state of TBC knowledge and identify critical gaps in the knowledge that hinder use in advanced applications. Perhaps more importantly, it was hoped that the Workshop would open a dialogue on TBCs that would allow exchange of factual information and more rapid advances in the field. These goals were addressed through presentations on topics ranging from defining the need for thermal barrier coatings to the design of future coatings. The participation of the 22 speakers and 200 attendees in wide ranging discussion sessions helped to provide a multifaceted view of the issues. This proceedings contains papers for 19 of the 22 presentations at the Workshop.

William J. Brindley
Chairman TBC Workshop

TABLE OF CONTENTS

Engine Experience With TBCs

Materials/Processing

Properties

Modeling

A DESIGN PERSPECTIVE ON THERMAL BARRIER COATINGS

Friedrich O. Soechting
Pratt & Whitney
West Palm Beach, Florida 33410-9600

ABSTRACT

This technical paper addresses the challenges for maximizing the benefit of thermal barrier coatings for turbine engine applications. The perspective is from a customer's viewpoint, a turbine airfoil designer, who is continuously challenged to increase the turbine inlet temperature capability for new products while maintaining cooling flow levels or even reducing them. This is a fundamental requirement to achieve increased engine thrust levels. Developing advanced material systems for the turbine flowpath airfoils is one approach to solve this challenge; such as high temperature nickel based superalloys or thermal barrier coatings to insulate the metal airfoils from the hot flowpath environment. The second approach is to increase the cooling performance of the turbine airfoil, which enables increased flowpath temperatures and reduced cooling flow levels.

Thermal barrier coatings have been employed in jet engine applications for almost 30 years. The initial application was on augmentor liners to provide thermal protection during afterburner operation. However, the production use of thermal barrier coating in the turbine section has only occurred in the past 15 years. The application was limited to stationary parts, and only recently incorporated on the rotating turbine blades. This lack of endorsement of thermal barrier coatings resulted from the poor initial durability of these coatings in high heat flux environments. Significant improvements have been made to enhance spallation resistance and erosion resistance which has resulted in increased reliability of these coatings in turbine applications.

INTRODUCTION

Gas turbine performance can be improved by increasing the efficiency of the fan, compressor and turbine components. This approach yields reduced specific fuel consumption of the gas turbine with a moderate increase in engine thrust. Large increases in thrust can be obtained by increasing the turbine inlet temperatures while maintaining or improving component efficiency levels. Figure 1, graphically illustrates the potential improvement that remains in increasing the core horsepower, defined as the horsepower generated per pound of airflow, of a gas turbine engine as a function of the turbine inlet temperature. The solid line represents components with 100% efficiencies. In other words, the maximum potential at a given temperature. Symbols on this

figure represent the status of current production engines as well as the original Whittle gas turbine demonstrator engine. There has been a significant improvement largely due to improvements in materials and the introduction of cooling technologies into the turbine. Each one of the production engines are near their optimum core horsepower level with the technology level incorporated into that engine. Therefore, each engine symbol represents continual improvements in technology. Note that turbine inlet temperature increases for a fixed technology level can actually cause the core horsepower to be reduced. The cause for this is parasitic loss increases in the turbine. This is due to increased cooling flow requirements for the turbine flow path, specifically the turbine vanes, blades, and blade outer air seals. As one can readily observe, there is significant potential for improving gas turbine power output by increasing turbine temperatures, however, technology improvements in materials, coatings, and cooling will be required to achieve the potential.

Material improvements have been dramatic over the past years. The composition of the alloys used for turbine airfoil materials and their processing methods have allowed increased metal temperature operation, and hence, increased turbine inlet temperatures. As the alloy compositions have been improved, the incipient (or onset) melt temperatures increased and the creep strength, fatigue strength and oxidation resistance was also increased. Increased temperature operation was therefore allowed because all of the material characteristics that affect turbine airfoil durability were improved. The material processing improvements resulted in investment cast airfoils produced in equiax, directionally solidified, and single crystal structures. Figure 2 shows the material temperature improvements obtained since 1960. A 100°C (180°F) improvement in turbine airfoil materials have been obtained in 25 years. This is a 4°C (7°F) improvement per year. To put this into perspective, for a turbine operating at constant operating temperature, the benefit is equivalent to doubling the durability every three and a half years. Turbine airfoil materials are nickel based superalloys; whose incipient melt temperatures have been increased to 1316°C (2400°F). Since 1985, there have been no major breakthroughs in the development of nickel based superalloys. The fundamental reason is that the incipient melt temperature has slowly approached the melting temperature of the nickel alloys. The melting point of nickel alloys is 1399°C (2550°F). There is further room for alloy improvement, however, the complexity of defining the alloy composition has become more difficult. A collaborative effort among the major United States gas turbine engine producers is underway to define the ultimate nickel alloy compositions. The goal is to improve the temperature capability another 27 to 42°C (50 to 75°F). To obtain increased turbine inlet temperature capability, improved cooling techniques or thermal barrier coatings need to be applied.

The amount of cooling that is required in a typical production turbine today is graphically illustrated in Figure 3. The gas temperature referred to in

this figure reflects the maximum inlet temperature to the first stage turbine vane. This temperature is higher than the average combustor exit temperature because combustor cooling requirements dictate the combustion and dilution processes occur with a minimum length of the burner. This results in a turbine inlet temperature that is not uniform. The allowable operating temperature for the metal is about half way between the maximum gas temperature and the temperature of the cooling flow supplied to the first vane. Also shown in this figure is the relationship of the allowable design metal temperature levels to the incipient melt temperatures. As shown, the allowable metal temperature levels are near the incipient melt point of nickel based superalloys. In addition, a small increase in operating metal temperatures results in a significant durability decrement. 13°C (25°F) produces a two-fold reduction in airfoil durability.

Efficient heat exchangers have been developed to cool turbine airfoils. Initially, simple internal convective cooling designs were employed. Advances in the development of airfoil cooling designs have been achieved by combining high convective cooling efficiencies with film cooling. Figure 4 shows the turbine inlet temperature increases possible with the use of cooled single crystal turbine blades. An example of this is the F100-PW-220, the cooling configuration shown in Figure 4, that was proven in accelerated mission testing where over 10 years of equivalent service was demonstrated. It should be noted that no thermal barrier coatings were employed in this engine model. However, thermal barrier coatings were beginning to be introduced into commercial and military products after the F100-PW-220 went into production. Cooling technology improvements will permit higher gaspath operating temperatures, similar to the application of thermal barrier coatings. Over time, small, incremental improvements in material and cooling will yield exponential increased gaspath temperature capability.

THERMAL BARRIER COATING DESIGN CONSIDERATIONS

Thermal barrier coatings were initially incorporated on turbine vanes. The benefit of these coatings were documented in back-to-back instrumented engine tests where turbine vanes were initially evaluated in an uncoated state. The instrumented vanes were removed from the engine and thermal barrier coating was applied for subsequent testing. Figure 5 shows that the reduction in operating metal temperatures with thermal barrier coatings are directly proportional to the coating thickness. The thickness was measured by sectioning the airfoils post test, and the data trends were as expected. The insulative benefit was also documented by measuring transient thermal response during a rapid engine acceleration from idle to intermediate power. Figure 6 presents a comparison of the uncoated and coated thermal response during this transient. The coated airfoil thermal response was slower than the uncoated airfoil. This demonstrated that the thermal barrier coating damped the thermal response of the airfoils to rapid engine acceleration or deceleration

transients. The benefit is that coating reduces thermal gradients within the metal airfoil. Since the thermal gradients in the metal are smaller, thermally-induced stresses and strains will also be smaller resulting in improved thermal fatigue capability.

Thermal barrier coatings have not been applied to the rotating turbine blades primarily due to the increase in load applied to the airfoil, attachment, and disk. Figure 7 dramatically illustrates the forces applied by the rotating blades, excluding their platforms and extended necks. The centrifugal force of a blade without thermal barrier coating is on the order of 6364 kg (or 7 tons). This is roughly equivalent to the weight of a Lockheed F-16 fighter aircraft, and considering that the number of blades on a disk ranges from 50 to 70, poses a very challenging structural design. Thermal barrier coatings, and the bond coating applied to the nickel based superalloy for adherence, result in significant increases in the centrifugal load transferred to the disk. Thermal barrier coatings do not have sufficient capability to support their own load in a rotating turbomachinery application. The load associated with the rotating mass of the coating must therefore be supported by the underlying superalloy structure. The mass of this structure must be increased to maintain acceptable stress levels while supporting the coating dead load. Additionally, attachment and disk masses must also be increased to provide a suitable blade/coating support structure. For rotating turbomachinery applications, it is extremely important to reduce the dead load, which means that thin, low thermal conductivity systems must be developed to maximize the benefit of thermal barrier coatings.

The benefit of thermal barrier coatings is schematically shown in Figure 8, where the metal temperature versus the coolant flow rate is respresented for an uncoated and a coated airfoil. For a fixed engine cycle, the addition of thermal barrier coating can be utilized to improve durability while maintaining constant airfoil cooling flow rates. In this situation, the airfoil operating metal temperatures are reduced, thus providing increased durability. The other approach is to improve the performance of the engine by increased thrust and reduced specific fuel consumption. In this approach the cooling flow rates to the airfoil are reduced while holding the operating metal temperatures constant. An alternate approach, not shown in this figure, is to maintain cooling flow levels and increase the turbine inlet temperature until the operating metal temperatures are maintained constant. This will provide greater thrust improvement than with the coolant flow reduction approach. The temperature reduction potential is dependent on the superalloy wall thickness and the thermal resistance of the thermal barrier coating as well as the magnitude of heat flux.

If thermal barrier coatings are utilized for improved engine performance, the integrity of the coating becomes increasingly important because loss of the coatings can result in a reduction of the durability of the airfoil. This effect is graphically shown in Figure 9. The loss of coating will result in increased metal

temperatures and accelerated loss of durability. Researchers in this field have commonly referred to the need for the development of "Prime Reliant" coatings to overcome the accelerated damage of the coatings if spallation were to occur. The issue here is not the development of a "Prime Reliant" coating, but rather the development of a design prediction system for determining when coating loss will occur. This enables design and overhaul trades to be made by defining inspection intervals that coincide with the projected coating spallation. This yields the largest performance benefit to the engine system while potentially increasing overhaul costs. Figure 3, previously described, showed that the operating metal temperatures are near the incipient melting point of the superalloys. Therefore, if the maximum performance advantage is utilized with thermal barrier coatings, the metal temperatures could exceed the incipient melting point of the alloy in a failure scenario. This would result in rapid deterioration of the airfoil. A design prediction system could also allow tailoring of the airfoil design to maximize durability for local spallation, however, this approach would require cooling flow to be increased locally to provide a more robust design.

There are several mechanisms in which thermal barrier coatings can spall from the turbine airfoil. These are from oxidation, fatigue, and particle erosion. Figure 10 shows that the applied forces that cause coating spallation are similar for both oxidation and fatigue. That is, the resultant forces at the interface between the thermal barrier coating and the metallic bond coat are similar in nature but the mechanisms are different. Thermal barrier coatings in use today are oxygen permeable, which allows oxygen to seep through the ceramic coating. When the oxygen is combined with the alumina-bearing metallic coating, an alumina oxide is formed. This alumina oxide produces a volumetric expansion above the bond coat which causes a delamination leading to the spallation of the thermal barrier coating. Under engine transient loading, cyclic stresses are introduced at the bond interface due to the combination of applied thermal gradients and thermal coefficient of expansion mismatch. The cyclic stresses can also result in coating spallation as demonstrated under laboratory testing sponsored by NASA. It is therefore important that both oxidation and cyclic damage be recognized and investigated during the selection and optimization of new thermal barrier coating systems. Future systems need to have a dual role capability for transports and military engine products by recognizing the difference in engine usage as shown in Figure 11.

Particulate erosion poses another concern for thermal barrier coating durability. These particles may be injected at the engine inlet, or they may be derived from abradable materials released during a compressor rub. These particles enter the turbine at a low axial velocity. Since they are more dense than air, inertial forces hinder their acceleration in the vane passage and as a result they exit the vane passage with a swirl velocity that is less than the freestream gas. Therefore, these particles impinge on the vane leading edge at

low velocities, but impact the suction side of the blade with high relative velocities. This is readily understood when the velocity triangles of a typical turbine blade are examined with particles exiting the vane at reduced swirl velocities relative to the mainstream gas (Figure 12). The impact zone for particulate erosion is downstream of the leading edge on the suction surface of the blade. It is therefore important that the erosion resistance of new coating systems be maximized in order to ensure the thermal protection is not diminished by erosion effects.

Thermal barier coating is applied using utilizing plasma spray, electron beam physical vapor deposition and chemical vapor deposition processes. The different processes produce dissimilar surface roughness levels. The surface roughness is significantly greater for the plasma spray process. Increased roughness results in higher aerodynamic losses as well as increased heat transfer to the airfoil. Figure 13 presents a comparison of the measured metal temperature from an uncoated vane with engine data obtained on turbine vanes with plasma spray thermal barrier coating. Both the concave and convex surfaces of the vane were instrumented with thermocouples that were imbedded into the metal. Plasma spray deposition is a line of sight process. Since the vanes were cast as a pair, a uniform thickness of thermal barrier coating could not be achieved for the convex surface of the vane which was shieded by the concave surface of the adjacent vane. The result was a thin coating application with increased local roughness on the convex surface on one vane in the pair. As shown in Figure 13, these combined effects caused the actual metal temperature beneath the coating to increase in this area. The objective in developing deposition processes should be to obtain uniform thicknesses of coating with a surface roughness no greater than the substrate.

Turbine airfoils residing in the highest heat flux regions typically utilize film cooling in conjunction with internal convective cooling. The principle of film cooling is to discharge spent cooling air out on the airfoil surface to provide a buffer between the airfoil surface and the hot mainstream gas flow. Since the heated cooling air is significantly cooler than the mainstream gas flow, reductions in the heat load and metal temperatures are obtained. However, to maximize the film cooling benefit, small hole sizes are used to distribute the convectively spent cooling flow along the entire airfoil surface. The meter area of these small film holes regulates the amount of cooling flow used in the airfoil for both convective and film cooling. Therefore any closedown of these holes by the deposition of a thermal barrier coating can result in large cooling flow reductions and increased part-to-part variations which deleteriously affect the durability of the coated airfoil. Figure 14 shows the flow reduction obtained by coating deposited on the surface of the cooling hole as a function of hole diameter. This figure demonstrates that a robust process is required to minimize the amount of coating deposited within a cooling hole. This again indicates that a low thermal conductivity thermal barrier coating, requiring reduced thickness

relative to today's state of art coatings, is the logical direction to focus development efforts. A thinner coating will naturally result in less potential deposition within cooling holes.

The surface temperature capability of thermal barrier coatings needs to be increased. Recommended maximum operating temperature limits are imposed on the designer to maintain the stability of ceramic matricies used in current state of the art coatings. However to maximize the potential benefit thermal barrier coatings can provide, a focused effort is required to increase the stability of the ceramic composition at elevated temperatures. The potential cooling flow reduction as a function of the maximum ceramic surface temperature is shown in Figure 15 for a first stage turbine vane application operating at stoichiometric conditions. This figure shows that large gains can be made with moderate temperature improvements. However, as the temperature capability increases, an associated reduction in the thermal conductivity is desired to minimize the coating thicknesses for turbine vanes and especially the rotating turbine blades. The challenge and benefits of such a system are unlimited.

SUMMARY

Significant advances in gas turbine propulsion capability can be obtained by incorporating the synergistic effects of improved materials, cooling, and advanced thin thermal barrier coatings into the next generation of turbine airfoils. However, to maximize the potential, there needs to be a focused and integrated technology development effort that combines the talents and expertise of airfoil designers, with materials, ceramic, and production engineering. To obtain success, calibrated life prediction methods must be developed to optimize the airfoil design. This must be accomplished with the minimum amount of coolant flow while ensuring that the protection provided by a thermal barrier coating will provide the durability expected.

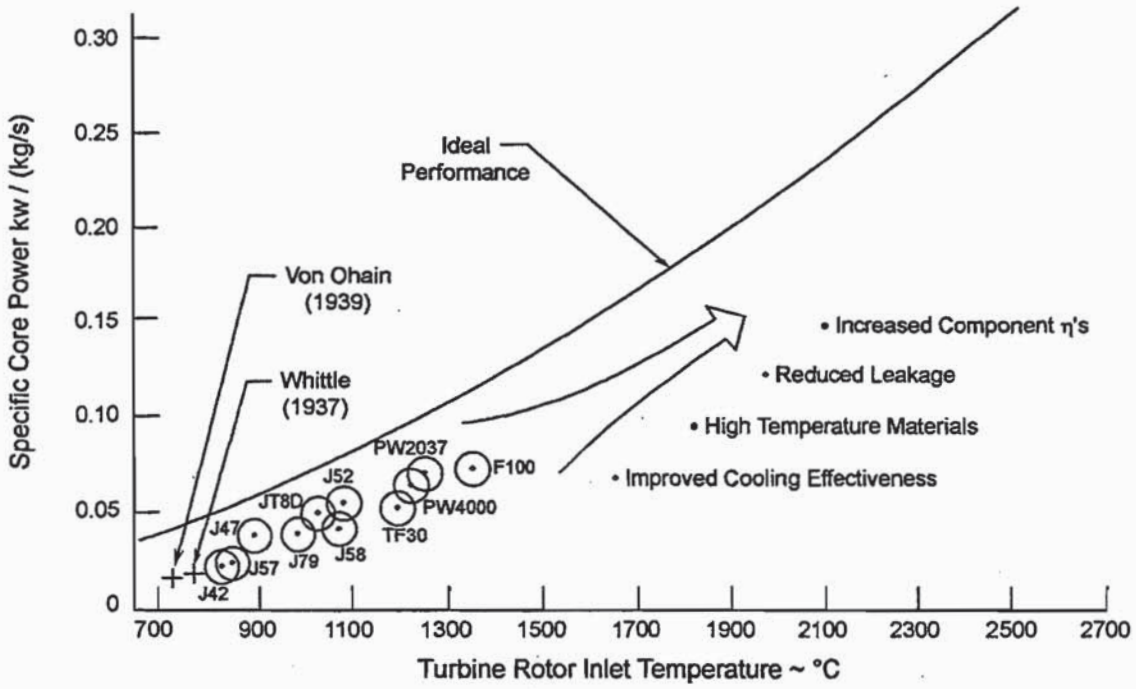

Figure 1: Increased Core Horsepower Attained With Increased Operating Temperatures and Turbine Technologies

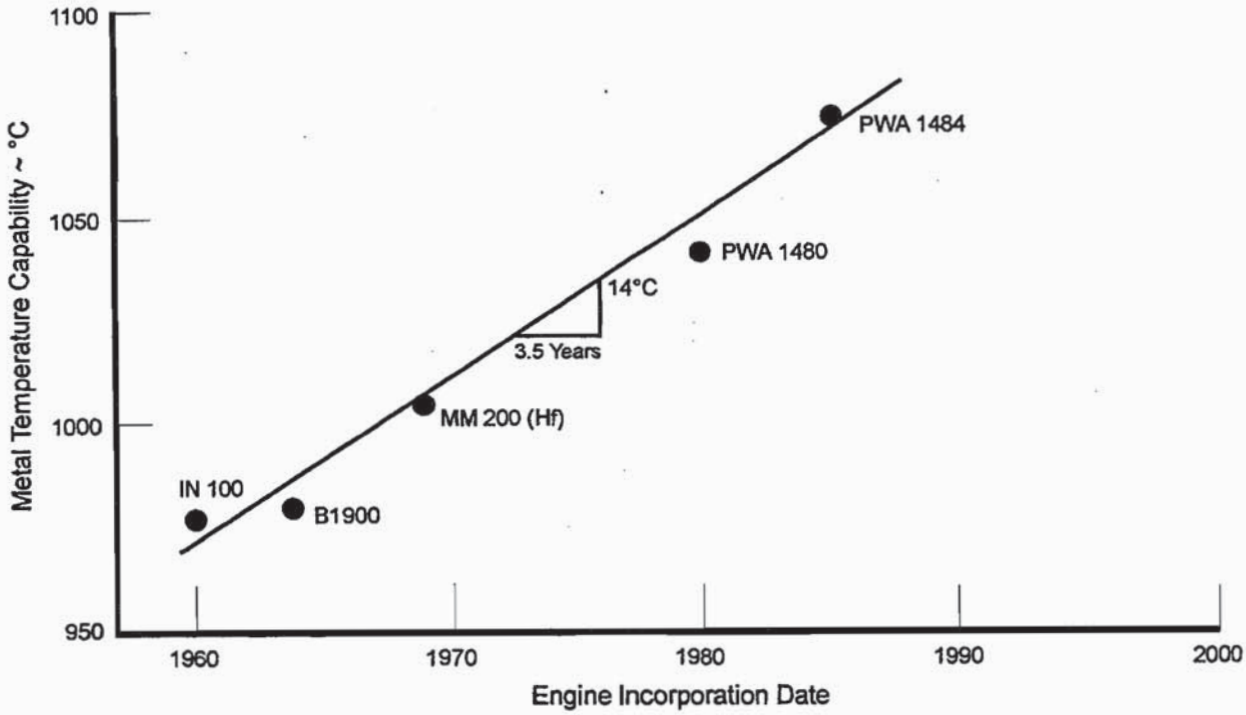

Figure 2: Turbine Blade Material Temperature Improvements

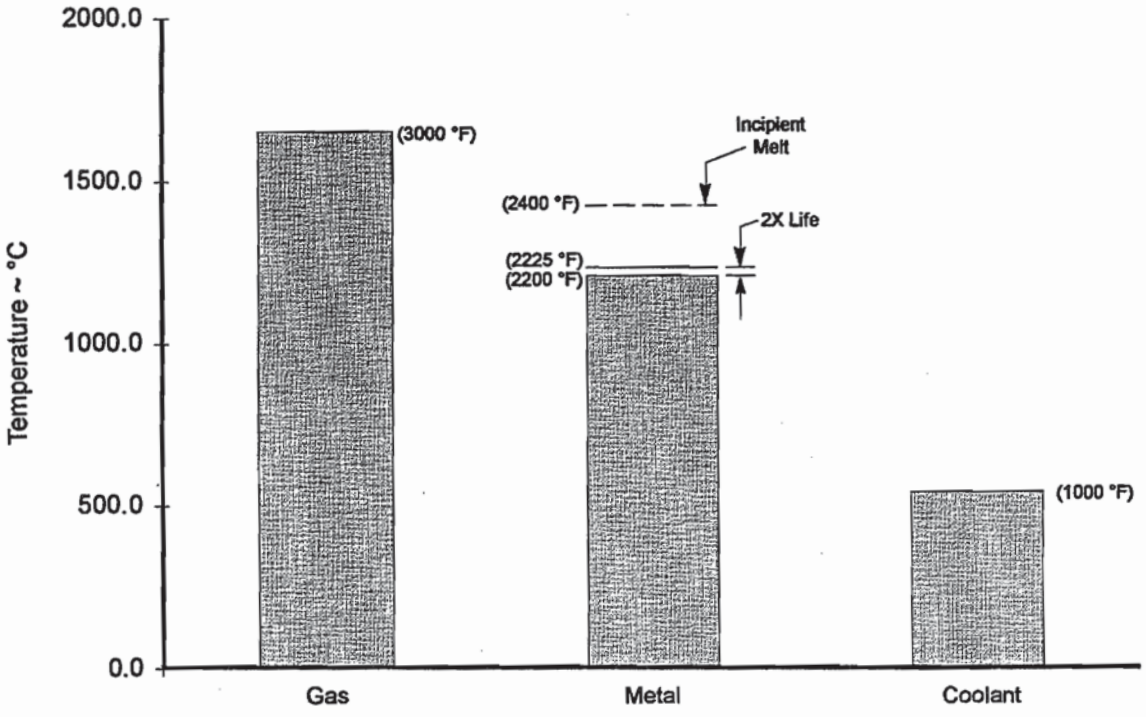

Figure 3: Typical Airfoil Cooling Requirements for Maximum Temperature Operation

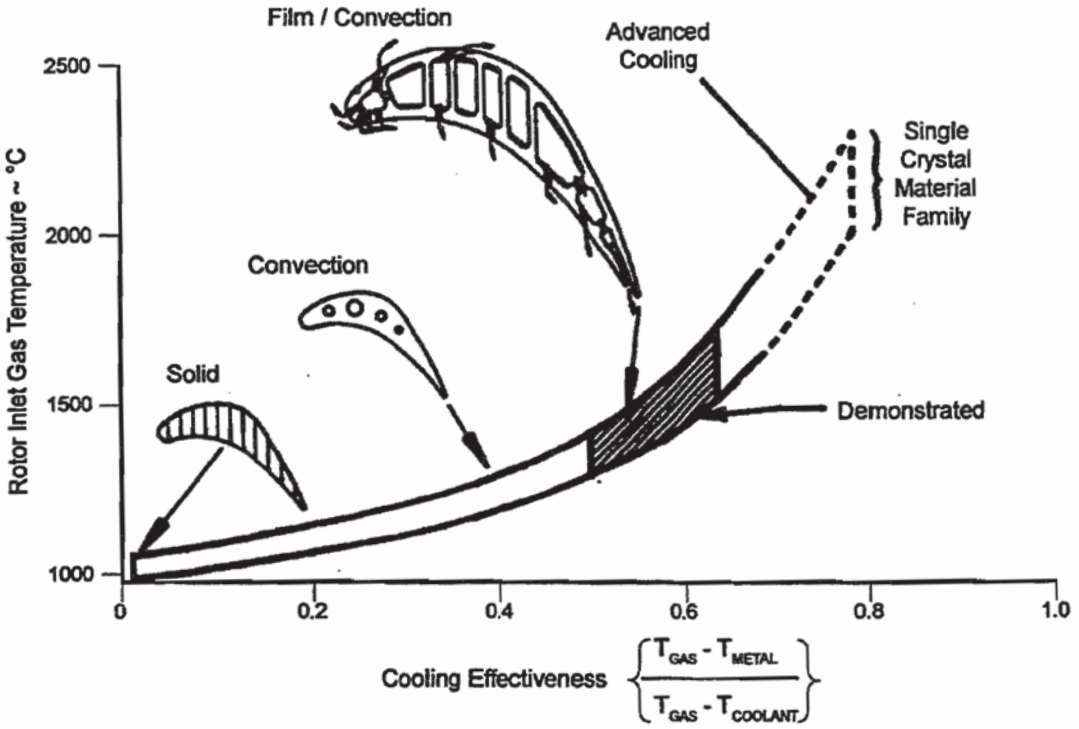

Figure 4: Dramatic Increase in Turbine Temperature Attained With Cooling, Augmented By Improved Materials

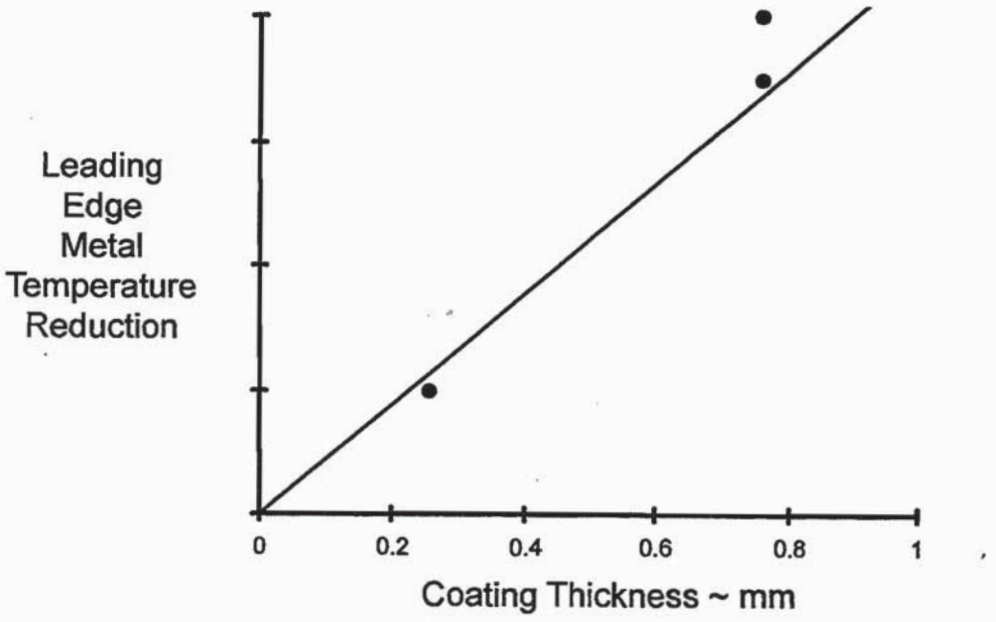

Figure 5: Engine Data Documents Dependency of Metal Temperature Reduction on Thermal Barrier Coating Thickness

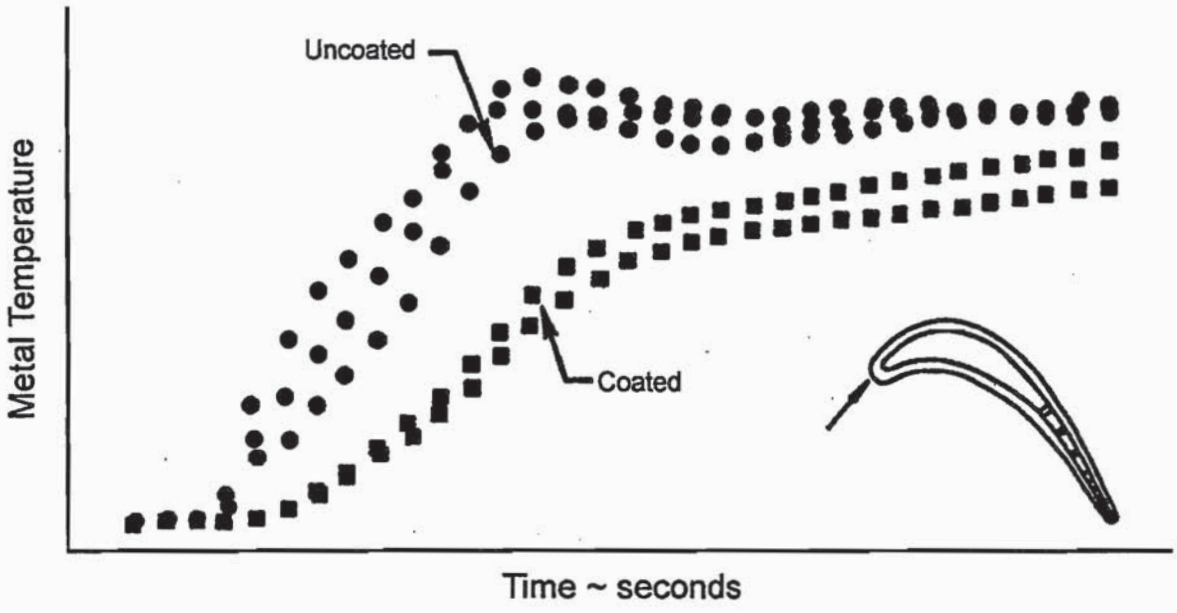

Figure 6: Transient Thermal Response is Damped With Thermal Barrier Coating

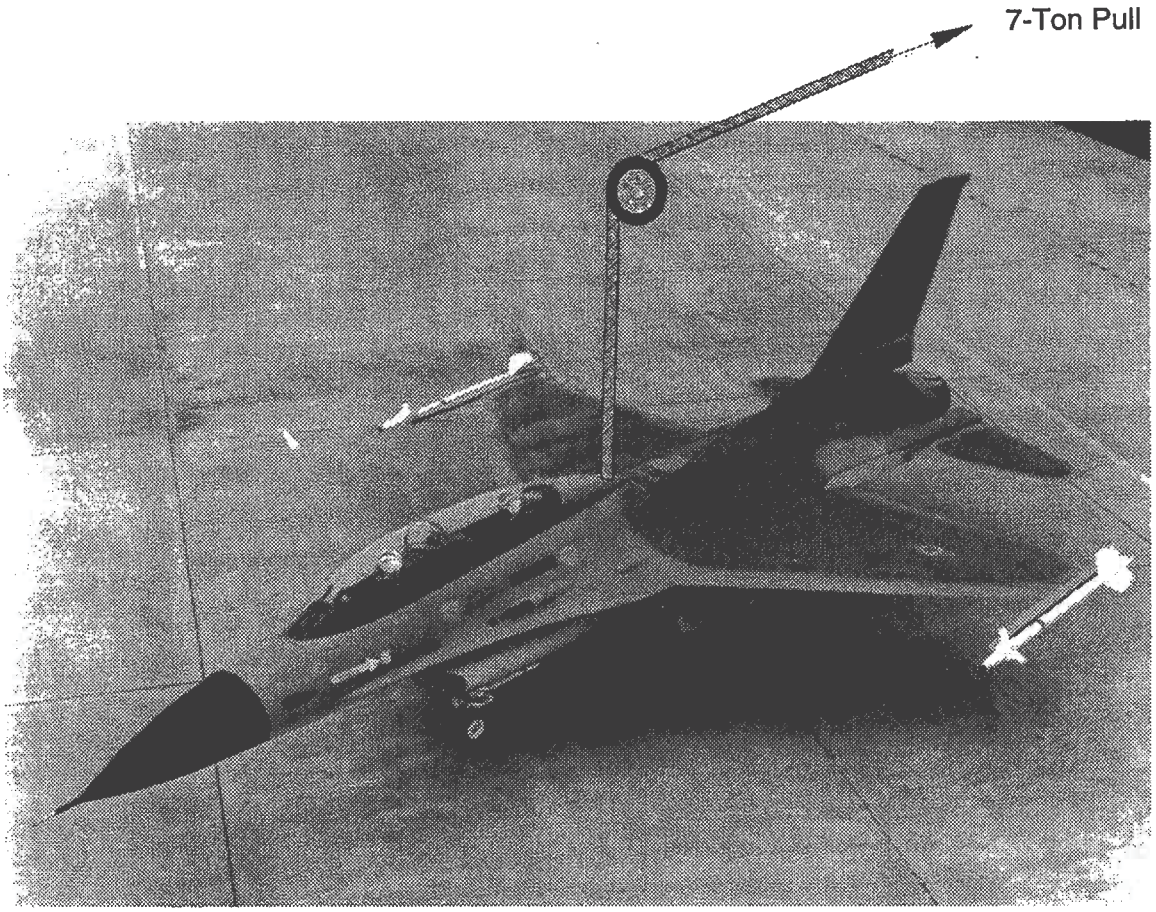

Figure 7: Turbine Blades Are Highly Loaded

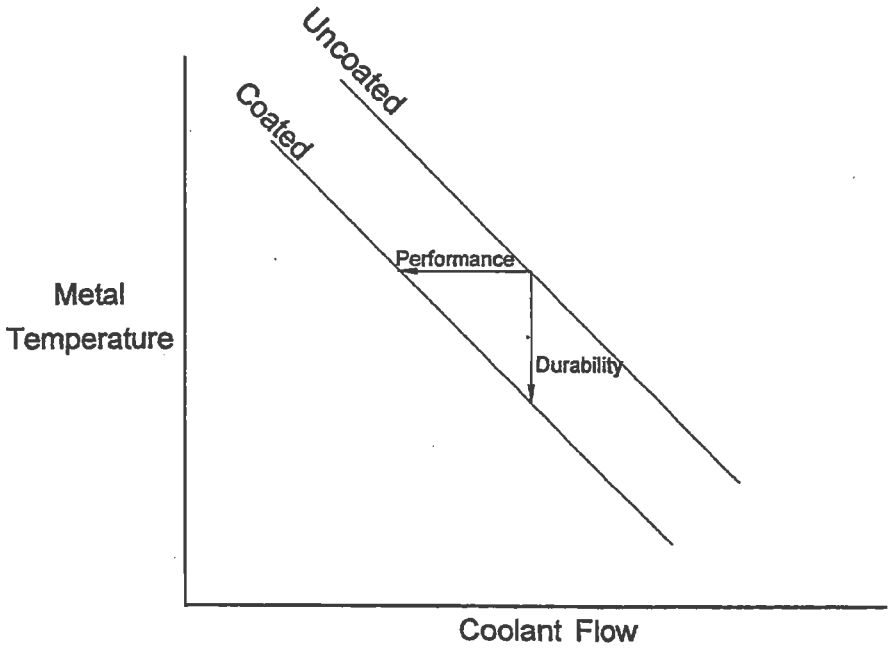

Figure 8: Thermal Barrier Coating Payoff - Reduced Airfoil Cooling / Improved Durability

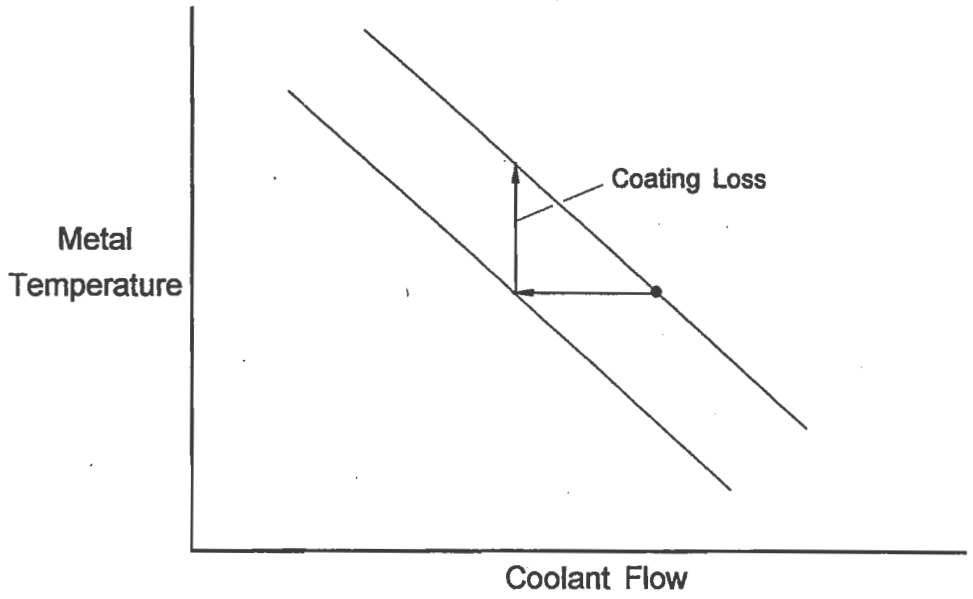

Figure 9: Thermal Barrier Coating Risk - Coating Loss Reduces Life as Flow is Reduced

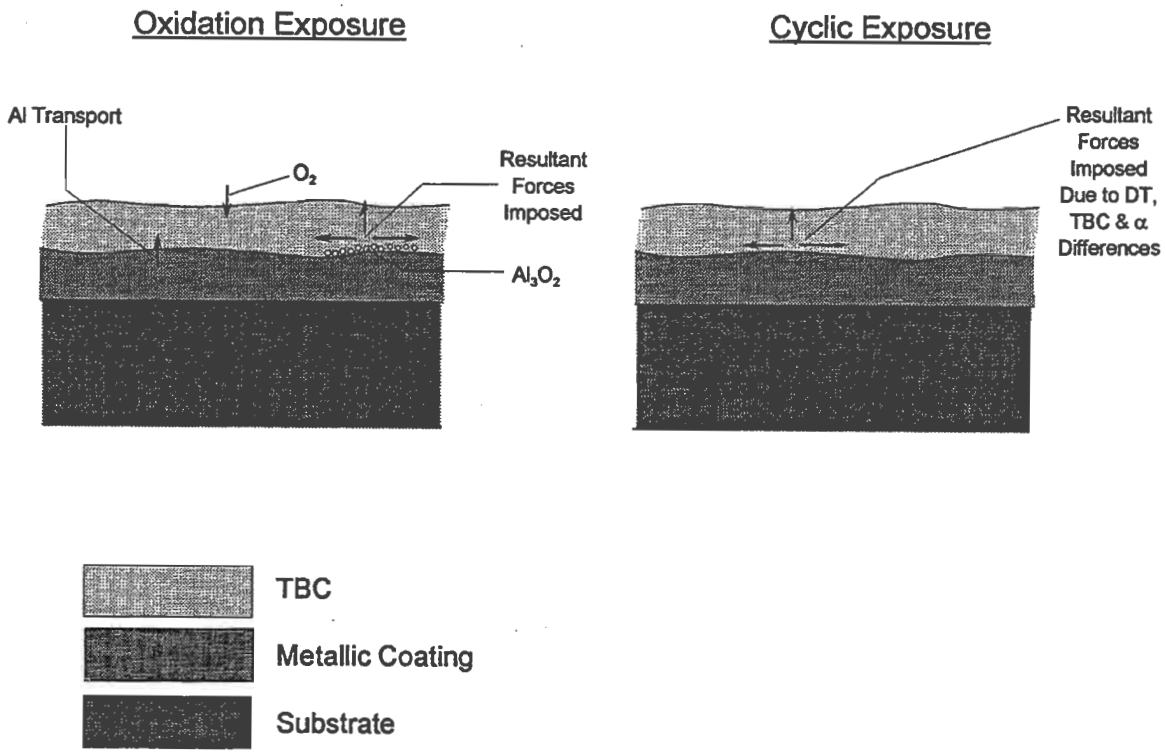

Figure 10: Spallation Mechanisms From Oxidation and Cyclic Strain Exposure is Similar

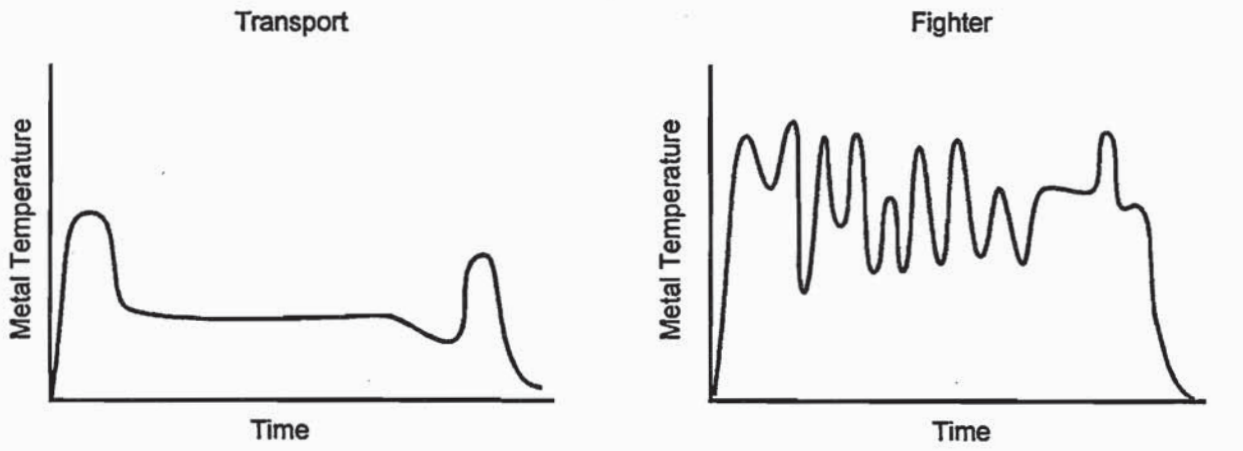

Primary Damage Mode: Oxidation / Creep

Primary Damage Mode: Fatigue / Oxidation

Figure 11: Engine Usage Can Produce Different Damage Modes

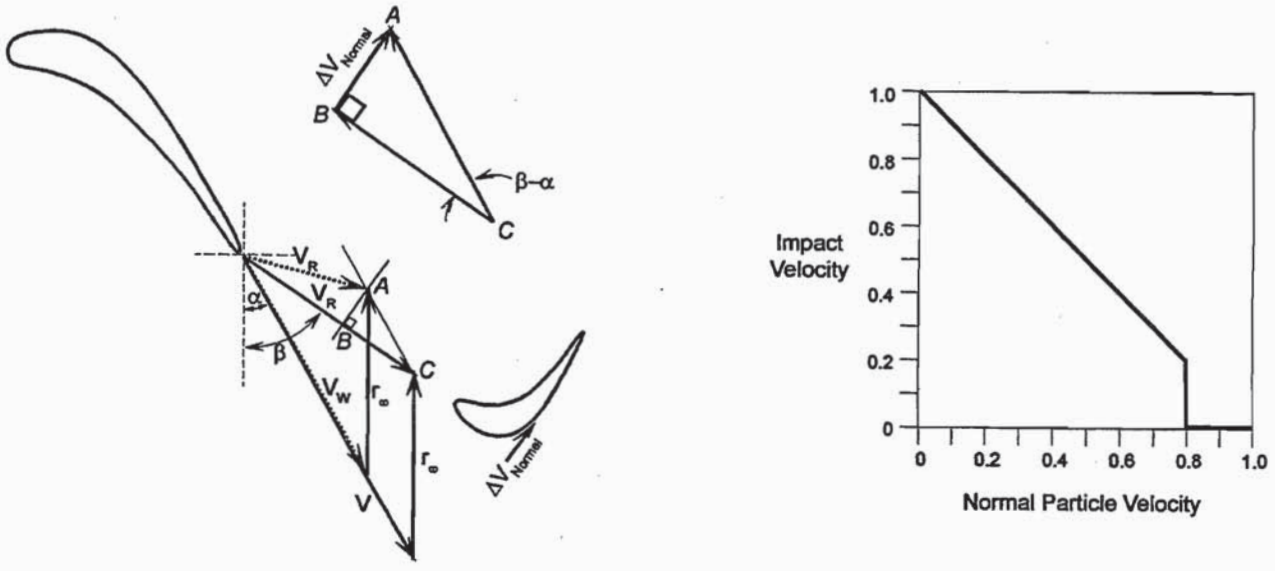

V	=	Gas Velocity
V_W	=	Particle Velocity
ΔV_{NORMAL}	=	Impact Velocity
$r\omega$	=	Rotational Velocity

Figure 12: Particle Erosion Most Prevalent on Blade Suction Side Thermal Barrier Coating

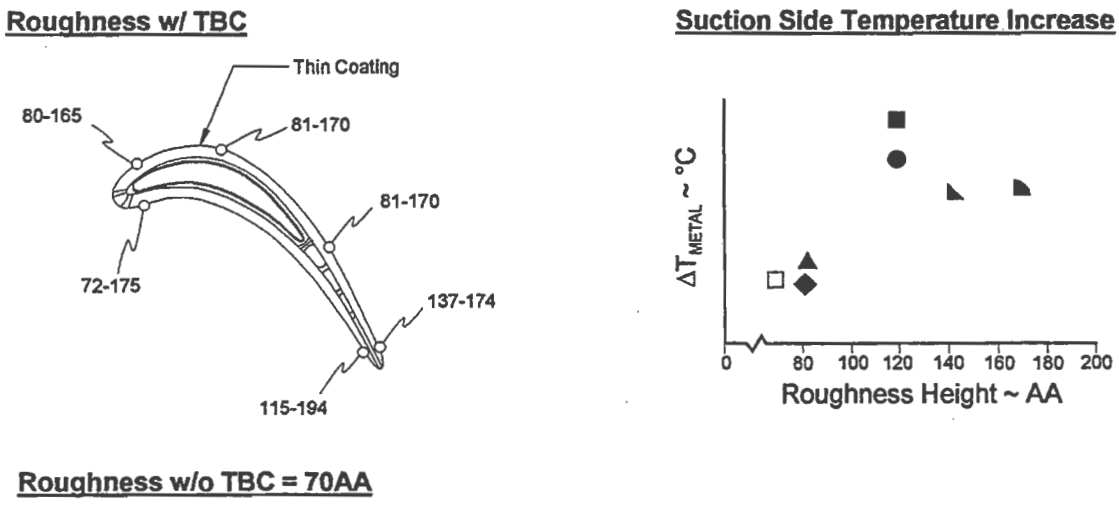

Figure 13: Increased Surface Roughness Can Produce Increased Operating Metal Temperatures

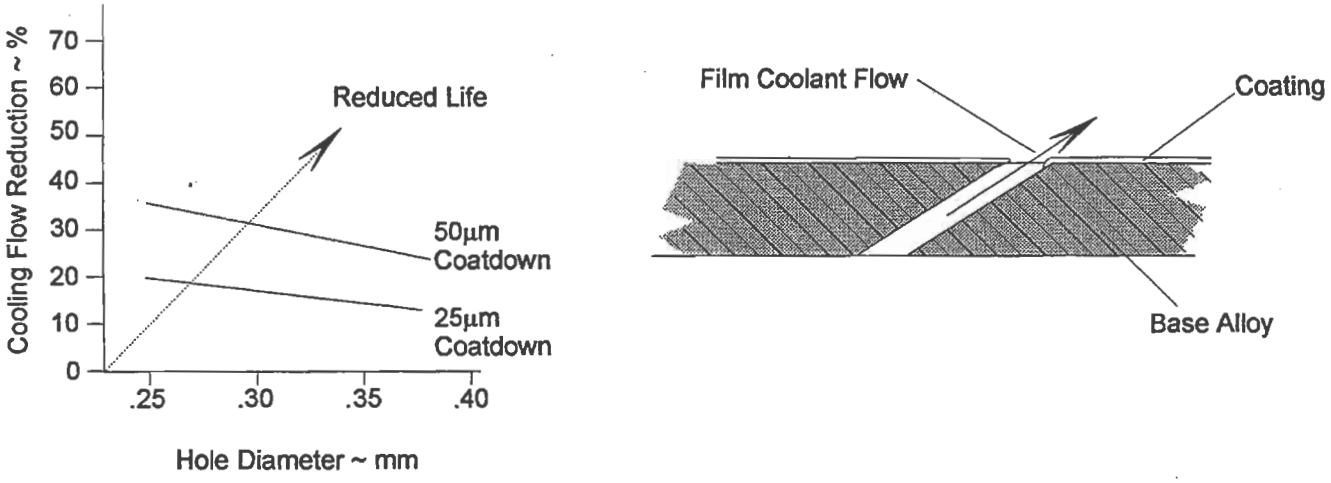

Figure 14: Coating Application Can Impact Flow Control and Durability

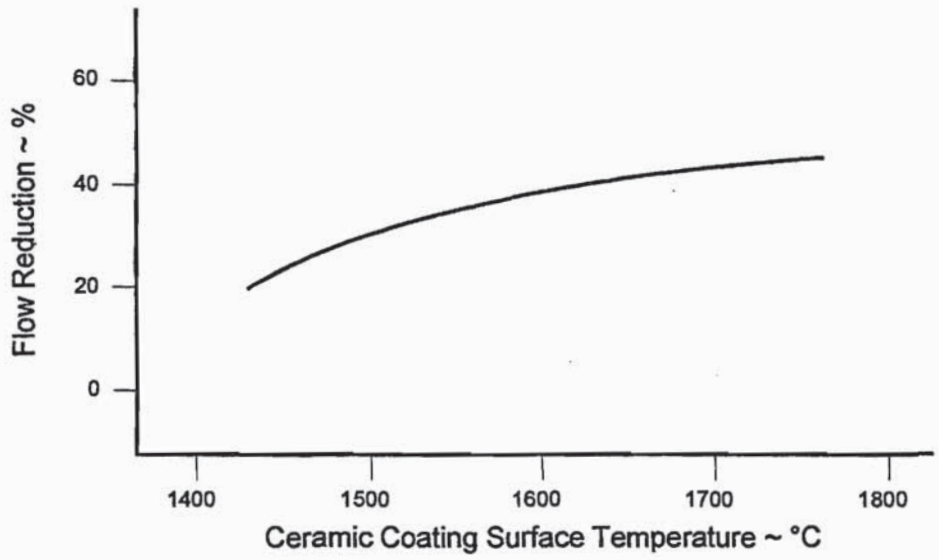

Figure 15: Large Potential Exists for High Temperature, Thin Thermal Barrier Coating System

Thermal Barrier Coatings for Aircraft Engines -- History and Directions

Robert A. Miller
NASA Lewis Research Center
Cleveland, OH 44135

Abstract

Thin thermal barrier coatings for protecting aircraft turbine section airfoils are examined in this paper. The discussion focusses on those advances that led first to their use for component life extension, and more recently as an integral part of airfoil design. Development has been driven by laboratory rig and furnace testing corroborated by engine testing and engine field experience. The technology has also been supported by performance modeling to demonstrate benefits and life modeling for mission analysis.

Factors which have led to the selection of the current state-of-the-art plasma sprayed and physical vapor deposited zirconia-yttria/MCrAlX TBCs are emphasized, as are observations fundamentally related to the their behavior.

Current directions in research into thermal barrier coatings and recent progress at NASA are also noted.

1. Introduction

Thermal barrier coatings were first successfully tested in the turbine section of a research gas turbine engine in the mid 70s. By the early 80s they entered revenue service on the vane platforms of aircraft gas turbine engine, and today they are flying in revenue service on vane and blade surfaces. Advanced engines, for the foreseeable future, may be expected to rely even more heavily on these coatings [1].

Two processes are used to apply today's thermal barrier coatings: plasma spraying and physical vapor deposition (PVD). Plasma sprayed coatings were brought into service first, and currently remain in service. By the 1990s, a second type of thermal barrier coating deposition process -- physical vapor deposition (PVD) -- was successfully brought into commercial service. The success of both types of coatings in commercial aircraft gas turbine applications, especially the PVD coatings, has played a pivotal role in the acceptance of this technology. However, with this acceptance comes ever increasing demands on these coatings to perform for longer and longer hot times under more and more severe conditions. This paper will focus primarily on the critical steps that led to the relatively rapid advancement of this technology.

2. Early ceramic coatings for aerospace applications

The earliest ceramic coatings for aerospace applications were frit enamels. The first of these frit coatings were developed by NACA and the NBS [2, 3]. Frit enamels were used in aircraft

engines throughout the 1950's [4]. Later, flame sprayed ceramic coatings were developed [5,6,7,8,9,10]. Of the various early ceramic materials that were evaluated for thermal barrier applications, alumina and zirconia-calcia where the most successful. The bond coat material for these early applications, if one was used at all, was typically nichrome or molybdenum for non-oxidizing environments. Early applications included the protection of sheet metal in jet engines and in rocket engine thrust chambers. The most visible coatings during this period were the flame sprayed zirconia-calcia coatings on the regeneratively cooled XLR99 thrust chambers for the X-15 experimental rocket planes [8, 9]. A portion of this coating is visible in figure 1. With the subsequent development of plasma spray processing -- which evolved from research into low thrust plasma arc engines for spacecraft and from plasma arc test facilities developed for reentry simulation [11] -- the utility of using the very high temperature plasmas for spraying ceramics was soon recognized [7,10,12,13]. In 1970, plasma sprayed thermal barrier coatings began to be used on hot section transition ducts and other hot section sheet metal components in commercial gas turbine engines [14].

Alumina and zirconia-calcia did not prove to be viable materials for the more advanced thermal barrier applications. In the case of alumina this is primarily because its thermal conductivity is relatively high [15]. Also, alumina forms non-equilibrium phases which are variously described as gamma, eta, or delta and these non-equilibrium phases shrink when they convert to the equilibrium alpha phase upon high temperature exposure. This shrinkage and the associated cracking would have a detrimental effect on coating life. The phase transformation to alpha alumina appears to become a factor above about 1100 °C [5,13,17,18]. The problem with zirconia-calcia and zirconia-magnesia is related to "destabilization" from the cubic fluorite (F-ZrO_2) phase that is observed in the as-sprayed material to the monoclinic (M-ZrO_2) phase. Zirconia-based ceramics containing excessive amounts of this monoclinic phase are not usable as structural materials due to the volume change associated with a martensitic phase transformation on cooling from the higher temperature tetragonal phase to the low temperature monoclinic phase. Although the calcia or magnesia are added to zirconia with the intent of extending the high temperature cubic phase field down to room temperature, it is now known that the cubic phases are actually not stable below about 1140 °C for zirconia-calcia and 1400 °C for zirconia-magnesia [19]. Toriz et al. [20] gave 950 °C as the practical upper use temperature for zirconia magnesia in gas turbine applications, and a similar upper use temperature may apply for zirconia-calcia.

3. Current State-of the Art

3.1 *Plasma-Sprayed TBC Development*

The current era in thermal barrier coatings began in the mid 1970's with the development at NASA-Lewis of a two layer TBC consisting of a porous atmospheric pressure plasma sprayed zirconia-yttria (ZrO_2-Y_2O_3) ceramic over a plasma sprayed NiCrAlY bond coat [21,22,23], and the successful testing of this coating on the turbine blades in a research gas turbine engine [24]. Figure 2 shows the coated J-75 turbine blades after testing.

There were three keys to the success of this new coating system. First, yttria was used to stabilize the zirconia. Second, the bond coat was an oxidation resistant NiCrAlY alloy of the type that was then being developed for metallic overlay coatings. Finally, this new approach

employed only two layers -- the ceramic and the bond coat -- with no intermediate layer for grading thermal expansion mismatch. Although there were attempts to include an intermediate region of mixed metal and ceramic to mitigate thermal expansion mismatch stresses, it was soon discovered that this graded expansion approach was inappropriate for temperatures high enough for oxidation to occur in the graded region [25]. Later work places an upper limit of about 800 °C for the maximum temperature to which the graded region may be exposed [26,27]. Union Carbide was another early developer of zirconia-yttria/MCrAlY TBCs [28].

The initial zirconia-yttria TBCs contained from 12 to 20% of yttria, which was added to fully stabilize the cubic phase. Later, Stecura showed that better performance could be achieved by lowering the yttria level to between 6 and 8% [29]; a portion of this data is shown in figure 3. The TBC literature, in general, now supports the view that zirconia-(6-8%)yttria is superior to zirconia-(12-20%)yttria for advanced gas turbine applications and that zirconia-yttria TBCs are in turn superior to zirconia-magnesia and zirconia-calcia [20,26,27,30,31,]. Also, it has been shown that residual stress control via substrate cooling is required for optimum ceramic coating life [32]. There is also general agreement that low pressure plasma sprayed (LPPS) bond coats [33,34] (or shrouded bond coats [35]) are superior to atmospheric pressure plasma sprayed bond coats. A cross sectional micrograph of the current optimum zirconia-yttria/MCrAlX TBC is shown in figure 4.

3.2 *Physical Vapor Deposited TBC Development*

Electron beam-physical vapor deposited zirconia-yttria coatings were first developed at Pratt & Whitney in the late 70s [32,36,37,38]. Other early players were Airco-Temescal [39] and Chromalloy [40]. The burner rig lives of the early PVD coatings were reported to have been far better than the early dense, fully stabilized zirconia-yttria coatings and comparable to the lives achieved for optimized fully stabilized zirconia-yttria [32]. By the early 80s, lives of the best PVD zirconia-yttria coatings were exceeding the lives of the modern partially stabilized zirconia-yttria coatings [34,36]. However, early PVD coatings suffered from poor reproduciblity which was attributed to small differences in the coating microstructure caused by subtle differences in processing parameters [36]. By mid-decade the reproducibility problems had been solved [37,38,41] and laboratory tests and, more importantly, engine tests indicated that this type of coating was well suited for protecting airfoils in subsonic engines. Among the advances were the replacement of the earlier ZrO_2-20%Y_2O_3 compositions with ZrO_2-(6-8)%Y_2O_3. Also the earlier work tended to be limited to PVD MCrAlX bond coats whereas currently it is recognized that PVD zirconia-yttria coatings may be applied to LPPS MCrAlX bond coats as well as to aluminide coatings. Engine experience will be discussed further elsewhere in this volume [Bose and DeMasi; Bartz, Maricocchi, and Wortman].

The columnar microstructure characteristic of PVD coatings (shown in figure 5) imparts excellent strain tolerance to the material. As a result, PVD coatings are favored for the more demanding applications involving frequent cycling. Other characteristics of physical vapor deposited ceramic coatings are excellent adherence to smooth surfaces, a relatively smooth surface finish, and the ability to not clog fine cooling holes when deposited. However, PVD TBCs do not insulate as well as APPS TBCs and they may be less durable in missions requiring very infrequent cycling based on rather poor results when subjected to relatively rapid

cooling after 10 to 20 hour cycling. [42]

4. Supporting Developments

The advances that have led to the acceptance of thermal barrier coatings in gas turbine engines are not limited to materials optimization. Advances in life prediction modeling and performance benefit modeling have played key roles. TBC durability testing has also played a critical role.

4.1 *Life Prediction*

In the mid 70s, thermal barrier coatings had successfully entered service in the turbine section of certain advanced gas turbine engines. While the early application was one of relatively low risk, it was recognized that the full potential of this technology could only be achieved if they were placed in higher risk locations. Establishment of an engine life prediction methodology was at that time a prerequisite to further advancement.

The development of life prediction methodologies consists generally of identification of critical failure mechanisms, stress/strain modeling, and the development of mathematical expressions that define life in terms of stress state and relevant failure criteria. To be useful, the model must be able to extrapolate the life of a given coating system beyond the experimental space achievable in the laboratory and must be extendable to engine service. Related efforts at NASA in the early 80s consisted of research into failure mechanism understanding [43], followed by the development of a prototype laboratory mathematical model [44,45]. The NASA model focussed on thermal expansion mismatch stress between the ceramic and the bond coat/substrate (which is at a maximum after cooling to room temperature) and high temperature oxidation of the bond coat. Although NASA was conducting stress/strain modeling at the time [46], modeled stresses were not coupled to the NASA life model -- rather, cyclic stress was treated as an adjustable parameter. This model was applied to laboratory life data at NASA. It was extended by Pratt & Whitney and subcontractor Southwest Research to engine modeling. This included the direct incorporation of modeled strain and replacement of oxidative weight gain by oxide scale thickness.[47,48]. Later, this model was extended to PVD coatings [42].

Another model, developed by GE [49], employed time-dependent, non-linear finite element modeling of the stresses and strains present in the thermal barrier coating system, followed by correlation of these stresses and strains with test lives. A third model, developed by Garrett [50], involves estimated rate constants and scale factors for cycle length, oxidation life, zirconia time-at-temperature effects and damage due to salt deposition.

4.2 *Performance Modeling*

The potential benefits provided by thermally insulating thermal barrier coatings were recognized at the time of the NASA J-75 engine test [51]. The benefits include considerable reduction in component temperatures and/or reduced coolant air flow requirements for a given turbine inlet temperature. Alternatively, the benefits could be taken in terms of higher allowable turbine inlet temperatures for given component temperatures and reduced coolant flows. At the same time, potential problem areas were identified; these included potential efficiency losses resulting from increased roughness and increased airfoil leading edge thickness. TBC performance analyses, such as the one described above and others [52,53,54], were important

factors that helped to drive TBC development.

Although the details of these calculations may often be proprietary, the results of an early analysis were reported for a vane coated with 0.25 cm of plasma sprayed zirconia-yttria. The benefits were expressed in terms of component temperature reductions of up to about 170°C (300°F) with component durability improvement of 3-4X or reduced cooling air flows corresponding to a 1% specific fuel consumption savings. [34,37]

Another example of temperature benefits theoretically attainable with plasma sprayed zirconia-yttria are given in figure 6 [53]. This figure gives coating surface, interface, and inner metal temperatures for both the pressure and suction side of the airfoil as a function of ceramic layer thickness for a film-cooled turbine vane subjected to a very high hot-spot temperature of 2280°C (4130°F). For this calculation the cooling airflow is sufficient to reduce the temperature of an uncoated blade to 1055°C (1930°F) on the suction side with a similar value reached on the pressure side. The addition of just 0.0127 cm (0.005 in) of ceramic, while maintaining the same high coolant flow, is expected to reduce the interface temperature to only about 870°C (1600°F). Metal temperatures are somewhat higher on the pressure side, but the reduction is still very significant. Thus, for this example, 0.0127 cm (0.005 in) of coating has lowered the component surface(interface) temperature by about 190°C. Note, however, that the second 0.0127 (0.005 in) of ceramic reduced the temperature less than an additional 100°C (180°F); i.e., a decreasing benefit with increasing coating thickness is predicted. Since there is a coating durability penalty associated with thicker coatings, turbine section coatings are typically limited to between 0.0127 (0.005 in.) and 0.0254 (0.010 in.). Another reason to limit the coating thickness is to limit the surface temperature of the ceramic. Generally, the interface temperature drop is accompanied by a comparable rise in the ceramic surface temperature. If temperatures rise too high, then sintering and phase transformations begin to occur. Phase transformations have been observed after 100 hours at 1200°C (2200°F) [55].

4.3 *TBC Durability Testing*

Durability testing, defined as coating life under high temperature cyclic exposure, has tended to guide TBC development. The assessment of durability has been much more important than independent measures of the various properties that affect durability (such as mechanical properties, environmental durability, and phase stability). This reliance on durability testing follows from the complexity of TBC failure mechanisms, which involves a complicated interplay of numerous high temperature effects. In the bond coat, these effects include oxidation, thermal expansion, phase transformations, thermal fatigue, creep/stress relaxation, and bond coat-substrate interaction. In the ceramic, these effects include thickness, structure, chemistry, thermal expansion, phase stability, the effect of microcracking, thermal gradient, and tensile and creep strength. Between layers there are also complicated issues involving thermal expansion and adhesion strength, and the complex interaction between these properties and bond coat oxidation.

While understanding of the above effects is necessary for life prediction, these effects are not independently useful for durability ranking. Nor, generally, is stress modeling useful for durability ranking. Therefore, ranking is generally first carried out in laboratory furnaces or burner rigs (or other laboratory torch rigs). These two types of durability tests each have associated advantages and disadvantages. Furnace tests have several advantages over burner

rig tests; they are generally 1) low cost, 2) temperature can be measured accurately, 3) specimen weight gains can be monitored (if all surfaces are coated), and 4) contaminants are less likely to be a problem. Burner rig tests (figure 7) may be used 1) to force hot spots (thereby avoiding edge effect failures), 2) to allow internal cooling, 3) to heat specimens relatively rapidly (so that short duration cycle durability representative of subsonic engine takeoff and climb can be investigated), 4) to expose specimens to relatively high gas velocity (which may be important when volatility is an issue) or 5) to expose specimens to injected salt contaminants. The burner rig also has somewhat higher heating and cooling rates than the furnace, but they are significantly less than in the engine. Generally the greatest problem in the burner rig involves the difficulties in measuring temperature as discussed in references 56 and 57.

5. Current Directions in Thermal Barrier Coatings Research

It is now evident that, for the foreseeable future, aircraft turbine airfoils will be fabricated from air-cooled superalloys which will be protected by thermal barrier coatings [1]. This represents a departure from the more optimistic predictions of the potential of advanced ceramic and metallic composites. Furthermore, even when these new materials come on line they are likely to require thermal barrier coatings. Therefore there will be more and more demanding requirements placed on this technology, and there will be a continuing need to develop coatings with increased durability. The following is a list of research areas being investigated at or sponsored by NASA-Lewis.

5.1 *Enabling Propulsion Materials Program*

One of the more demanding of the projected future applications of thermal barrier coatings will be to protect airfoils in the next generation of supersonic gas turbine engines. These engines will operate at peak temperatures for several hours per cycle. This contrasts to current subsonic engines which operate at peak temperatures for several minutes per cycle (during take-off-and-climb). NASA is currently actively pursuing research in this area through the Enabling Propulsion Materials program with prime contractors Pratt & Whitney and General Electric.

5.2 *TBCs for Alternative Substrates*

Many new applications of thermal barrier coatings will involve adapting the coatings to the special requirements of new substrate materials. One example of such a material is the NiAl+Zr intermetallic alloy. This material is highly oxidation resistant and may not require a bond coat. In one study at NASA [58], it was shown that zirconia-yttria could be plasma sprayed onto smooth NiAl+Zr if the first mil or so of the ceramic is applied by low pressure plasma spraying. This initial layer of LPPS zirconia-yttria is then followed by a close-out layer of conventionally air-plasma sprayed ceramic. Later, unpublished work, showed that the conventional APPS ceramic could be applied to grit blasted NiAl. Very long lives of over 800 hours at 1200°C were observed in furnace tests.

Another new class of substrates are silicon-based ceramics. While silicon-based ceramics may be a very long way off for the turbine section of aircraft gas turbine engines, certain land based engines are currently investigating silicon-based blades. Also, silicon-based ceramics may be used in other regions of advanced gas turbine engines, and it appears that in many applications

these new ceramics will need thermal barrier and/or environmental coatings. Mullite-based coatings are being developed for Si-based ceramics [59]. Mullite is attractive because of an excellent coefficient of thermal expansion match between it and silicon carbide. However, it was discovered at NASA that plasma sprayed mullite tends to deposit as an amorphous phase which converts to crystalline mullite, with shrinkage and cracking, when heated to above 1000°C. This shrinkage also occurs more slowly beginning at about 600°C. It was discovered that it is possible to deposit mullite in a stable crystalline form if the deposition is carried out above 1000°C, as shown in figure 8. Although this work has been promising, there is still a considerable amount of work that needs to be done, including the development of multilayered ceramics tailored for specific requirements [60] and the development of better approaches for coating silicon nitride based ceramics.

5.3 *Second Generation Life Prediction Modeling*

One important direction for future research involves life prediction modeling, the definition of which has grown to include failure mechanism understanding and stress modeling. This work builds on the prior life prediction work described previously. One example of a current direction in failure mechanism understanding are experiments designed to explore the role of time dependent bond coat properties and the bond coat thermal expansion coefficient on TBC life [W.J. Brindley, this volume]. This work grew out of attempts to understand why high chromium bond coat compositions such as Ni-35%Cr-6%Al-1%Y perform better than lower chromium, higher aluminum bond coats such as Ni-18%Cr-12%Al-0.3%Y [61,62]. This is true even though the lower chromium, higher aluminum compositions would be superior as an oxidation resistant overlay coating. The reason for this surprising behavior was found to be related to a comparatively low thermal expansion for the high chromium bond coat at lower temperatures [63,64] combined with greater stress relaxation for the higher chromium bond coat at higher temperatures. Initial approximate stress modeling [Brindley, this volume] and ongoing finite element modeling are quantifying these effects. While the above analysis suggests that bond coat stress relaxation can be beneficial, it should be noted that an alternative approach involving high strength bond coats has also been advocated [65].

5.4 *Alternative Compositions*

It is interesting to note that no clearly superior successor to yttria as a stabilizer for zirconia has been developed over the past two decades. One promising material is zirconia-ytterbia which has performed well in furnace tests. The optimum composition of those tested was 12% (by weight), i.e. 4 mol% [66]. This composition appears to be in the same position relative to the equilibrium phase diagram [67] as zirconia-yttria in the 6 to 8% range. In more recent unpublished work Yb_2O_3 as well as Er_2O_3 and Dy_2O_3 were evaluated in furnace tests. All three materials performed well, but none were clearly superior to a reference ZrO_2-8%Y_2O_3 coating.

In contrast, great changes in life have been achieved by controlling the silica level on sol gel prepared ZrO_2-8%Y_2O_3 (figure 9). That is, recent work at NASA has shown a strong correlation between TBC durability and the level of silica impurity in plasma sprayed zirconia-yttria coatings that were produced from sol gel processed powders. It was shown that

increasing the silica level from 0.1% to 1.0% caused a five-fold decrease in burner rig life [68]. This is apparently due to increased stress relaxation in the higher silica coating. Work is continuing in this area. The effect of silica on the sintering of the plasma sprayed material is being evaluated by dilatometry and the durability of TBCs prepared from sintered and crushed powders are being determined.

Recently, at NASA, hafnia-yttria based coatings have been evaluated [69]. Hafnia is an element that is chemically similar to zirconia, and plasma sprayed HfO_2-Y_2O_3 TBCs have performed well in laboratory tests. However the best performing hafnia-based coatings appear to be no better than zirconia-based coatings. Interestingly, the best hafnia-yttria coatings contain high levels of yttria stabilizer, up to and including 27%, and are fully cubic. Therefore, they may be more stable at very high surface temperatures which would cause destabilization of the optimum, partially stabilized zirconia-ytrria compositions. However, this has not been demonstrated experimentally. Also, we have begun to investigate the performance of zirconia-scandia in burner rig and furnace tests in cooperation with the Naval Research Laboratory.

Another area under consideration involves metal/ceramic composite bond coats for the purpose of lowering the thermal expansion mismatch between the ceramic and metal layers. [70] This is similar to the intermediate layers produced in graded coatings. However, a major difference is that these composite coatings are low pressure plasma sprayed. Results in this area have been mixed.

5.6 *Programs Sponsored by Other Organizations*

A currently important area of research at NASA involves thick coatings for diesel engines. This effort, sponsored by the Army Research Laboratory, is primarily designed to develop laboratory tests that can be used to screen new concepts in diesel TBCs. Also, U.S. Department of Energy funding has been used to sponsor a Cooperative Agreement with Vanderbilt University to evaluate the mechanical high cycle fatigue behavior of thick TBCs and to develop tests to measure and understand the role of the tensile and shear strengths of these coatings.

Also, NASA expects to become more involved in the near future in the area of thermal barrier coatings for electric utility engines. This is in response to new Department of Energy programs, and it represents a return to an area in which NASA was once active in the past. However, unlike past efforts, the new efforts will not emphasize fuels with high impurity levels.

6. Concluding Remarks

In summary, thermal barrier coatings have evolved from laboratory tests to low risk turbine section applications and then to a state where they are an integral part of engine design. These coatings applied to advanced, air-cooled, superalloy components will be the materials systems of choice in advanced engines for the foreseeable future. Even as non-superalloy components gradually come into service, it is anticipated that these new materials will require the protection of a thermal barrier coating.

References

1. C.T. Sims, Non-Metallic Materials for Gas Turbine Engines -- Are They Real?, Adv. Mater. Process, 139,(1991),32-39.

2. W.N. Harrison, D.G. Moore, and J.C. Richmond, Review of an Investigation of Ceramic Coatings for Metallic Turbine Parts and Other High Temperature Applications. NACA TN-1186,1947

3. F.G. Garrett and C.A. Gyorgak, Adhesive and Protective Characteristics of Ceramic Coating A-417 and Its Effects on Engine Life of Forged Refractory-26 (AMS 5760) and Cast Stellite (AMS 5385) Turbine Blades. NACA RM-E52130,1953.

4. N.I. Cannistraro, Where Do We Stand in Ceramic Coatings, Met. Prog, 74,(1958)111-113.

5. N.N. Ault, Characteristics of Refractory Oxide Coatings Produced by Flame Spraying, J. Amer. Ceram. Soc., 40,(1957)69-74.

6. W.M. Wheildon Jr, Oxide Coated Metal Articles with Metal Undercoating. U.S. Patent 3,006,782. Oct. 1961.

7. A.V. Levy, Ceramic Coating for Insulation, Met. Prog. 75,(1959)86-89.

8. L.N. Hjelm and B.R. Bornhorst, Research-Airplane-Committee Report on Conference on the Progress of the X-15 Project. NASA TM X-57072, 1961, pp 227-253..

9. H. Davies, The Design and Development of the Thiokol XRL99 Rocket Engine for the X-15 Aircraft. J. Royal Aeronat. Soc 67,(1963)79-91.

10, S.G. Grisaffe, Simplified Guide to Thermal-Spray Coatings. Mach. Des., 39,(1967) 174-181.

11. P.R. Dennis, O.W. Gates, C.R Smith, and J.B. Bond, Technological Survey -- Plasma Jet Technology. NASA SP-5033, 1965, pp. 117-120.

12. H.S. Ingham and A.P. Shepard, Metco Flame Spray Handbook vol II, Powder Processes. Second ed. Metco Inc, Westbury, NY, 1964.

13. A.N. Curren, S.G. Grisaffe, and K.C. Wycoff. Hydrogen Plasma Tests of Some Insulating Coating Systems for the Nuclear Rocket Thrust Chamber. NASA TM X-2461, 1972.

14. G.W. Goward, Seventeen Years of Thermal Barrier Coatings, Proceedings of the 1987 Coatings for Advanced Heat Engines Workshop, 27-30 July 1987, U.S. Department of Energy, CONF-870762, pp. III-1--III-9.

15. K.E. Wilkes and J.F. Lagedrost. Thermophysical Properties of Plasma Sprayed Coatings.

NASA CR-121144, 1973.

16. J. Humink Jr, High Temperature Inorganic Coatings, Reinhold Publishing Co, New York, 1963, pp14-15.

17. R. McPherson. the Relationship Between the Mechanism of Formation, Microstructure and Properties of Plasma-Sprayed Coatings, Thin Solid Films, 83,(1981)807-811.

18. D, Chuanian, R.A. Zatorski, and H. Herman, Oxide Powders for Plasma Spraying -- The Relationship Between Powder Characteristics and Coating Properties. Thin Solid Films, 118,(1984)467-475.

19. V.S. Stubican, Pahase Equilibria and Metastabilities in the Systems ZrO_2-MgO, ZrO_2-CaO, and ZrO_2-Y_2O_3, Adv. Ceram. 24A,(1984)71-85.

20. F.C. Toriz, A.B. Thakker, and S.K. Gupta, Thermal Barrier Coating for Jet Engines. ASME 88-GT-279, 1988.

21. S. Stecura, Two-Layer Thermal Barrier Thermal Barrier Coating for Turbine Airfoils -- Furnace and Burner Rig Test Results, NASA TM X-3425, 1976.

22. S. Stecura and G.H. Liebert, Thermal Barrier Coating System. U.S. Patent 4,055,705, Oct. 1977.

23. S. Stecura, Two Layer Thermal Barrier Coating for High Temperature Components. Amer. Ceram. Soc. Bull., 56,(1977)1082-1085.

24. C.H. Liebert et al., Durability of Zirconia Thermal-Barrier Ceramic Coatings on Air-Cooled Turbine Blades in CYclic Jet Engine Operation. NASA TM X-3410, 1976.

25. J.T. DeMasi-Marcin, K.D. Sheffler, and S. Bose, Mechanisms of Degradation and Failure in a Plasma Deposited Thermal Barrier Coating, ASME Paper 89-GT-132, 1989.

26. R.J. Bratton, S.K. Lau, and S.Y. Lee, Evaluation of Present Thermal Barrier Coatings for Potential Service in Electric Utility Gas Turbines. NASA CR-165545, 1982.

27. S.R. Levine and R.A. Miller, Thermal Barrier Coatings for Utility Gas Turbines. NASA TM-85349, 1982.

28. R.C. Tucker, T.A. Taylor, and M.H. Weatherly, Plasma Deposited NiCrAlY Airfoil and Zirconia/NiCrAlY Thermal Barrier Coatings. Presented at the Third Conference on Gas Turbine Materials in a Marine Environment, Bath University, Bath , England, Sept. 20-23, 1976, Session VII, Paper 2.

29. S. Stecura, Effects of Compositional Changes on the Performance of a Thermal Barrier Coating System. NASA TM-78976, 1978.

30. P. Boch, et al., Plasma-Sprayed Zirconia Coatings. Adv. Ceram., 12(1984)488-502.

31. E.C. Duderstadt and P. Agarwal, Energy Efficient Engine, High Pressure Turbine Thermal Barrier Coating Support Technology Report. NASA CR-168037, 1983.

32. I.E. Summner and D.L. Ruckle, Development of Improved Durability Plasma Sprayed Ceramic Coatings for Gas Turbine Engines, AIAA Paper 80-1193, 1980.

33. P.A. Siemers and W.B. Hillig, Thermal-Barrier-Coated Turbine Blade Study, NASA CR-165351, 1981.

34. N.P. Anderson and K.D. Sheffler, Development of Strain Tolerant Thermal Barrier Coating Systems, Tasks I-III, NASA CR-168251, 1983.

35. T.A. Taylor, D.L. Appleby, A.E. Weatherill, and J. Griffiths, Plasma-Sprayed Yttria-Stabilized Zirconia Coatings: Structure-Property Relationships, Surf. Coatings Technol., 43/44,(1990)470-480.

36. D.S. Duvall, Processing Technology for Advanced Metallic and Ceramic Turbine Airfoil Coatings, Proceedings of the Second Conference on Advanced Materials for Alternative-Fuel-Capable Heat Engines, 24-28 August 1981, EPRI RD-2369-SR, pp. 6-102--6-117.

37. S. M. Meier, D. M. Nissley, and K.D. Sheffler, Status of Ceramic Thermal Barrier Coatings -- Gas Turbine Applications and Life Prediction, Proceedings of the 1990 Coatings for Advanced Heat Engines Workshop, 6-9 August 1990, U.S. Department of Energy, CONF-9008151, pp. II-57--II-65.

38. T. E. Strangman, Development and Performance of Physical Vapor deposition Thermal Barrier Coating Systms, Proceedings of the 1987 Coatings for Advanced Heat Engines Workshop, 27-30 July 1987, U.S. Department of Energy, CONF-870762, pp. III-63 -- III-71.

39. R.E. Demaray, W.K. Halnan, ans S. Shen, Development of Electron Beam Physical Vapor Deposition of Ceramic Coatings, Proceedings of the Second Conference on Advanced Materials for Alternative-Fuel-Capable Heat Engines, 24-28 August 1981, EPRI RD-2369-SR, pp.

40. R. Shankar, Electron-Beam Physical Vapor Seposition Development of Zirconia Coatings (Abstract only), Proceedings of the 1987 Coatings for Advanced Heat Engines Workshop, 27-30 July 1987, U.S. Department of Energy, CONF-870762, p. III-43.

41. H.Lammermann and G. Kienel, PVD Coatings for Aircraft Turbine Blades, Adv. Mater. Proc., 140,no. 6, (1991)18-23.

42. S.M. Meier, D.M. Nissely, K.D. Sheffler, Thermal Barrier Coating Life Prediction Model Development, Phase II -- Final Report, NASA CR-189111, 1991.

43. R.A. Miller and C.E. Lowell, Failure Mechanisms of Thermal Barrier Coatings Exposed

to Elevated Temperatures, Thin Solid Films, 95, (1982)265-273.

44. R.A. Miller, Oxidation-Based Model for Thermal Barrier Coating Life, J Amer Ceram Soc., 67,(1984)517-521.

45. R.A. Miller, Life Modeling of Thermal Barrier Coatings for Aircraft Gas Turbine Engines, J. Eng. Gas Turbines Power, 3,(1989)301-305.

46. G.C. Chang, W. Phucharoen, and R.A. Miller, Behavior of Thermal Barrier Coatings for Advanced Gas Turbine Blades, Surf. Coatings Technol. 30, (1987)13-28.

47. J.T. Demasi, K.D. Sheffler, and M. Ortiz, Thermal Barrier Coating Life Prediction Model Development, Phase I -- Final Report, NASA CR-182230, 1989.

48. T.A. Cruse, S.E. Stewart, and M. Ortiz, Thermal Barrier Coating Life Prediction Model Development, J, Enginering Gas Turb. Power, 110,(1988)610-616.

49. R.V. Hillery, B.H. Pilsner, R.L. McKnight, T.S. Cook, and M.S. Hartle, Thermal Barrier Coating life Prediction Model Development, Final Report, NASA CR-180807.

50. T.E. Strangman, J. Neumann, and A. Liu, Thermal Barrier Coating Life-Prediction Model Development, NASA CR-179648, 1987

51. C.H. Liebert and F.S. Stepka, Potential Use of Ceramic Coating as a Thermal Insulation on Cooled Turbine Hardware, NASA TM X-3352, 1976.

C.H. Liebert and F.S. Stepka, Ceramic Thermal-Barrier Coatings for Cooled Turbines, J. Aircraft, 14,(1977)487-493.

52. D.E. Andress, An Analytical Study of Thermal Barrier Coated First-Stage Blades in an F100 Engine, NASA CR-135359, 1978.

54. H.J. Gladden and C.H. Liebert, Effects of a Ceramic Coating on a Metal Temperatures of an Air-Cooled Turbine Vane, NASA TP-1598, 1980.

53. P. L. Meitner, Analysis of Metal Temperature and Coolant Flow with a Thermal Barrier Coating on a Full-Coverage-Film-Cooled Turbine vane, NASA TP-1310, 1978.

55. R.A. Miller, R.G. Garlick, and J,L. Smialek, Phase Stability in Plasma-Sprayed Zirconia-Yttria, Amer. Ceram. Soc. Bull. 62,(1983)1355-1358.

56. R.A. Miller and W.J. Brindley, Thermal Properties of Thermal Barrier Coatings, NASA TM-105923, 1991.

57. C.C. Berndt et al., Current Problems in Plasma Spray Processing, J. Thermal Spray Technol., 1,(1992)341-356.

58. R.A. Miller and J. Doychak, Plasma Sprayed Ceramic Thermal Barrier Coatings for Smooth Intermetallic Alloys. J. Thermal Spray Technol., 1,(1992)211-213.

59. K.N. Lee, R.A. Miller, and N.S. Jacobson, Development of Thermal Shock Resistant Mullite Coating on Silicon Carbide. Ceramamic Transactions: Advances in Ceramic Matrix Composites, N.P. Bansal, ed., American Ceramic Soc., Columbus, OH, 1994. pp.565-575.

60. K.N. Lee, N.S. Jacobson, and R.A. Miller, Refractory Oxide Coatings on Silicon-Based Ceramics, MRS Bulletin, XIX,(1994)35-38.

61. S. Stecura, Advanced Thermal Barrier System Bond Coatings for Use on Ni-, Co-, and Fe-Base Alloy Substrates, NASA TM-87062, 1985.

62. W.J. Brindley and R.A. Miller, Thermal Barrier Coating Life and Isothermal Oxidation of Low-Pressure Plasma-Sprayed Bond Coat Alloys, Surf. and Coat, Technol, 43/44,(1990)446-457.

63. C.E. Lowell, R.G. GArlick, and B. Henry, Thermal Expansion in the Ni-Cr-Al and Co-Cr-Al Systems to 1200°C Determined by High-Temperature X-Ray Diffraction; Metall. Trans. 7A, (1076)655-660.

64. W.J. Brindley and J.D. Whittenberger, Stress Relaxation of Low Pressure Plasma-Sprayed NiCrAlY Alloys. Mat. Sci. Engr., A163,(1993)33-41.

65. D J. Wortman, E.C. Duderstadt, And W.A. Nelson, Bond Coat Development for Thermal Barrier Coatings, ASME Paper 89-GT-134(1989).

66. S. Stecura, New ZrO_2-Yb_2O_3 Plasma-Sprayed Coatings for Thermal Barrier Applications. Thin Solid Films 150,(1987)15-40

67. V.S. Stubican, G.S. Corman, J.R. Hellmann, and G. Senft, Phase Relationships in Some ZrO_2 Systems, Adv. Ceram. 12,(1984)96-106.

68. R.A. Miller, W.J. Brindley, J.G. Goedjen, R. Tiwari, and D. Mess, The Effect of Silica on the Cyclic Life of a Zirconia-Yttria Thermal Barrier Coating, Proceedings of the 7th National Thermal Spray Conference, 20-24 June 1994, C.C. Berndt and S. Sampath, Eds, pp. 49-54.

69. R.A. Miller and G.W. Leissler, Characterization and Durability Testing of Plasma-Sprayed Zirconia-Yttria and Hafnia-Yttria Thermal Barrier Coatings, Part II. Effect of Spray Parameters on the Performance of Several Hafnia-Yttria and Zirconia-Yttria Coatings, NASA TP-3296, 1993.

70. R.A. Miller, W.J. Brindley, C.J. Rouge, and G.W. Leissler, Metal/Ceramic Bond Coatings for High Temperatures, NASA Tech Brief 12, (1988)51.

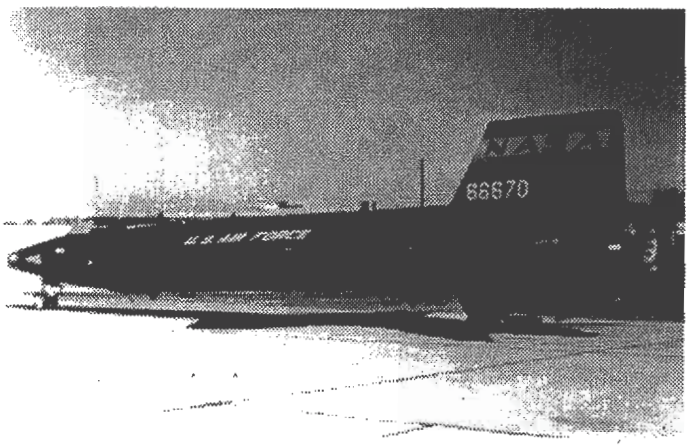

Figure 1. Zirconia-calcia/NiCr TBC visible on the exhaust nozzle of the X-15 manned rocket plane. This is believed to be the first use of thermal barrier coatings in manned flight.

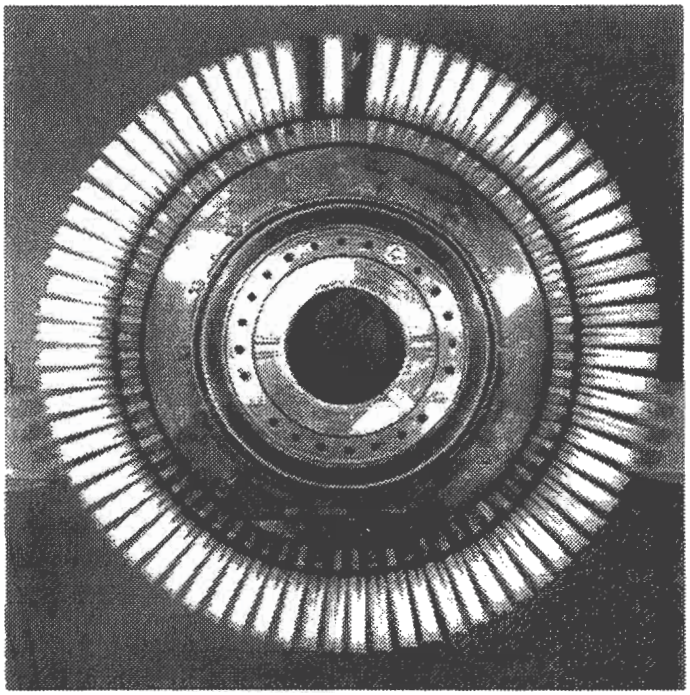

Figure 2. Post test, zirconia-12% yttria/NiCrALY coated turbine J-75 blades. This test marked the beginning of the modern era of thermal barrier coatings.

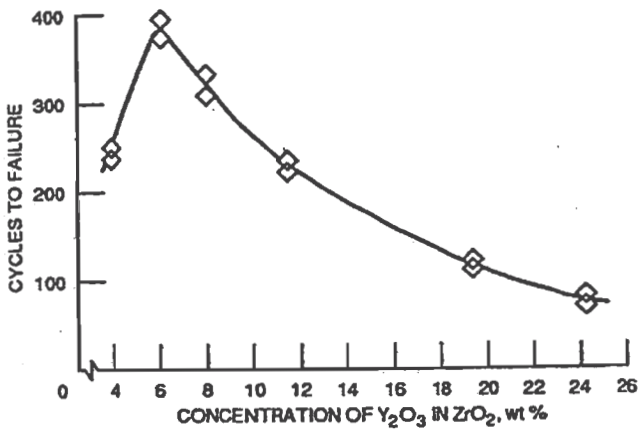

Figure 3. Laboratory test results showing that the optimum thermal barrier coating composition occurs in the ZrO_2-(6-8)%Y_2O_3 range.

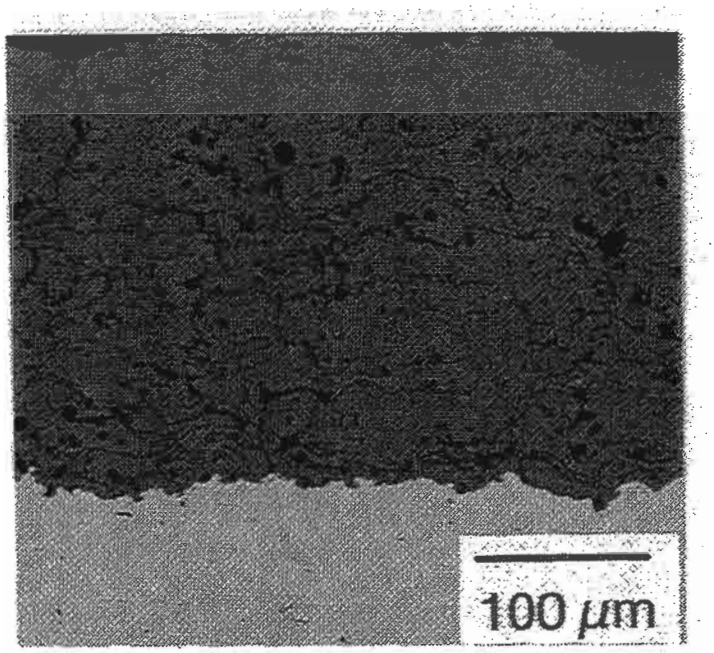

Figure 4. Cross sectional micrograph of a current state-of-the-art plasma sprayed zirconia-yttria/MCrAlX TBC showing porous and microcracked ceramic layer over relatively dense metallic bond coat.

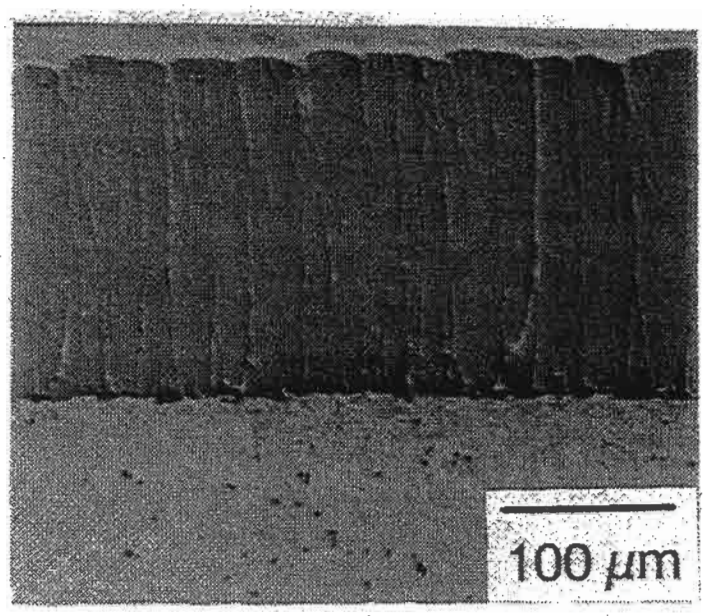

Figure 5. Cross sectional photomicrograph of a current state-of-the-art electron beam-physical vapor deposited zirconia-yttria/MCrAlX TBC showing columnar ceramic over relatively dense bond coat.

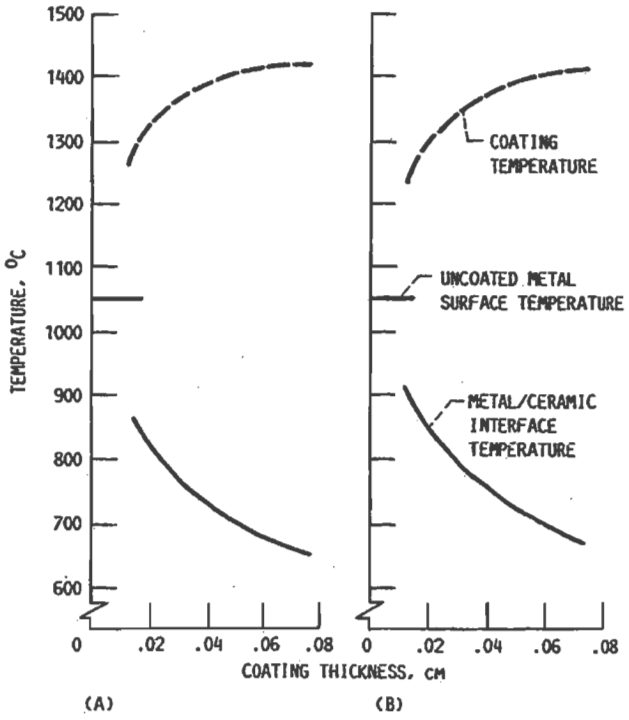

Figure 6. Modeled temperatures for a film-cooled thermal barrier coated turbine blade; a) suction and b) pressure side.

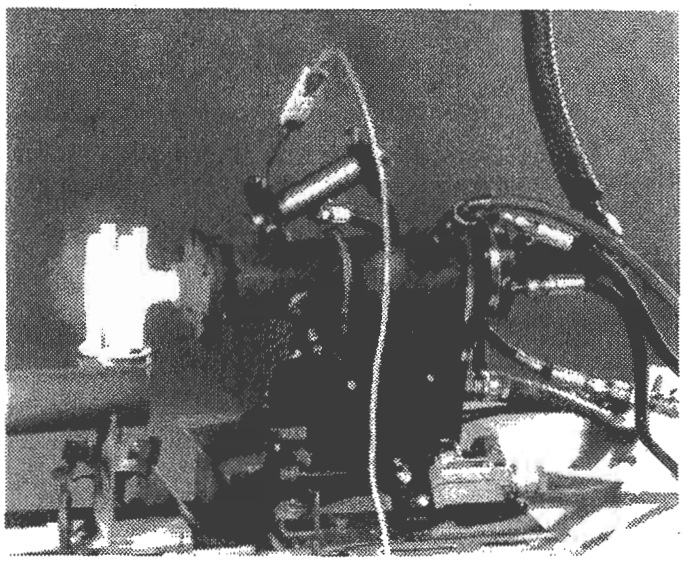

Figure 7. Mach 0.3 burner rig test of four cylindrical, TBC-coated specimens in a rotating carousel.

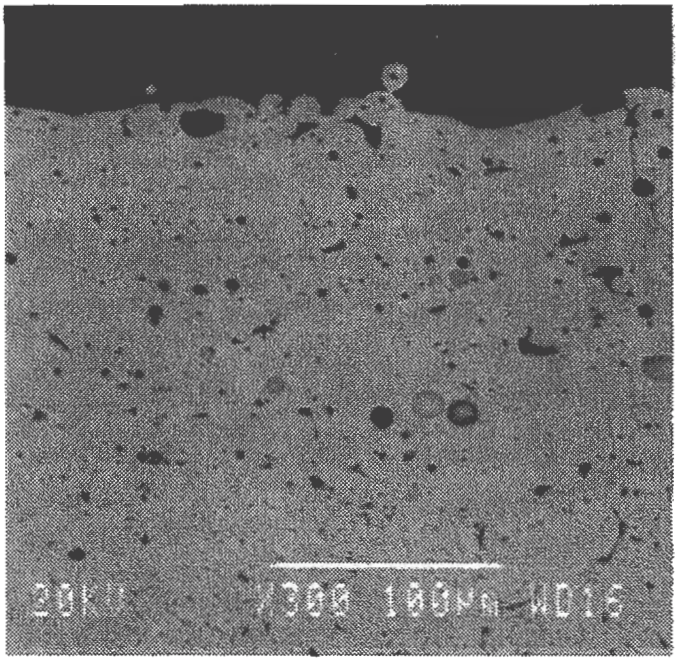

Figure 8. Cross sectional micrograph of plasma sprayed mullite over silicon carbide.

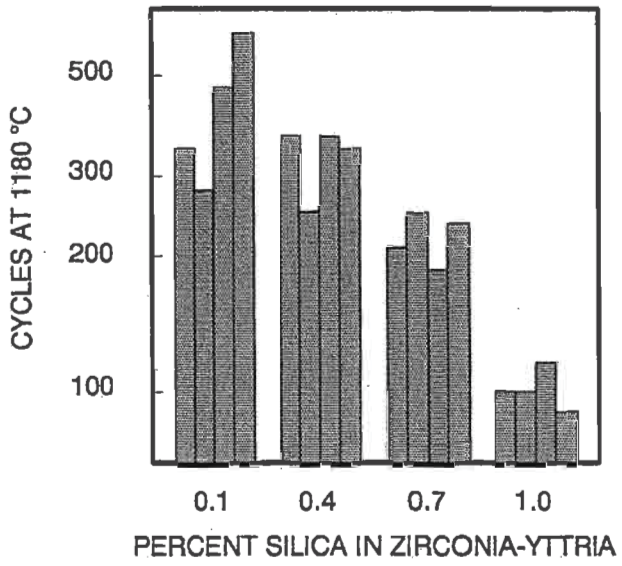

Figure 9. Effect of silica level in sol-gel-processed ZrO_2-$8Y_2O_3$ on the burner rig life of TBC coated specimens.

THERMAL BARRIER COATINGS ISSUES IN ADVANCED LAND-BASED GAS TURBINES

William P. Parks
Department of Energy
Office of Industrial Technologies
Washington, DC 20585

Eugene E. Hoffman
Department of Energy
Oak Ridge Operations Office
Oak Ridge, TN 37831

Woo Y. Lee, and Ian G. Wright
Oak Ridge National Laboratory
Oak Ridge, TN 37831

ABSTRACT

The Department of Energy's Advanced Turbine Systems (ATS) program is aimed at fostering the development of a new generation of land-based gas turbine systems with overall efficiencies significantly beyond those of current state-of-the-art machines, as well as greatly increased times between inspection and refurbishment, improved environmental impact, and decreased cost. The proposed duty cycle of ATS machines will emphasize different criteria in the selection of materials for the critical components. In particular, thermal barrier coatings (TBCs) will be an essential feature of the hot gas path components in these machines. In fact, the goals of the ATS will require significant improvements in TBC technology, since these turbines will be totally reliant on TBCs, which will be required to function on critical components such as the first stage vanes and blades for times considerably in excess of those experienced in current applications. Issues that assume increased importance are the mechanical and chemical stability of the ceramic layer and of the metallic bond coat; the thermal expansion characteristics and compliance of the ceramic layer; and the thermal conductivity across the thickness of the ceramic layer. Obviously, the ATS program provides a very challenging opportunity for TBCs, and involves some significant opportunities to extend this technology. A significant TBC development effort is planned in the ATS program which will address these key issues.

INTRODUCTION

The predicted worldwide need for new electricity-generation capacity in the 1990's is 600 GW. In the U. S., energy consumption is expected to increase by 46 percent in the next 10 years or so[1] which suggests a market in the U. S. alone for new base-load electricity generation capacity of 20 GW per year. Approximately 44 percent of the

current electricity generating capacity in the U. S. will be more than 40 years old by the year 2010[2] and its replacement will be required to meet stringent emissions standards. The technology required by conventional fossil fuel-fired steam boilers to meet these requirements is ready and available; however, substantial reductions in CO_2 emissions will probably require some fuel switching, since approximately 40% of all the carbon-emissions in the U. S. currently are produced by the electric utilities[2]. The projected efficiency of the best available coal-fired steam boiler technology, represented by the Electric Power Research Institute's State-of-the Art Power Plant (SOAPP)[3], is 42 percent [8,100 Btu/kWh net at full load, based on the higher heating value of the fuel (HHV)] when an advanced supercritical steam cycle is employed, which compares with approximately 38 percent for the best coal-fired plants currently in operation in the U. S.

Gas-fired gas turbine combined cycle systems are expected to account for a significant fraction of the projected new capacity. Such plants are available in a range of sizes, up to more than 200 MWe per turbine, which allows the concept of modular build-up of new capacity to meet growth needs. Also, gas turbine power generation equipment offers a low risk, low capital cost, quick-return option. Current combined-cycle plants have claimed cycle efficiencies of the order of 49 percent (7,000 Btu/kWh, based on the HHV), and can achieve environmental compliance for SO_2 and NO_x with minimal effluent or byproduct streams. Further, they can be installed in a very short time frame as a turnkey operation—less than 12 months is possible. Given that gas turbines will likely account for an increasing fraction of the base-load generating capacity, developments to improve their efficiency and improve their environmental compatibility would have a significant positive effect on the economics of power industry.

OVERVIEW OF THE ATS PROGRAM

The overall goals of the ATS program are to develop advanced gas turbine systems to serve both utility and industrial power generation markets. The systems intended for utility application will have an efficiency rating of at least 60 percent (based on the lower heating value; better than 54 percent, based on the HHV), whereas the industrial power generation systems will be at least 15 percent more efficient than current gas turbines. The baseline fuel is natural gas. The ATS machines will have superior environmental compliance, with NO_x levels less than 8 ppm, and CO and hydrocarbon emissions less than 2 ppm. The goal of these systems is to reduce the cost of electricity by at least 10 percent. There is also a requirement that the systems developed will be adaptable to coal and biomass firing; this assumes that gasification processes will be developed as planned[4] to allow a smooth transition from natural gas to coal when that is economical and strategically necessary.

APPROACHES TO ACHIEVING THE ATS PROGRAM GOALS

The approaches available for achieving the program goals were analyzed in an initial phase, in which systems studies were conducted by Allison Engines; ABB Power Generation, Inc., the General Electric Co.; Solar Turbines, Inc.; United Technologies; and Westinghouse Electric Corp. The major areas identified where improvements could be made, and where significant investment would be required were:

- Recuperation to preheat the air entering the combustor.
- Advanced combustors/catalytic combustion to achieve significant reduction in NO_x levels.
- Methods for increasing the TRIT: An increase of 55°C (100°F) in turbine inlet temperature (TRIT) can provide an 8 to 13 percent increase in power output, and a 1 to 4 percent increase in simple cycle efficiency. Suggested approaches include items such as:
  —introduction of single crystal alloys,
  —introduction of low-sulfur alloys,
  —adaption of advanced cooling designs,
  —development of closed-circuit cooling with steam,
  —development of new alloys and advanced cooling designs, which could require ceramic core and mold development,
  —use of thermal barrier coatings (TBCs; a TBC is essentially a materials system which consists of a thermally-insulating ceramic bonded to an oxidation-resistant metal coating which is integral with the substrate), and
  —development of ceramic vanes and blades.
- Increased aerodynamic efficiency from the use of improved sealing and advanced airfoil designs (also applies to steam turbine).
- Improved steam cycles: generation of higher-temperature steam (from 10 MPa/538°C/538°C (1450 psi/1000°F /1000°F) to 12.4 MPa/593°C/593°C (1,800 psi/1100°F /1100°F), or 10 MPa/816°C (1500 psi/1500°F) once-through).
- Thermodynamic recuperation: use of exhaust heat in a methane reforming process to produce fuel gas which would augment the normal fuel.

Some indication of the potential gains associated with some of these approaches can be seen from the following:

Approach	Potential Efficiency Gain
Advanced materials, TBCs	3-4%[5]
Thermodynamic recuperation	2%[6]
Advanced air cooling	1-2%[7]
Reduced leakage (clearance)	0.5-0.6%[5]
Improved aerodynamics (gas turbines & steam turbines)	0.2-0.4%[5]

MATERIALS DEVELOPMENT NEEDS

Some of the materials developments required to realize the goals of the ATS program will be based in part on technology already in use in modern aircraft engines. These engines emphasize maximization of specific thrust, and especially peak thrust in the case of military applications, which is achieved largely through increased turbine inlet temperatures and increased pressure ratios. The pressure ratios of military engines may be as high as 40:1, with the gas temperature at the first stage blade (TRIT) upwards of 1500°C (2732°F). Compact engine dimensions are obtained through the use of multi-spool designs to achieve high pressure ratios, and high individual high-pressure turbine stage loadings. A premium has, therefore, been placed on the development of alloys with appropriate strength at extreme temperatures, and the improvements in aircraft engine performance with time can be accurately tracked by developments in alloy design and processing. Current single crystal alloys experience bulk metal temperatures up to 1000°C (1832°F) in aircraft engine service, reaching 1075 to 1100°C (1967 to 2012°F) at hot spots, but the useful lifetime under these conditions (in the absence of a TBC) is usually less than 5,000 hours. It is considered that alloying technology will allow one more generation of single crystal alloys (which are now in the 3rd generation), which may give a further 28°C (50°F) increase in temperature capability. Further increases in the temperature capability of metallic blade and vanes will probably have to rely on advances in cooling techniques and TBCs, in the absence of alloy technology breakthroughs[8].

Since superalloys begin to melt at 1260-1290°C (2300-2350°F) or so, it has been necessary to use advanced cooling of the critical components, such as combustors, transition ducts, and the first stage vanes and blades. This is currently accomplished by a combination of air cooling, and the use of thermal barrier coatings. The air for turbine cooling is bled from the compressor, and can be as much as 20 percent of the compressor capacity. Since this air bypasses the combustion process, a significant efficiency penalty results. The need for more efficient use of this cooling air has led to progressively more complicated cooling passage designs, hence more complicated blade and vane castings. TBCs were introduced in combustors of advanced engines approximately ten years ago, and now are used routinely on transition ducts as well as combustor liners. Trials are in progress using TBCs on the platforms and, in some cases, as patches on the airfoils of first stage vanes and blades; in this application, the TBC is an added benefit, and no credit is taken for it by reducing the amount of cooling air.

The design of heavy frame turbines has been typically conservative, with greater emphasis on long service life and minimized maintenance requirements than on higher performance and efficiency. However, the performance of these turbines has been gradually improved without much sacrifice of service life and reliability as new materials and designs incorporating aircraft engine experience have been evolved. As a result, the TRIT of a state-of-the-art heavy frame engine is of the order of 1300°C (2370°F), and pressure ratios range up to 16:1. It is expected that the application of advanced air-cooling techniques as well as TBCs will be required to allow an increase in

the TRIT to 1427°C (2600°F), together with a lifetime in excess of 25,000 hours. Further increases in the TRIT probably would require the use of newer cooling technologies such as closed-loop cooling with air or steam.

The transfer of aircraft engine technology for the ATS application must be made with the recognition that the different duty cycle envisioned for these engines will impose different requirements on the critical components and associated materials. In particular, ATS engines will run for a large fraction of their operating lives at close to full power, in contrast to the use of close to full power by aircraft engines only during take off and landing (and combat). In addition, the required time between overhauls and refurbishment is 25,000 hours, which is some five times that required for aircraft engines. The inherently longer time at temperature suggests that time-dependent processes such as creep, corrosion, and sintering (of ceramic thermal barrier coatings) will play an increased role in the degradation processes experienced by ATS engine components. Since the bulk metal temperature must be commensurate with the creep allowances, blade temperatures may have to be somewhat lower than those tolerated in aircraft engines, or more creep-resistant alloys must be introduced.

The short-term and long-term materials needs for developing advanced land-based turbines were recently identified using input from gas turbine manufacturers, materials suppliers, universities, and government laboratories[9]. The key technical areas were considered to be:

- coatings and process development,
- directional solidification and single crystal airfoils manufacturing technology,
- turbine airfoil development; ceramics development,
- materials characterization,
- catalytic combustor materials, and
- efficient technology information exchange to fully use parallel efforts.

Materials issues inherent in coatings and airfoil development are: corrosion, fouling, uniformity of cooling, the impact of steam cooling, leakage, and operation on coal or coal-derived fuels. The development of TBCs with improved bond coats was rated by many respondents as the most important element for advanced land-based turbine applications.

TBC DEVELOPMENT NEEDS

TBCs are currently used on combustors, vane and blade platforms (and airfoil surfaces, but usually as patches) of aircraft engines as a means of increasing the component life, rather than as life-dependent coatings. TBC thicknesses of 500 to 1,000 μm (20 to 40 mil) are used routinely on combustors, and 250 to 500 μm (10 to 20 mil) on first stage vanes whereas, on rotating parts, the thickness is limited by weight and aerodynamic considerations to approximately 125 to 250 μm (or possibly 380 μm) [5-10 mil (or possibly 15 mil)]. Given that ATS machines will operate for significantly longer times at

close to full power than do aircraft engines, it may be necessary to reduce the average bulk metal temperature of the first-stage blades below that permitted for aircraft engines to minimize creep. Even without such a requirement, the relatively thin TBC layer currently applicable to the blade surfaces suggests that substantial cooling of the blade still will be necessary. As a result of these considerations, it appears that developments are needed to increase the effectiveness of the TBC that can be applied to blade surfaces. The necessary improvements may involve developements to allow the use of increased coating thickness, coatings with decreased density, or decreased thermal conductivity. A further approach to minimize the efficiency penalty associated with cooling requirements may involve cooling the air before it enters the blades, or the introduction of steam-cooling for the first-stage vanes to provide more air for the blades.

The key technical issues to be addressed in the development of current TBCs for use on the hot section components of ATS machines are, therefore, the mechanical and chemical stability of the ceramic layer (YSZ) and of the bond coat; the thermal expansion characteristics and compliance of the YSZ layer; and the thermal conductivity across the thickness of the ceramic layer.

PROPOSED EFFORT ON TBCs IN THE ATS PROGRAM

The effort proposed on the ATS program in support of TBCs will address the following issues:

(1) TBC Materials and Process Development

In order to hold the turbine blade temperatures to the limits required for ≥25,000 hours, there are several materials issues to be considered for designing and manufacturing TBCs. These issues include sintering, phase changes, damage due to high angle impact of ingested particles, corrosion and destabilization of the YSZ layer, and long-term thermal and oxidation stability at the bond coat interface.

The mechanical integrity and compatibility with the substrate depend on careful control of the TBC microstructure. For rotating components, a columnar grain microstructure (grain boundaries oriented perpendicular to the surface) as produced by electron beam-assisted physical vapor deposition (EB-PVD) is preferred, since it produces a lower elastic modulus parallel to the metal substrate, and a higher modulus across the thickness. The increased coating compliance parallel to the substrate results in significantly improved spallation resistance. The ability to control this columnar orientation along with coating uniformity, while accommodating cooling holes and maintaining the desired aerodynamic airfoil surfaces, is a major consideration in the development of processes for coating large airfoils. TBCs are also deposited by plasma spraying, which often results in a more porous structure consisting of an agglomeration of solidified splats oriented parallel to the substrate surface. This process is less expensive than EB-PVD, and better-suited to coating large components.

Sintering and phase changes of the TBCs have been shown to occur at the turbine operating temperatures. Sintering increases the tendency for spallation, as well as thermal conductivity, both of which result in increases in the temperature of the metal substrate. The longer-term exposure to high-temperatures projected for ATS machines will accentuate this problem. Characterization of the thermal and physical properties of the TBC as a function of exposure conditions and of its mechanical performance at rated heat fluxes is, therefore, an essential part of any process development.

The deposition of corrodents and their adverse influence on the chemical and mechanical integrity of the TBC layer is a potentially serious threat for coal- and biomass-based fuels. For example, the Y_2O_3 phase in the YSZ system is known to be susceptible to fluxing in the presence of molten salts containing sodium and vanadium[10]. Also, infiltration of the surface of the TBC by deposited salts that are molten at operating temperature could promote spalling of the YSZ when they solidify on cool-down.

Current coating processes, especially plasma spraying, can result in plugging of cooling holes in turbine airfoils, and so lead to the need for secondary processing for removal of the coating in the holes. In advanced turbine airfoils, shaped holes are used to enhance film cooling; a coating that distorts the hole shape, hence the cooling air flow, could negate the benefits of the TBC. The surface finish of the coating is also important to maintain aerodynamic performance. Secondary processing that uses coolants that could contaminate the relatively porous TBC would be highly undesirable.

Manufacturing process developments will be required that improve the reliability and reproducibility of TBCs. Intelligent processing of materials is being emphasized in programs sponsored by the National Institute of Standards and Technology and the Advanced Research Development Agency.

(2) Bond Coat and Metallic Coating Development

Two general types of bond coat have been used: overlaid MCrAlY, where M is typically Ni or NiCo, and diffusion aluminide (or Pt-aluminide). These are shown schematically in Figure 1. The first coating is formed by plasma-spraying directly on to the component, whereas the second is formed by the diffusion of aluminum into the alloy substrate.

A major concern associated with the longer design life for advanced land-based gas turbines is the stability of the bond coat. The ease of transport of oxygen through YSZ ensures that the bond coat will be subject to continued oxidation, as well as hot corrosion if deposited salts can penetrate to the bond-coat region. The ability of the bond coat to continue to support the growth of an alumina scale depends on the total amount of aluminum available; the effective reservoir of aluminum in the bond coat is depleted not only by consumption by the growth of the alumina scale, but also by diffusion into the alloy substrate. If a point is reached where the aluminum level of the bond coat falls below that at which alumina can be formed preferentially, faster-

growing oxides of the other constituents of the bond coat will form, and the adherence of the TBC could be significantly degraded. Another factor is that the continuing growth of the otherwise protective Al_2O_3 at the bond coat-YSZ interface is a source of increasing strain, which may affect the adherence of the external ceramic layer.

Spallation of the YSZ layer induced by the oxidation of the bond coat is considered to be the ultimate failure mode for EB-PVD TBCs. Failure usually occurs at the interface between the bond coat and its oxide scale, whether the bond coat is diffusion aluminide or overlaid MCrAlY. This observation suggests that the life of these TBCs is largely controlled by the factors that govern the bonding at the scale-bond coat interface. For air plasma-sprayed TBCs, spallation usually occurs within the ceramic layer, but very near to the bond coat-YSZ interface. The major sources of stress leading to degradation of TBCs appear to be[11]: thermal mismatch with the bond coat; temperature gradient through the TBC; stress at the YSZ-bond coat interface from oxide growth; and transformations in the YSZ, especially tetragonal to monoclinic which results in a 3 to 5 percent volume change.

A recent discovery is that even trace amounts (≈1 ppm) of sulfur impurity in airfoil alloys can degrade the integrity of the bonding at the scale-alloy interface. This sulfur effect can be minimized by reducing the inherent sulfur impurity level in the alloy through in-melt or post-solidification processing, or through the incorporation of reactive elements additions (such as Y). The use of Y-containing alloys requires the use of alumina for cores and molds, with inherent difficulties of handling and core extraction. The alternative is modification of current melt practices, as well as bond coating processes. There is, therefore, a need for definitive microstructural studies of the effectiveness of approaches to minimize the sulfur effect on the rate of scale growth on bond coat alloys, and on the adhesion of TBCs to such alloys, as a function of exposure time and temperature. These issues are shown schematically in Figure 2.

(3) TBC Analytical Modeling, Life Prediction, and Maintenance and Repair

The development of an analytical model that could predict TBC performance and life based on key TBC parameters and operating conditions could be a major step toward enhanced TBC reliability in an application which is totally dependent on the TBC to reduce airfoil temperature as well as increase airfoil life. The model should address interrelationships among geometric factors (thickness and surface curvature); thermomechanical considerations (gas temperature, cooling characteristics, mechanical stresses, and mechanisms for damage accumulation); material parameters (conductivity and coefficient of expansion; coating strength; bond strength; long-term creep properties; oxidation resistance, corrosion resistance, and microstructural stability). These issues are summarized in Figure 3.

It may be necessary to incorporate several different but related models into the overall model, such as: heat transfer model (prediction of temperature and gradients); materials models (prediction of thermal conductivity and stress-strain response); and mechanistic model (prediction of thermal and mechanical stress fields in the coating, substrate, and

interface as a function of configuration, temperature, environment, and time). Experimental validation of the interrelationships in these models is key to the implementation and use of the overall model in the TBC manufacturing process. In this manner, such a model and its experimental verification could aid in establishing system tradeoffs and synergistic improvements.

The time-temperature exposures and projected thermal gradients in TBCs to meet ATS needs are beyond the current TBC experience base. Laboratory test facilities will be required that can measure properties needed for modeling as described above. In addition, rig test facilities that can simulate the temperatures and high thermal gradients, gas velocities, and pressure on the TBCs are required. Built-in sensors capable of predicting imminent TBC failure in the field would reduce the risk associated with applications where the higher inlet temperature and reduced cooling air are dependent on the TBCs.

Given the critical role of TBCs, reliable inspection procedures will be needed to determine coating section thicknesses and detect defects. A methodology must also be established for the repair of components, either on-site or at a designated depot. Techniques that can establish non-destructively the remaining life of turbine airfoils are actively being sought for aircraft turbines, and such techniques will become even more critical for land-based gas turbines, where time-dependent properties such as creep assume greater importance.

(4) Revolutionary TBC Concepts

TBCs with better thermal properties than achievable by current concepts (YSZ) may be needed to reach the target operating temperature of the ATS hot gas path components. Simply increasing the thickness of a given monolithic coating does not necessarily produce a corresponding increase in thermal resistance, since radiation contributes significantly to the overall heat transfer process at the ATS design temperature. The goal of radically new concepts for TBCs would be to maximize thermal resistance while minimizing coating thickness; thinner coatings might be expected to exhibit improved mechanical properties. There are several approaches for increasing the thermal resistance of a TBC; examples include:

(1) controlled increase in the population of microstructural discontinuities (grain boundaries, voids) in currently-used materials, to increase the thermal resistance
(2) multiple layers of precisely-controlled thickness to provide light-refracting interfaces for selected wavelengths, or
(3) compositionally-graded structures to provide a transition in mechanical properties (such as coefficient of expansion) across the bond coat-TBC interface; and, less revolutionary,
(4) diffusion barriers to reduce the permeability of the TBC to oxygen (and to alkali metal salts), and slow the growth of the oxide on the bond coat.

SUMMARY

The ATS program has the goal of developing gas turbine systems for both utility and industrial power generation applications that will have efficiency ratings significantly higher than current gas turbine systems, that will operate for significantly longer periods between scheduled maintenance outages and, in addition, will have superior emissions performance. Realization of these goals will make use of hot gas path component technologies developed for aircraft engines, but adapted to the quite different duty cycle of ATS machines, which will operate mostly at close to full power rating and exhibit significantly longer lifetimes. A major difference will be that the ATS machines will depend on TBCs to allow a reduction in the cooling air requirements and to realize extended component lifetimes whereas, in aircraft engines, TBCs are used on blades and vanes only to gain added service life benefits, and no reliance is placed on them so that cooling air can be reduced. A significant TBC development effort is, therefore, planned in the ATS program which will address the following issues: improvement of the performance of TBC materials, including the ceramic insulator and the metallic bond coating; development of processes for applying TBCs to large, complex structures with good control of the coating thickness and structure; analytical modeling of the coating degradation processes to allow life prediction, maintenance and repair, and the exploration of revolutionary TBC concepts that have potential for increased thermal resistance and thinner coatings. The Department of Energy is currently pursuing solicitations for major research programs in these areas.

ACKNOWLEDGMENTS

We would like to acknowledge the contributions of our colleagues at the Oak Ridge National Laboratory: J. H. DeVan, R. S. Holcomb, and M. A. Karnitz, and consultant R. W. Harrison for their invaluable discussions during the preparation of this paper.

REFERENCES

1 C. A. Ervin, "The Role of Advanced Turbine Systems in Energy Efficiency and Renewable Energy's Mission," presented at the Advanced Turbine System Annual Program Review Meeting, Washington, D. C. (Nov. 1994).

2 P. Godley, "The Role of Gas Turbines in Utility Research and Development," presented at the Advanced Turbine System Annual Program Review Meeting, Washington, D. C. (Nov. 1994).

3 S. Pace, D. Sopocy, et al., "State of the Art Power Plant (SOAPP)," Sargent and Lundy Engineering Conference, Chicago, IL (Spring, 1992).

4 N. A. H. Holt, "Advanced Gas Turbines Ready to Produce Coal-Based Power," Private Power Executive, Vol. 2, No. 2, 1994, p36-41.

5 H. E. Miller, "Technologies for Next Generation Power Systems," presented at the Advanced Turbine System Annual Program Review Meeting, Washington, D. C. (Nov. 1994).

6 R. L. Bannister, "Overview of Westinghouse's Advanced Turbine Systems Program," pp. 21-26 in *Proc. Advanced Turbine System Annual Program Review Meeting*, DOE/OR-2025 (Nov. 1994).

7 J. C. Corman, "Gas Turbine Power Generation Evolution Advances for the Future," presented at the Advanced Turbine System Annual Program Review Meeting, Washington, D. C. (Nov. 1994).

8 R. V. Hillery, "Coatings for High-Temperature Structural Materials," presented at the Advanced Turbine System Annual Program Review Meeting, Washington, D. C. (Nov. 1994).

9 E. E. Hoffman, M. A. Karnitz, J. H. DeVan, R. S. Holcomb, D. Anson, R. W. Harrison, and R. P. Allen, *Materials/Manufacturing Plan for Advanced Turbine Systems Program*, Report No. DOE/OR-2007, Office of Industrial Technologies, U.S. Department of Energy, Washington, DC (April 1994).

10 R. L. Jones and R. F. Reidy, "Development of Hot Corrosion-Resistant Scandia-Stabilized Zirconia Thermal Barrier Coatings," presented at ASM Materials Week, Session on Ceramic Coatings, Rosemont, IL (Oct. 1994).

11 Y. H. Sohn, K. Cho, and R. D. Sisson, "The Role of Diffusion, Oxidation, and Interfacial Reactions in the Failure of Thermal Barrier Coatings," presented at ASM Materials Week, Session on Ceramic Coatings, Rosemont, IL (Oct. 1994).

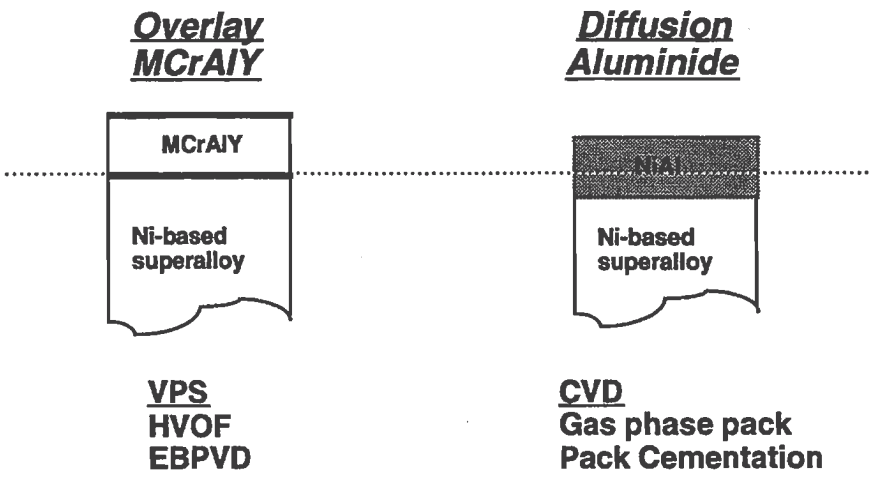

Figure 1 Major Types of Bond Coat

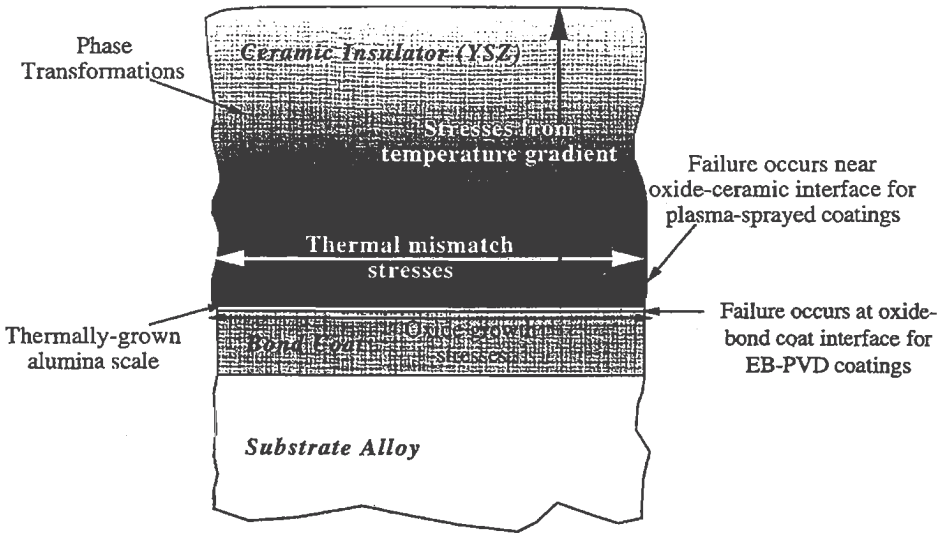

Figure 2 Factors Affecting the Cyclic Oxidation Life of the Bond Coat

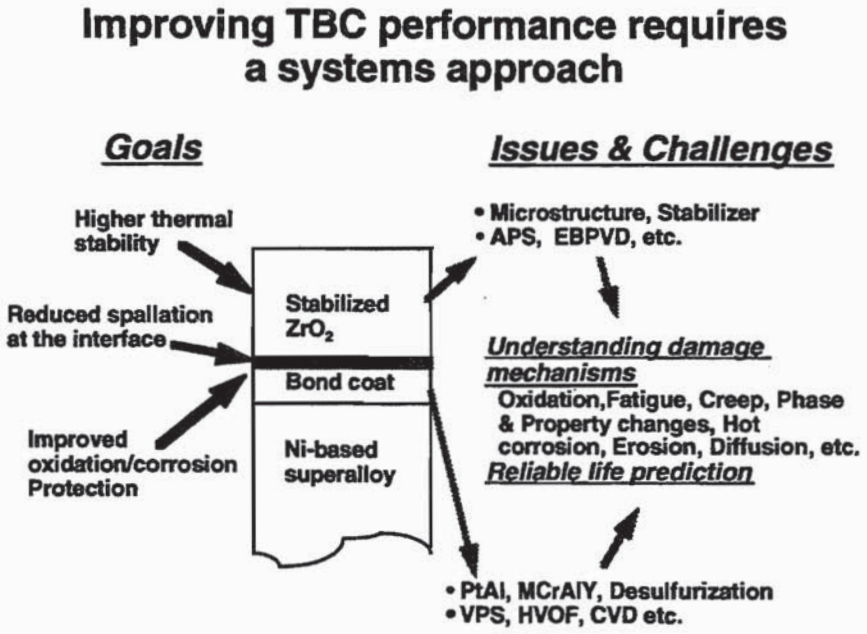

Figure 3 Approaches for Improving TBC Performance

MEASUREMENT METHODS AND STANDARDS FOR PROCESSING AND APPLICATION OF THERMAL BARRIER COATINGS

Stanley J. Dapkunas
Ceramics Division
National Institute of Standards and Technology
Gaithersburg, Maryland 20899

ABSTRACT

Application of thermal barrier coatings deposited by thermal spray, physical vapor and possibly other methods is expected to be extended from aircraft gas turbines to industrial and utility gas turbines as well as diesel engines. This increased usage implies the participation of greater numbers of processors and users, making the availability of standards for process control and property measurement more important. Available standards for processing and evaluation of thermal barrier coatings are identified as well as those needed in the future but currently unavailable.

INTRODUCTION

Thermal barrier coatings (TBC's) based on stabilized zirconia have been applied to aircraft gas turbines for several years with early application on combustor components extended to airfoils. The increased system thermodynamic efficiency due to higher operating temperatures allowed by these coatings, as well as extended substrate lifetimes due to lower metal temperatures, has warranted consideration for non-aircraft turbine as well as diesel engine applications. The increased commerce in coating services and number of coated parts customers expected for these new applications implies a greater need for standardized methods of describing and controlling processing conditions and measurement of coating properties.

Commerce between material or coating suppliers and component manufacturers is conducted by reference to specifications. Specifications are instituted to address two primary concerns: (1) cost, which is driven by process reproducibility manifested as scrap or reject rate and material utilization manifested as waste; and (2) performance which is driven by predictable properties and optimized design. Standard test methods (for mechanical properties, e. g.) and analytical techniques (for chemical or microstructural analysis, e. g.)

Certain trade names and products of companies are identified in this paper to adequately describe materials and equipment. In no case does such identification imply that the products are necessarily the best for the purpose or that they are recommended by NIST.

are, or can be, utilized in determining compliance to specifications. Standard test and analysis methods often rely on, or are based on, reference materials with well characterized properties which are relevant to specific measurements. It is also important that standard test methods and standard reference materials be appropriate to the accuracy, speed requirements, instrumentation and skill capabilities of the intended users. Therefore, development of standards and reference materials is best conducted through the consensus and participation of interested users. It is important that the standard or reference material be developed with a sufficient understanding of the phenomena or property of interest to ensure that the limits of applicability be defined.

In applications where coatings are an integral element of the design of structural components (often termed "prime reliant", in contrast to an added element which improves an already acceptable design), increased precision in control of the coating deposition process and more accurate measurement of coating properties are desirable.

The value of standardized measurement methods for coatings has been recognized in the United States by the Department of Defense, primarily for plasma sprayed (PS) or detonation gun (DG) coatings. In addition to military specifications, Society of Automotive Engineers (SAE) and American Society for Testing and Materials (ASTM) consensus standards have been developed, for primarily wear resistant PS coatings. Foreign standards developed in Great Britain (British Standards Institute, BSI), Germany (Deutsches Institut fur Normung, DIN), Japan (Japanese Institute of Standards, JIS) address primarily thin coatings not intended for thermal barrier application and largely focus on measurement of physical characteristics such as thickness and qualitative measures of adhesion. The increased interest in coatings of all types has fostered a Committee for European Normalization (CEN) effort on development of standard measurement methods for coatings as Working Group 5, Ceramic Coatings, under Technical Committee 184, Advanced Technical Ceramics. It may be expected that these national and regional standards will be incorporated into International Standards Organization (ISO) standards eventually.

In the long term, the use of materials more precisely designed at finer levels, such as functionally graded and nanolayered coatings, will require the development of characterization and measurement standards which are now experimental techniques.

RELEVANT MEASUREMENTS

The efficacy of TBC's relies on two major factors: adhesion to metallic substrates and the thermal insulation provided by the ceramic. The primary means of TBC deposition, PS and PVD, create anisotropic materials which have a low elastic modulus due to the presence of widely-distributed microcracks or porosity. This low modulus allows compliance with the substrate during dimensional changes caused by mechanical or thermal loading. Long term operability of TBC's relies upon adherence of the stabilized zirconia topcoat to a metallic undercoat (bondcoat) applied to the structural component. The importance of adhesion and an understanding of the nature of adhesion has encouraged research to identify the causes of

spallation and the development of models utilizing coating thermal, mechanical and chemical properties to predict coating behavior. Studies [1,2,3] have identified or utilized several key properties which influence PS coating lifetime defined by spallation resistance. These include: coefficient of thermal expansion, thermal conductivity, tensile strength, creep, elastic modulus, Poisson's ratio and, especially, the growth and nature of the oxide layer on the undercoat at the topcoat (zirconia) interface. In these model developments, properties were measured on free standing materials removed from substrates and processed to provide microstructures similar to those in relevant coatings. The same properties are important to the prediction of PVD coatings.

Processing parameter measurement and control is critical to reproducible, cost effective coating deposition. Typical process parameters controlled for both PS and PVD include: power supplied, feedstock chemistry and homogeneity, spacial relationship of feedstock source to substrate, feed rate of coating material, substrate temperature and, for PVD, oxygen partial pressure in the deposition chamber. Control of these parameters influences deposition rate and efficiency as well as microstructural features such as porosity, microcracking, dendrite or splat size, chemistry and phase content, and thermal conductivity.

STANDARD MEASUREMENT TECHNIQUES

Processing

Procedures for the deposition of coatings are generally developed by coating purchasers in cooperation with coating processors and constitute valuable proprietary knowledge. Although not standards in themselves, these procedures can utilize standard analysis and measurement methods to ensure that both parties agree on the values of particular specified process parameters. The importance of specifying processing parameters has resulted in the issue of military specifications for thermal spray deposition. Standards for processing which focus on the characterization and measurement of plasma spray feedstock have been developed through the ASTM and SAE. These standards and specifications are listed in Table 1. With the exception of MIL-Z-81572 and SAE AMS 2436B, these standards address metallic coatings and may be applicable to plasma sprayed bond coats. Standard procedures for chemical and phase content analysis for stabilized zirconia are lacking as are certified reference materials used to calibrate instruments which measure these and other properties such as feedstock powder size and size distribution.

Standard procedures for the analysis of thermal spray (TS), physical vapor deposition (PVD) or chemical vapor (CVD) process parameter are unavailable. However, commercially available systems have been developed to monitor several TS process parameters such as particle velocity and spacial distribution and could conceivably be related to standard calibration procedures. Techniques for analysis of vapor composition in PVD and CVD processes could also be calibrated to known gaseous compositions via reference materials.

Mechanical Properties

The durability of thermal barrier coatings relies on their mechanical properties. These properties, particularly as a function of temperature, are the subject of considerable research but their measurement has not been widely codified as standard measurement techniques. Coating adhesion to the substrate, i.e., zirconia adhesion to the metallic bond coat, is the primary measure of suitability for application. Cohesive strength is also important, but less investigated. Methods for the qualitative evaluation of adhesion, such as flexure, scratch or impact testing have been developed for less complex materials, like zinc coatings. These are of limited value but have been included in ASTM, BSI standards and have been used for the analysis of TBC's. The most commonly used adhesion test is ASTM C 633-79, the tensile tab test[4,5], which is comparable to DIN 50 160-A, and JIS H8666-80. This technique is limited by the use of epoxy adhesive grip attachment to test temperatures significantly lower than application temperatures. These standards are included in Table 1.

Brown et al[6] have reviewed methods used to measure adherence of coatings applied by thermal spray, including flexure and fracture mechanics techniques, and conclude that widely used tests do not provide information required and that simulation of service conditions is vital. Beardsley[7] has addressed the mechanical behavior of coatings intended for diesel applications and developed techniques for the evaluation of compressive tensile fatigue on PS coatings removed from substrates. These techniques have not been developed as standards.

Recognition of the importance of more subtle properties such as fracture toughness, thermal shock response and thermomechanical fatigue has been manifested in research on the modeling of coating behavior and was the subject of a recent conference[8]. However, standards for the measurement of these properties are not available.

Hardness is commonly used as a process control measure and its application to coatings has been recognized in the development of BS 5411-part 6, Vickers and Knoop microhardness, for metallic coatings. Fracture mechanics analysis has been combined with microindentation to measure the fracture behavior of ceramic coatings[9]. However, this more sophisticated analytical technique has not been developed as a standard test method.

It should be noted that significant research has been conducted to utilize scratch techniques to evaluate the adhesion of thin coatings[10]. Although not particularly applicable for thick coatings, the ease of this technique to evaluate coating/substrate systems offers potential for study of the much thinner coatings now being developed.

Corrosion Behavior

Significant levels of effort have been directed to the evaluation of the high temperature corrosion behavior of TBC's for gas turbine applications. Laboratory tests, such as static furnace, and high and low velocity burner rig exposure[11], have been related to

coating behavior in specific engine environments. Specimen geometry and test conditions vary among manufacturers and have evolved to simulate engine conditions, allowing a degree of performance prediction. Because this evaluation is so closely related to application in a competitive market, development of a standard test methodology is unlikely.

Erosion Behavior

The erosion resistance of coatings for gas turbine applications has been the topic of research for many years. Like corrosion evaluation, this testing is intended to simulate performance in an engine and the development of standard test methodologies representative of gas turbine or diesel conditions is unlikely. ASTM G76-83-Standard Practice for Conducting Erosion Tests by Solid Particle Impact Using Gas Jets, included in Table 1, has been developed for low velocity, low temperature evaluation. It does not provide appropriate information for TBC operating conditions.

Thermal Properties

The measurement of thermal conductivity and coefficient of thermal expansion are obviously important to TBC design and performance prediction. Measurement of these properties over the temperature range of application is required. Thermal conductivity of bulk materials and coatings is often measured by the laser flash technique. ASTM E-1461 addresses the use of laser flash for bulk materials and could be extended to coated materials. Similarly, ASTM C-177 proscribes the more complex guarded hotplate method which is generally regarded as the most accurate measure of conductivity. Like ASTM E-1461 it may be extended to coatings. More importantly, the relationship of less expensive and less labor intensive methods to the more sophisticated method is worth establishing

Concerns over the apparent low thermal conductivity of thin films used in electronic and laser optic applications and the adverse effects that poor heat dissipation would have on device performance led to the development of techniques such as the thermal comparator method[12,13] for conductivity measurement. These methods have the potential for development as standard measurement techniques and may be suitable for thin TBCs in particular.

Microstructure

Accurate measurement of coating features such as thickness, porosity, splat and column sizes is necessary for the specification of coatings. In the longer term, measurement of these characteristics may be used to tailor coatings for specific applications. Optical metallographic preparation and analysis is skill dependent and standard reference materials with known characteristics would aid in interpretation. Currently, ASTM C 577-92, Refractory Permeability, is used to measure connected porosity by means of the BET gas absorption method. This method does not allow for size or orientation analysis, nor does it address the analysis of closed porosity.

Microstructural design to achieve specific thermal and metallic properties is expected to gain interest as techniques of modelling coating behavior evolve. These models require measurement of properties at levels commensurate with elements in the models. Methods of measurement for this scale (less than 10 micrometers) are limited. Measurement of details such as porosity and crack size, size distribution and orientation by X-ray and neutron scattering show promise and provide valuable data for modelling. Measurement of elastic modulus and cohesive strength by the use of nanoindentation offer similar promise.

SUMMARY

Increased commerce in TBC's is expected due to the improved performance and component life they provide to both gas turbines and diesel engines. This increased commerce, reflected in greater numbers of suppliers and users, will necessitate the use of broadly accepted methods for analysis and characterization of processing parameters and coatings. Standard measurement techniques and standard reference materials suitable for the analysis of properties are not available for TBC's specifically. Conventional TBC's processed by TS and PVD, and particularly low conductivity thin film coatings, require examination as coated systems which include substrates to properly analyze critical interfacial strength and thermal effects. Available property measurement standards and reference materials are in some cases applicable to or can be extended to coatings. Improved methods of measurement of adhesion and cohesion as well as thermal properties for conventional coatings are necessary. In the longer term, the development and application of nanolayered and functionally graded coatings will require the development of techniques for measurement of properties on scales characteristic of the microstructural features of these materials.

REFERENCES

1. R. A. Miller, Oxidation-Based Model for Thermal Barrier Coating Life, *J. Amer. Cer. Soc.* Vol. 67, No. 8, 1984, p 517-521

2. R. V. Hillery, B. H. Pilsner, R. L. McKnight, T. S. Cook and M. S. Hartle, Thermal Barrier Coating Life Prediction Model Development, Final Report, *NASA Contractor Report 180807,* November 1988

3. J. T. DeMasi, Thermal Barrier Coating Life Prediction Model Development, Second Annual Report, *NASA Report CR-179508,* April 1986

4. Christopher C. Berndt, Tensile Adhesion Testing Methodology for Thermally Sprayed Coatings, *J. Mater. Eng.* Vol. 12, 1990, p 151-158

5. C. C. Berndt and C. K, Lin, Measurement of Adhesion for Thermally Sprayed Materials, *J. Adhesion Sci. Technol.*, Vol. 7, No. 12, 1993, p 1235-1264

6. S. D. Brown, B. A. Chapman and G. B. Wirth, Fracture Kinetics and the Mechanical Measurement of Adherence, in *Proceedings of the National Thermal Spray Conference,* Ed. David Hauck, Pub. ASM International,Materials Park, Ohio,1988,p 147-157

7. M. Brad Beardsley, Thick Thermal Barrier Coatings, in *Proceedings of the Annual Automotive Technology Development Contractors' Coordination Meeting*, Pub. Society of Automotive Engineers, Warrendale, PA, 1992, p 567-572

8. Ceramic Coatings, *Proceedings of the 1993 ASME Winter Annual Meeting, Materials Division, MD-Vol 44*, Ed. K. Kokini, Pub. American Society of Mechanical Engineers, New York, NY, 1993

9. G. K. Besich, C. W. Florey, F. J. Worzala, and W. J. Lenling, Fracture Toughness of Thermal Spray Ceramic Coatings Determined by the Indentation Technique, *J. Thermal Spray Tech*, Vol. 2, No. 1, 1993, p 35-38

10. S. J. Bull and D. S. Rickersby, Evaluation of Coatings, *Br. Ceram. Trans. J.* Vol. 88, 1989, 177-183

11. Robert A. Miller, George W. Lissler, and J. Marcus Jobe, Characterization and durability of Plasma Sprayed Zirconia-Yttria and Hafnia-Yttria Thermal Barrier Coatings, *NASA Technical Paper 3295*, 1993

12. J. C. Lambropoulos, S. D. Jacobs, S. J. Burns, L. Shaw-Klein, and S.-S. Hwang, Thermal Conductivity of Thin Films: Measurement and Microstructural Effects, *Thin Film Heat Transfer-Properties and Processing, HTD-Vol 184*, Ed. M. K. Alam, et al, Pub American Society of Mechanical Engineers, Book No H 00671, 1993

13. K. E. Goodson and M. I. Flik, Solid Layer Thermal Conductivity Measurement Techniques, *Appl. Mech. Rev.*, Vol. 47, No. 3, 1994, p 101-112

Table 1. Available Standards for Coatings

PROCESSING

AMERICAN SOCIETY FOR TESTING AND MATERIALS (ASTM)

B 212-89 Standard Test Method for Apparent Density of Free - Flowing Metal Powders

B 213-90 Standard test Method for Flow Rate of Metal Powders

B 214-92 Standard Test Method for Sieve Analysis of Granular Metal Powders

B 215-90 Test Methods of Sampling Finished Lots of Metal Powders

C 702-87 Standard Practice for Reducing Field Samples of Aggregate to Testing Size

SOCIETY OF AUTOMOTIVE ENGINEERS (SAE)

AMS 2435C Detonation Process - Tungsten Carbide/Cobalt Coating

AMS 2436B Coating, Aluminum Oxide - Detonation Deposition

AMS 2437B Coating, Plasma Spray Deposition

AMS 5791 Powder, Plasma Spray, 56. 5Co-25. 5Cr-10. 5Ni-7. 5W
AMS 5792 Powder Plasma Spray, 50(88W-12Co)+35(70Ni-16.5Cr-4Fe-4Si-3.8B)+15(80Ni-20Al)

AMS 5793 Powder, Plasma Spray, (95Ni-5Al)

AMS 7875 Chromium Carbide Plus Nickel-Chromium Alloy Powder, 75Cr2C3 + 25 (80Ni-20Cr Alloy)

AMS 7878 Tungsten Carbide Powder, Cobalt Coated

AMS 7879 Tungsten Carbide-Cobalt Powder, Cast and Crushed

AMS 7880 Tungsten Carbide-Cobalt Powder, Sintered and Crushed

Department of Defense

MIL-C-52023 Coating: Ceramic, Refractory, for High Temperature Protection of Low Carbon Steel - 1958

MIL-STD-1886 (AT) Tungsten Carbide-Cobalt Coating, Detonation Process For - 1992

MIL-C-81751B Coating, Metallic Ceramic

MIL-M-80141C Metallizing Outfits, Powder Guns and Accessories-1987

MIL-STD-1884A (AT) Coating, Plasma Spray Deposition - 1991

MIL-Z-81572 (AS) Zirconium Oxide, Lime Stabilized, Powder and Rod, for Flame Spraying - 1991

PROPERTIES

ASTM

B 571-91 Standard Test Methods for Adhesion of Metallic Coatings (Bend, Burnishing, Chisel-Knife, Draw, File, Grind-Saw, Heat-Quench, Impact, Peel, Push, Scribe-Grid Tests; Qualitative Only; similar to BS 5411/Part 10)

C 177-85 Steady State Heat Flux Measurements and Thermal Transmission Properties by Means of the Guarded-Hot-Plate Apparatus

C 633-79 Standard Test Method for Adhesion or Cohesive Strength of Flame Sprayed Coatings (Reapproved 1993)

C 577-92 Standard test Method for Permeability of Refractories

E 228-85 Standard Test Method for Linear Thermal Expansion of Solid Materials with a Vitreous Silica Dilatometer (Reapproved 1989)

E 289-94 Standard Test Method for Linear Thermal Expansion of Rigid Solids with Interferometry

E 831-93 Standard Test Method for Linear Thermal Expansion of Solid Materials by Thermomechanical Analysis

Other

D 4541-85 Standard Test Method for Pull-Off Strength of Coatings Using Portable Adhesion Testers

F 692-80 Standard Test Method for Measuring Adhesion Strength of Solderable Films to Substrates (Reapproved 1991)

BRITISH STANDARDS INSTITUTE (BSI)

BS 5411 Methods of Test for Metallic and Related Coatings
Part 1 - Definitions and Conventions Concerning the

Measurements of Thickness
Part 2 - Review of Methods for the Measurement of Thickness
Part 3 - Eddy Current Method for Measurement of Thickness of Non-conductive coatings on Non-Magnetic Basis Materials
Part 4 - Coulometric Method for the Measurement of Coating Thickness
Part 5 - Measurement of Local Thickness
Part 6 - Vickers and Knoop Microhardness Tests
Part 7 - Profilometric Method for Measurements of Coating Thickness
Part 8 - Measurement of Coating Thickness of Metallic Coatings: X-Ray Spectrometric Methods
Part 9 - Measurement of Coating Thickness of Electrodeposited Nickel Coatings on Magnetic and Non Magnetic Substrates-Magnetic Method
Part 10 - 1981/ISO 2819-1980 Review of Methods for Testing Adhesion of Electrodeposited and Chemically Deposited Metallic Coatings on Metallic Substrates (Burnishing, Ball Burnishing, Shot Peening, Peel [less than 125 microns], File, Grinding and Sawing, Chisel[greater than 125 microns], Scribe and Grid, Bending, Twisting, Tensile, Thermal Shock, Drawing, Cathodic; Qualitative Only)
Part 11 - Measurement of Coating Thickness of Non-Magnetic Metallic and Vitreous or Porcelain Enamel Coatings on Magnetic Basis Metals: Magnetic Method
Part 12 - Beta Backscatter Method for Measurement of Thickness
Part 13 - Chromate Conversion Coatings on Zinc and Cadmium
Part 14 - Gravimetric Method for Determination of Coating Mass per Unit Area of Conversion Coatings on Metallic Materials
Part 15 - Review of Methods of Measurement of Ductility
Part 16 - Scanning Electron Microscopy Method for Measurement of Local Thickness of Coatings by Examination of Cross Sections

BSI M. 40 Aerospace Series-Methods for Measuring Coating Thickness by Non-Destructive Testing

DIN

50933-87 Measurement of Coating Thickness by Differential Measurement Using a Stylus

50949-84 Non-Destructive Testing of Anodic Oxidation Coatings on Pure Aluminum and Aluminum Alloys by Measurement of Admittance

50955-83 Measurement of Coating Thickness. Measurement of Thickness of Metallic Coatings by Local Anodic Dissolution: Coulometric Method

50976-89 Corrosion Protection: Hot Dip Batch Galvanzing: Requirements and Testing

50978-85 Testing of Metallic Coatings: Adherence of Hot Dip Zinc Coatings[up to 150 microns]

50982 Part 1-87 Principles of Coating Thickness Measurement: Terminology Associated with Coating Thickness and Measuring Areas

50982 Part 2-87 Principles of Coating Thickness Measurement: Review of Commonly Used Methods of Measurement

50982 Part 3-87 Principles of Coating Thickness Measurement: Selection Criteria and Basic Measurement Procedures

50987-87 Measurement of Coating Thickness by the X-Ray Spectrometric Method

50160-A Tensile Adhesion

JAPAN INSTITUTE OF STANDARDS (JIS)

H8666-90 Testing Methods for Thermal Sprayed Ceramic Coatings

R4204 Method of Testing Ceramic Coating

THERMAL BARRIER COATINGS APPLICATION IN DIESEL ENGINES

J.W. Fairbanks
Office of Transportation Technologies
Department of Energy
Washington, DC

Commercial use of thermal barrier coatings in diesel engines began in the mid 70's by Dr. Ingard Kvernes at the Central Institute for Industrial Research in Oslo, Norway. Dr. Kvernes attributed attack on diesel engine valves and piston crowns encountered in marine diesel engines in Norwegian ships as hot-corrosion attributed to a reduced quality of residual fuel. His solution was to coat these components to reduce metal temperature below the threshold of aggressive hot-corrosion and also provide protection.

Roy Kamo introduced thermal barrier coatings in his "Adiabatic Diesel Engine" in the late 70's. Kamo's concept was to eliminate the engine block water cooling system and reduce heat losses. Roy reported significant performance improvements in his thermally insulated engine at the SAE Congress in 1982.

Kamo's work stimulates major programs with insulated engines, particularly in Europe. Most of the major diesel engine manufacturers conducted some level of test with insulated combustion chamber components. They initially ran into increased fuel consumption. The German engine consortium had Prof. Woschni of the Technical Institute in Munich. Woschni conducted testing with pistons with air gaps to provide the insulation effects. Woschni indicated the hot walls of the insulated engine created a major increase in heat transfer he refers to as "convection vive." Woschni's work was a major factor in the abrupt curtailment of insulated diesel engine work in continental Europe. Ricardo in the UK suggested that combustion should be reoptimized for the hot-wall effects of the insulated combustion chamber and showed under a narrow range of conditions fuel economy could be improved.

The Department of Energy has supported thermal barrier coating development for diesel engine applications. In the Clean Diesel - 50 Percent Efficient (CD-50) engine for the year 2000, thermal barrier coatings will be used on piston crowns and possibly other components. The primary purpose of the thermal barrier coatings will be to reduce thermal fatigue as the engine peak cylinder pressure will nearly be doubled. As the coatings result in higher available energy in the exhaust gas, efficiency gains are achieved through use of this energy by turbochargers, turbocompounding or thermoelectric generators.

THERMAL BARRIER COATING EXPERIENCE IN GAS TURBINE ENGINE AT PRATT & WHITNEY

Sudhangshu Bose and Jeanine DeMasi - Marcin
Pratt and Whitney
East Hartford, Connecticut 06108

ABSTRACT

Pratt and Whitney has accumulated over three decades of experience with thermal barrier coatings (TBC). TBCs were originally developed to reduce surface temperatures of combustors of JT8D gas turbine engines to increase the thermal fatigue life of the components. Continual improvements in design, processing and properties of TBCs have extended their applications to other turbine components such as vanes, vane platforms and blades with attendant increases in performance and component durability. Plasma spray based generation I (Gen I) combustor TBC with 7 w/o yttria partially stabilized zirconia deposited by air plasma spray (APS) on an APS NiCoCrAlY bond coat continues to perform extremely well in all product line engines. Durability of this TBC has been further improved in Gen II TBC for vanes by incorporating low pressure chamber plasma sprayed (LPPS) NiCoCrAlY as a bond coat. The modification has improved TBC durability by a factor of 2.5 and altered the failure mode from a "black failure" within the bond coat to a "white failure" within the ceramic. Further improvements have been accomplished by instituting a more strain tolerant ceramic top layer with electron beam physical vapor deposition (EB-PVD) processing. This Gen III TBC has demonstrated exceptional performance on rotating airfoils in high thrust rated engines by improving blade durability by 3x, by eliminating blade creep, fracture and rumpling of metallic coatings used for oxidation protection of the airfoil surfaces. A TBC durability model for plasma sprayed as well as EB-PVD systems is proposed which involves the accumulation of compressive stresses during cyclic thermal exposure. The model attempts to correlate failure of the various TBCs with elements of their structure and its degradation with thermocyclic exposure.

INTRODUCTION

Gas turbine engines use nickel and cobalt based superalloys in the turbine components, such as airfoils, combustors, transition ducts and seals. Increased thermal efficiency demands of the newer engines dictate that the turbine inlet temperature be significantly increased. This needs to be accomplished without structural failure of components from melting, creep, oxidation, thermal fatigue and other degradation mechanisms. The surface temperature of these components must, therefore, be maintained low enough to retain materials properties within acceptable bounds. The demand is partially met by innovative component cooling schemes using compressor discharge air. However cooling air is only available at a premium at the expense of loss of thrust, and added fuel consumption. The major element in meeting the demand without significant performance loss, however, comes from two parallel materials innovations: improvement in the temperature capability of superalloys on the order of 80 - 85°C and development of thermal barrier coatings (TBC) capable of providing thermal insulation equivalent to about 165 - 170°C. The relative magnitude of the thermal benefit provided by TBCs highlights their extreme importance as enablers of the super high thrust engines such as Pratt & Whitney's PW 4084.

Typically TBCs are a bilayer system, consisting of a metallic layer (the bond coat) on the substrate on which a ceramic layer is deposited. In addition to providing oxidation protection to the substrate, the metallic bond coat layer provides an adequately prepared surface to which ceramic layer adheres. The ceramic layer composition is selected based on thermal conductivity, high temperature stability and thermal expansion compatibility with the substrate. Due to its low thermal conductivity, good thermocyclic durability when stabilized against phase transformation, zirconia has become the ceramic of choice. The current bilayer design and composition of TBC have evolved from a multitude of designs and a number of compositions tested by Pratt and Whitney over a period of several decades.

Historical background..— Pratt and Whitney first introduced TBC on burner cans in JT8D engines in 1963. This TBC consisted of zirconia stabilized by the addition of 22 w/o MgO (22MSZ) to avoid the detrimental tetragonal (high temperature phase) to monoclinic (low temperature phase) phase transformation. The ceramic was deposited on a flame sprayed Ni-Al bond coat. Subsequent evolution of TBC at Pratt and Whitney, incorporating refinements that allowed increamental increases in combustor exit

temperature, are summarized in Table 1. In current systems, the ceramic consists of 7 w/o yttria partially stabilized zirconia (7YSZ). Depending on the application requirements, the bond coat is a variation of NiCoCrAlY composition applied either by air plasma spray (APS) or low pressure chamber plasma spray (LPPS). The ceramic deposition is accomplished either by APS or electron beam physical vapor deposition technique (EB-PVD). In the present generation high thrust engines, the major turbine components protected by TBCs and the the TBC systems used are summarized in Table 2. A review of general experience on the various TBC systems in Pratt & Whitney engines has been presented by Meier et. al. [1]. However, some details beyond those covered by the review, with specific observations, are discussed below.

Combustor plasma sprayed TBC.— Magnesia stabilized zirconia (MSZ) used to be the ceramic top layer for combustor application. However, due to its susceptibility to destabilization and relatively low temperature capability (~ 982°C), MSZ has been replaced with 7YSZ as the ceramic coat. This modification has resulted in 4x improvement in durability. The 7 YSZ based combustor TBC system, henceforth called generation I (Gen I) TBC, has performed extremely well in all engines. Failure of Gen I TBC usually occurs within the bond coat with the appearance of the so called "black failure". The bond coat is NiCoCrAlY deposited by air plasma spray, since large component size does not allow for processing in low pressure chamber. X ray diffraction analyses indicate that the bond coat oxidizes to a structure akin to NiO. It is speculated that kinetics favors the growth of this oxide because of the pre-existence of the oxide nuclei formed during air plasma spraying. This oxide is voluminous and is relatively weak in comparison with the thin oxide that forms on alumina formers. With increased thermocyclic exposure, biaxial in-plane compressive stresses develop within the oxide. When these stresses exceed the compressive strength of the oxidized bond coat, failure seems to occur within the bond coat giving the black appearance of the oxide. The compressive stresses are acerbated in the presence of sharp changes of radius of curvature. In combustor designs, therefore, such abrupt changes are carefully avoided.

Airfoil plasma sprayed TBC.— Experience on Gen I combustor TBC showed that the weak link in the system was the bond coat. The next improvement therefore, focused on the strengthening of the bond coat, particularly its oxidation resistance. This was accomplished in the second generation (Gen II) TBC system by incorporating a low pressure chamber plasma spayed NiCoCrAlY bond coat in place of the air plasma sprayed bond coat of Gen I. The absence of oxygen during deposition of the bond layer

eliminated the pre-existing oxide nuclei to a great extent and altered the oxidation mode, eliminating the "black failure" observed previously.

Vane airfoil surfaces and platforms, with operating environment structurally and thermally more severe than that experienced by the combustor, are usually protected by Gen II TBC. It has demonstrated outstanding performance in all engines with a durability improvement of 2.5x over Gen I. The failure mode of Gen II, extensively investigated under NASA's HOST Program [2], is characterized by spallation of the ceramic with resulting "white failure" in which major cracks develop and propagate parallel to and near the bond coat - ceramic interface but always remaining within the ceramic. These major cracks are a result of linking of microcracks that form early in the ceramic due to cyclic thermal exposure. Bond coat oxidation results in the formation of a slow growing thin alumina layer. Due to the strengthening of the bond coat and the resulting oxide, the weak link in Gen II TBC, relative to Gen I, is now within the ceramic layer itself, thus providing white appearance.

The thickness of the TBC has been found to be an important parameter, because while increased ceramic thickness provides additional thermal insulation, it adds to component weight and accelerates TBC spallation.

The nominal thickness of TBC systems calls for a 0.125 mm bond coat and 0.250 mm ceramic top coat. These thickness values have been arrived at from experience balancing thermal protection against additional weight imposed by the TBC. The durability of TBCs was found to be strongly thickness dependent. In order to understand the ceramic thickness issue in greater detail, an effort was made at Pratt and Whitney to determine in laboratory tests the effects of ceramic thickness on cyclic durability as determined in burner rig tests. Burner rig bars were coated with Gen II TBC of increasing ceramic thickness. These bars, in combination with base line Gen II TBC with 0.25 mm ceramic layer, were exposed in thermocyclic endurance test at 1120°C. The results in the form of relative durability vs. ceramic thickness, with data scatter, are shown in Figure 1. The data show that increased thickness has a strong debit on durability. The failure mode of the ceramic also changed with increased thickness, moving from a compressive failure within the ceramic for nominal 0.25 mm ceramic thickness to tensile cracking at higher thicknesses. It is speculated that with increased thickness of the ceramic, the temperature of the top surface increases, introducing sintering as a degradation mechanism of growing importance. Sintering and associated shrinkage introduce tensile stresses which result in

transverse cracking of the ceramic perpendicular to the interface. Such failure modes have indeed been observed with thicker TBCs in the laboratory and in engine testing.

Airfoil Electron Beam Physical Vapor Deposited (EB-PVD) TBC.— The successful application of TBC on the vane airfoil surface and platform logically leads to the question of rotating airfoil applications. Earlier engine tests at Pratt and Whitney had indicated that improvement beyond Gen II TBC would be required because of the combination of rotational stresess and high temperatures that blades experience. TBC with LPPS NiCoCrAlY bond coat and the ceramic layer consisting of the strain tolerant EB-PVD 7YSZ structure [1], designated Gen III TBC, appeared very attractive based on burner rig tests in which it exhibited 10x durability improvement relative to Gen II TBC. This translates roughly into an anticipated 3x improvement in blade life. Due to the importance of this TBC as enabler of high thrust engines such as PW4000, early engine validation was conducted. The test was comparative in nature, conducted on first stage turbine blades of JT9D engine. Blades coated with patches of Gen III TBC on the concave side, were run in the same engine, in a rainbow configuration, with two additional sets of blades, one coated with an equivalent patch of plasma deposited Gen II TBC and the other with just the LPPS metallic bond coat which only provides oxidation protection. As shown in Figure 2, both the metallic coating and Gen II patches exhibited significant blade distress. However, EB-PVD based Gen III patch performed extremely well. This excellent performance has been verified on blades in JT9D revenue engines with total run time on TBC exceeding 15000 hrs on the same blade. The repeated demonstration of excellent performance of Gen III TBC has led to its becoming bill-of-material for blade application on all PW high thrust engines, with cumulative experience exceeding 4 million hours. Figure 3 shows the excellent condition of Gen III TBC on a cluster of first-stage blades after 1666 endurance cycles in PW4084 experimental engine. While the third generation TBC performance is at least an order of magnitude improved in thermocyclic durability, eventual failure still occurs by spallation. However, the failure mode of this TBC is unlike those for both Gen I and II. A very thin aluminum oxide layer grows on the bond coat at the ceramic - bond coat interface. This very tenacious thermally grown oxide (TGO) plays a key role in the adhesion of the ceramic layer of the TBC. Failure occurs usually by spallation due to the propagation of cracks either within the TGO or at the TGO - bond coat interface. Frequently, the ceramic spalls at room temperature after the component had been out of test for considerable length of time. Such delayed failures are clear indications of the role of accumulating residual stresses in the ceramic - bond coat system.

Specific Observations.— The overall benefit of TBC lies in the lowering of the substrate temperature, thereby retaining significant portion of the structural properties of the substrate materials. However, under this overall benefit umbrella lie some nuances that are spectacular exhibit of specific performance advantages of TBC.

Suppression of thermal transient effects: Figure 4 shows a generic strain - metal temperature cycle, the so-called "peanut curve" of a turbine blade. The Figure illustrates that the particular operating points within the mission cycle of an engine can have significant effects on both the component mechanical strain and the metal temperature, and every change in the operating point introduces thermal transients. The effect of these thermal transients is non-uniform temperature distribution and temperature gradients across the airfoil. These can result in distortion and thermomechanical fatigue cracking of the components. In addition to the transients, component design and associated cooling patterns also generate non-uniform temperature distribution and temperature gradients, which can contribute to distortion and cracking. Distortion induced by non-uniform temperature distribution is illustrated by Figure 5 which shows the cross section of the airfoil section of an engine tested blade. Due to its operating environment, the blade experienced a temperature difference of ~85°C between the concave pressure side and the convex suction side. In combination with the high operating temperature, the ΔT translated into a significant thermal stress to creep distort the pressure side. The distortion has two effects. First, it disturbs the aerodynamic flow. Second, the distortion reduces blade life. A solution to the distortion issue was the use of TBC on the airfoil surface. Application of Gen III TBC has alleviated the problem by lowering the overall temperature and reducing the temperature gradient across the airfoil surface. Figure 6 shows the cross section of an airfoil section of a blade tested with Gen III TBC under similar condition. It shows no signs of creep distortion seen in Figure 5.

Creep of metallic coatings: To impart oxidation protection, turbine blades are coated with an oxidation resistant metallic coating. The first and the second turbine blades are usually coated with LPPS NiCoCrAlY overlay coating. Above the brittle to ductile transition temperature of the intermetallic NiCoCrAlY, the coating tends to creep, behaving superplastically at higher temperatures. The creep stresses originate from the blade rotation with minor contribution from the coating - substrate thermal expansion mismatch. As a result of creep of the metallic coating, an originally smooth surface of the coated airfoil tends to take a "rumpled" appearance, as shown in Figure 7. The resulting

distortion has impact both on the aerodynamic performance of the airfoil and the durability of the component. Since creep is a thermally activated process, a simple solution would be to lower the temperature of the metallic coating. Application of TBC has indeed alleviated the problem by lowering the temperature. As can be seen in Figure 7, there are no signs of creep in areas protected by TBC, while adjacent areas with metallic coating not protected by TBC exhibit the creep "rumples".

Generic failure mechanism.— Based on the experimental engine experience and laboratory data generated to date, a model emerges that explains the thermocyclic behavior of TBCs including plasma sprayed Gen I, Gen II and EB-PVD based Gen III systems. The details of the model depend on individual TBC systems, the time dependent stress - strain response and materials degradation mechanism of individual elements of the TBC. However, in all cases, it has been established that coating failure occurs due to in-plane compressive residual stresses. In-plane tensile residual stresses only result in transverse cracks which do not generally contribute to coating spalls except in thicker TBCs as explained before. The influence of oxidation on plasma deposited TBC life is well demonstrated [3]. A significant portion of the residual stress develops due to the constrained oxide growth on the bond coat at the ceramic-bond coat interface. Depending on the kinetics of the oxide growth in the presence of the ceramic top layer, the compressive residual stresses increase with time as depicted schematically in Figure 8. Superimposed on this increasing compression, lies the cyclic stresses generated by the thermal expansion mismatch between the ceramic and the underlying layer, the cycles being the heating and cooling associated with engine operation. Failure occurs when the cumulative compressive stress exceeds the compressive strength of the elements at the failure sites. The failure locations are coating specific. In MSZ based TBC, failure takes place in the ceramic due to destabilization of MSZ. In Gen I TBC, failure occurs in the bond coat. In Gen II failure takes place within the ceramic but near the ceramic - bond coat interface. EB-PVD based Gen III TBC, on the other hand, fails either within the TGO or at the TGO - substrate interface. The failure sites are the weak links in the TBC structure. In Gen I with air plasma sprayed bond layer, the weakest link lies within the bond coat. The oxidized bond coat, with predominantly NiO structure, has a relatively low compressive strength. In PWA 264, replacement of the bond layer with LPPS deposited NiCoCrAlY favorably altered the oxidation characteristics. Instead of a weak and voluminous NiO structure, a thin and strong alumina forms. The strengthening of the bond layer, therefore, moved the weak link from the bond coat into the ceramic, initiating failures within the ceramic coating. Any further durability improvement now would

require enhancement of the ceramic. Such enhancement has been achieved by replacing the plasma sprayed ceramic layer with the strain tolerant structure of EB-PVD ceramic. Due to the strengthening of the ceramic, the weak link has now shifted within the TGO or at the TGO-bond coat interface.

Concluding Remarks.— Thermal insulation benefits provided by TBCs and the resulting impact on component creep and thermomechanical fatigue life have made them enablers of high thrust gas turbine engines. Of particular importance is the EB-PVD based TBC which is anticipated to improve blade life by a factor of 3. This new generation of TBC has evolved from an understanding of and improvements to the structure, properties, processing and failure modes of earlier TBC systems. Such understanding will continue to extend TBC performance beyond what is accomplished today.

Table 1 TBC Development at Pratt and Whitney

TBC System	Year of Introduction	Bond Coat	Ceramic Coat	Design of Layers
Early Combustor TBC	1963	Flame sprayed Ni-Al	APS 22MSZ	Ceramic / Bond coat
"	1973	APS Ni-Cr / Al	APS 22MSZ	Ceramic/Cermet/Bond coat
"	1974	APS CoCrAlY	APS 22MSZ	Graded
"	1980	APS NiCoCrAlY	APS 22MSZ	Ceramic/Bond coat
Gen I	1984	APS NiCoCrAlY	APS 7YSZ	Ceramic / Bond coat
Gen II	1982	LPPS NiCoCrAlY	APS 7YSZ	Ceramic / Bond coat
Gen III	1987	LPPS N NiCoCrAlY	EB-PVD 7YSZ	Ceramic / Bond coat

Table 2 Application of current TBC systems in Pratt and Whitney gas turbine engines

Turbine Component	TBC System	Size Requirement	Structural/ Thermal Environment	Specific Engines
Combustor	Gen I	Large	Moderate Thermal	JT8D, JT9D, PW2000 PW4000, V2500
Vane Airfoils	Gen II	Small	High Thermal	First and second stages in JT9D, PW2000, PW4000 and V2500
Vane Platforms	Gen II	Small	Moderate Thermal	First and second stages in JT9D, PW2000, PW4000 and V2500
Blade Airfoils and Platforms	Gen III	Small	High Mechanical & Thermal	First in JT9D, PW2000, PW4000

REFERENCES

1. S. M. Meier and D. K. Gupta, The Evolution of Thermal Barrier Coatings in Gas Turbine Engine Applications, ASME Journal of Engineering for Gas Turbines and Power, Vol 116, 1994, p250-257

2. J. T. DeMasi, M. Ortiz and K. D. Sheffler, Thermal Barrier coating Life Prediction Model Development, Phase I Final Report, NASA Cr-182230, 1989, Pub. NASA-LeRC, Cleveland, OH

3. R. A. Miller and C. E. Lowell, Failure Mechanisms of Thermal Barrier Coatings Exposed to Elevated Temperature, Thin Solid Films, Vol 99, 1982, p265

ACKNOWLEDGEMENT

The authors would like to thank Drs D. N. Duhl and D. K. Gupta of Pratt and Whitney, East Hartford, Connecticut, for their suggestions and for reading the manuscript.

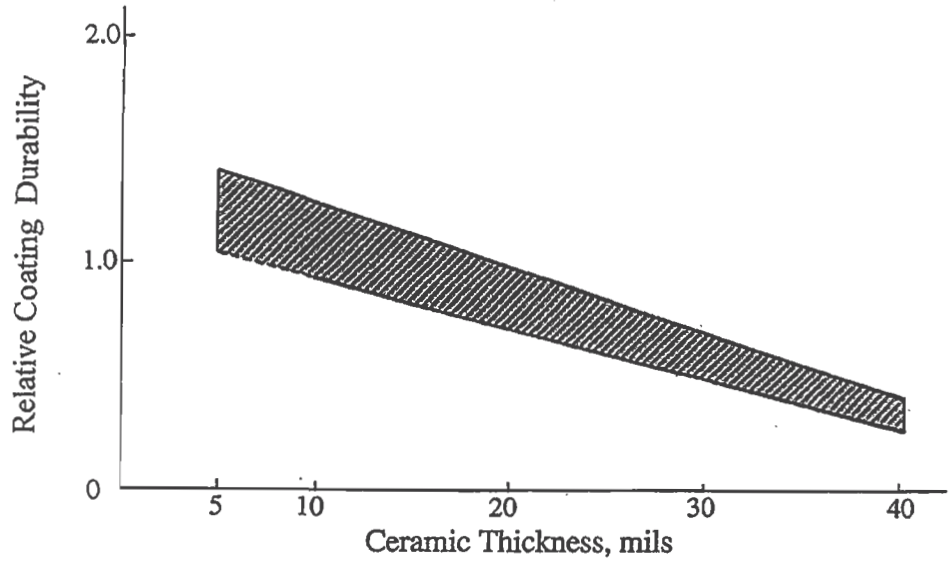

Figure 1. Debit on durability due to increased TBC thickness as demonstrated in burner rig testing.

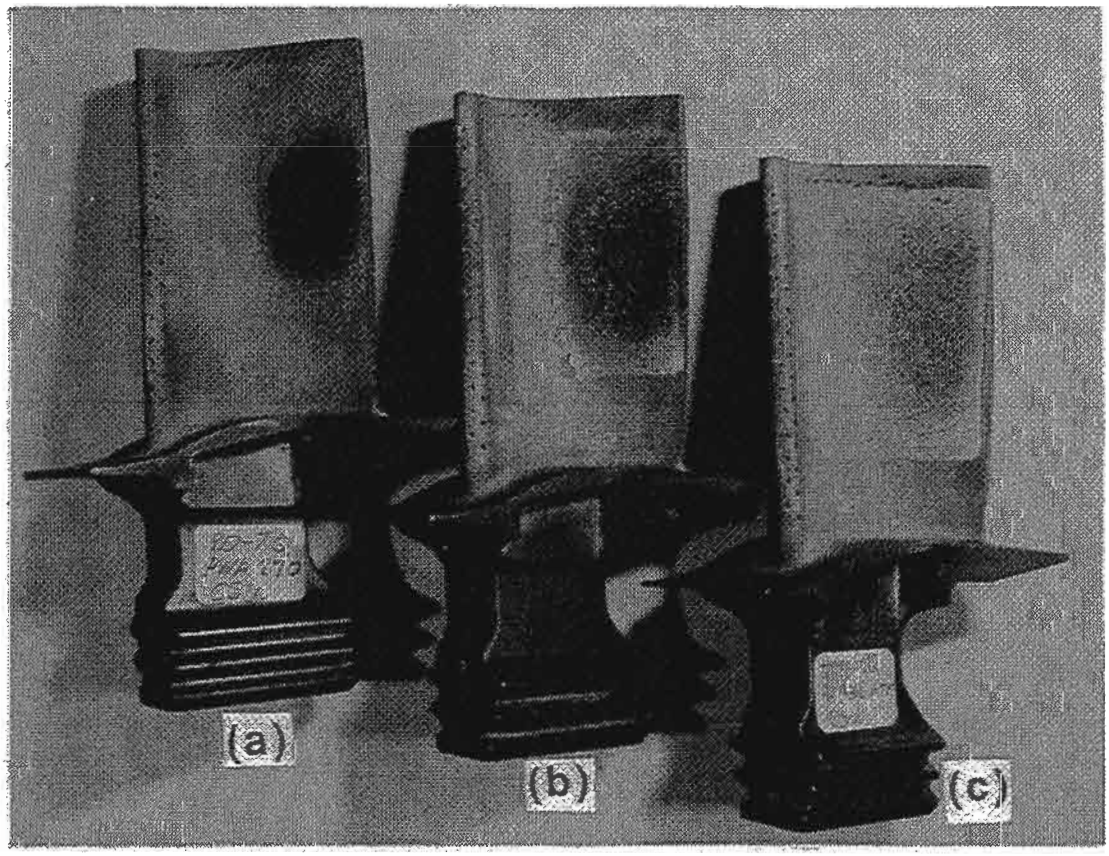

Figure 2. Relative durability of (a) Metallic coating for oxidation resistance, (b) Plasma sprayed TBC and (c) EB-PVD TBC demonstrated by application of respective patches on the concave airfoil surface of JT9D first stage blade. While the metallic coating and plasma TBC exhibited distress, EB-PVD TBC performed extremely well.

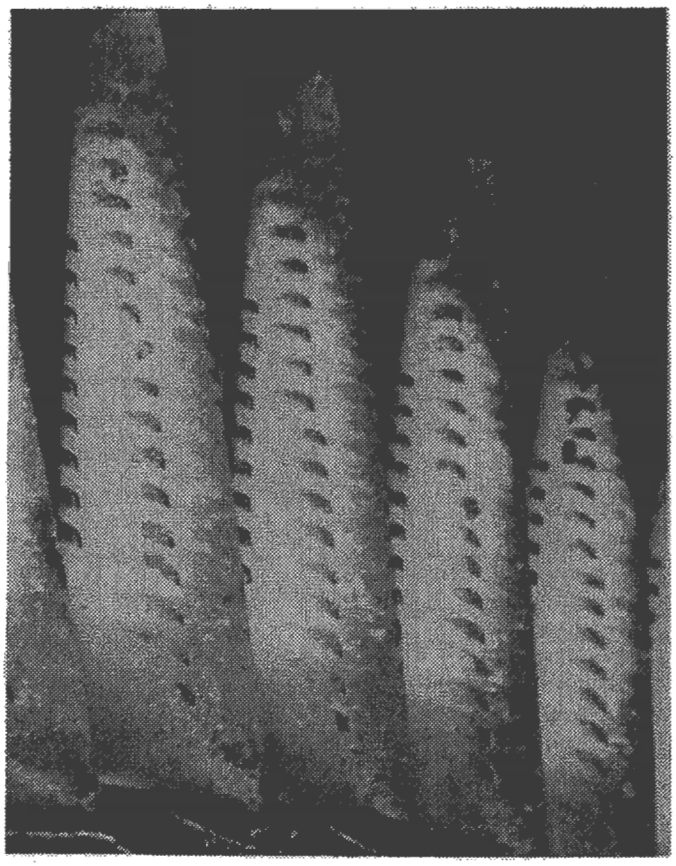

Figure 3. Leading edge cluster of first stage blades tested in PW4084 engine exhibiting excellent performance of EB-PVD TBC

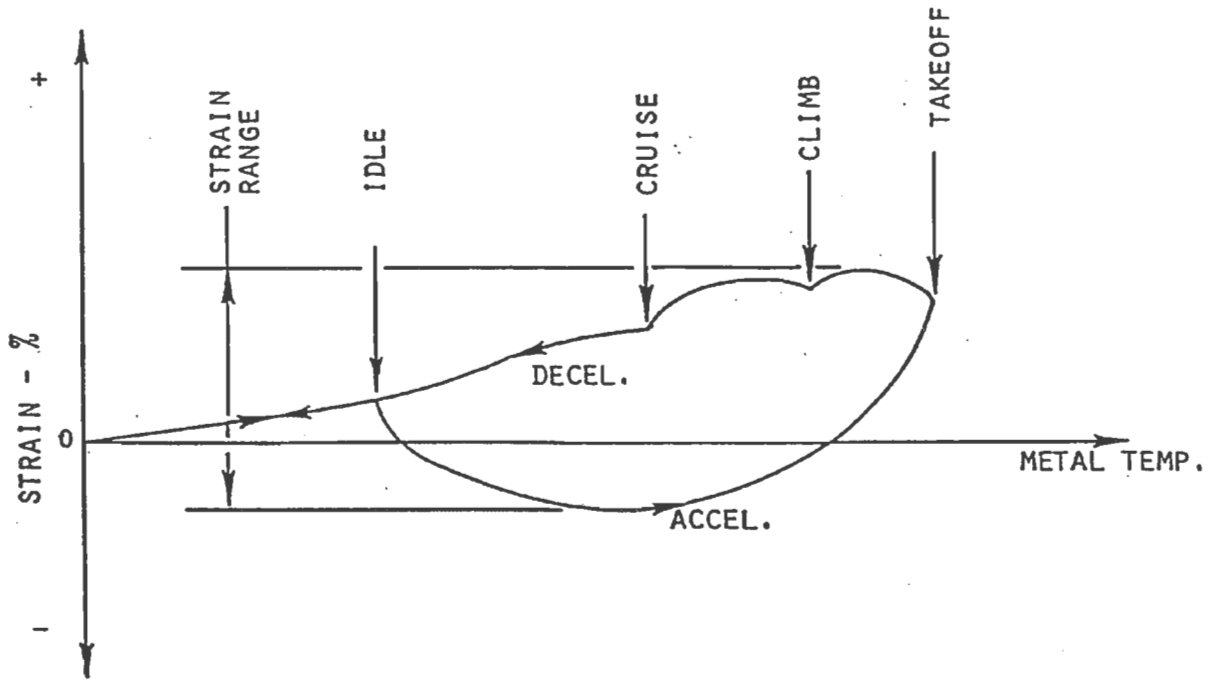

Figure 4. Generic "Peanut curve" for a turbine blade shows the transient nature of strain vs metal temperature cycle.

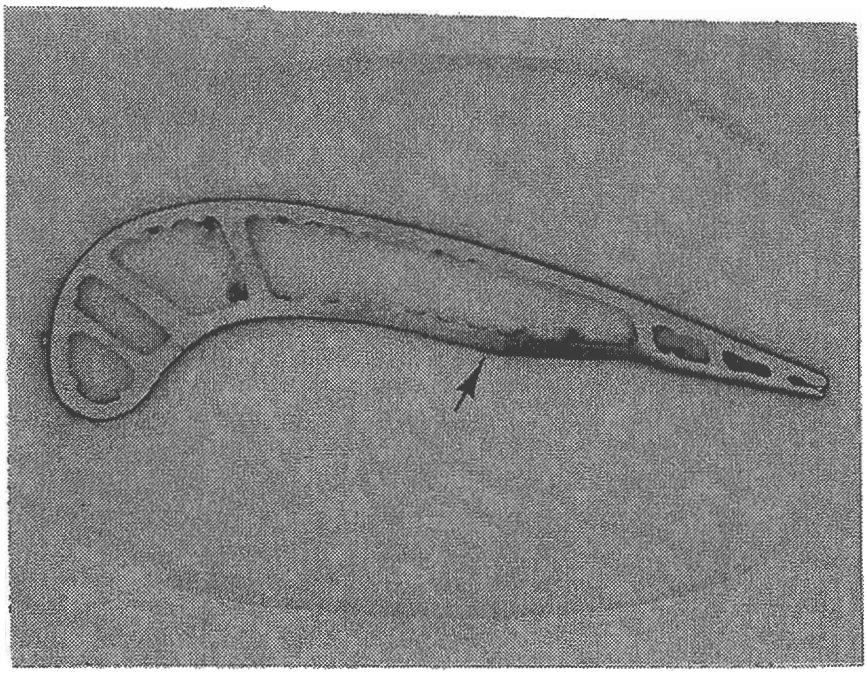

Figure 5. Creep distortion of airfoil due to nonuniform temperature distribution.

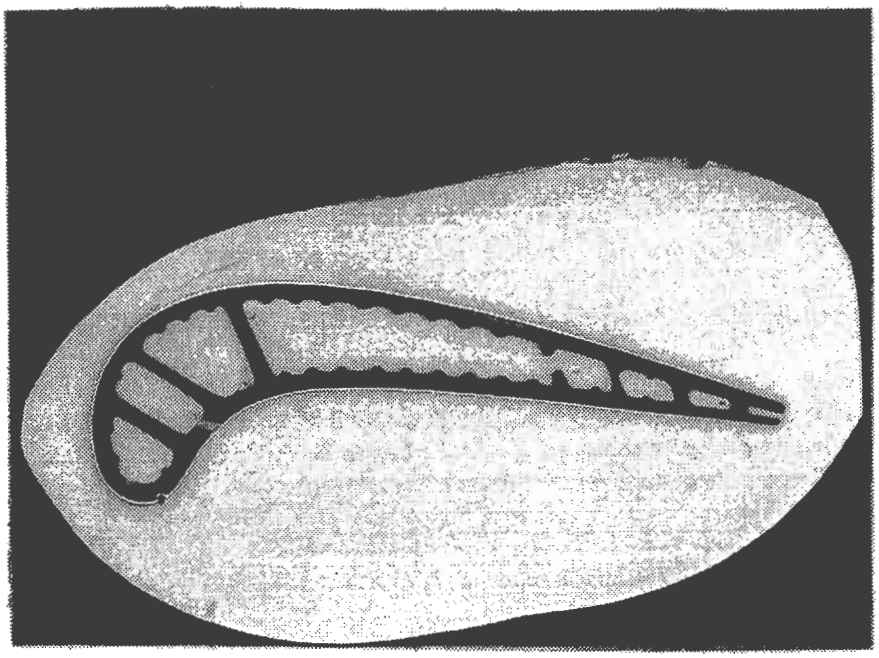

Figure 6. Creep distortion of airfoil eliminated due to the application of TBC.

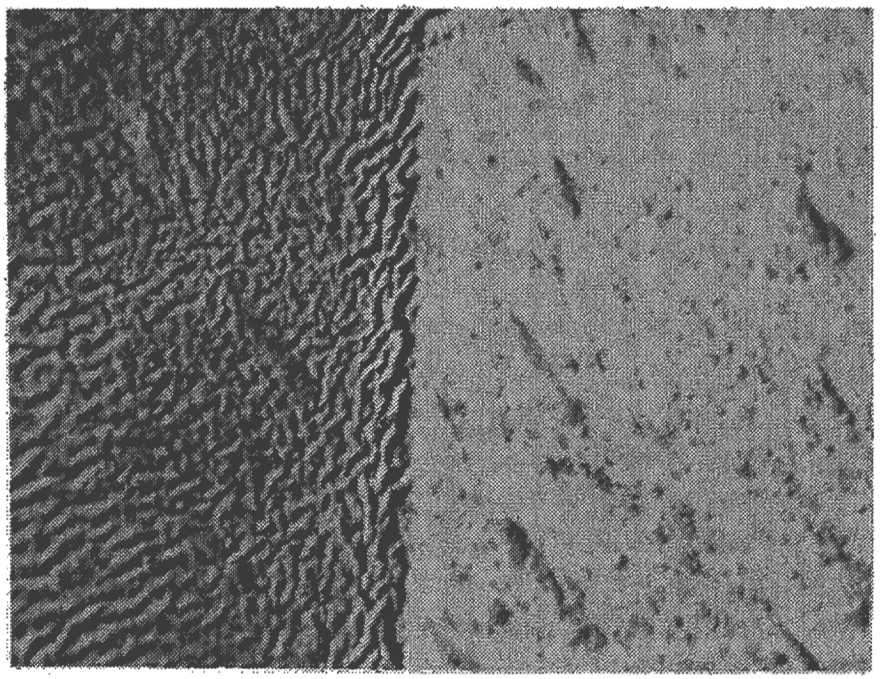

Figure 7. Bond coat creep eliminated by TBC application.

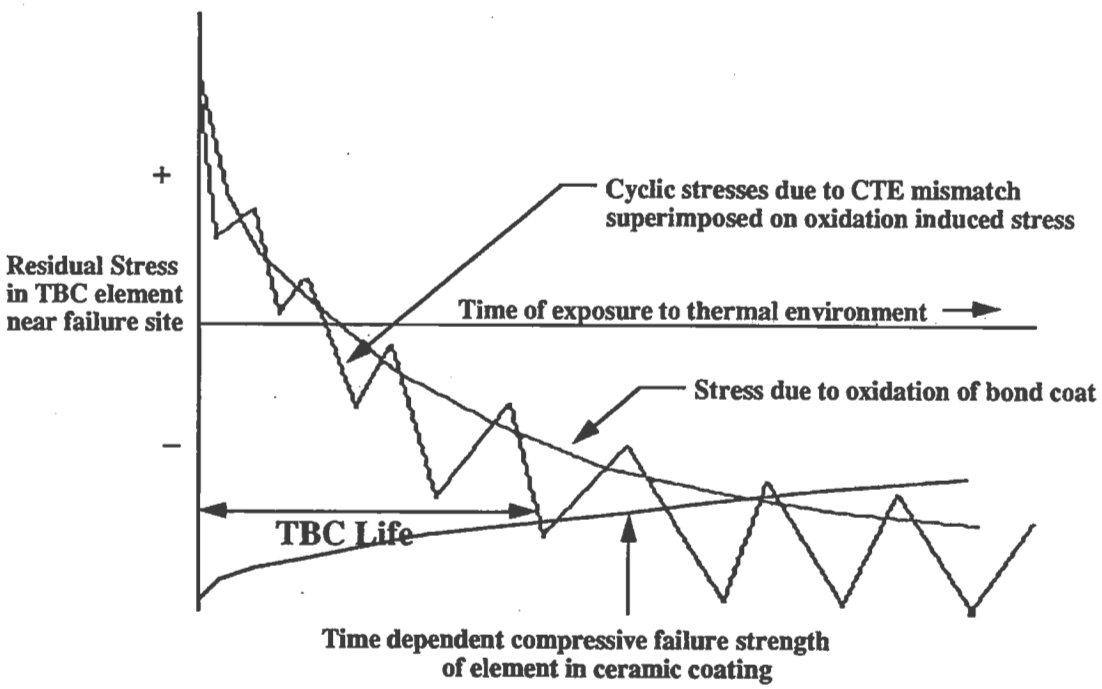

Figure 8. "Weak Link" model of TBC failure. In plane compressive residual stresses in the TBC increases with thermocyclic exposure time. Failure occurs when these stresses exceed compressive stress of elements at the failure location.

PVD TBC EXPERIENCE on GE AIRCRAFT ENGINES

Antonio Maricocchi, Andi Bartz, and David Wortman
GE Aircraft Engines
1 Neumann Way MD H-85
Cincinnati, Ohio 45215

ABSTRACT

The higher performance levels of modern gas turbine engines present significant challenges in the reliability of materials in the turbine. The increased engine temperatures required to achieve the higher performance levels reduce the strength of the materials used in the turbine sections of the engine. Various forms of Thermal Barrier Coatings (TBCs) have been used for many years to increase the reliability of gas turbine engine components. Recent experience with the Physical Vapor Deposition (PVD) process using ceramic material has demonstrated success in extending the service life of turbine blades and nozzles. Engine test results of turbine components with a 125 μm (0.005 in) PVD TBC have demonstrated component operating temperatures of 56-83 °C (100-150 °F) lower than non PVD TBC components.

Engine testing has also revealed the TBC is susceptible to high angle particle impact damage. Sand particles and other engine debris impact the TBC surface at the leading edge of airfoils and fracture the PVD columns. As the impacting continues, the TBC erodes away in local areas. Analysis of the eroded areas has shown a slight increase in temperature over a fully coated area, however a significant temperature reduction was realized over an airfoil without TBC.

INTRODUCTION

The drive for increased aircraft engine thrust and fuel efficiency has resulted in continual increases in hot section temperatures. Several generations of superalloys have been developed over the past 20 years to make these increases in turbine inlet temperature possible. However the limits of stress rupture, surface protection, and melting point make this increasingly difficult. In addition, the amount of air which can be used for cooling in high performance engines is limited. The use of thermal barrier coating (TBCs) has the potential of extending these advances in aircraft engine development by providing a layer of thermal insulation between the superalloy turbine airfoil and the hot gasses (Fig 1). With the turbine airfoil cooling technology available today, a 250 μm (0.010 in) thick TBC can reduce the average metal temperature by 111-167 °C (200-300 °F) (1). Designing with a TBC for its full thermal insulating benefit requires a very high degree of confidence since loss of the TBC could result in rapid component degradation. The payoff in increased engine thrust or fuel efficiency is significant and therefore much effort is currently being focused on improvements in the reliability of TBCs. Additional effort is being expended to further the understanding of the behavior of TBCs.

Thermal barrier coatings have been used extensively since the mid 70's for life extension of combustor and afterburner components. Plasma sprayed zirconia with 7% yttria (YSZ) for stabilization of the tetragonal phase was determined to be most successful for these applications. Zirconia's very low thermal conductivity, high melting point, inertness and relatively high coefficient of thermal expansion (CTE) make it ideal as a TBC. Although YSZ has one of the highest CTEs of any high temperature ceramic, it is still only about 70% that of the superalloy substrate. To help accommodate the large compressive stresses that result on

cool down from service temperatures, the YSZ must be sprayed to achieve a microstructure that will accommodate these strains. Both porous (2) and dense, vertically cracked (3) microstructures have been successful in accomplishing this strain tolerance. A plasma spray MCrAlY (where M equals any combination of Co, Ni, or Fe) bond coat is applied prior to the YSZ for adherence to the metal substrate.

The roughness of the plasma sprayed bond coat was found to be essential to the adherence of the plasma sprayed YSZ because it provided a mechanical bonding of the YSZ to the bond coat. Use of plasma spray TBCs was extended to high pressure turbine (HPT) nozzles in the late 80's through use of low pressure plasma sprayed bond coats which have greater oxidation resistance than atmospheric plasma sprayed bond coats (4).

PHYSICAL VAPOR DEPOSITED THERMAL BARRIER COATINGS

Physical vapor deposition (PVD) processes such as sputtering will produce highly columnar deposits under certain conditions of evaporation. The ability of sputtering to produce a strain tolerant microstructure with YSZ was observed by Bush *et al* (5). The higher deposition rates achievable by electron beam physical vapor deposition make this process economically feasible for deposition of highly strain tolerant TBCs. Figure 2 depicts the features of a PVD TBC. Bond coats are required for adherence and oxidation resistance of the substrate. As opposed to the plasma sprayed TBC, the PVD TBC relies on a chemical bond between a smooth bond coat, the alumina scale that forms on the bond coat, and the YSZ. The alumina scale between the bond coat and the TBC continues to grow during engine operation. Alumina forming bond coats are successfully used for PVD TBC bonding and controlling the growth of the alumina scale is a key feature in increasing the life of these systems. Control of the PVD processing parameters is also key to producing the strain tolerance necessary for reliability.

This paper will describe the successful testing of PVD TBC on high pressure turbine (HPT) nozzles and blades (gamma prime (γ') strengthened nickel based superalloys) where the TBC significantly extends the life of the components.

APPLICATION OF PVD TBCs TO AEROSPACE COMPONENTS

The PVD process was used to apply the TBC to several jet engine components to evaluate its effectiveness under operating conditions. High pressure turbine blades and nozzles were selected since these components reside in the hottest section of the engine and are most susceptible to base material degradation.

One of the advantages of the PVD TBC is the smooth surface finish that is generated on the surface of a component. The PVD TBC surface as deposited produces a 1.0 μm-1.5 μm Ra (40-60 μin Ra) finish. A surface finishing operation can also be performed on the PVD TBC to reduce the finish of the surface to the 0.5 μm-0.75 μm Ra (20-30 μin Ra). The finishing operation removes the tips of the columns to create the smooth surface.

Spallation is a major concern with components treated with the PVD TBC process. This is the loss of coating due to chipping or other operating environment factors. Spallation occurs when stresses are generated through the coefficient of thermal expansion mismatch between the YSZ ceramic and the metal substrate. Stresses are also generated through the coefficient of thermal expansion mismatch between the substrate and the aluminum oxide that grows at the bond coat surface. Through control of the PVD process parameters, the YSZ can be deposited with a columnar microstructures that accommodates the thermal expansion mismatch without

generating compressive stresses in the YSZ on cool down from deposition or operating temperatures. Measurement of residual stress in PVD YSZ show room temperature stresses that are less than 10 Ksi. Calculation of room temperature stresses assuming the deposition temperature as a stress free temperature predict compressive stresses greater than 100 Ksi. Control of the stresses in the thermally grown alumina is more difficult since a dense microstructure is both desired (to slow subsequent oxidation) and naturally formed. With thermally grown alumina, the assumption that the growth temperature is the stress free temperature is probably valid. Inward diffusion of oxygen anions may even produce compressive growth stresses at the thermal exposure temperature. Calculation of the room temperature stresses due to the coefficient of thermal expansion mismatch with the substrate predicts a 300-400 Ksi compressive stress.

The interfacial strength of the PVD TBC system is greater than 10 Ksi in the as-deposited condition as demonstrated by epoxy failures in bond strength tests. After thermal exposure, the bond strength drops below 6 Ksi with separation occurring at the alumina bond coat interface. It is believed that the two effects are occurring during thermal exposure; 1) the alumina scale becomes thicker and therefore the compressive force (proportional to the thickness of the alumina) increases and 2) the bond strength decreases due to any of several mechanisms (void formation under the alumina, sulfur migration to the scale metal interface, or thermal cycle induced cracking in the scale). The tensile bond test cannot differentiate between these two effects, however the result is clear; exposure to elevated temperature eventually leads to compressive loads that produce buckling at the interface between the alumina scale and the bond coat and subsequent spallation of the TBC (Figure 3).

ENGINE TURBINE BLADE TESTING OF PVD TBCs

The PVD TBC has been tested on the stage 1 High Pressure Turbine Blades (HPTB) of a high by-pass engine. The test was conducted for 1820 endurance engine cycles where one cycle simulates the take-off, climb, cruise and thrust reverse. The TBC was deposited over the entire airfoil surface to a thickness of 125 μm (0.005 in).

The test included both coated and uncoated blades to accurately evaluate the impact of the PVD TBC. Figure 4 contains post test photographs of one of the test blades without the PVD TBC. The blade contained an axial crack at the 55% span and a radial crack on the suction side from the 40% to the 80% span. The blade has failed due to rupture of the base material.

Figure 5 contains photographs of a TBC coated blade after the engine test and shows no spallation on the concave airfoil and no spallation on the convex airfoil after the leading edge region. However, there is some TBC spallation at the leading edge and on the suction side leading edge. Both of these spalls are attributed to impact damage or erosion damage from debris coming through the turbine. This blade did not have any cracks and can be reserviced using a strip and recoat procedure.

Closer examination of the blades was performed to determine how the PVD TBC responded when impacted by debris. The microstructure of the TBC near the spalled regions are shown in Figure 6. The engine debris impacted the ceramic at the surface, cracking the columns. The cracks propagated to the interface and eventually spalled the ceramic.

The percent volume of γ' precipitant in the alloy was measured through microstructure analysis. This measurement was then compared to the solubility curve (percent precipitate versus temperature) of the alloy to estimate the highest operating temperature at that specific location of the blade. This is an acceptable approach to estimate the operating temperature of

the blades when direct measurement was not performed. These examinations were taken at the mid-wall between the blade surface and the internal cavity of the blade. The γ percent volume of blades with and without the TBC were compared to the alloy solubility curve. The results indicate that the blade with the TBC ran at a temperature 56-83 °C (100-150 °F) lower than the blade without the TBC.

For the next engine test, blades were prepared with the TBC intentionally missing from certain areas of the blade. The TBC was applied to the entire airfoil then locally grit blasted to remove the TBC. (Figure 7). The 3 locations of the blade with missing TBC are: 1) the nose of the blade between the 50%-80% span designated as location A, 2) the suction side leading edge between the 50%-80% span (location B) and 3) the pressure side at the midchord between the 50%-80% span (location C). The blades were tested for 2000 engine endurance cycles along with blades that contained a full TBC and blades without a TBC.

Figure 8 contains photographs of the blades after engine test. The intentionally grit blasted areas did not grow in size after the 2000 engine cycles and no distress was observed. The blades were then metallographically examined to determine the maximum metal operating temperatures through γ' analysis. In location A, along the leading edge nose, no temperature reduction was observed between the blade with the intentionally spalled TBC and the blade that did not have TBC. In location B, the temperature reduction on the intentionally spalled TBC blade was minimal and in location C, the temperature reduction was estimated to be 75 °F at the mid-wall location for the intentionally spalled TBC. At the surface of locations B and C, the temperature reduction is estimated to be 100 °F for the spalled TBC blade when compared to the blade without TBC.

ENGINE NOZZLE TESTING OF PVD TBCs

Tests of the PVD TBC were also performed on the High Pressure Turbine Nozzle (HPTN) of a high bypass engine. The test was conducted for 750 endurance engine cycles where one cycle again simulates takeoff, climb, cruise, and thrust reverse. The engine was operated at or above standard "red line" conditions resulting in an engine test which exceeded normal operating parameters. The TBC was deposited on the airfoil surface to a thickness of 125 μm (0.005 in).

The TBC was only applied to the suction side of the nozzle as shown in Figure 9. The PVD TBC has an application advantage in that it provides a smooth transition from the non-coated region to the coated region. This eliminated aerodynamic effects with turbulence which would be caused if the process created a step between the TBC and non-TBC regions. The turbulence created when the boundary layer air is forced to cross a step in the coating will reduce the cooling effectiveness of the air which then increases the temperature of the material.

Figure 10 shows the TBC HPT nozzle following the engine test. The TBC remained intact with no spallation. The minor chipping at the trailing edge was caused by assembly. Figure 11 is a photograph of an HPT Nozzle that did not have a TBC. The extreme conditions of the test resulted in massive thermal fatigue cracks on the suction side of the nozzle that extended through the wall of the base alloy. There were no thermal fatigue cracks extending through the walls of the nozzle with the TBC but there was some cracking in the environmental bond coating.

SUMMARY

The engine tests of the PVD TBC resulted in a 38-66 °C (100-150 °F) temperature reduction on the Stage 1 HPTB and the HPTN. The tests also indicated that the TBC is susceptible to leading edge damage due to impact from particles running through the engine or various other engine debris. The PVD TBC has been introduced for Stage 1 high pressure turbine blades. Additionally, over 10,000 cycles of engine testing has been accumulated on nozzles with the TBC. The TBC of nozzles was introduced in the early '90s.

1) S.M. Meier, and D.K. Gupta, "The evolution of thermal barrier Coatings in Gas Turbine Engine Application," ASME Conf. Publication, 92-GT-203.

2) J.T. DeMasi, K.D. Scheffler and S. Bose, "Mechanisms of Degradation and Failure in a Plasma-Deposited Thermal Barrier Coating," *Journal of Engineering for Gas Turbies and Power*, Vol. 112, October 1990, pgs. 521-526

3) G. Johner, and K.K. Schweitzer, "Flame rig testing of thermal barrier coatings and correlation with engine results," *Journal Vacuum Science Technology,* Nov/Dec 1985, pps, 2516-2524.

4) D.J. Wortman, B.A. Nagaraj, and E.C. Duderstadt, "Thermal Barrier Coatings for Gas Turbine Use," *Materials Science and Engineering,*, A121 (1989) 433-440

5) R. Bush, J. Patten, and J. Fairbanks, High Rate Sputter Depositions of Protective Coatings on Marine Gas Turbine Hot-Section Superalloys," Proceedings, 1974 Gas Turbine Materials in the Marine Environment Conference, Castine, Maine, Metals and Ceramics Information Centers, MCIC 75-27, July 1974.

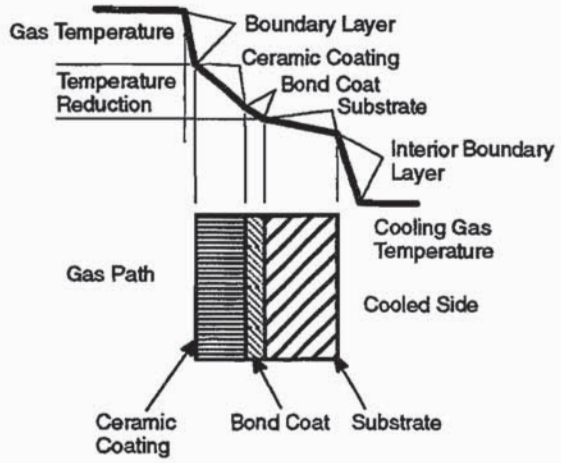

Figure 1. Schematic of a Thermal Barrier Coating.

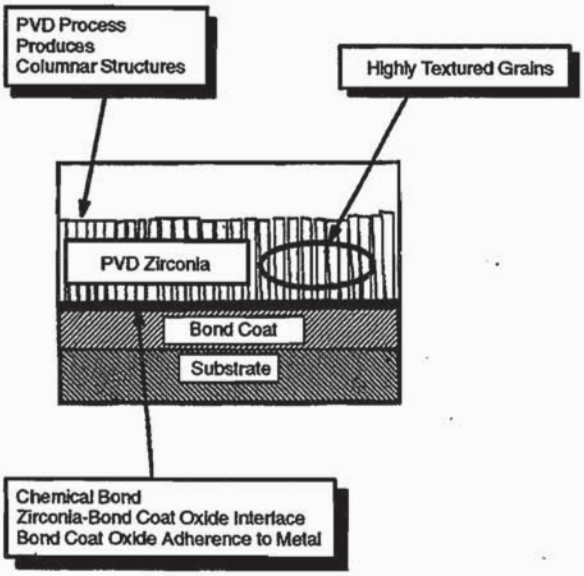

Figure 2. Typical Physical Vapor Deposited Thermal Barrier Coating.

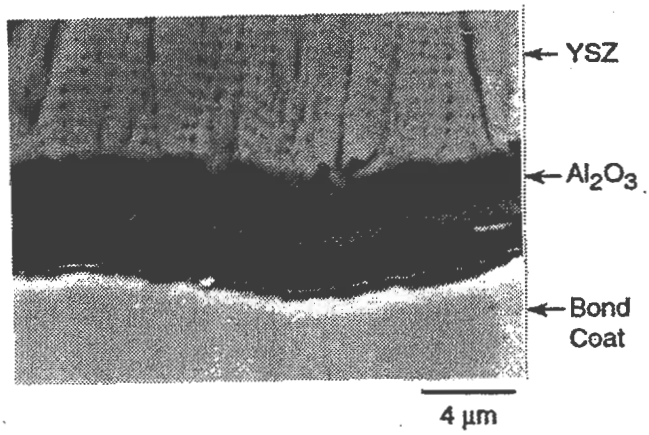

Figure 3. Micrograph Showing Separation Between Al_2O_3 Scale and Bond Coat.

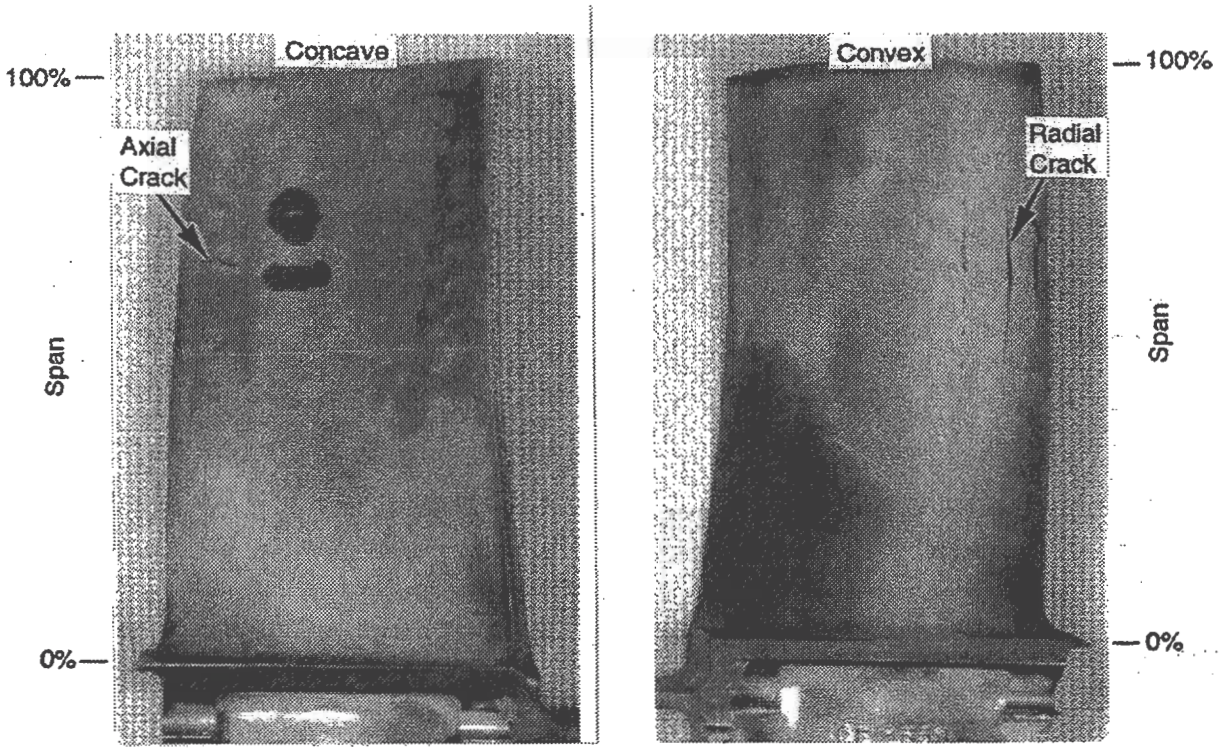

Figure 4. A Stage 1 HPTB Without TBC Showing Axial and Radial Cracking of Material After 1820 Cycles.

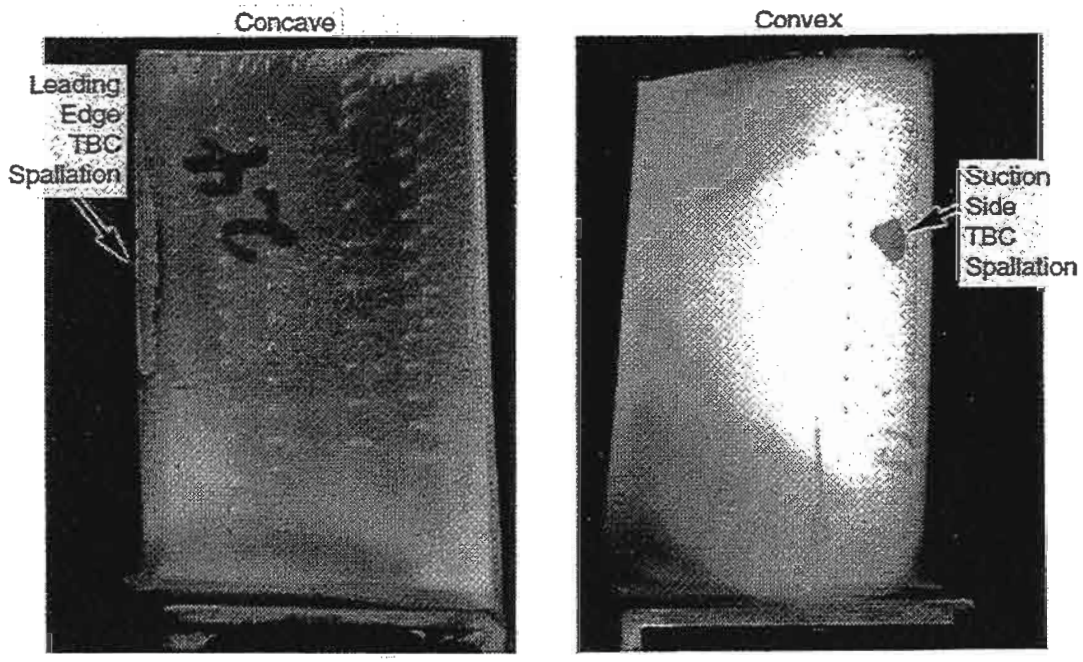

Figure 5. Photograph of a Stage 1 HPTB With TBC Showing Leading Edge and Suction Side TBC Spallation After 1820 Cycles.

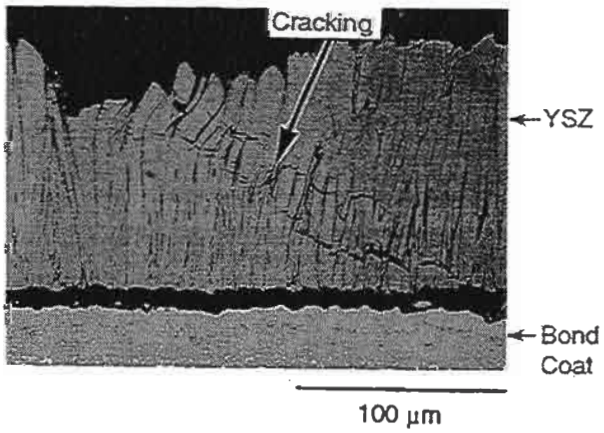

Figure 6. Micrograph of the TBC Cracking Due to Particle Impact Damage.

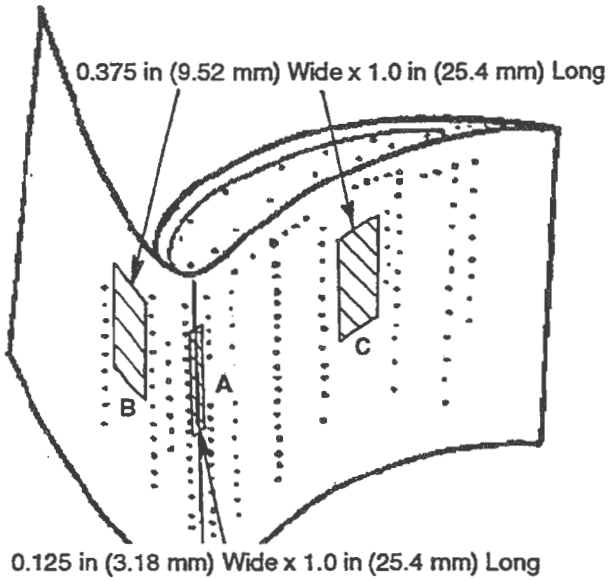

Figure 7. Schematic of Blade Airfoil Showing Location of Intentionally Missing TBC.

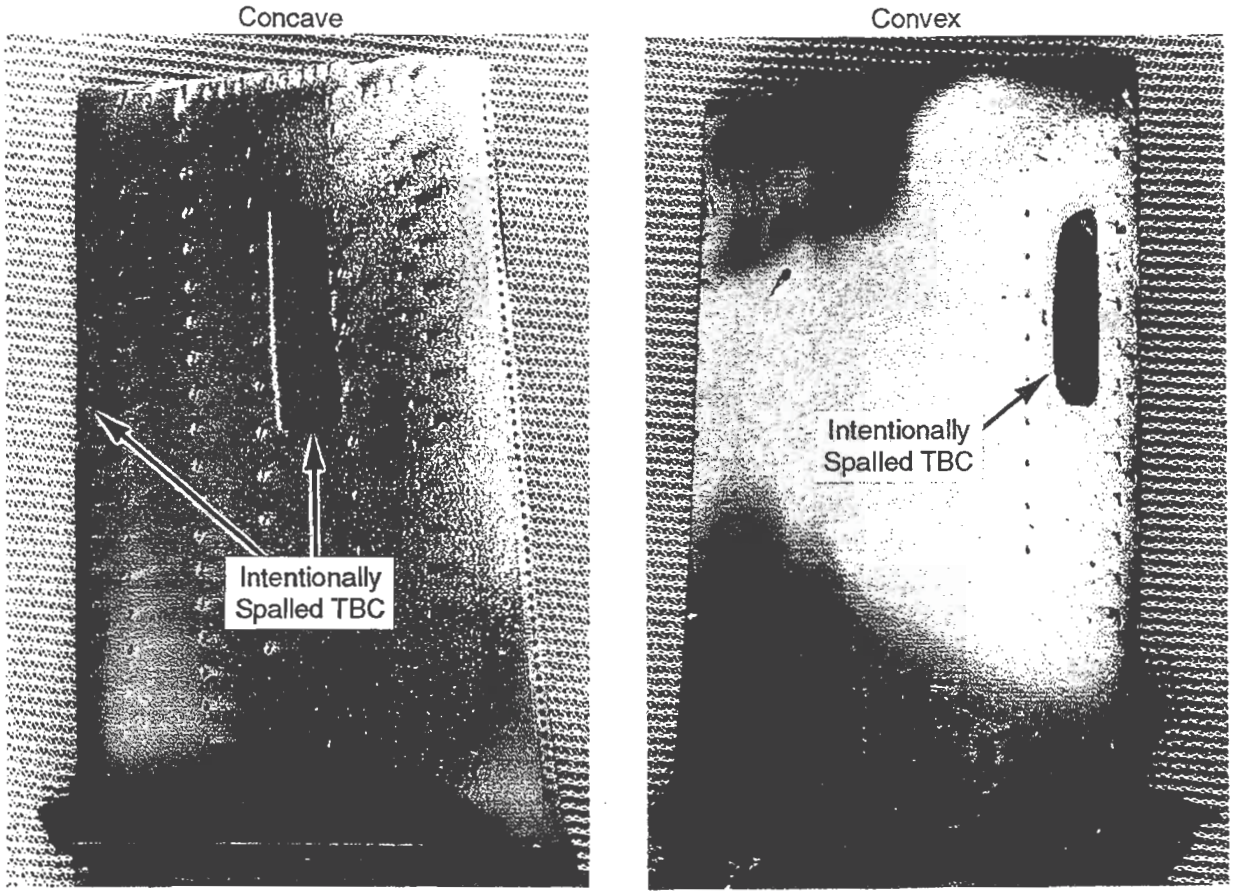

Figure 8. A Stage 1 HPTB Showing the Areas of Intentionally Spalled TBC After 2000 Cycles.

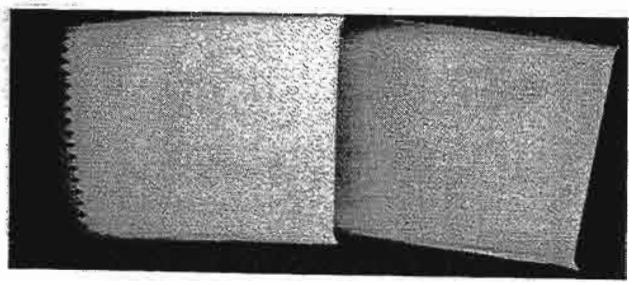

Figure 9. High Pressure Turbine Nozzles With a PVD TBC Prior to Engine Testing.

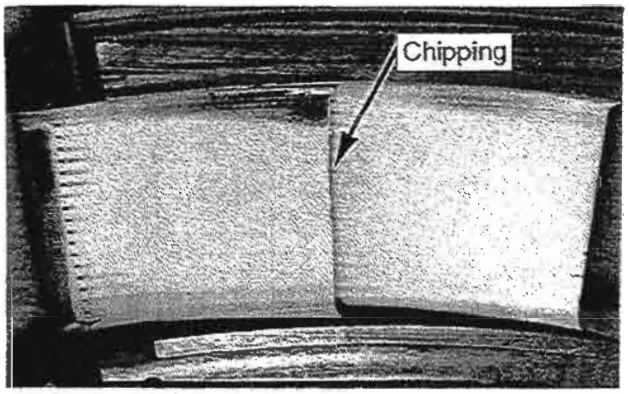

Figure 10. High Pressure Turbine Nozzle With a PVD TBC After 750 Cycles of Engine Testing.

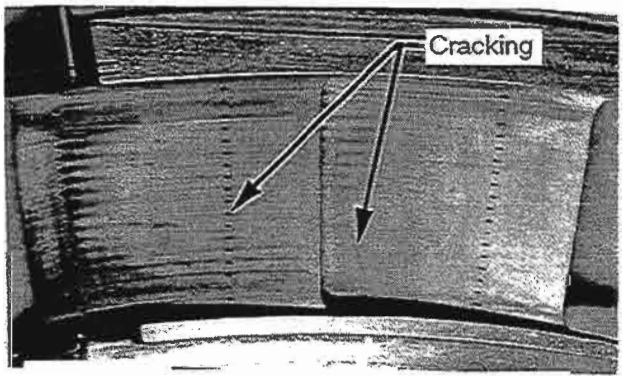

Figure 11. High Pressure Turbine Nozzle Without TBC After 750 Cycles of Testing Showing Thermal Fatigue Cracking in the Airfoil Material.

TBC EXPERIENCE IN LAND BASED GAS TURBINES

Warren A. Nelson, Robert M. Orenstein
GE Power Generation Engineering
Materials and Processes Engineering
Schenectady, NY 12345

ABSTRACT

This paper summarizes prior and on-going machine evaluations of TBC coatings for power generation applications. Rainbow testing of TBCs on turbine nozzles, shrouds, and buckets are described along with a test on combustor liners. GEPG has conducted over 15 machine tests with TBC coated turbine nozzles of various coatings. TBC performance has been quite good and additional testing, including TBCs on shrouds and buckets, is continuing. Included is a brief comparison of TBC requirements for power generation and aircraft turbines.

INTRODUCTION

Yttria-stabilized zirconia (YSZ) ceramic thermal barrier coatings (TBCs) on superalloy components are being used successfully in heavy duty gas turbines and aircraft engines. At GE Power Generation, TBCs applied by air plasma spray (APS) are used in the combustor and turbine sections, at ceramic thicknesses up to 0.51 mm (0.02 inch). GE Power Generation production experience is summarized in Table 1.

A thermal barrier coating (TBC) is typically comprised of 2 layers: 1) ceramic oxide top coat and 2) metallic bond coat. The low thermal conductivity ceramic top coat provides thermal insulation while the bond coat provides a suitable interlayer to improve adherence of the ceramic top coat and to provide environmental protection to the underlying superalloy substrate. GE state-of-the-art TBC systems use top coats of 6-8 wt. % yttria-stabilized zirconias (YSZs) while the bond coats are based on Ni(Co)-Cr-Al-Y alloys. Bond coat material development has been successful in improving the high temperature oxidation resistance and thermal cycle lives of plasma-sprayed TBCs.

In general, the aircraft engine industry has led turbine technology improvements and these improvements were later adapted in power generation machines; this is also true in area of TBCs. The experience base of TBC usage in aircraft turbine applications is greater than in power generation equipment. While operating conditions in aircraft turbines, especially peak temperature and number of cycles, are typically more severe than in power generation equipment, the time requirements are much longer in power generation equipment. Table 2 highlights some of the differences between aircraft and power generation requirements for TBC. The aircraft engine duty cycle is highly cyclic with only a small percentage of its time at maximum temperature conditions, i.e., during takeoff and climb. Conversely, power generation equipment sees different duty cycles, varying from one cycle per day for peaking power applications to one cycle per year

for baseload machines. Coating life, i.e., time to refurbishment for aircraft turbines is in the order of 8,000 hours, of which only 5-15% is at maximum conditions. In contrast life in a power generation component should be 24,000 hours with a majority of all service time at maximum conditions.

The following time and temperature effects should be considered for power generation use of TBCs: 1) bond coat oxidation, 2) interdiffusion of bond coat and substrate, 3) coating densification and 4) changes in thermal or mechanical properties of the coating. Accessibility for inspection, repair and refurbishment is also more difficult in power generation machines than in aircraft engines.

Another significant difference between aircraft and power generation equipment is the component size as shown in Figure 1. This impacts coating fabrication capabilities. Plasma spray processing has a significant advantage in being able to accommodate the large size components found in today's large power generation machines. The large nozzles of power generation machines, especially those with multiple airfoil configuration, could not be accommodated in today's EB-PVD coaters. Plasma spray processing with turbine parts on turntables and robot gun manipulation can more readily accommodate large parts. Each component application of a TBC requires careful review and study to determine whether APS or EB-PVD is most appropriate since there is no clear overall advantage of one versus the other.

The following sections highlight some of the experience of TBC usage in GEPG. In particular, observations from numerous field trials are discussed.

MACHINE EXPERIENCE

GEPG frequently uses "Rainbow" field tests to assess the capabilities of new materials in actual operating machines. Rainbow refers to the simultaneous test of a variety of materials or coatings in customers' machines; the nickname "Rainbow"comes from differences in the physical appearance of different coatings or materials. Virtually all production gas path materials have seen initial evaluation in Rainbow tests as a prerequisite to actual production introduction. Rainbow test times generally range between 10,000 to 24,000 hours. The main purposes of Rainbow test programs are to 1) assess the capabilities of new materials in field conditions. 2) restrict any risk with new materials to a few machines rather than to the entire fleet, and 3) provide evidence to customers that a new technology has been proven in the field. Rainbow tests bridge the gap between laboratory tests and production. GEPG has conducted over 80 rainbow tests since the mid-50s on numerous alloys and coatings; TBCs have seen testing in several of the more recent tests since 1987.

The earlier TBC rainbows evaluated various top coat and bond coat compositions as well as differing methods of bond coat application. First stage turbine nozzles of MS6000 or MS7000 machines were coated and tested. The nozzles were doublets, i.e., comprised of two airfoil sections, which precluded the ability to fully coat the vanes. Typically only selected portions of the nozzle outer band and airfoil were coated. Over 15 different rainbow tests were conducted

with test durations between 6,000 and 45,000 hours. Table 3 lists some of the variables investigated.

The interest in TBCs has expanded recently and additional rainbows have been initiated with TBCs on combustor liners, turbine shrouds and buckets on today's higher firing temperature machines. Three recent Rainbow tests are of particular interest:

1) Combustor Liners: A machine set of 10 combustor liners, 2 with each of the 5 coating systems detailed in Table 4, was installed in an MS7001EA gas turbine fired by natural gas. The entire inner surface of each liner was coated with TBC. The coating variations yielded microstructures ranging from random porosity, as shown in Figure 2 to denser, more oriented microstructure such as that shown in Figure 3.

2) Turbine Shrouds: Fifteen S1 inner shrouds with four APS TBCs were installed in a MS7001FA gas turbine in October, 1993. Full shroud cooling is used for this test, which will run for approximately 24,000 hours. The shrouds were coated by two different sources. Coating variables include: 1) the bond coat composition: NiCrAlY and CoNiCrAlY, 2) bond coat fabrication method: air plasma spray and shrouded arc plasma spray; and 3) top coat density and microstructure. Bond coats were 8-12 mils thick while the ceramic topcoats were sprayed to 1.4 mm (55 mils) and ground back to approximately 1 mm (40 mils). A photograph of the shrouds prior to installation is shown in Figure 4.

3) Turbine Buckets: Seven S1 buckets with APS and EB-PVD TBCs were installed in an MS9001E gas turbine in 1993. These buckets will provide a side-to-side comparison of APS and EB-PVD coatings (Figure 5). The buckets were installed in a peaking machine that will operate less than 2000 hours per year but will be cycled frequently. The machine will be operated for two to three years prior to removal of the test buckets.

Rainbow testing of prototype components in commercial machines involves several shortcomings as compared to factory testing. Rainbow hardware must often be procured with very limited lead time in order to meet machine outage schedules. This may preclude complete development of the coating process and performing a suitable number of coating trials for TBC optimization on specific hardware. Production implementation may then require additional development and process refinement. A second shortcoming of rainbow testing is that the components may be refurbished and put back into service following the test and thus are not always available for detailed post test evaluations.

RESULTS

Nozzle Rainbows: The nozzle rainbows initiated in the late 80's are now coming off test. Most of the conclusions are based upon visual observations rather than metallurgical cutup and analysis although, loss of the ceramic top coat is easy to see. An MS7000E nozzle after 16,700 hours operation is shown in Figure 1. The results show that APS TBCs can survive in power generation machines for long periods of time. Nozzle degradation at the outer band due to oxidation and, or erosion was reduced by the presence of the TBC. A key result that 6-8YSZ top

coat outperformed other compositions, and is consistent with the results of laboratory tests and aircraft experience. These early tests also showed that APS NiCrAlY is an adequate bond coat; HVOF NiCrAlY was a close runner-up with CoNiCrAlY slightly poorer. It was observed that coating source was a factor in performance; similar coatings from different sources performed differently. This reinforces the need to ensure adequate development and understanding of the coating processes. Occasional loss of coatings have been observed in operating machines due to abnormal operating conditions, foreign object damage (FOD), and buildup of deposits. TBC loss was more prevalent at the outer side wall and at nozzle leading edges. TBC loss may also have resulted from accumulation of dust and dirt on nozzle surfaces. NASA and others have recently reported TBC degradation due to environmental contamination from airborne dust. The overall result of these early nozzle rainbows is quite encouraging and gives confidence for expanding TBC usage.

Combustor Liners: The 5 coatings described in Table 4 ran for over 6000 hours at a customer site and have provided insight into coating thickness and microstructure effects. This machine utilized water injection that is used by some utilities for NOx abatement, oxides of nitrogen, and power augmentation. On the test machine, water was introduced from 8 nozzles upstream of the fuel nozzle swirl tip, which does not completely atomize and vaporize the water at high flow rates. As a result, high velocity water droplets impinged directly upon the TBC under some operating conditions.

TBC spallation occurred in 9 of the 10 liners, with significant differences in the size and morphology of the spalled regions. In all cases, spallation resulted from the impingement of water onto the TBC. The differences in spallation were attributed to TBC microstructure and thickness. The results are summarized as follows: 1) thinner coatings, 0.3 and 0.5 mm. (12 and 20 mils) thickness, all showed approximately 77 sq. cm. (12 sq. in) of coating loss 2) thicker coatings, 0.75 and 1.1 mm. (30 and 45 mils), had considerably less spalling, approximately 6 sq. cm. (1 sq. in.). Porous coatings tended to fail adjacent to the bond coat / top coat interface while the denser coatings failed higher within the ceramic layer. The thicker coatings had less porosity and a more oriented microstructure which is stronger, as evidenced by higher through thickness tensile strengths, and more strain tolerant due to low in-plane modulus.

Turbine Shrouds: An initial borescope inspection of the shrouds was performed after ~4600 hours. All coatings appear to be performing very well. Four of the 15 test shrouds showed minor spallation at the shroud edges. Evidence of FOD was noted on some of the adjacent metal shrouds. No rubbing, i.e. contact with bucket tips, was observed for these parts. Additional inspections are expected twice per year.

Turbine Buckets: An inspection of this rainbow test was performed at ~1000 hours. The EB-PVD coatings tended to show erosive loss at the platform aft of the trailing edge. The EB-PVD microstructure is poorer on the platform due to its orientation during processing and hence more likely to erode. The APS coatings showed minor spalls at the platform edges possibly due to handling or part-to-part contact. One APS bucket was removed from the machine due to distress of the TBC on the airfoil. Analysis is in progress to understand this result.

SUMMARY

The earlier rainbow tests which evaluated various top coat compositions resulted in confirmation of the superiority of YSZ and especially 6-8YSZ composition. On-going tests are more focused on TBC process and property variations. The prevalent failure modes seen thusfar in the various rainbow tests are spalling, erosion, FOD, and buildup of deposits. Additional post test analysis is required to investigate bond coat oxidation and other time/temperature dependent changes to the system. Water injection, at very high levels, has been detrimental to TBC coatings in combustor applications.

Despite the experience gained from operating ceramic-coated components in current generation gas turbines, much more remains to be learned about TBC behavior in the gas turbine hot section. The full advantage of TBCs can be achieved only when the reliability of the coating approaches that of the superalloy component substrate. Rainbow test programs will serve to improve confidence in TBCs, but these tests must be supported by an improved understanding of TBC thermomechanical behavior and process variability. Ultimately the linkage of process / properties and/ performance relationships to component design rules and guidelines must be achieved.

ACKNOWLEDGMENTS

The efforts of Allan Foster to initiate and track the early nozzle rainbows were instrumental to this activity. Eric Brambani was key to the execution of the combustor rainbow test.

Table 1. GEPG Machines employing TBCs for component life extension.

Machine	Component	Introduction Date
Frame 6B	Combustor	After market only
Frame 7E	Combustor	1982
Frame 7F	Combustor	1990
Frame 7FA	Nozzle	1992
Frame 9E	Combustor	1986
Frame 9F	Combustor	1992

Table 2. Comparison of nominal TBC requirements for aircraft and power generation turbine applications

Requirement	Commercial Aircraft	Power Generation
# Cycles	8000	2400
Total hours	8000	24,000
Hours at peak conditions	300	24,000
Peak surface temperature	>2200 F (1204 C)	<2200 F (1204 C)
Peak bond coat temperature	2000 F (1093 C)	1750 F (954 C)
Relative size	1X	5X

Table 3. TBC coating variables investigated in early nozzle rainbow tests.

Bond Coat	Top Coat
APS CoCrAlY	
APS NiCrAlY	20 YSZ
HVOF NiCrAlY	8YSZ
APS CoNiCrAlY	8YSZ (less porosity)
HVOF CoNiCrAlY	CeSZ
HVOF CoNiCrAlY (higher Al content)	thickness: .1 , .3 and .5 mm. (5, 12, 20 mils)

Table 4. TBC coating variables in combustor liner rainbow test

Liner #	Coating Vendor	Bond coat	Bond coat thickness mm. (mils)	Top coat thickness mm. (mils)
1	A	NiCrAlY	0.1 (4)	0.33 (13)
2	A	NiCrAlY	0.3 (12)	0.48 (19)
3	B	CoNiCrAlY	0.25 (10)	0.5 (20)
4	B	CoNiCrAlY	0.25 (10)	0.75 (30)
5	B	CoNiCrAlY	0.25 (10)	1.08 (43)
6	A	NiCrAlY	0.1 (4)	0.33 (13)
7	A	NiCrAlY	0.25 (10)	0.6 (24)
8	B	CoNiCrAlY	0.28 (11)	0.5 (20)
9	B	CoNiCrAlY	0.25 (10)	0.78 (31)
10	B	CoNiCrAlY	0.23 (9)	1.13 (45)

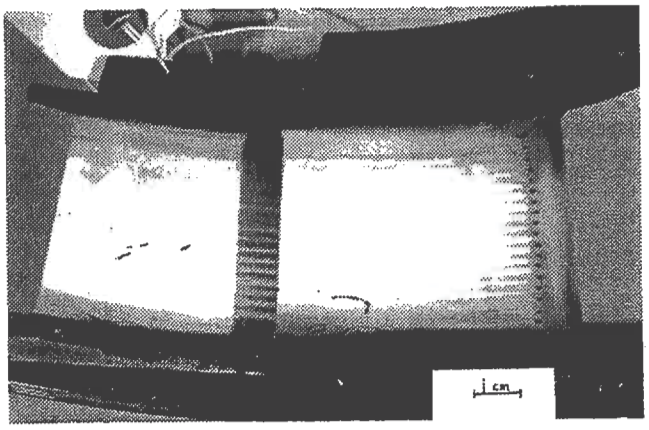

a) aircraft (CFM56) nozzle after 1000 cycles of factory engine test

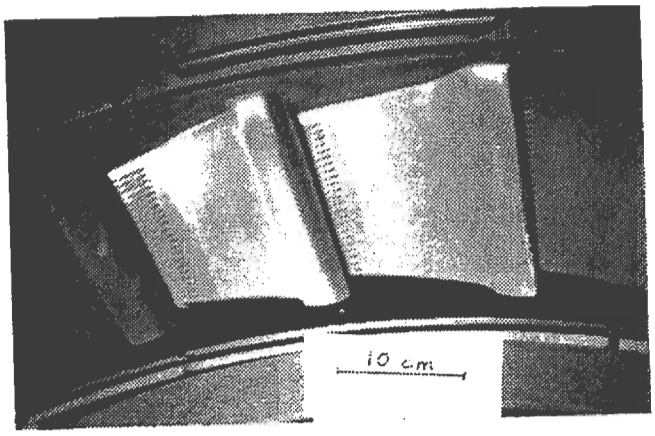

b) MS7000 after almost 17,000 hours of machine operation.

Figure 1. Photographs of TBC coated aircraft and power generation turbine nozzles comparing relative sizes.

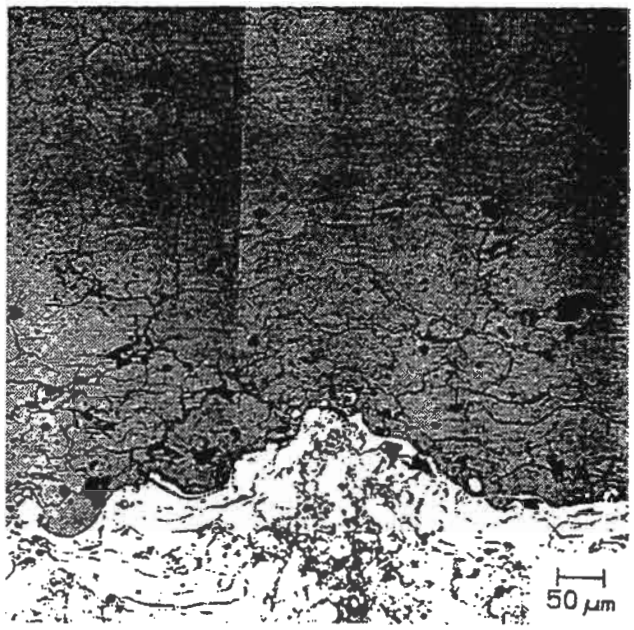

Figure 2. Photomicrograph of typical TBC coating microstructure showing random porosity and microcracking.

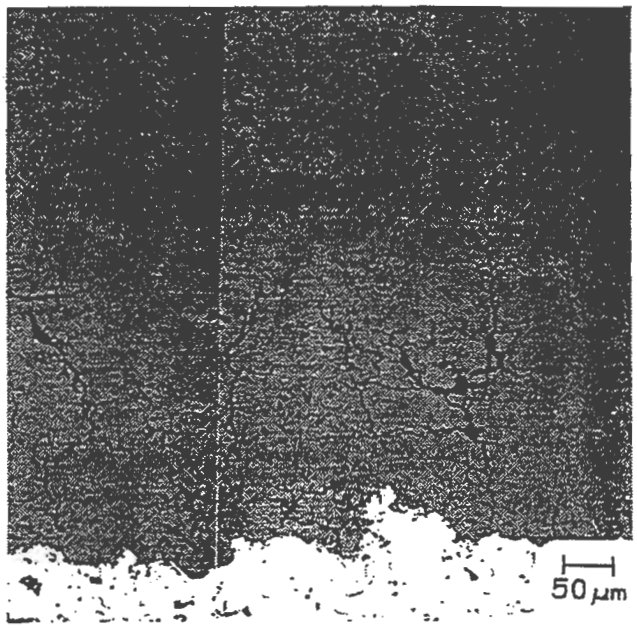

Figure 3. Photograph of TBC microstructure showing reduced porosity and oriented microcracks.

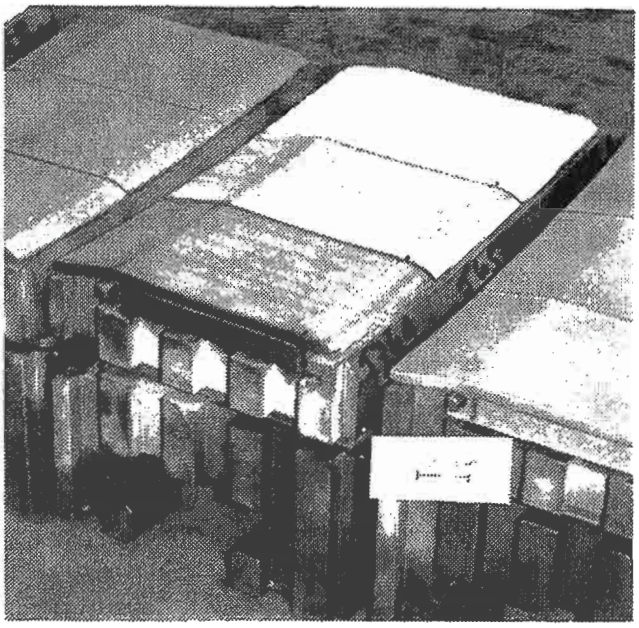

Figure 4. Photograph of TBC coated MS7001FA shrouds in outer shroud hanger prior to installation into machine.

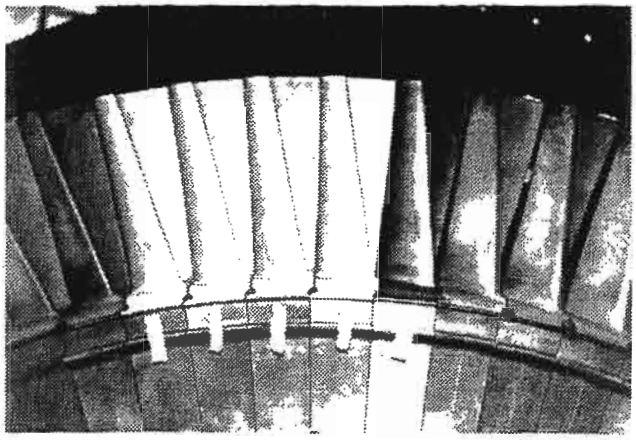

a) APS TBC

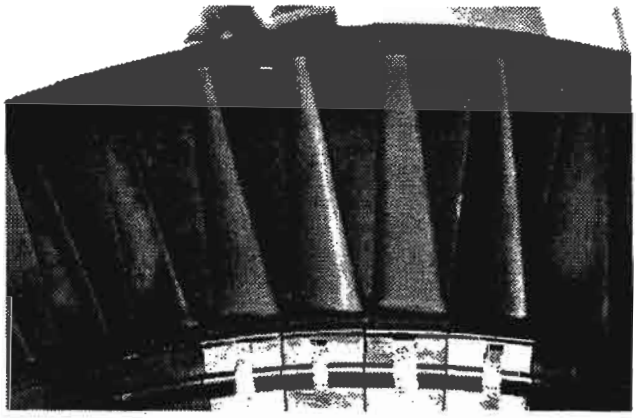

b) EB-PVD TBC

Figure 5. Photographs of APS and EB-PVD TBC coated MS90001E buckets installed in rotor prior to installation into machine.

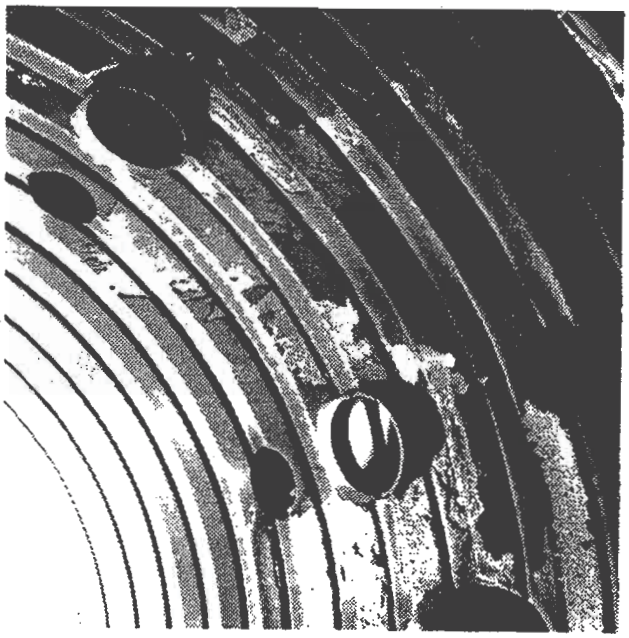

a) 0.5 mm. (20 mil) thick porous coating

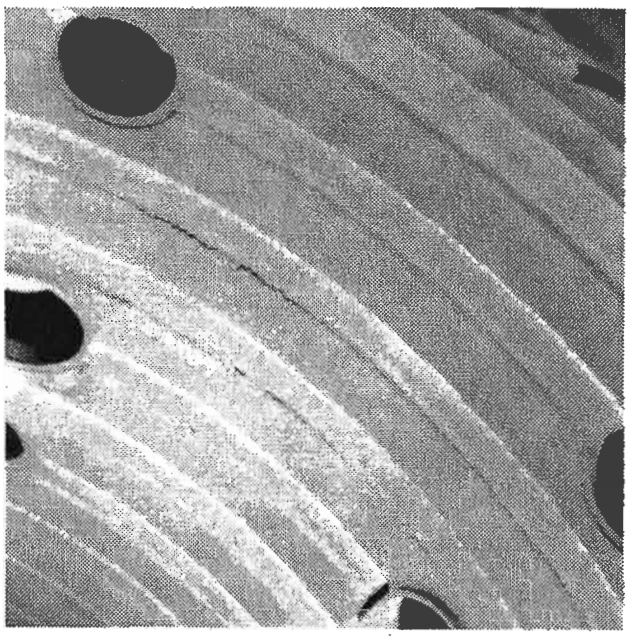

b) 1.1 mm. (45 mil) thick dense coating.

Figure 6. Photographs of TBC coated combustion liners after over 6000 hours in MS7001E machine.

PERSPECTIVE ON THERMAL BARRIER COATINGS FOR INDUSTRIAL GAS TURBINE APPLICATIONS

Zaher Mutasim and William Brentnall
Solar Turbines Incorporated
San Diego, California

ABSTRACT

Thermal barrier coatings (TBC's) have been used in high thrust aircraft engines for many years, and have proved to be very effective in providing thermal protection and increasing engine efficiencies. TBC life requirements for aircraft engines are typically less than those required for industrial gas turbines. This paper describes current and future applications of TBC's in industrial gas turbine engines. Early testing and applications of TBC's is reviewed. Areas of concern from the engine designer's and materials engineer's perspective are identified and evaluated. This paper focuses on the key factors that are expected to influence utilization of TBC's in advanced industrial gas turbine engines. It is anticipated that reliable, durable and highly effective coating systems will be produced that will ultimately improve engine efficiency and performance.

BACKGROUND

Thermal barrier coatings (TBC's) have been used for many years on gas turbine components. TBC's provide thermal resistance to the external surfaces of turbine components and reduce metal surface temperatures. TBC's have been extensively used for high thrust aircraft engines, where the expected coating life is in the order of few hundred hours. For industrial gas turbines (IGT's), where the time between overhaul (TBO) is approximately 10 fold those of aircraft engines, coating life becomes very critical for the successful application of TBC's. Furthermore, IGT's operating cycles are longer than aircraft engine cycles, which would raise other concerns with regards to coating long term stability and adherence. The use of TBC's for industrial gas turbines will increase if durability and longer service life are successfully demonstrated. The objective of this paper is to provide a perspective on the use of TBC's for industrial gas turbine applications.

TBC DEVELOPMENT EXPERIENCE

Most of the TBC development activities conducted during the last twenty years has focused on aircraft engine applications, where the turbine component requirements are high operating temperatures, large number of cycles, and relatively short lives. In contrast, few development activities have been conducted for industrial gas turbine applications. Aircraft and

industrial gas turbines differ mainly by the cycling frequencies and TBO. The use of TBC's for IGT applications is strongly influenced by the long term stability of the TBC system. Many researchers (Ref. 1 to 4) have reported that the dominant failure mode observed from TBC systems is the spallation of the oxide scale which forms on the surface of the metallic bond coat upon exposure to oxidative environments. Spallation is caused by residual, thermal, and mechanical stresses present at the oxide-metal interface. As a result, bond coat material development has increased in the last few years since it has been determined that TBC system durability is a function of bond coat properties. It was reported that TBC life could increase by the use of creep-resistant bond coat compositions and by overaluminizing the bond coat (Ref. 5).

Field data for the long term durability of TBC systems for IGT applications, is scarce. Early programs for developing advanced ceramic coatings for IGT's were conducted (Ref. 6), and included field engine data for candidate TBC systems. Various TBC systems applied on gas producer turbine blades were run in a 550-hour rainbow engine endurance test. The TBC systems included plasma sprayed calcium silicate, calcium titanate, and yttria stabilized zirconia ceramic top coats, and various NiCrAlY compositions for the metallic bond coats. The calcium titanate, and yttria stabilized zirconia systems survived the full test duration, but exhibited some coating erosion at the blades leading edges (Figure 1). It was concluded that both systems have potential for IGT applications. In addition, TBC's were applied on utility turbine blades (Ref. 7) as part of a field engine study. The effects of TBC's on the lifetimes of turbine components and on the performance of the utility turbine were demonstrated. When operating the turbine under constant cooling flow, the turbine airfoils experienced a 55°C drop, which could translate to 10 times the creep rupture life, and twice the corrosion life. When operated at constant metal temperatures, and reduced cooling flow, both specific power and efficiency increased, with no change in component lifetime. For IGT applications, an engine test was conducted (Ref. 8) with a TBC system applied using the electron-beam physical vapor deposition (EB-PVD) process. Gas producer blades and nozzles (Figure 2) were coated with EB-PVD ytrria stabilized zirconia, and were placed in an engine for a 5500-hour field test. The thermal barrier coatings appeared to be effective in protecting the component airfoil surfaces from high temperature oxidation. However, due to the limitations imposed by the line-of-sight nature of the EB-PVD process, coating uniformity was inconsistent between the airfoils of the turbine nozzles. The coating thickness varied from 0.125 mm at the airfoil leading edge and 0.025 mm between the adjacent airfoils. This limitation resulted in lower coating thickness between the airfoils due to the shadowing effect produced by the airfoils during coating deposition. As a result, the TBC coated nozzles did not perform as was expected for this application. With better coating application optimization, this problem could have been eliminated. Another field test was conducted (Ref. 9) on EB-PVD thermal barrier coated turbine blades. The engine operated for over 10,000 hours using a low grade liquid fuel, and in a harsh glass manufacturing environment. After service, the coating experienced some hot corrosion attack near the blade base, however the coating remained mostly intact with some distress and cracks near the blade trailing edge (Figure 3). The coating distress was attributed to blockage in the trailing edge cooling holes (Figure 4). This test determined that those available TBC's did not have adequate hot corrosion resistance.

CURRENT TBC APPLICATION

The use of TBC's for industrial gas turbines is expanding. Currently, thermal barrier coatings are more commonly used on combustors and in other low-risk applications to extend the useful lives of those components. Thermal barrier coatings are applied to combustion liners and transition pieces to virtually all of GE's advanced gas turbines (Ref. 10). GE's Power Generation experience has been excellent, with some TBC coated combustion components accumulating over 30,000 hours of total life. The application of plasma sprayed TBC's to hot combustors and turbine vanes is also being conducted on Mitsubishi heavy-duty gas turbines (Ref. 11). For Solar's medium size industrial gas turbine applications (Ref. 12), a NiCrAlY metallic bond coat with a calcium titanate ceramic top coat is applied on fuel injector tips (Figure 5) and sliding shroud rings. This TBC system has been successfully applied and operated in the field, where it provided thermal protection to the components, thus preventing cracking and deformation during service. However, few production applications of TBC's could be found on IGT airfoil components. Those could be attributed to the more complex and added processing costs associated with applying coatings to airfoils.

FUTURE TBC APPLICATIONS

Advanced industrial gas turbines with higher turbine efficiencies must operate at progressively higher temperatures. Even the most sophisticated cooling schemes have practical limits, and use of cooling air imposes severe penalties on performance. The application of TBC's on the external surfaces of turbine airfoils will provide the thermal resistance to the base metal, which will be capable of operating at the higher gas temperatures. TBC's are being considered for usage on turbine nozzles and blades, where they experience the highest temperature gradients. The advances in the EB-PVD processing controls and parts manipulation could facilitate the uniform deposition of TBC's on curved airfoils and between adjacent and partially overlapping airfoils. Furthermore, it is expected that engineered coatings which are capable of withstanding the harsh environment that IGT's are exposed to, and provide the long term coating life expected before TBO, could be achieved by the EB-PVD process.

AREAS OF CONCERN

As discussed earlier, industrial gas turbines are subjected to a more severe environment than aircraft engines. This would raise some areas of concern regarding coating reliability and durability. These concerns are related to the quality of fuels used for IGT's, oxide scale long term kinetics, and coating life.

Exposure of plasma sprayed yttria stabilized zirconia TBC's to combustion environments using clean fuels does little to degrade their properties. However, the presence of impurities in the fuel can be very detrimental. This is most likely to occur when lower grade fuels are used which involve the presence of vanadium and sodium. In combination with these impurities, SO_3

gas also adversely affects the performance of these coatings because thin films of molten salts can be deposited on the surface of the coated components. The principal reasons for coating failure in a dirtt environment is the localized destabilization of the original tetragonal/cubic structure of the zirconia material, and transformation to the monoclinic phase. This transformation has a 4% volume change associated with it and can therefore cause cracking of the coating. With the utilization of the EB-PVD deposition process, yttria stabilized zirconia TBC's can be tailored to be stable in combustion environments and to inhibit penetration of the corrosive molten salts (Ref. 13).

Another area of concern related to IGT applications, is the long term stability of the thin oxide scale formed at the bond coat/ceramic coat interface during service even when using clean fuels. Many reports (Ref. 1 to 4) indicated that TBC failure occurred at the oxide scale. With long term exposures and short cycles, the oxide scale will grow at different rates than those experienced in aircraft engines. A better understanding of the oxide scale growth kinetics is necessary for the design of more reliable TBC's.

Thermal barrier coating life is the limiting factor for the reliability of the TBC coated component. To understand this limitation, analytical models that describe the mechanical stress distribution and heat transfer of coated components are essential for component design. Models that can accurately describe TBC system life during specified service conditions are important to designers in defining component lives. Development of life prediction models are necessary to understand the TBC system behavior and be able to estimate time before coating failure. Life prediction modeling incorporates materials properties, component stress and heat transfer analyses, non-destructive techniques for detecting impending coating failures, and definition of failure modes. With better understanding of these parameters, the use of thermal barrier coatings on IGT components will become increasingly more attractive by reducing the uncertainties associated with TBC's.

EXPECTED BENEFITS

The use of TBC's on industrial gas turbine components is expected to provide many benefits. First and foremost, TBC's act as thermal insulators reducing the amount of heat transmitted to the component from the hot gas flux. The heat flux is dissipated through radiation back into the hot gas path, and through conduction across the coating and base metal, where the excess heat is absorbed by the back side cooling air. The temperature gradient across the coating allows for higher operating temperatures without distortion or degradation of the base metal. Second, TBC's provide thermal shock protection to turbine components during cold starts. The application of TBC's on turbine blades and nozzles could allow for higher turbine inlet temperatures, reduction in air cooling, and therefore increased volume of the working fluid in the turbine section which could translate to greater total efficiency.

The expected benefits of TBC's are very realistic to industrial gas turbines. Thermal analysis was conducted on existing airfoil designs coated with a nominal TBC system, and using

literature-available heat transfer properties. A 3-D thermal analysis was conducted to estimate heat flux and temperature distribution around the airfoil with and without a TBC. With a TBC, preliminary calculations using assumptions for thermal and physical properties for the TBC show that the temperature distribution drops by approximately 65°C at the leading and trailing edges and 38°C near the airfoil platform. These temperature reductions were achieved without requiring any optimization of the airfoil cooling schemes, or optimization of TBC properties. The 3-D thermal analysis model also indicated that the temperature reduction at the metallic surface is a function of coating thickness, and it was estimated that internal cooling requirements may be decreased by as much as 30 to 50%, resulting in an increase in overall thermal efficiency.

CONCLUDING REMARKS

For advanced industrial gas turbines, it is recognized that the use of thermal barrier coatings on turbine components will reduce maximum temperatures and thermal stresses on the components, allow for higher turbine inlet temperature, and reduce the extent of back side air cooling. Together, all of these positive factors will translate to an increase in total engine efficiency. The use of TBC's for industrial gas turbines will increase dramatically if durability and longer service life are successfully demonstrated.

REFERENCES

1. W.J. Brindley, and R.A. Miller, TBCs for Better Engine Efficiency, *Advanced Materials and processes*, 8/89, 1989, p29-33.

2. S.M. Meier and D.K. Gupta, The Evolution of Thermal Barrier Coatings in Gas Turbine Applications, IGTI, ASME 92-GT-203, 1992.

3. J.T. DeMasi-Marcin, K.D. Sheffler, and S. Bose, Mechanisms of Degradation and Failure in a Plasma-Deposited Thermal Barrier Coating, *Journal of Engineering for Gas Turbines and Power*, October 1990, Vol 112, p521-526.

4. T.E Strangman, A. Liu, and J. Neumann, Thermal barrier Coating Life - Prediction Model Development Final Report, NASA CR-179648, October 1987, Pub. NASA LeRC, Cleveland, OH

5. D.J. Wortman, B.A. Nagaraj, and E.C. Duderstadt, Thermal Barrier Coatings for Gas Turbine Use", *Materials Science and Engineering*, A121, 1989, p433-440.

6. J. W. Vogan and A. R. Stetson, Advanced Ceramic Coating Development for Industrial/utility Gas Turbines, NASA CR-169852, January 1982, Pub. NASA LeRC, Cleveland, OH

7. C.A. Andersson, S.K. Lau, R.J. Bratton, S.Y. Lee, and K.L. Rieke, Advanced Ceramic Coating Development for Industrial/Utility Gas Turbine Applications, NASA-CR-165619, February 1982, Pub. NASA LerC, Cleveland, OH.

8. J. Aurrecoechea, Analysis of TBC Coated Turbine Components After a 5500-Hour Engine Test, *Solar Turbine Incorporated*, SR88-F-5538-00, June 1989.

9. M. Van Roode, and J. Aurrecoechea, Rainbow Field Test of Coatings for Hot Corrosion Protection of Gas Turbine Blades and Vanes, IGTI, ASME 89-GT-242, 1989.

10. D.W. Parker, Thermal Barrier Coatings - Taking The Heat, *Turbomachinary International*, September/October 1991.

11. K. Takahashi, I. tsuji, N. Hirota, H. Kawai, and K. Takeishi, The Application of Advanced Plasma Coating To Hot Parts For Heavy-Duty Gas Turbine, *Thermal Spray Research and Applications*, ASM International, 1990, p439-441.

12. R.G. Mills, Advanced Concepts in Turbomachinary Technology, *Turbomachinary Technology Seminar*, Solar Turbines Incorporated, TTS48/186, 1986

13. T.E. Strangman, and J.L. Schienle, Tailoring Zirconia Coatings for Performance in a

Marine Gas Turbine Environment, *Journal of Engineering for Gas Turbines and Power*, October 1990, Vol 112, p531-535.

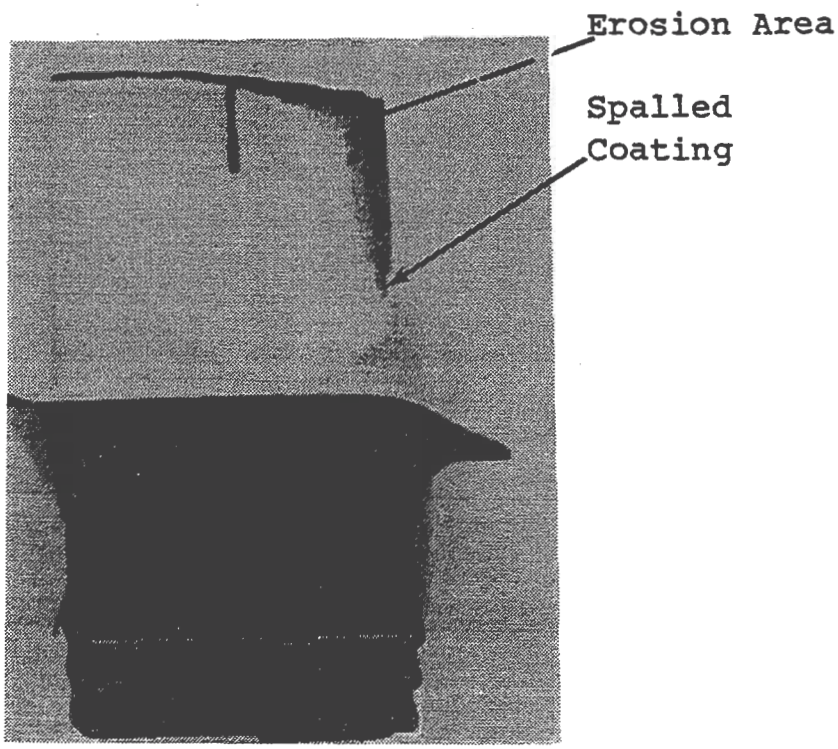

Figure 1. Yttria Stabilized Zirconia Plasma Spray Coated Blade After 550 Engine Test

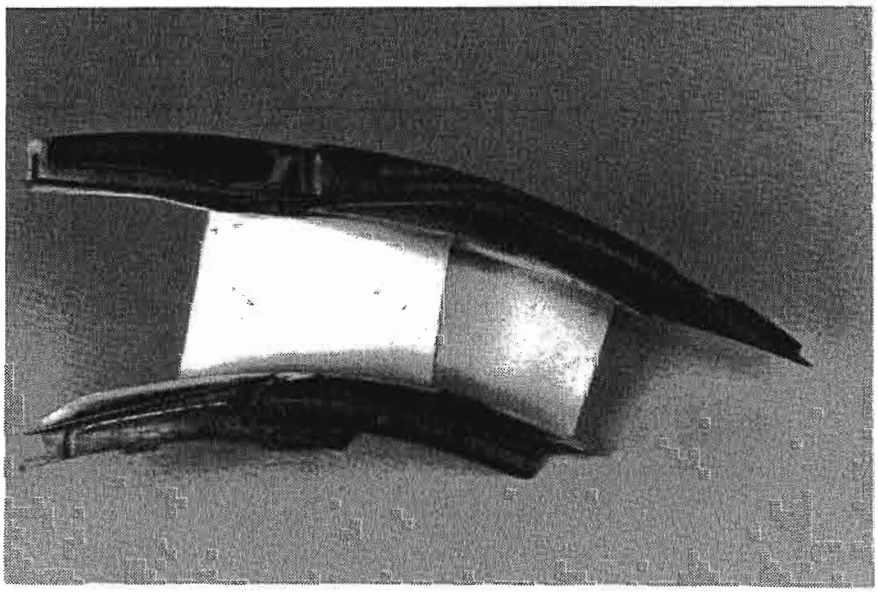

Figure 2. EB-PVD Yttria Stabilized Zirconia Coated Nozzle After 5500 Engine Test

Figure 3. EB-PVD Yttria Stabilized Zirconia Coated Blade Showing Coating Distress and Cracking Near Trailing Edge

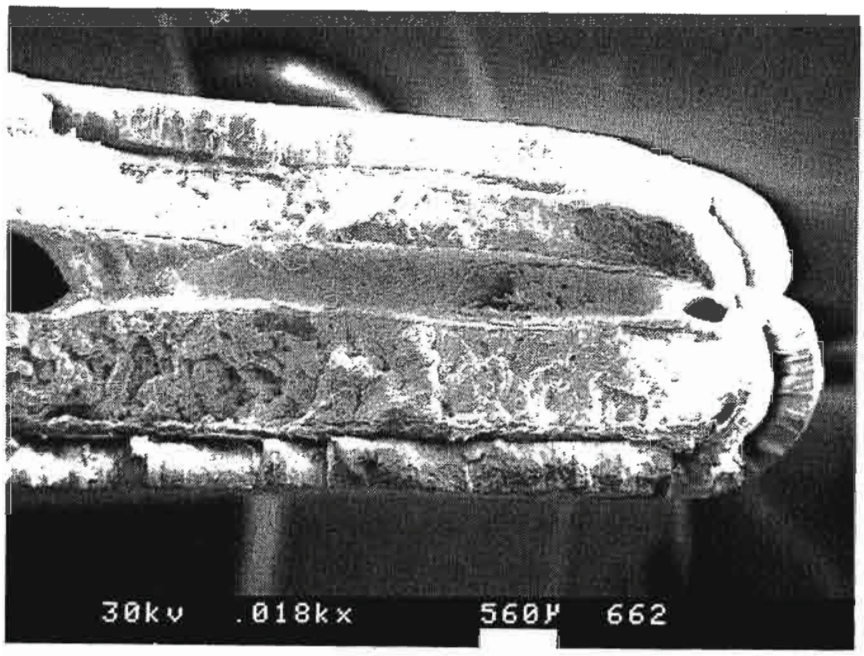

Figure 4. Scanning Electron Micrograph of EB-PVD Yttria Stabilized Zirconia Coated Blade Showing Blockage Inside Cooling Hole

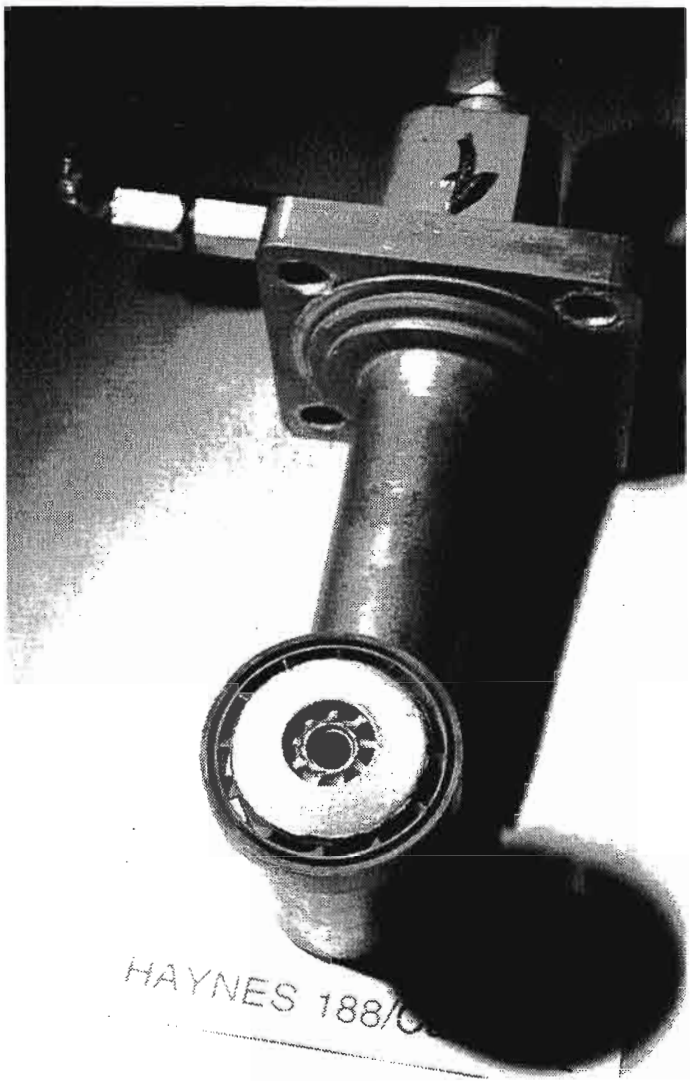

Figure 5. Fuel Injector Tip Coated With Plasma Spray Calcium Titanate Coating

OVERVIEW OF THERMAL BARRIER COATINGS IN DIESEL ENGINES

Thomas M. Yonushonis
Cummins Engine Company, Inc.
Columbus, IN 47202-3005

ABSTRACT

An understanding of delamination mechanisms in thermal barrier coatings has been developed for diesel engine applications through rig tests, structural analysis modeling, nondestructive evaluation, and engine evaluation of various thermal barrier coatings. This knowledge has resulted in improved thermal barrier coatings which survive abusive cyclic fatigue tests in high output diesel engines.

Although much conflicting literature now exists regarding the impact of thermal barrier coatings on engine performance and fuel consumption, the changes in fuel consumption appear to be less than a few percent and can be negative for state-of-the-art diesel engines. The ability of the thermal barrier coating to improve fuel economy tends to be dependent on a number of factors including the fuel injection system, combustion chamber design, and the initial engine fuel economy. Limited investigations on state-of-the-art diesel engines have indicated that the surface connected porosity and coating surface roughness may influence engine fuel economy.

Current research efforts on thermal barrier coatings are primarily directed at reducing in-cylinder heat rejection, thermal fatigue protection of underlying metal surfaces and a possible reduction in diesel engine emissions. Significant efforts are still required to improve the plasma spray processing capability and the economics for complex geometry diesel engine components.

BACKGROUND

Thermal barrier coatings were initially investigated for "adiabatic" diesel engines due to first law thermodynamic predictions of significant fuel economy improvements, reduction in heat rejection, and the potential to increase power density of the diesel engine. Cummins Engine Company, Inc. conducted extensive evaluation of existing thermal barrier coatings using the Cummins V903 diesel engine. These initial exploratory efforts were conducted using duplex coatings consisting of a NiCrAlY bond coating and a yttria stabilized zirconia top layer. Total coating thickness was on the order of 1.5 mm with the bond coating thickness approximately 0.1 mm. These investigations conducted in the early 80's revealed that the existing thermal barrier coatings were insufficient to survive short duration tests in a high output diesel engine (1.38 MPa brake mean effective pressures (BMEP)). Extensive trial and error development efforts conducted at that time using plasma sprayed zirconia coatings did not result in acceptable or reproducible coating lives.

Efforts sponsored by the Department of Energy(DOE) /NASA, Tank Automotive Command (TACOM), and Cummins internal funds in the mid-80's focused on understanding the stresses in the thermal barrier coatings with a goal of significantly improving the life of the coatings in diesel engines. Approximately two orders of magnitude in thermal barrier coating life improvements were necessary for utilization of the coatings in advanced diesel engines.

The DOE/NASA program[1] had an objective to develop zirconia based thermal barrier coatings with a thermal conductance of 410 W/m^2K which could survive 100 hours of operation in a research single cylinder engine. The engine chosen for this program was the Cummins V903 direct injection diesel engine with a 140 mm bore and 120 mm stroke. The V-8 engine was rated at 360 kW at 2100 RPM for the turbocharged configuration. The geometric compression ratio chosen for this work was 13.5:1, and the peak cylinder pressure was limited to a maximum of 13.8 MPa.

Extensive diesel engine cycle simulation and finite element analysis of the coatings were conducted to understand the effects of a coating on diesel engine performance and the stress state in the coating and underlying metal substructure. The TACOM program[2] expanded the effort initiated with DOE to develop improved thermal barrier coatings which could survive the high cylinder pressures and thermal loads projected for military applications.

An engineered coatings approach was utilized in the DOE program which consisted of utilizing existing databases augmented where necessary by the collection of additional data, modeling of stresses in the coatings by finite element techniques, and extensive rig and engine tests. Cummins and United Technologies Research Center cooperated on this program to modify thick thermal barrier coatings developed for turbine tip seals for diesel applications.

COATING DEVELOPMENT FOR DIESEL ENGINES

Diesel engine performance modeling was conducted which projected that the maximum benefits of the thermal barrier coatings was obtained by applying the coatings to the piston and cylinder head surfaces. The effects of the coatings on valves and cylinder liners were not projected to result in significant fuel economy improvements. Therefore, research efforts on the DOE/NASA and TACOM programs concentrated on cylinder head and piston coating development. With the insulation levels defined by the coatings thermal conductance, diesel engine performance models predicted that the in-cylinder heat rejection would be reduced by 38% and that the fuel economy would be improved by 2% for a turbocharged engine and 3% for a turbocompound version of the engine.

United Technologies Research Center (UTRC) used one-dimensional thermal-structural modeling to select preferred coating systems for spray fabrication trials and rig tests.
A one-dimensional thermal-structural model was established to predict both the temperature gradients across layer interfaces of candidate coating systems and overall coating state-of-stress at maximum operating conditions. Predicted temperatures from the thermal analysis were used to predict stresses within the coating systems at a diesel engine maximum operating condition. The modeling indicated that single layer coatings systems were in compression at the top of the

coating and in tension at the bond/substrate interface. Previous single layer coatings have been shown to delaminate in the zirconia coating in this tensile region above the bond coating.

It was determined that the multilayer coatings reduce in-plane tensile stresses in the ceramic top layers. Figure 1 shows that the thermal stresses were significantly less than the measured coating strength. The coating was in compression at the top surface which was 2.5 mm from the bond coating-ceramic coating interface. Metal substrates were also analyzed and it was determined that substrate yielding should not be expected. Additionally, thermal modeling indicated that the metal temperatures were insufficient to result in bond coating oxidation in the short time that engine coating delamination was experienced in previous engine tests.

Two dimensional finite element modeling using the cycle average boundary conditions also suggested that a multilayer thermal barrier coatings could survive engine conditions. Efforts concentrated on the understanding of one coatings system, a multilayer 2.5 mm coating. This coating consisted of mechanical mixtures of CoCrAlY and zirconia fully stabilized by yttria. The 2.5 mm coating consisted of 0.5 mm layer of 40 % zirconia/ 60% CoCrAlY, followed by a 0.5 mm 85% zirconia/ 15% CoCrAlY layer , followed by a 1.5 mm thick 100% zirconia layer. The zirconia layer was approximately 85% dense. Processing conditions were developed to generate residual stresses in the thermal barrier coatings by controlling the substrate temperature during the deposition process.

It is also important to consider thermal transients when designing with ceramic materials. The low thermal diffusivity of the ceramics causes their temperatures to quickly respond to changes in operating environment while the temperatures of the base materials respond much more slowly. This thermal response behavior causes significantly different temperature and thermal stress profiles to be encountered under transient operation than those observed at steady-state.

The first thermal transient considered was a sudden cooling of the combustion face. Calculations were made at steady-state for conditions representative of full load operation at rated speed. At time zero, the in-cylinder conditions were suddenly changed to those representative of no-load conditions. The resulting transient spatial thermal response within the coating is summarized in Figure 2. As can be seen in Figure 2, the surface temperature drops rapidly while the interior temperature reacts more slowly. With increasing time, the coating temperature decreases. The predicted thermal stresses in the coating are shown in Figure 3. The trend shows a relaxation of the compressive stress at the surface with increasing time. This relaxation results in a slight reduction in the tensile stress experienced in the bond coat adjacent to the substrate. Cycle to cycle transients and rapid heating of the coating were also modeled.

Through transient analysis using a simple finite element model, it was determined that:

1. Temperature and stress profiles under transient conditions were found to be significantly different than those at steady-state.

2. Engine load changes, though resulting in a change in stress profiles, were not predicted to result in coating failure for the cases considered.

3. Firing cycle transients resulted in a predicted surface temperature swing of 225 C, and an increase compressive stresses in the surface layers of the coating. These compressive stresses were predicted to not penetrate further than 0.13 mm into the coating.

UTRC developed a spray fabrication technique to define material properties most representative of actual coating material. Flat-plate substrates were attached to a rotating holding fixture in areas representing the piston crown diameter. Heat was applied to the panels through the use of small propane torches mounted on a ring that surrounded the base plate. A thermocouple placed on the backside of the substrates provided the processing temperature and allowed for manual adjustment of the propane to maintain the desired prestress temperature through the spray run. The actual robot motion control and spray processing parameters used to coat the piston crowns were used to coat the substrates. Test specimens were fabricated from the substrates in locations indicative of the crown rim and center dome areas of the piston. This approach was needed to verify uniformity of properties across the crown diameter.

Based on preliminary one-dimensional transient analysis performed by Cummins for the baseline multilayer-layer coating on ductile iron, the rig thermal cycle was targeted to achieve a maximum surface temperature of approximately 675-730 C with a maximum thermal gradient across the coating of approximately 480-537 C at a 7 second time point into the cycle.

Test rig conditions were calibrated using the baseline multilayer-layer coating system on a nickel-based superalloy test panel that had been instrumented with embedded thermocouples. A test cycle which closely reflects the predicted diesel engine thermal environment was created with a maximum thermal gradient across the coating of approximately 510 C in seven seconds and a top surface temperature of 675 C. Two additional test cycles representing maximum thermal gradients of 555 C and 705 C respectively were used to further screen thermal strain capability at higher temperatures.

Ductile iron test panels with the baseline multilayer coating system were fabricated at both a medium fabrication temperature and a medium (hybrid) fabrication temperature which incorporated a temperature spike through the bond coat region. These panels were then exposed to the same thermal cyclic test conditions. The panel fabricated at the medium fabrication temperature was initially tested and survived the 510 C thermal gradient. Examination of the panel after the five cycles yielded no visible damage. The panel was then subjected to the more severe 555 C and 705 C thermal gradients. No damage was noted to occur after the 555 C cycle; however, after the 705 C cycle the coating showed moderate cracking of a secondary nature at the 40/60 zirconia/CoCrAlY to 85/15 zirconia/CoCrAlY interface.

The panel fabricated at the medium (hybrid) prestress temperature profile was exposed to the 705 C thermal gradient and showed minimum cracking sensitivity. These test results showed

the superior strain capacity of the baseline multilayer coating system fabricated with the medium (hybrid) fabrication temperature control.

A prototype plasma spray facility with the capabilities needed to continuously apply multilayer-layered thermal barrier coatings was set up to coat Cummins V903 and L10 piston crowns and single cylinder heads[3]. The facility was equipped with a six-axis articulating robot to provide gun motion control. Part holding fixturing for all diesel engine components was developed for both simulations and actual hardware. The fixturing for the piston crown was made to incorporate a flame shroud to provide the capability to heat the piston crown substrate during the spray processing to control fabrication temperature. A powder feed delivery system was used to provide continuous feed rate control during coating deposition. It had the capability to deliver four coating materials sequentially.

Spray process parameters to produce zirconia-based thermal barrier coatings on V903 piston crowns and cylinder heads were developed by translating UTRC's experience in producing turbine seal coatings on curved duct segments. Fundamental issues addressed included prestressing technology and special processing techniques needed to coat each of the specific diesel engine components.

Initial processing efforts focused on developing robotic control software for the plasma gun motion. Applying the coating system across the piston crown diameter proved to be difficult and variable due to the complex bowl geometry. Simulated piston crowns were machined and used to assess the magnitude of the coating thickness variation across the actual piston crown contour. A combination of single-layer and multilayer coating systems were sprayed on the simulated crown. The simulation was then cut in half and the resulting diameter polished for metallographic examination of the thickness variation of the individual layers, particularly in the bowl area of the crown. From thickness measurements it could be seen that the deposition was not as efficient as areas where a 90 degree angle of the plasma gun to the sprayed surface was maintained. A "circular" type gun motion control including a gun rotation into the wall area was developed to achieve the highest degree of thickness, microstructure and properties uniformity across the crown diameter. Baseline robotic control parameters such as speeds and program increments were determined empirically by conducting a series of coating trials on piston crown simulations.

ENGINE EVALUATION

Single cylinder engine tests confirmed that the multilayer thermal barrier coatings had significantly longer lives than previously evaluated duplex thermal barrier coatings. These multilayer zirconia based coatings achieved the DOE/NASA contractual goals of 100 hours at rated engine conditions, approximately 1.38 MPa BMEP, while meeting the thermal conductance goals. However, engine fuel economy was not improved and coating life capability was marginal. Further evaluation of similar multilayer zirconia coatings in commercial L10 engine revealed that the coatings could survive steady state operation at 1.83 MPa BMEP. However, cyclic tests resulted in coating deterioration and coating loss. Further confounding was the observation that the zirconia coatings had open crack patterns at the surface of the coating while finite element

stress calculations predicted the coating to be in compression for the input boundary conditions. Additional improvements in coating life and capability were required for the technology to be commercially viable.

TACOM sponsored efforts concentrated on the engine evaluation of thermal barrier coatings on an articulated steel piston in a multicylinder L10 engine to further define coating durability at higher brake mean effective pressures, 1.83 MPa. Initial tests at steady state operation confirmed that multilayer zirconia coatings would survive steady state operation for 200+ hours. Cyclic tests were conducted between high idle and full power condition. Coating loss was experienced in these cyclic tests. Further coating evaluation concentrated on the evaluation of the coating in cyclic tests which were conducted for 75 hours followed by removal of the cylinder head. Various zirconia multilayer coating strategies were evaluated including varying residual stresses, utilizing partially stabilized zirconia instead of fully stabilized zirconia, varying plasma gun power, and other coating changes. These modifications had essentially no measurable effect on the coating life.

Contrary to intuition and predicted stresses, a mullite based multilayer coating was tested. Mullite was selected due to the materials lower thermal expansion and higher thermal conductivity. The mullite based coatings had significantly improved performance compared to the zirconia based coatings as shown in Figure 4. Diesel engine evaluation of zirconia and mullite based coatings has demonstrated that the mullite coatings significantly outperform the zirconia coatings in steady state and cyclic engine tests. In multiple engine builds, the mullite multilayer coatings have survived transient conditions that have extensively damaged zirconia based coatings.

NONDESTRUCTIVE EVALUATION

Although state-of-the-art plasma control systems and robotics have been used to deposit thermal barrier coatings, minor errors in plasma gun manipulation, concentric powder feed and plasma alignment and slight changes in coating deposition rates can alter the coating structure and coating performance. Since the thermal barrier coatings are applied individually to the pistons and limited production studies have been conducted, a reliable inspection process is required for the coatings. At the period of time that the coatings were being developed, Cummins initiated efforts with Wayne State University to apply infrared imaging techniques to understand the coatings appearance before and after engine test. Thermal wave imaging was found to offer significant advantages including speed of data collection and user friendly interpretation of the images[4]. Destructive evaluation of the coatings confirmed that delaminations or coating inconsistencies were detected by the thermal wave imaging technique. Infrared imaging is currently used to inspect the thermal barrier coating prior to and after engine evaluation. This nondestructive evaluation technique has led into new areas of research and confirmed a number of hypothesis. Infrared imaging has shown that the center portion of the piston is difficult to coat and may be delaminated in the region prior to engine evaluation.

COATING CRACK INITIATION

As a gradual increase in coating durability was realized, the coating life was still inadequate for many advanced diesel applications. A critical factor missing in many investigations was the understanding of the crack initiation and propagation mechanisms in the thermal barrier coatings. Purdue University and Cummins began an investigation to determine the mechanisms responsible for surface crack initiation at conditions that simulate the engine thermal loading conditions in a diesel engine[5].

A simple experiment was designed to simulate the boundary conditions imposed during diesel engine combustion. In direct injection diesel engines, combustion of the fuel results in localized high heat flux regions on the piston and cylinder head. These areas of high heat flux concentration correlate with coating damage observed during diesel engine evaluation of thermal barrier coatings. Previous analytical modeling had predicted that the thermal barrier coating was in compression through all engine operating conditions. This resulted in a paradox, since crack opening due to tensile stresses was observed in thermal barrier coatings. To understand the observations from diesel engine tests, an experiment was designed as a two dimensional representation of the diesel engine combustion. An advantage of this specimen design was that the during crack formation the depth of the surface crack and the presence of interface cracks could be determined by low power optical inspection. The specimens consisted of multilayer beam specimens with a concentrated heat flux in the center of the sample. The experiments and analysis were conducted on three specimen configurations.

The concentrated heat flux region was created by high powered infrared lamps. Temperature measurements were recorded at multiple points on the coating surface and the substrate. Tests were conducted by heating the specimen by turning the lamps on at full power and then maintaining a steady state temperature for two hours. A two hour test time was used in order to allow the surface stresses to equilibrate. At the end of the test, the specimen was cooled to room temperature under natural convective cooling.

In order to develop an understanding of the stress distribution in the specimens, analytical models of the specimens were developed using the finite element method. The magnitude of the in-plane stress in the top layer governed the formation of the surface crack. The temperatures and the stresses were calculated in four discrete steps.

1. The residual stresses were calculated by assuming a uniform stress free temperature of 618 C which approximates the manufacturing temperature used in the coating deposition for the test specimens.

2. The thermal stresses were calculated at steady state temperatures based on measurements of the heat flux generated by the lamps.

3. Stress relaxation was allowed to occur for a two hour period.

4. The specimen was uniformly cooled back to room temperature.

The stress relaxation of the zirconia was estimated using a strain gauge mounted to the bottom of the substrate to measure the strain change as a function of time during steady state heating.

Experimental measurements showed that the temperature of the coating surfaces reached approximately 870 C for a thick zirconia specimen and 760 C for a comparable mullite coating thickness. The stress relaxation was modeled as $\varepsilon = A\sigma^n$ where $A = 4.03*10^{-19}$ and $n = 1.59$ for zirconia at 870 C and $A = 2.98*10^{-17}$ and $n = 1.1$ for mullite at 760 C. Surface crack formation was observed the thicker zirconia specimen, but was not observed in the thick mullite. Crack formation started at the zirconia surface thus indicating that a tensile stress at the surface governs crack initiation behavior. In order to understand the thermal crack initiation behavior in the zirconia, the stress distributions were calculated analytically. The stress in the thick zirconia coating is in compression at approximately 200 MPa near the surface. During the heating of the zirconia surface, the zirconia coating surface reaches a much higher temperature than the metal underlying surface. The result of this thermal gradient is that the zirconia coating expands more than the underlying metal which results in a large calculated compressive stress in the ceramic coating. However, at the higher temperatures, stress relaxation locally reduces the magnitude of the compressive stress. This stress relaxation results in a local tensile residual stress in the coating at room temperature. The new residual tensile stress is sufficient to crack the zirconia coatings.

The model suggests that to extend the service life of the coating that the stress relaxation properties should be reduced. Since stress relaxation is highly temperature and material dependent, analysis was conducted for a mullite coatings. The model predicts that the temperatures were not sufficient to induce cracking for the lower temperature and different mechanical properties of mullite.

EMISSIONS AND ENGINE FUEL ECONOMY

An extensive data set of engine performance measurements have been made comparing a single cylinder 1.67 liter diesel engine using steel articulated pistons to pistons with an insulated coating of yttria stabilized zirconia or mullite. Measurements made on back-to-back single cylinder tests included cylinder pressure, brake torque, NOx, unburned HC, and particulate as a function of timing at four speed-load operating conditions. The effect on heat transfer of insulated pistons was determined based on indicated fuel consumption versus centroid of heat release curves. Engine performance using the zirconia coated piston was measured to have 1 - 3% higher indicated and brake specific fuel consumption in comparison to the baseline, Figure 5. The difference between the two pistons was greatest at the most advanced injection timings. The mullite coated pistons displayed a fuel consumption increase which was as much as 8% at advanced timings, Figure 6. Heat release was slightly extended for the zirconia pistons and extended even longer on the mullite pistons. Error analysis of the measurement methods showed an uncertainty of $\pm 3\%$ in the indicated specific fuel consumption and ± 2 crank angles in the centroid could be expected for this set of measurements. The data was therefore inconclusive on the effect of insulation on heat transfer for the zirconia coated pistons, but the mullite coated pistons displayed a measurable reduction in indicated mean effective pressure which was

interpreted to be caused by increased heat transfer. Emissions for the insulated pistons showed similar NOx particulate trade-off curves at retarded timings, but the particulate increased at advanced timings on the mullite coated pistons. The zirconia coated pistons displaced a slight increase in particulate and NOx at advanced timings as shown in Figure 7.

SUMMARY

Thermal barrier coating life has been significantly enhanced by understanding the mechanisms that control the coating life. Initial diesel cycle average boundary conditions did not adequately represent the thermal loading applied to the thermal barrier coating. Nondestructive evaluation based on the infrared imaging technique was instrumental in understanding the thermal barrier coatings structure as deposited and after engine evaluation. Thermal wave imaging confirmed that some coatings were delaminated prior to engine evaluation. This technique also confirmed that local thermal gradients tied to the diesel combustion process were resulting in localized damage. This information led to the development of a low thermal expansion mullite based coating system [6] which had better thermal fatigue resistance than the zirconia coatings.

Use of robust thermal barrier coatings permitted the engine fuel economy and emissions data collection which was not complicated by combustion chamber changes due to coating loss. Engine fuel economy and emissions performance improvements were not realized for the state-of-the-art diesel engines evaluated. Metal temperatures underneath the coatings have been shown to be reduced which impacts thermal fatigue life of these components.

ACKNOWLEDGMENTS

Many people contributed to the efforts described in this overview of thermal barrier coating development for diesel engines. Research was conducted at the following organizations described in this paper. Cummins Engine Company, United Technologies Research Center and a spin-off company Engineered Coatings, Inc., Wayne State University, and Purdue University. Funding was provided by the Department of Energy monitored by NASA, TACOM, and Cummins Engine Company, Inc. Major contributors include the following people: Cummins Engine Company, Inc. - Kevin Hoag, Dan Oren, Mike Pasini, Dr. Jim Patten, Pat Pierz, Randy Stafford, Dale Tree, and Paul Wiczynski; United Research Technology Center - Dick Novak, Roberta Huston, Janet Linsey, Al Matarese, and Al Scharman; Wayne State University - Tasdiq Ahmed, L. Favro, P. K. Kao, and Dr. Bob Thomas; Purdue University - Dr. Klod Kokini and Yoshimi Takeuchi.

NASA contributors included Murray Bailey and Jim Wood and funding from Contracts DEN3-331 and DEN3-375 is acknowledged. Assistance from John Fairbanks at DOE is gratefully acknowledged. Support from U. S. Army Tank Automotive Command (TACOM) under Contracts DAAE 07-84-C-R082 and DAAE 07-91-C-R005 and the support of Chuck Raffa and Ernie Schwarz is acknowledged.

REFERENCES

1. T. M. Yonushonis, "Thick Thermal Barrier Coatings for Diesel Components", NASA CR-187111, August 1991.
2. U. S. Army Tank Automotive Command (TACOM) under Contracts DAAE 07-84-C-R082 and DAAE 07-91-C-R005.
3. R. C. Novak, A. P. Matarese, R. P. Huston, A. J. Scharman, and T. M. Yonushonis, "Development of Thick Thermal Barrier Coatings For Diesel Applications", *Materials and Manufacturing Processes*, 7(1), 15-30 (1992).
4. T. M. Yonushonis, R. J. Stafford, T. Ahmed, L. D. Favro, P. K. Kuo, and R. L. Thomas, "Infrared Thermal Wave Imaging of Thermal Barrier Coatings For Diesel Applications", *Bulletin of the American Ceramic Society*, 71 (8), (1992).
5. Y. Takeuchi, K. Kokini, and T. M. Yonushonis, "Thermal Barrier Coating Development for Pistons", *Proceedings of the 1992 Coatings for Advanced Heat Engines Workshop*, Aug. 3-6 (1992).
6. A. J. Scharman and T. M. Yonushonis, Ceramic Thermal Barrier Coating for Rapid Thermal Cycling Applications, Patent No. 5,320,909, (June 14, 1994).

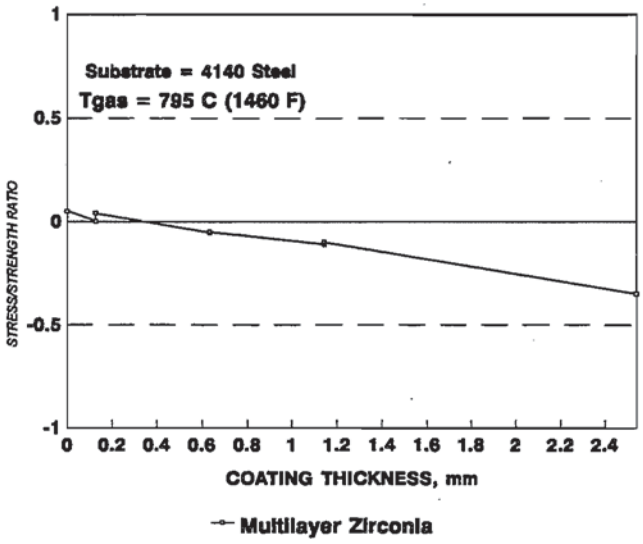

Figure 1. Coating Strength to Stress Ratio through the Thickness of a Multilayer Zirconia Based Coating.

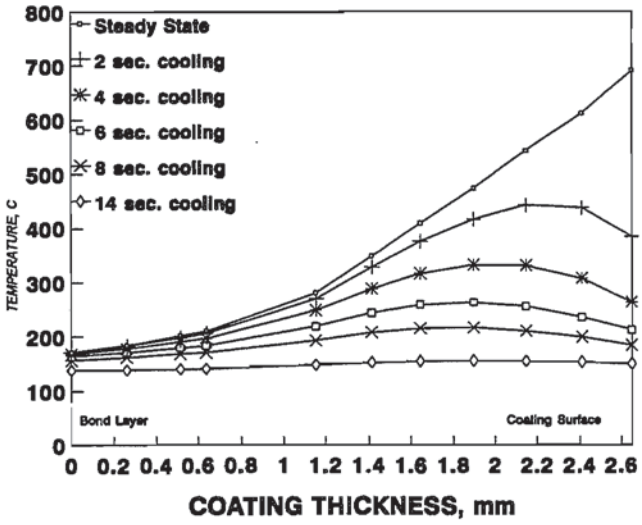

Figure 2. Coating Temperature Changes During Cooling from Steady State Engine Conditions.

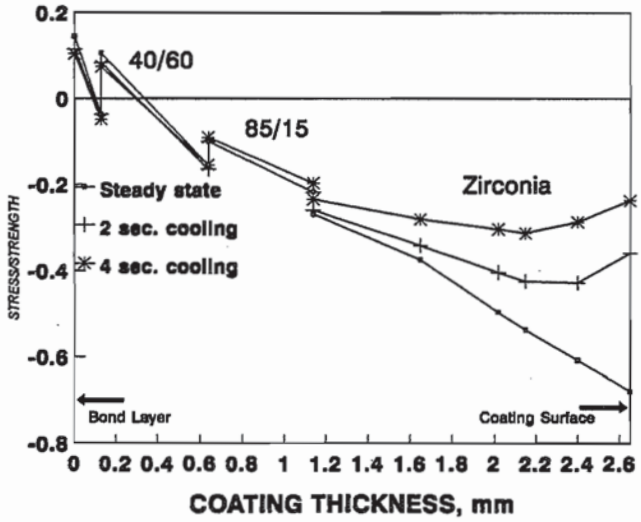

Figure 3. Estimated Stresses in a Multilayer Zirconia Based Coating During Cooling.

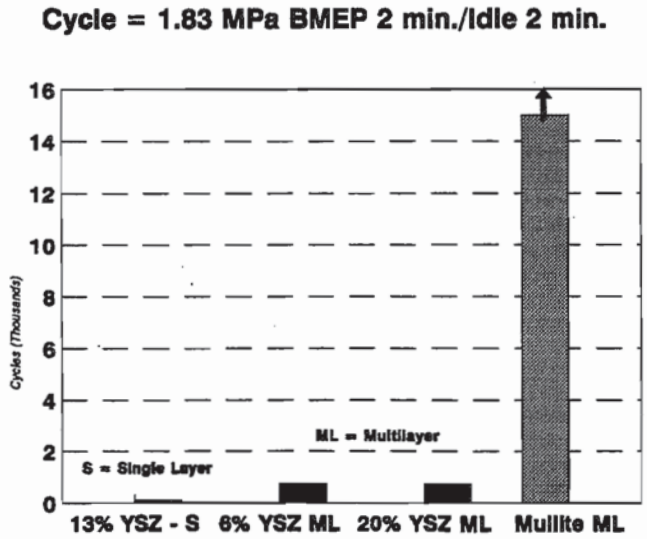

Figure 4. Improvements in Thermal Barrier Coatings in Cyclic Diesel Engine Tests.

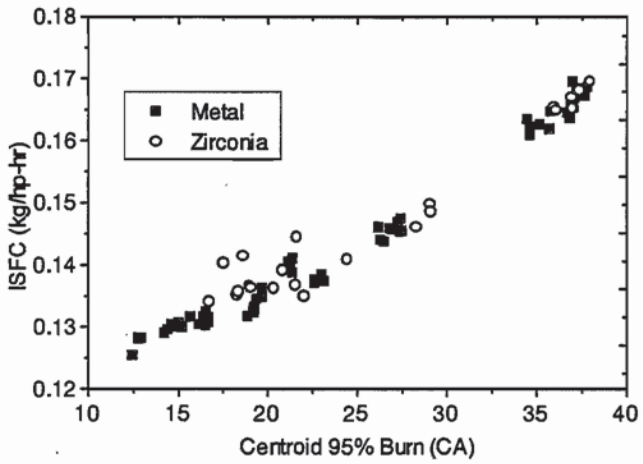

Figure 5. Comparison of Metal and Zirconia Coated Pistons at 1800 rpm and Rated Load.

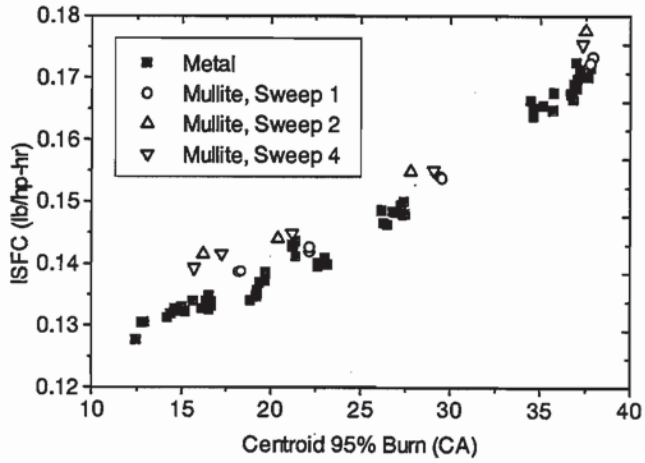

Figure 6. Comparison of Metal and Mullite Coated Pistons at 1800 rpm and Rated Load.

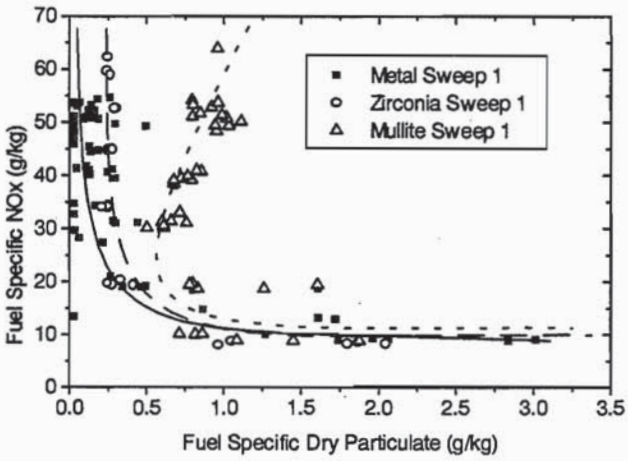

Figure 7. Fuel Specific NOx and Particulate Trade-off Curve for Metal, Zirconia and Mullite Coated Pistons at 1800 rpm and Part Load Conditions.

PLASMA SPRAY PROCESSING OF TBCs

H. Herman and C.C. Berndt
Thermal Spray Laboratory
Dept. of Materials Science and Engineering
State University of New York
Stony Brook, NY 11794-2275

ABSTRACT

Thermal spray processing has been used for a number of years to cost-effectively apply TBCs for a wide range of heat engine applications. In particular, bond coats are applied by vacuum plasma spray or HVOF techniques and partially-stabilized zirconia top coats are applied by plasma spray methods. Thermal spray involves melting and rapid transport of the molten particles to the substrate, where high-rate solidification and coating build-up occur. It is the very nature of this melt processing that leads to the unique layered microstructure, as well as the apparent imperfections, so readily identified with thermal spray. Therefore, although the plasma spray of TBCs has been largely successful, it is clear that a major step forward in terms reliability and performance can be gained by a fundamental understanding of the TBC microstructure with respect to the processing technology and operating environment.

INTRODUCTION

Thermal barrier coatings (TBCs) for gas turbine applications are applied by plasma spray to thicknesses of ~0.020 inches. The sprayed TBC has a few volume percent porosity, which contributes further to a decrease in thermal conductivity. The remarkable feature of the TBC is survivability, both in thermal shock and in the difficult environmental conditions within the gas turbine. The scientific answer to the performance of TBCs lies in the uniqueness of their micrographic characteristics. Furthermore, the origin of this microstructure lies in the means through which the molten ceramic droplets undergo impact-solidification on the substrate and then onto previously deposited layers, yielding chaotic layers of splats. There have been numerous studies involving modeling of the evolution of such deposits, but serious questions remain, which become particularly important when dealing with thermal barrier coatings.

The prototypical TBC, and the one most used in heat engines, is partially-stabilized zirconia (PSZ). While there is considerable commonality in the behavior of all ceramic plasma sprayed deposits, PSZ has unique and important features which explain its survivability in the extreme environments

encountered in, for example, gas turbine engines. Coupled closely with the performance of PSZs is the process of deposition. It is widely known that plasma sprayed ceramics have layered microstructures, not unlike hand-laid New England stone fences. And like those fences, the flat stones have associated with them gaps and fractures of various morphologies and sizes. But the analogy ends there. For, in the case of plasma sprayed coatings, "mortar" is used, which originates from solidification-bonded splats. The character of the interbonding and the voids and cracks are crucial to the behavior of the TBC both at high operating temperatures and under thermal cycling conditions.

With regard to microstructure, it is important to compare the plasma sprayed layered structure to what is commonly obtained from its closest competing process, electron-beam physical vapor deposition (EBPVD). Due to the nature of the latter process, PVD microstructures are strongly columnar, enabling sought after strain tolerance. However, this same microstructural feature which allows compliant behavior under thermal cycling, due to the columns being able to move relative to one-another, also allows entry of oxygen and corrodants. In addition, the distribution of voids and cracks will differ between the layered and columnar microstructures, thereby influencing behavior in-service.

This paper will explore plasma spraying of TBCs, with special reference to process-related microstructure and imperfections and how these influence coating performance. Of principal concern will be the anisotropic nature of the deposits, that is, the layers of splats. This is also reflected in the anisotropic array of porosity, which specialized neutron diffraction methods have recently resolved. In fact, through the application of a variety of characterization methods, plasma sprayed TBCs can be reasonably well understood, leading to the process-control of microstructure.

PLASMA SPRAY PROCESSING

TORCH AND PARTICLE DYNAMICS

The gas stabilized non-transferred dc plasma spray torch is able to sustain a electric arc between a thoriated tungsten cathode and an annular water-cooled copper anode. Usually an inert arc gas (generally, argon) is introduced such that the gas enters as a vortex and exits from the front of the anode. The electric arc from the cathode to the anode completes the circuit, forming an exiting plasma flame. For a typical torch operating at 40 kW, the temperature of the plasma is in excess of 15,000K; this temperature dropping off rapidly from the exit of the anode (1) . Feedstock powder particles, which are injected either internally or externally are approximately 40 micrometers in diameter. The particles are accelerated and melted in the flame on their high speed (100-300 m/sec)

path to the substrate, where they impact and undergo rapid solidification (10^6 K/sec). There are a number of reviews on the theory and practice of gas stabilized plasma spray torches (2,3). It should be especially noted that the French school of Fauchais has pioneered experimental diagnostics of the non-transferred plasma spray torch (e.g., Ref. 3).

The interaction between a solid particle and the plasma flame is of vital importance, because this interaction must result in proper melting of the feedstock powder. The particles, on being introduced, must achieve sufficient kinetic energy to accelerate to some velocity approaching that of the flame, and to take from the flame sufficient enthalpy to fully melt. Additionally, a large proportion of the powder particles must have trajectories through the center of the flame, this yielding the highest deposition efficiency. In the ideal case, the plasma effluent would not be turbulent and the particle, on entering the plasma, would not perturb the flame. In reality, however, the flame is non-lamellar and, further, the powder carrier gas does disturb the flame, creating significant flame distortions. It is widely recognized that thermal plasmas are very different from the ideal, making modeling of the process difficult. However, the plasma gun should be able to approximate the following goals:

1. Particle velocity should be sufficient to result in a dense deposit but not so high as to cause an "explosion" of the particle on impact
2. The particles should all have the same uniform velocity upon impact
3. The particles should all be uniformly heated.
4. The particles should be fully molten or plastic without significant vaporization and without undesired chemical reactions.

The plasma spray process has experienced enhanced scientific maturation, leading to the ability to control and to reproduce plasma spray parameters. The enhanced reproducibility which has in recent years been available is due largely to the introduction of microprocessors. But also important has been statistical process control, with which it is possible to rationalize optimization of the plasma process into a reasonable number of experiments. There are dozens of variables controlling the process, and it is essential to determine the level of sensitivity of a given parameter. Statistical process control is now used widely to minimize the time and effort required to obtain optimized plasma spray parameters. In the past, plasma spray processing of coatings has been an, essentially, manual procedure. All process parameters, such as gun current, gas flow, powder feed rate, and spray distances, were preset (and, frequently, were based upon empiricism) and adjusted manually during operation. Thus, significant part-to-part, operator-to-operator, and booth-to-booth

variations could occur, since small changes in these parameters can adversely affect the coating quality.

Equally important have been developments in feedstock powder materials (4). There has been heightened recognition of the relation between the means through which the powders are processed and the sprayed product. For example, a fused-and-crushed and a sintered-and-crushed mixed-oxide powder may show significantly different properties when sprayed with identical plasma parameters (5). And new, previously difficult-to-spray materials are being effectively plasma sprayed, sometimes in environmental chambers.

ALTERNATE PLASMA PROCESSES

At the other end of the plasma spray spectrum is the limitation in obtaining thin films. A major shortcoming of traditional thermal spray technology has been the thinness to which a deposit could be formed. Fine-sized feedstock particles would be required for the production of thin film deposits (< 1 micrometer). To force fine particles into such a flame would require increasing the carrier gas pressure, leading to increased flame turbulence, and thus to unacceptably disturbed particle trajectories. These problems, as well as others, could be largely overcome by using axial injection of the materials feedstock. Axial-feed plasma guns can avoid many of the limitations imposed by non-axial plasma devices. The operation of a recently developed axial gun is based on the "electromagnetic coalesced plasma" (EMCP), allowing four off-centered coalescing 1 kW pilot plasmas to transfer energy to a downwind central anode (6). The feedstock material, in the form, for example, of fine powder or sol gel fluid, is injected axially using essentially any carrier gas, such as oxygen, hydrocarbon, nitride or diamond-forming reactive gas (leading to, for example, thermal plasma CVD reactions), etc. The nozzle is designed to preclude internal contact of the feed material with the ID of the anode. One interesting benefit of the EMCP gun is obtaining nano-sized grains within the deposit from the sol-gel feed, with the attendant well known potentially interesting properties associated with these unique microstructures. Additionally, due to its well controlled fine flame, together with uniform particle size distribution, one could consider EMCP as a valuable means for spraying a fine pattern or for repairing TBCs as well as other coatings having process- or service-related damage or holidays in coatings.

An alternative plasma torch is the Czech-developed "Water-Stabilized Plasma" (WSP) gun (7). In this device, the working inert plasma gas is replaced by a water vortex within the inner wall of the cylindrical arc chamber. An arc is created between an expendable graphite cathode, continuously introduced from the rear of the torch, and an external, internally water cooled anode, positioned at a point outside of the gun. The plasma arises from water, the ionic recombination outside of the

torch delivering considerable enthalpy. The WSP operates at 160 kW, enabling the gun to process well over 100 kg/hr of metal powder and over 35 kg/hr of refractory ceramics. With these high through-puts and no need for a plasma gas, one can think in terms of new spray coating economics. In a joint international program, the Czech Institute and the Thermal Spray Laboratory, State University of New York at Stony Brook, are exploring the use of the WSP spraying of metal-ceramic graded deposits to enhance the thermal shock properties of high performance composite materials.

Environmental chamber spraying (also referred to as "vacuum plasma spraying" or "low pressure plasma spraying") allows plasma spraying within a low partial pressure of oxygen (8,9). This results in an oxide-free deposit having mechanical properties superior to those obtained with the traditional plasma gun in air. By plasma spraying in reduced pressure (say, 50 mbar) the flame extends and the velocity of the particles will typically increase from approximately 200 M/sec to perhaps 800 M/sec. This greater particle velocity, coupled with a significantly higher substrate-deposit operating temperature of 800-1000C, yields a coating with a much greater strength-of-adhesion to the substrate and a substantially higher overall density, in many cases approaching theoretical density. Vacuum plasma spraying is commonly employed for the production of bond coats prior to the application of the TBC.

There is a competitive means of applying bond coats using advanced combustion techniques, which yield sonic level particle velocities and thus very well bonded, dense coatings. The so called "high velocity oxy-fuel" (HVOF) methods are being increasingly employed to form bond coats of Ni-base alloys (e.g., NiCrAlY) for intermediate layers.

POROSITY: MEASUREMENTS AND SIGNIFICANCE

Plasma sprayed TBCs have a perplexing array of pores and microcracks which at first sight appear inaccessible to characterization. In particular, it is difficult to distinguish between pores and cracks. In fact, their designation as such may at times be ambiguous. In any case, microcracks can intersect one-another as well as pores, thus, for example, limiting the use of the commonly employed liquid intrusion techniques.

Porosity of plasma sprayed ceramics can be evaluated using Archimedean (water) immersion, mercury intrusion porosimetry (MIP), two techniques of small-angle neutron scattering (SANS - multiple scattering and Porod internal specific surface analysis), optical and scanning electron microscopy (SEM) in conjunction with image analysis. MIP yields a measurement of the surface connected through-porosity; i.e., the total connected porosity. Water immersion measures a lower

porosity volume, i.e., only those pores opened to the surface at atmospheric pressure. On the matter of the SANS measurements, all of the internal porosity contributes to the scattering and, thus, all of the porosity is gauged, within the limits of detectability. Further, it can be demonstrated that SANS measures pores with a margin of error equal to that of the MIP method (10).

In addition to pore size distribution, SANS allows an evaluation of pore shape anisotropy and to some extent, pore orientation. In a joint Stony Brook-NIST program, the pores in plasma sprayed alumina have been modeled as tube-like or disk-like, depending on the neutron beam angle relative to the spray normal. For as-sprayed alumina, pore sizes measured by multiple SANS (MSANS) are in the range 0.6 to 1.2 micrometers and the pore specific surface area is in the range $2\text{-}3\text{x}10^4$ cm^2/cm^3. The majority of the pores are likely oriented with their long axes perpendicular to the deposit surface, i.e., parallel to the spraying direction - these are probably mainly cracks. The pores in the direction parallel to the deposit surface are likely interlamaler pores, not unlike those discussed by McPherson (11). The observed anisotropy as measured by SANS decreases with heat treatment, indicating that phase transformations and sintering lead, not surprisingly, to significant changes in the sprayed microstructure.

The question of the influence of pores on the properties and in-service performance of plasma sprayed TBCs has been the subject of some conjecture. The problem, of course, lies in the difficulty of pore characterization: size, shape orientation, distribution, etc. To a large extent, intuition has played a greater role than good experimental work. Nonetheless, a picture has emerged of the porosity which is at least consistent with the results of many measurements of thermal diffusivity and mechanical properties. And, interestingly, these conclusions, in general, are in accord with the ideas proposed by McPherson who modeled a pore system such that there were essentially two sets of pores: thin, intersplat voids, some 0.1 micrometers in thickness, and pore-like voids, perpendicular to the splats. The latter were identified as cracks and the former were associated with incomplete bonding between layered splats. McPherson also argued that only 20% of the intersplat area was actually physically connected, leaving the rest to voids containing gas or vacuum, depending on the ambient environment. This model is consistent with a reasonable amount of physical data as well as the SANS results discussed above.

MECHANICAL PROPERTIES OF COATINGS

The data base on physical properties developed for TBCs is virtually non-existent; at least data that is available in the public domain. Moreover, testing at operational temperatures has only been by expensive burner rig or engine tests which lead to relative schemes for coatings rather than rigorous fundamental understanding of coatings. As well, limited (and often unverified) predictive

capability of TBC performance has been published. There is, indeed, a dire need to methodically characterize the mechanical properties of TBCs and several approaches are detailed in this section with respect to "understanding the microstructure" of these coatings. Clearly required, then, are qualified testing methods that can measure thermo-mechanical properties of TBCs that can reflect processing variables experienced in the production line.

The ASTM C 633 standard pull-test is used throughout the TBC industry. Normally several (~3 to 5) tests are performed and on the basis of these coating adhesion to the substrate is said to have been verified. There are many fallacies to performing the adhesion test as it is specified in the current ASTM standard; for instance there are (i) strong arguments that the testing procedures are statistically invalid and (ii) that stress concentration around the test specimen leads to a poor reflection of the true material property. However, the fact remains that there is much resistance to alter the *status quo* since then qualification and specification procedures for existing coatings which have proven performance under operating conditions will need to be re-evaluated.

CONCLUDING REMARKS

It is clear that great progress has been made in the design and processing of TBCs. It has become a pressing goal for the gas turbine industry to employ the TBCs thus developed for a greater range of high temperature components. A significantly improved picture of the processing-microstructure-behavior relations will be required to achieve this goal. An additional challenge is to create TBCs systems which are prime reliant and not afterthoughts. The NASA-Lewis group has for many years sought to achieve this and have contributed importantly to life modeling and process dependencies for TBCs.

Fundamental knowledge is required for a better understanding of the complex mechanical properties associated with ceramic coatings. Experimental techniques must be explored which will allow us to understand properties anisotropy, cracking mechanisms, fatigue, etc. And thermal conductivity, controlled through both intrinsic materials limitations and porosity, needs to be carefully characterized and modeled to improve TBC efficiency.

Thermal spray has and will continue to play an important role in TBC production. There are practical and economic reasons for making thermal spray the process of choice in many TBC applications. Precision controlled thermal spray processing methods are increasingly being introduced, lending to the technology reproducibility not previously thought possible. The future will see new processes and materials which will further enhance the utility of thermal spray technology for the gas turbine industry.

ACKNOWLEDGMENTS

The authors' research on TBCs was sponsored by NASA-Lewis in the 1980's and by Caterpillar Inc. in the area of thick TBCs in the early 1990's. We value the opportunities to have worked with these groups.

REFERENCES

1. H. Herman. MRS Bull., Vol. 13 (1988) 60.

2. E. Pfender, Plasma Chem. and Plasma Proc., 9 (1989) 167S-194S.

3. M.A. Vardelle, A. Vardelle, P. Fauchais, and M. Boulos, A.I.Ch.E.J., 29 (1983) 243.

4. H. Herman, KONA- Powder Science and Tech., No. 9 (1991) 187-199 and H. Herman, H. Wang and C.C. Berndt, in Ceramics Films and Coatings, (Ed. J. B.Wachtman and R. A. Haber), pp. 131-188, Noyes Publ., 1993.

.5. R.A. Zatorski and H. Herman, High Performance Cer. Films and Coatings, (Ed. P. Vincenzini) (1991)591.

6. D. R. Marantz, "Electromagnetically Coalesced Multi-Arc Plasma Torch with True Axial Powder Feed", 1990 National Thermal Spray Conf., Long Beach, CA. ASM Intern., Materials Park, OH.

7. P. Chraska and M. Hrabovsky, "Water Stabilized Plasma Spraying of Ceramics", Proc. Intern. Thermal Spray Conf., Orlando, Fla., ASM Intern., (1992) 81.

8."Microstructure of Vacuum Plasma Sprayed Coatings", S. Sampath and H. Herman, Proc. National Thermal Spray Conference, Cincinnati, ASM Inter., Metals Park, Ohio, (1989) 1.

9. W.J. Brindley and J.D. Whittenberger, Matls. Sci. and Engg. A163 (1993)33.

10. J. Ilavsky, "Porosity in Plasma Sprayed Ceramics", Ph.D. Thesis, SUNY-Stony Brook, 1994.

11. R. McPherson, Thin Solid Films, 112 (1984) 89..

PVD THERMAL BARRIER COATING APPLICATIONS AND PROCESS DEVELOPMENT FOR AIRCRAFT ENGINES

David V. Rigney, Rudolfo Viguie, and David J. Wortman
GE Aircraft Engines
Neumann Way
Cincinnati, OH 45215

and DW Skelly
GE Corporate Research
K1 Metallurgy
Schenectady, NY

ABSTRACT

Thermal barrier coatings (TBC's) have been developed for application to aircraft engine components to improve the life in an increasingly hostile thermal environment. The choice of TBC type is related to the component, intended use and economics. The selection of Electron Beam Physical Vapor Deposition (EB PVD) processing for turbine blades is due in part to part size, surface finish requirements, thickness control needs, and hole closure issues.

Process development of PVD TBC's has been carried out at several different sites including GEAE. Some of the influences of processing variables on microstructure are discussed. The GEAE development coater and initial experiences of pilot line operation are discussed.

INTRODUCTION

Increases in turbine inlet temperatures have led to a need for a thermal barrier coating (TBC) on turbine airfoils and other components for advanced engines. TBC's provide an insulating layer of yttria stabilized zirconia on the surface of the turbine airfoil. The low thermal conductivity of zirconia allows internal cooling air to more effectively cool the part, lessening the amount needed to achieve the design temperature. By requiring less cooling air, overall engine performance is improved and, by reducing the part temperature and reducing thermally induced strains, component life is increased.

Two types of thermal barrier coatings have been developed for aircraft engine use: plasma spray and PVD. Numerous versions of plasma spray TBC's have been used successfully on a wide range of components. The initial applications were in the combustor and afterburner where atmospheric plasma spray (APS) bond coats of NiCrAlY were successful with a porous 7% YSZ top coat. In the late 1980's, plasma spray TBC's were introduced to stationary nozzle components in the turbine. Here, higher temperatures forced the use of low pressure plasma spray MCrAlY bond coats for improved oxidation protection and longer life. Also in the late 1980's, PVD TBCs were developed to the point where production introduction on both turbine blades and vanes were practical.

Sufficient experience has since been gained to allow the designer and materials application engineer to wisely make selections of TBC for specific application needs. Selection of a plasma spray or PVD TBC are based on the ability of the coating to meet the performance and cost requirements of the application. Limited information on life

comparison of plasma and PVD TBCs available in the literature (1) shows that in both burner rig tests and engine tests, PVD TBCs have longer lives. However, improvements in plasma spray TBCs, both in processing and bond coat composition have been made (2) which may have reduced the differences significantly. Engine test experience with plasma spray TBCs at GEAE has been good with recent testing in an industrial power engine for times up to 20,000 hours.

Other than the life issue, there are significant differences between the two types of coatings that drive the selection process; surface finish, hole closure and cost. PVD TBCs are much smoother as deposited (56-60 μin vs. >200 μin). After surface finish improvement, PVD still has the advantage with better than 30 μin possible. The importance of surface finish depends on the application as shown in **Figure 1**. On stage 1 airfoils, with high pressures and velocities, a smooth finish is important whereas on latter stages this is not as important. Surface finish on combustor and end wall surfaces is less important as well.

Most HPT airfoils in advanced aircraft engines have many small (0.010-0.020" diameter) cooling holes which can be closed or the flow reduced by coating. PVD coatings taper very rapidly at the opening of the cooling hole (**Figure 2**). Plasma spray coatings however have a greater tendency to build up coating at the hole opening. The sticking and build up of the molten plasma sprayed particles can close over small cooling holes. Several approaches have been attempted to circumvent this problem including drilling holes after coating, filling holes with wires during spraying, and over sizing holes but none have proven to be universally acceptable.

Costs to apply plasma spray TBCs are generally lower than PVD, in large part the result of lower capital costs. However, other issues can make the PVD less expensive. For example, small parts favor PVD because many can be coated simultaneously. On the other hand, some applications where only one surface is being coated may allow a full ring of parts to be plasma spray coated at one time. For PVD the same space in the coater is taken up whether all surfaces or only one surface is being coated. The overall assessment from the above discussion is that both plasma and PVD TBCs will continue to have applications in aircraft engines. A multitude of issues will determine which process is best for a given part. In the balance of the paper, issues related to PVD processing of TBCs will be covered.

Adherence and durability as well as producibility and productivity are key issues for TBCs. Loss of the TBC will result in increased metal temperatures (at least in the area of TBC loss) and potentially shorter part lives. Initially, a very thin alumina scale exists between the bond coat and the zirconia (**Figure 3**). This alumina scale is formed by oxidation of the surface during preheat and the initial moments during deposition of the zirconia in the coating chamber. In service, growth of the alumina scale occurs through oxygen transport through the zirconia. The dense alumina scale will be under high compressive loads when cooled to room temperature due to the lower thermal expansion of the alumina scale compared to the metallic substrate. Ideally, the open columnar structure of the zirconia will not contribute additional compressive stresses. Eventually, thickening of the alumina scale produces sufficient compressive force such that the scale will buckle, carrying both the alumina and the overlying zirconia with it. (**Figure 4**) This failure should occur after a relatively long and predictable time and therefore would permit the designer to use the TBC capability in the design life consideration for the part. Unfortunately, very short lives can occur if the bond coat surface is not properly prepared or if the deposition process parameters are not well controlled or are sensitive to process variations beyond the capability to control.

An important aspect of PVD TBC development is selection of process parameters to provide a reliable, reproducible coating. Although much effort has been expended toward this goal by several sources, very little has been published and this remains an area of competitive development. Experience with different equipment designs has shown that results obtained in process development are closely linked to the equipment. In the following sections, some of the process development experiences at GE Aircraft Engines are discussed.

Processing of PVD TBC Coating

The PVD TBC system requires a multiple step coating sequence as shown in **Figure 5**. The development of a highly reliable PVD TBC requires establishment of precise process controls on all process steps.

The function of the bond coat is to provide a stable base for adherence of the ceramic insulation layer. The bond coat must generate a stable, slow-growing alumina scale.

In the PVD process the coating material is heated to vaporization temperatures through kinetic energy exchange between the electron beam (≈38 kV) and the coating material. The process is unique in that large amounts of energy can be focused in a small area. Evaporation from large areas can be achieved by sweeping the beam over the surface of the material. Ceramic materials like ZrO_2•7%Y_2O_3 have very high melting points (≈3200°C) and very low thermal conductivities. It is estimated that the evaporation temperature at the point of electron beam impact is > 5000°C. **(Figure 6)** The coating material evaporates atomistically (or molecularly) and condenses onto the part. The condensed atoms can move on the surface for short distances, and then form nuclei and begin grain growth. Columnar growth is the norm; however, grain orientation may be affected by processing temperature, surface morphology, etc.

To achieve good PVD TBC coatings, parts must be processed at elevated temperatures. The coating morphology is a function of the melting point of the coating material and the temperature of the substrate being coated (3,4, 5). The closer the part temperature is to the melting point of the coating material, the greater the surface mobility of the condensed atoms, and the denser the coating. The coating temperature limit for nickel-based alloys is about 1100 - 1150°C, owing to the melting point of the substrate and the stability of the bond coat - substrate system.

Process Sequence:

Below is a generalized process sequence used to apply ceramic coatings.

- Surface Preparation.

Proper engineering the bond coated surface for subsequent coating is critical to any successful coating process. For PVD TBC coatings, the surface preparation serves to normalize the chemical and physical natures of the part such that a predictable coating can be applied. Examples of the effect of different surface textures on a subsequent ceramic top coat microstructure are shown in **Figure 7**, for different coarseness of media: polished, 220 mesh, 80 mesh, and 54 mesh.

- Loading and Preheat

After cleaning and surface preparation, parts are weighed and fitted into mask/holders. Weighing the parts before and after the coating process has been found to be a rapid, precise technique to non-destructively determine the thickness of coating deposited. The weight gain during coating is compared against data from metallographic examinations in prior runs. Parts are loaded into a load lock, evacuated to a low pressure, and then moved into a separate preheat chamber. They are heated to coating temperature in a programmable heater.

- Coating

The microstructure of the resultant coating is a complex function of the many variables contributing to the coating: material, deposition rate, pressure, part rotation rate, geometric attitude, temperature, etc. The substrate temperature is one of the most important parameters affecting coating microstructure and life and the temperature must be kept within a defined temperature envelope during coating deposition. The parts to be coated are heated by several different sources during coating: heat of condensation, radiation from the hot pool, and heat from impingement of electrons reflected from the melt. If the thermal input from these sources is insufficient, additional heating must be provided by reflection (insulation), by an auxiliary electron beam source, or other means.

Unlike metallic systems, ceramic materials such as ZrO_2•8 Y_2O_3 dissociate during evaporation, and require addition of oxygen to compensate for gas pumped out of the chamber.

Removal and Post Coating Processing

After coating, the parts are returned to the load lock, where they are cooled and the lock vented. The parts are then removed and reweighed. Satisfactory comparison with weight gain envelopes derived from sectioned blades qualifies the parts for the next evaluation steps and further processing.

Line-of-Sight and Rotation Effects on PVD TBC Microstructure

The effects of line of sight deposition were studied by coating a stationary cylinder with a grit blasted surface finish over a single source. The thickness and structure shows a very thin (<1/2 mil) fine-grained coating deposited on the backside of the cylinder (**Figure 8**). A thicker, porous (open grain) coating is deposited at the tangency (grazing) point of the vapor. On the other hand, at the static - head-on position, the coating is much more dense, and thicker (>9 mils).

If a part is to be coated uniformly, it must be rotated or rotated and tilted. Most production coaters use a N/C control system to control orientation and rotation. (**Figure 9**) Others may use complex tooling and fixturing concepts to achieve similar results. (**Figure 10**).

The substructure of the coating crystals is significantly altered by the effects of rotation. **Figure 11** shows different substructures generated by the rotation of a simulated part over the coating source. The two photos show a view of the growth of 'c' shaped structures formed during each revolution within the main crystal at two different rotation rates. The character of each is the same. The relationship of the 'c' structures is a function of rotation rate and the vapor flux at the surface (Evaporation rate and distance from the source). Thus, the beginning of the structure results from the small amount of deposit on the substrate when facing away from the source. As the substrate rotates into

the main stream of evaporated vapor, the condensation rate greatly increases. Continued rotation results in decreasing condensation rates. The fine structured grains were deposited onto a surface rotating at ≈ 6 rpm; the coarser structure was grown on a surface rotating at about 0.4 rpm.

The use of TBC's for performance benefit depends on a high degree of confidence in the life of the product. As part of the development effort to produce this improved TBC, a pilot production scale PVD Coater was purchased in 1989 and installed in 1992. The coater was designed with a full production-scale evaporation chamber, but with only one parts handling chamber. While this reduced the throughput, added space was available for process monitors and controls for development work. **(Figure 12)**

The coater is equipped with two 200 kW evaporation EB guns which evaporate from two ceramic sources and one over source heating EB gun. The coater can coat ten CF6-80C2 Stage 1 HPT blades simultaneously in a uniform 140 mm x 420 mm coating zone. Three minicomputers allow for easy programming and control of the processing conditions and continuous logging of more than 90 process and equipment variables. Coating pressure, rotation, rate, lateral and tilt position, electron beam parameters and adjustments; cooling water temperature, and time since oil change (pumps) are examples of logged items.

Initial development efforts at GEAE concentrated on producing a coating equivalent to the industry standard, i.e. that which is available on the commercial market. A designed experiment was conducted to evaluate significant parameters, including those shown below:

1. Part temperature during preheat
2. Part temperature during coating
3. Pressure in the coating chamber
4. Oxygen partial pressure in coating chamber
5. Part rotation rate during coating

As part of the experiment, bond coated alloy button specimens were prepared. The primary evaluation method was cyclic exposure in a furnace (FCT Test) at 1093°C (2000°F) and 1135°C (2075°F). Each cycle consisted of 45 minutes at temperature and 20 minutes heating and cooling. The number of cycles to ≥10% spall of the ceramic coating constituted coating life. All the parameters exhibited acceptable furnace cycle lives and compared favorably to concurrent and past cyclic test results obtained from specimens prepared at commercial sources, showing that the overall process is robust, at least with regard to these parameters. Three parameters were determined to have a significant effect on spallation life: 1) preheat temperature, 2) coating temperature, and 3) part rotation rate. Preheat and coating temperature were shown to be most significant pairings necessary to produce consistent performances in the FCT Test.

The initial result of the program was the establishment of a Baseline TBC coating which is currently being applied on a pilot scale. The objectives of operating the pilot line are to provide parts for field evaluation, gain operating experience with the coater's systems, and assess the continuing constancy of the TBC process. As part of the pilot line, two lots of bond coated R'N5 buttons were coated along with pilot production hardware over a period of more than 18 months. The results of furnace cycle testing is

shown in **Figure 13**. The data show - happily - that there were no infant mortalities. On the other hand, there developed an increase in scatter in both bond coat lots after about six months into the sequence, and the 3-sigma value of the data is rises from about 36% of the mean to ±66 % of the mean (over all the data). At this point, the causes for these variations have not been sorted through. Some of the variations have been attributed to piece-to-piece variation in bond coat application, surface treatment, and run-to-run variations in the ceramic deposition. Data is being gathered on the durability and reliability of the mechanical and electronic systems that make up the coater.

Summary

Development activities are continuing, and clearly must focus on several process aspects of the TBC system: the bond coats; the surface preparation and cleanliness; PVD process parameters, monitors and controls. Additional engine testing and feedback of performance of coated hardware from field exposures will provide additional insight into the performance capabilities of the TBC. The continued use of the coater for pilot production is very complementary to the project. Quality issues observed in producing coated hardware within the same coater can be addressed by modifying the development plans. Likewise, the production experience helps maintain a focus towards development of a producible TBC process.

1. Meier, S.M., and Gupta, D.K., "The Evolution of Thermal Barrier Coatings in Gas Turbine Engine Applications," ASME Conf. Pub., **92**-GT-203
2. Wortman, D.W., Nagaraj, B.A., and Duderstadt, E.C., Mat. Sci. and Eng., **A121**, 433 (1989)
3. Movchan, B.A., and Demchishian, A. V., Phys. Met. Metallography, **28**, 83 (1969)
4. Thornton, J.A., J. Vac. Technology **11**, 666 (1974)
5. Thornton, J. A., Ann. Rev. Mater. Sci. **7**, 239 (1977)

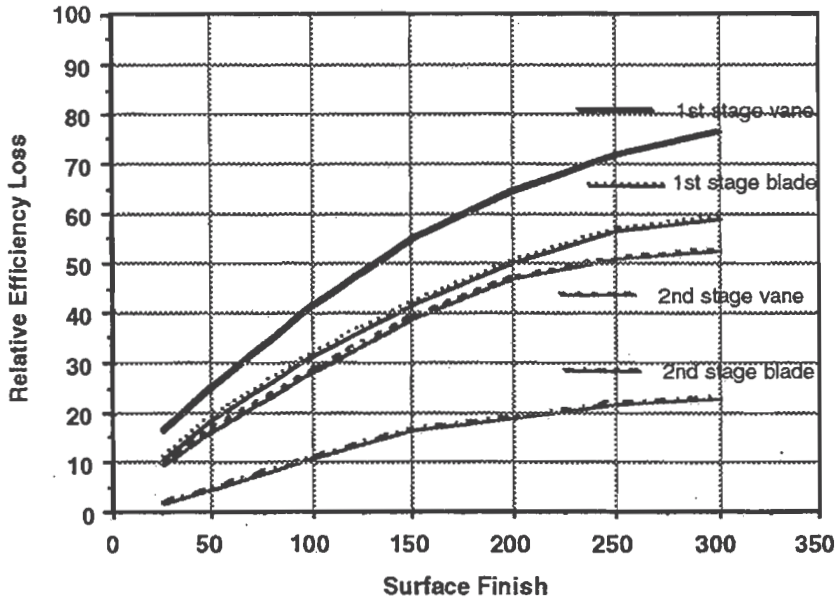

Figure 1. Effects of Surface Roughness on Loss of Efficiency.
The aerodynamic efficiency of the stage 1 and 2 high pressure turbine vanes and the stage 1 high pressure turbine blades is very sensitive to the surface roughness of the suction wall surface finish.

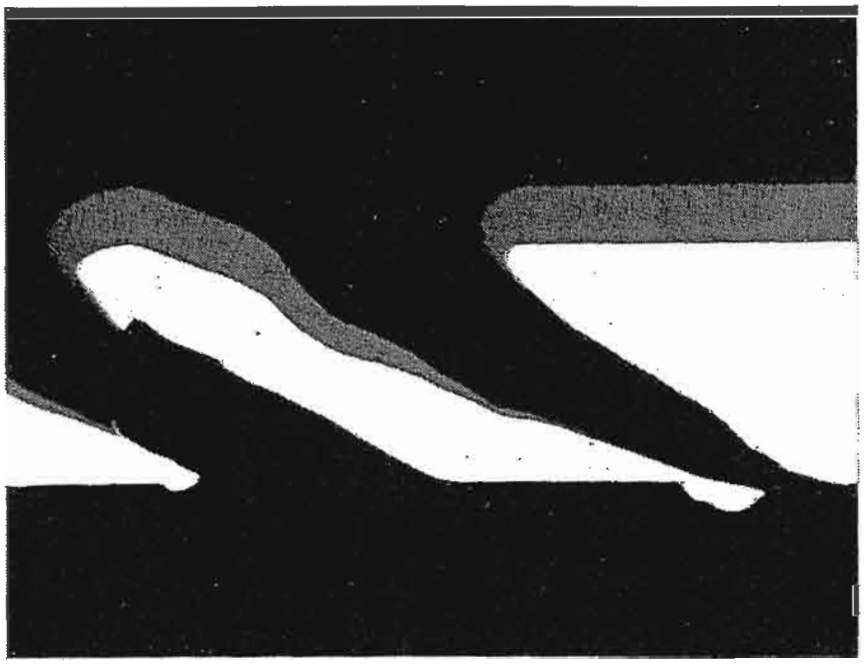

Figure 2. Component Showing PVD Coating in Region of Cooling Holes.
Deposit is approximately 0.014 inch (350 microns) thick. The atomistic nature of the PVD coating process results in a rapidly, smoothly tapered coating at the hole entrance. Laser drilling usually results in the throat of the hole (the narrowest dimension) to be located near the interior end of the hole.

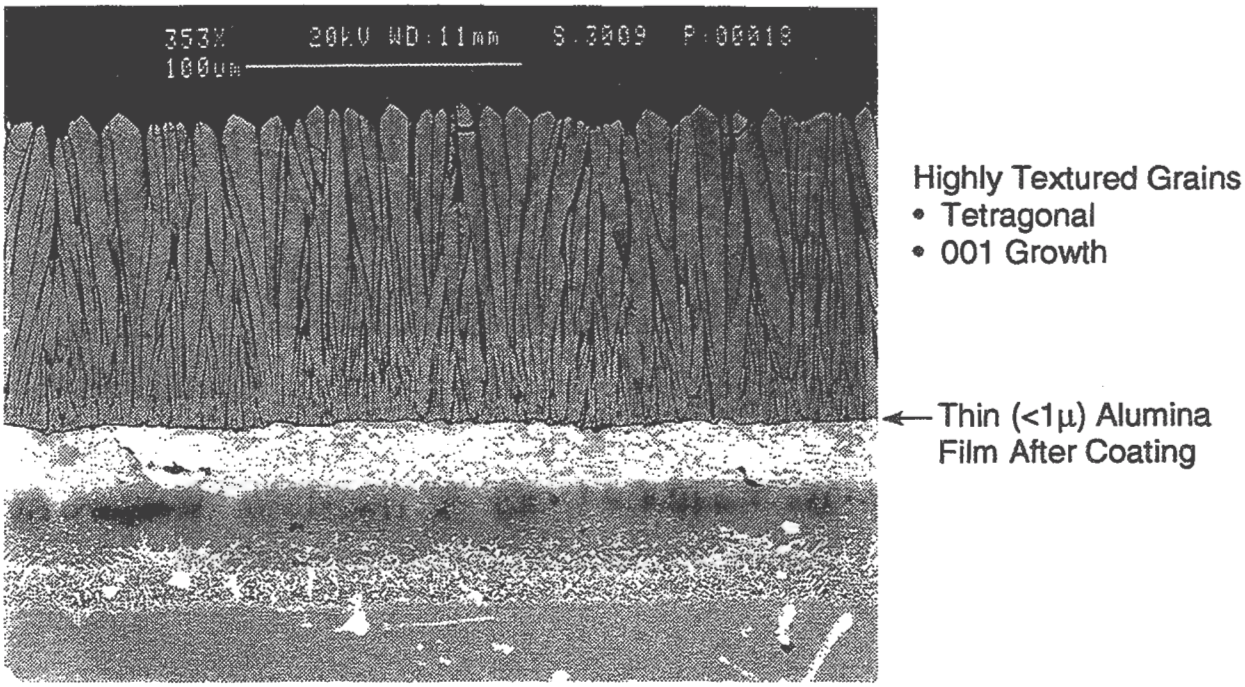

Figure 3. Cross Section of Thermal Barrier Coating Characterizing PVD YSZ Deposit.
Thin alumina film chemically bonds the YSZ to the bond coat. High modulus, oriented columnar grains are characteristic of PVD coatings. Low modulus in surface plane results in ability to withstand high strain rates.

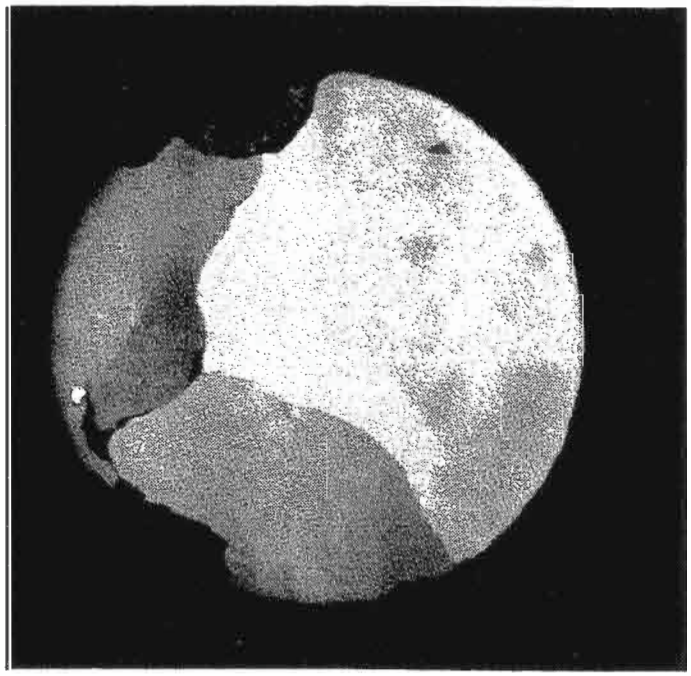

Figure 4. PVD TBC Coated Button at End of Cyclic Test.
Button shows Oxidation growth causes compressive loading on Al_2O_3 and results in lifting of both Al_2O_3 and thermal barrier.

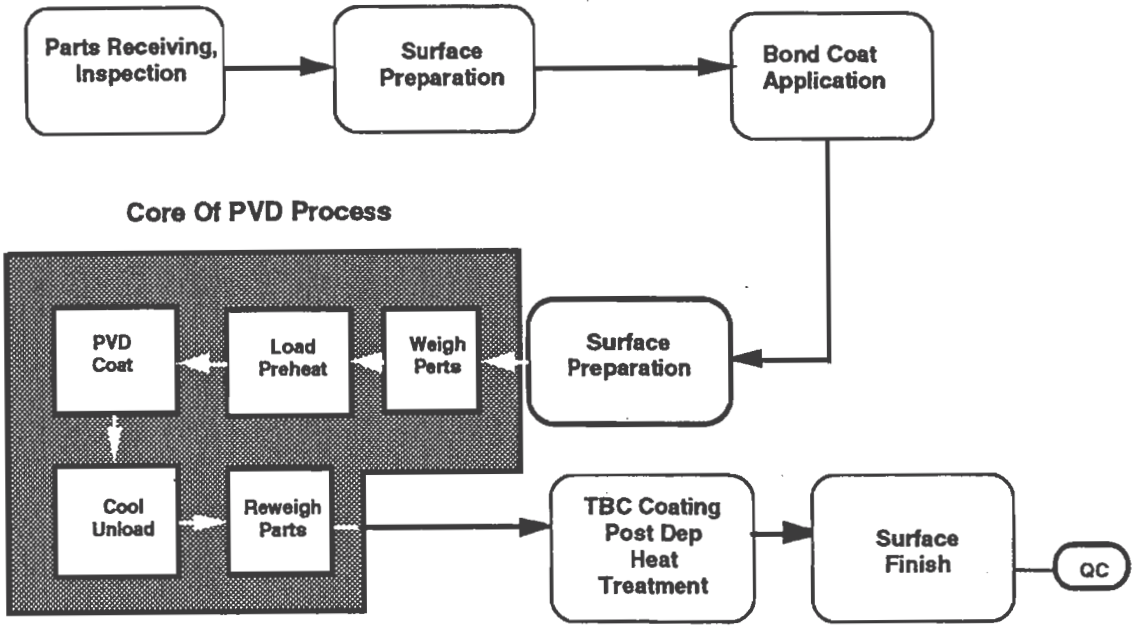

Figure 5. Schematic of PVD TBC Process Sequence.

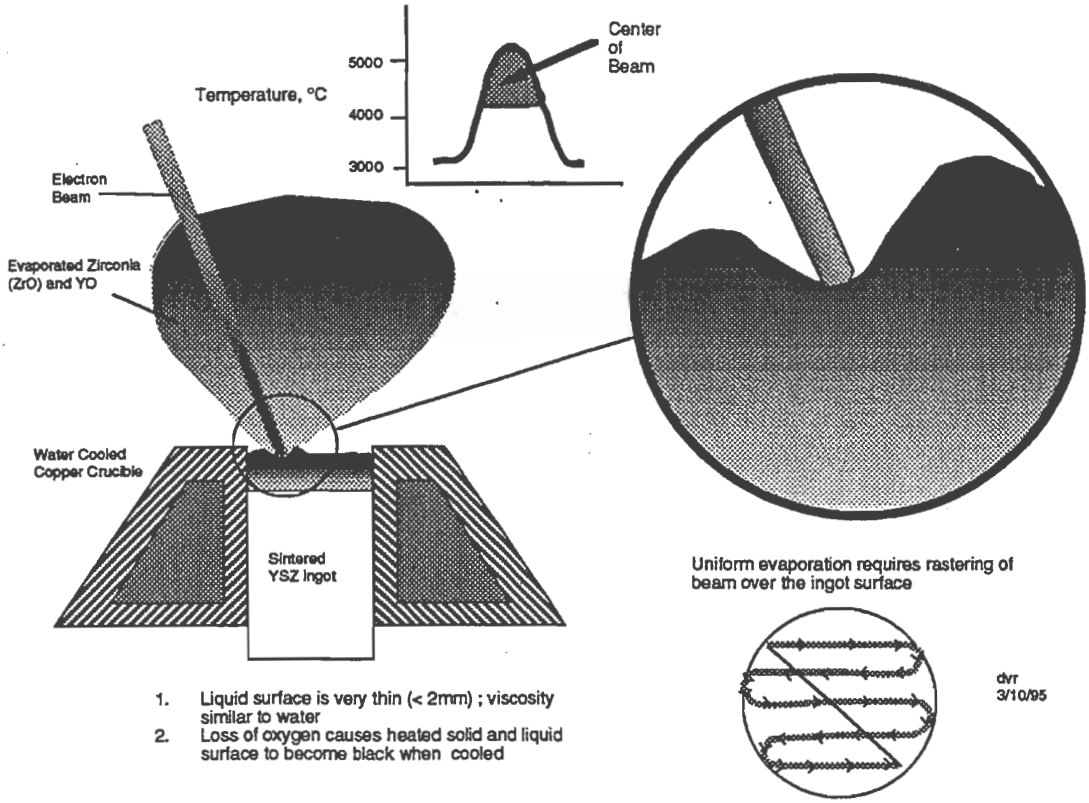

Figure 6. Schematic Illustrating Evaporation from Ceramic Pool.
Evaporation takes place when liquid being directly impinged by electrons is super heated. In the YSZ system, the liquid pool is only two to three millimeters deep.

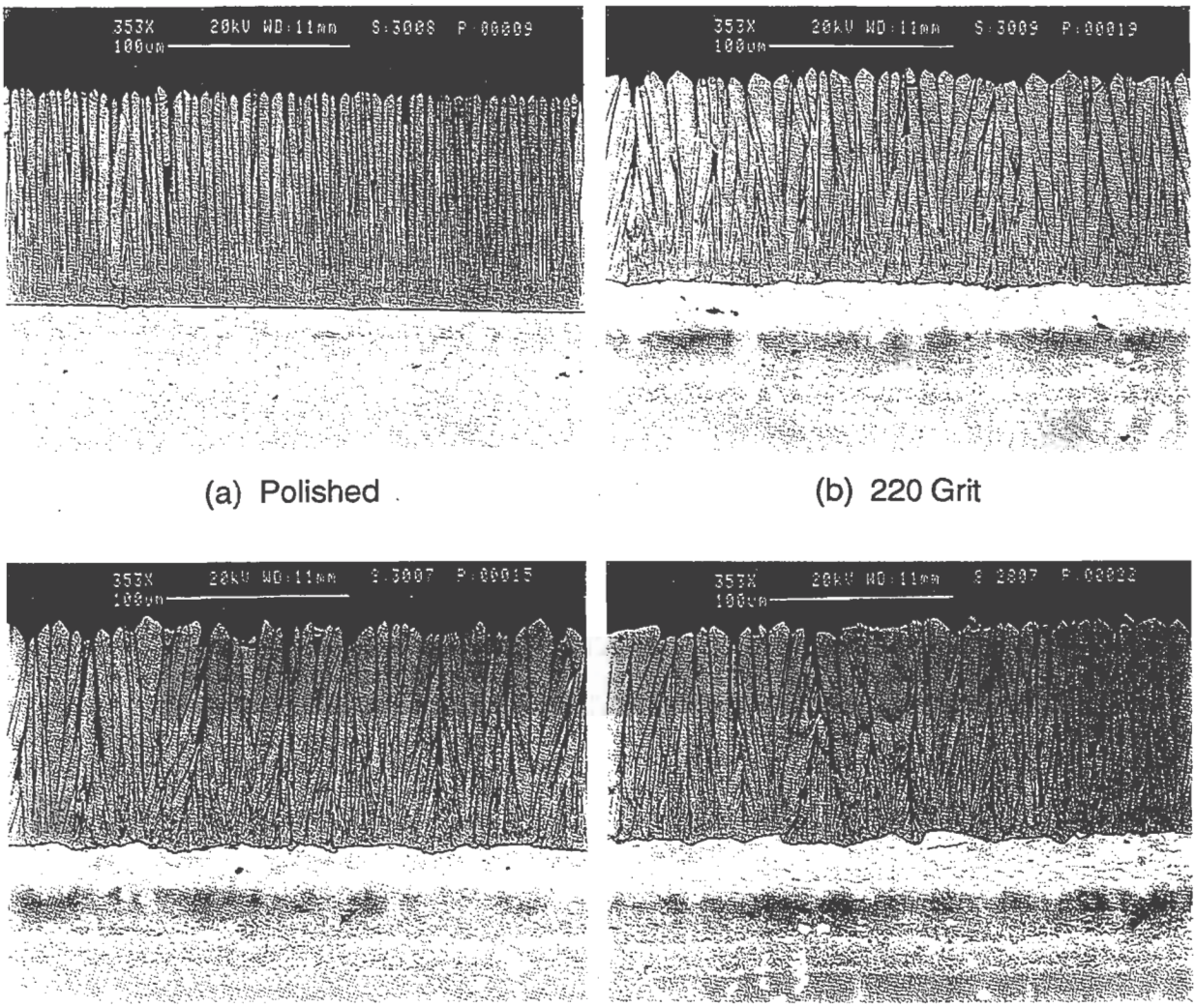

Figure 7. Bond Coat Surface Texture has a Major Influence on Ceramic Top Coat Microstructure. *Figure 7a shows a polished surface resulting in deposition of uniform, dense columnar structure, whereas 7b, c, and d show gradations of greater porosity and nodularization from 220, 80, and 54 mesh grit blasted surfaces .*

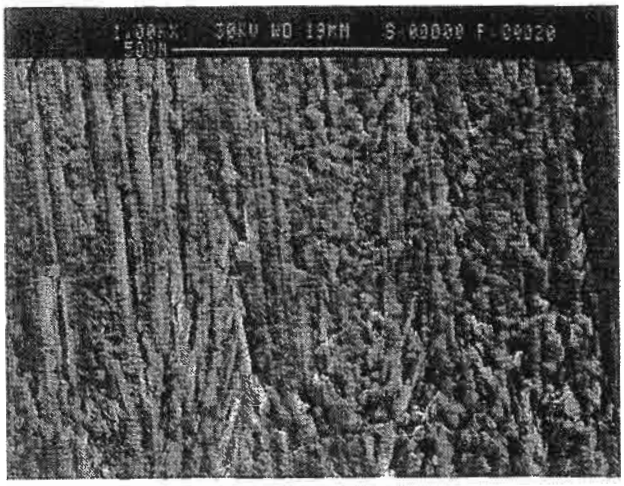

(a) Front Side

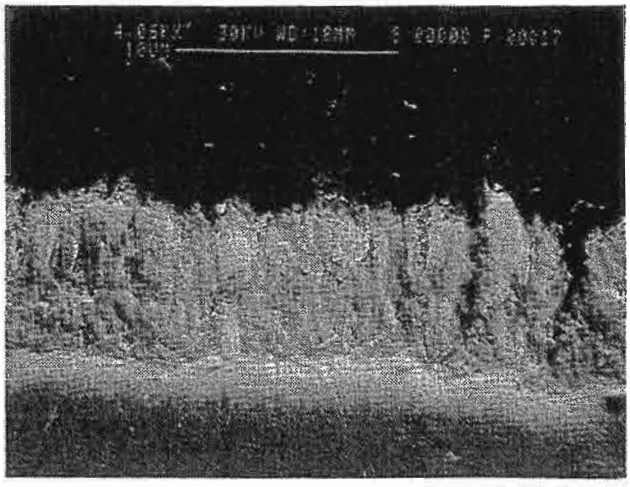

(b) Back Side

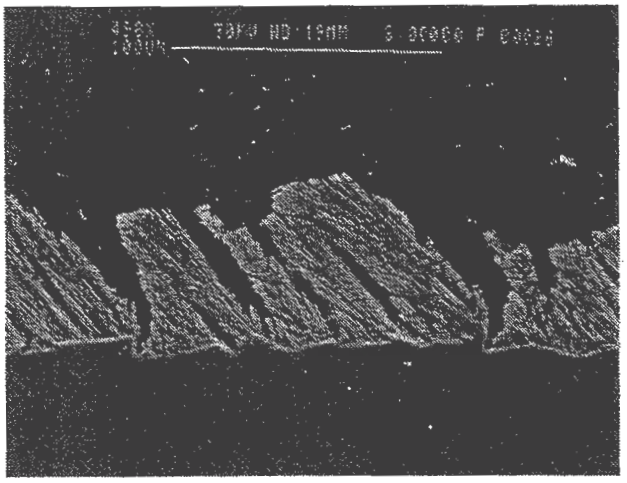

(c) Grazing

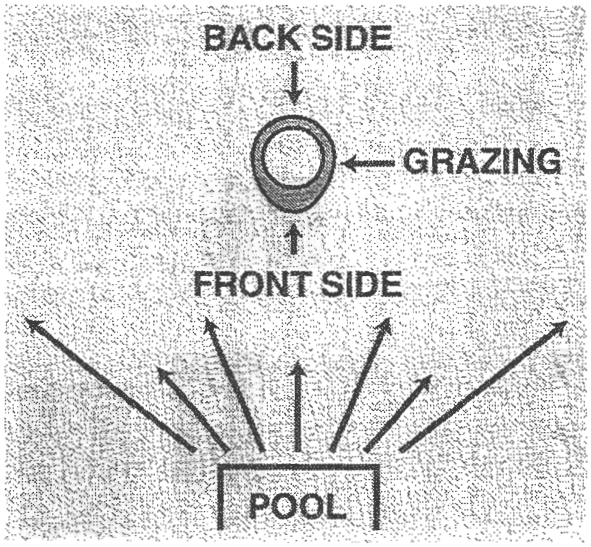

Figure 8. Coating Structures Deposited on Stationary Cylinder. *(a) Thin fine-grained columnar film deposited by gas-scattering on part facing away from source. (b) Open, feathery deposit at tangency point on cylinder of vapor flux from pool. (c) Thick, dense structure deposited on surface facing pool.*

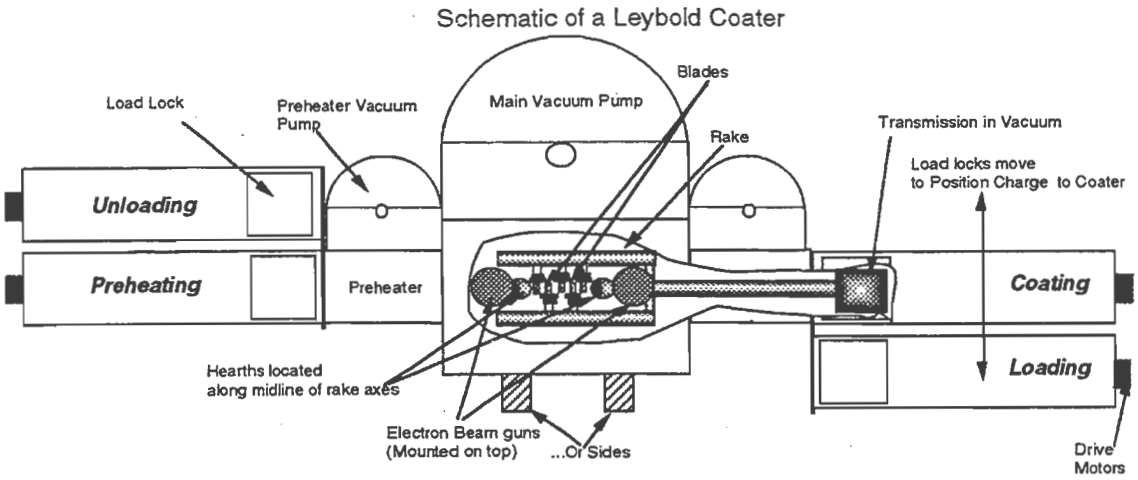

Figure 9. Schematic of Generic Leybold-design PVD Coater. *Coater uses multiple pools to generate a large vapor cloud. These pools may be heated from above the pools or , using magnetics to assist in directing the electron beams, from sources aimed from the side. Parts are oriented over the pools on numerically controlled gear-driven holders on shafts to allow multiple part coating. The parts can be tilted to coat platforms and other surfaces. Multiple shafts allow nearly continuous coating of parts by timing the major process events in a four lock system: (1) loading of parts; (2) preheating parts to coating temperature; (3) coating deposition; and (4) Cooling and unloading.*

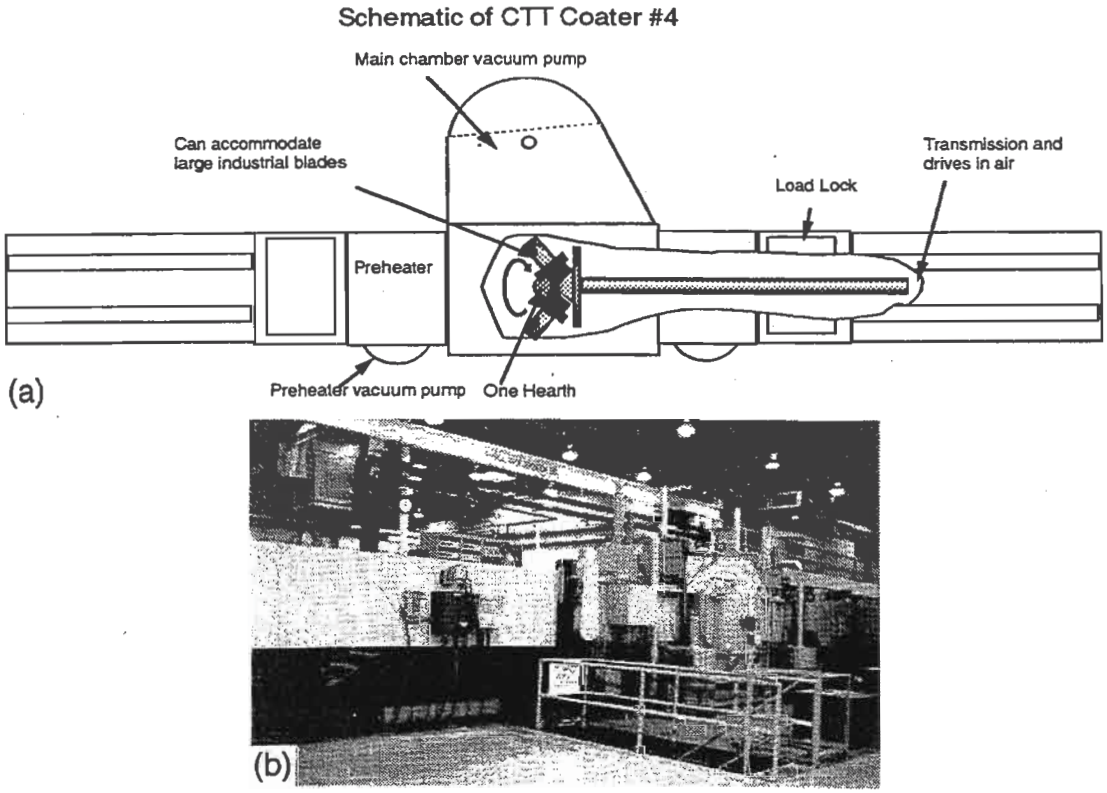

Figure 10. (a) Schematic of Large Coater Made by Temescal. *Coater uses complex tooling and large weight carrying capability of shaft to achieve coating of many parts simultaneously. Weight carrying capability and size allows large industrial turbine components (>10 kg) to be coated. Opposed load locks and shafts allow efficient use of coater evaporation time. (b) Photograph of large Temescal Coater. Note operator just behind coater. Courtesy Chromalloy Turbine Technologies.*

0.18μ/Rev. 2.6μ/Rev.

Figure 11. Photomicrographs Showing Grain Substructures Resulting from Rotation Effects.

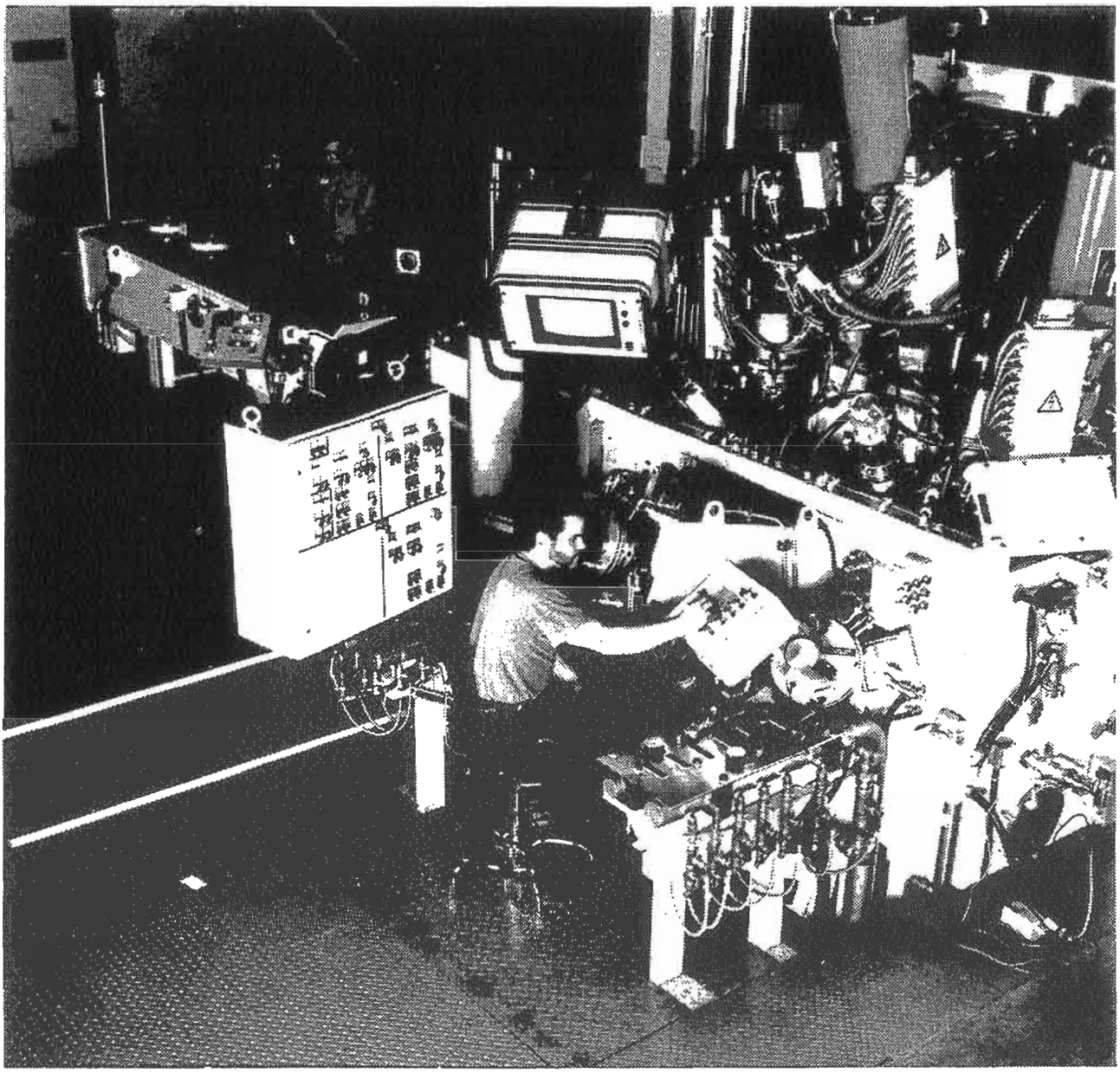

Figure 12. General Electric Prototype EB PVD Coater. *Coating chamber is production-scale as is the loading chamber.*

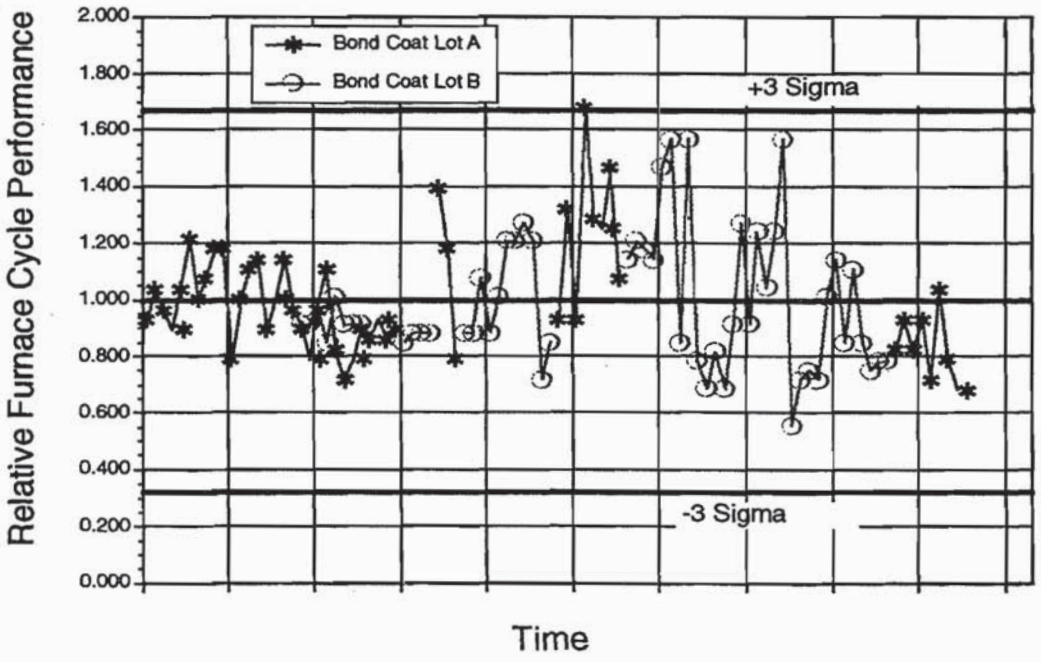

Figure 13. Relative Furnace Cycle Tests Performed on Specimens Coated During Pilot Production Operations in the GE Prototype Coater Over an 18 month Period.

JET ENGINE APPLICATIONS FOR MATERIALS WITH NANOMETER-SCALE DIMENSIONS

J.W. Appleby, Jr.
Pratt & Whitney
West Palm Beach, Florida

The performance of advanced military and commercial gas turbine engines is often linked to advances in materials technology. High performance gas turbine engines being developed require major material advances in strength, toughness, reduced density and improved temperature capability. The emerging technology of nanostructured materials has enormous potential for producing materials with significant improvements in these properties. Extraordinary properties demonstrated in the laboratory include material strengths approaching theoretical limit, ceramics that demonstrate ductility and toughness, and materials with ultra-high hardness. Nanostructured materials and coatings have the potential for meeting future gas turbine engine requirements for improved performance, reduced weight and lower fuel consumption.

PROCESS, PROPERTIES, AND ENVIRONMENTAL RESPONSE OF PLASMA SPRAYED THERMAL BARRIER COATINGS

Richard C. Novak
Pratt & Whitney Talon, Inc.
Rocky Hill, Connecticut 06067

ABSTRACT

Experimental results are shown which demonstrate that the properties of plasma sprayed fully stabilized zirconia are strongly influenced by the process parameters. Properties of the coatings in the as-sprayed condition are shown to be additionally influenced by environmental exposure. This behavior is dependent on raw material considerations and processing conditions as well as exposure time and temperature.

Process control methodology is described which can take into consideration these complex interactions and help to produce thermal barrier coatings in a cost effective way while meeting coating technical requirements.

INTRODUCTION

The key to producing thermal barrier coatings which meet technical and manufacturing requirements is to carefully integrate the design, materials and processing aspects of the development work at the earliest possible stage. Through this approach all aspects of the problem can be considered in an integrated manner, and the most cost effective solution can be obtained, given the time and funding constraints of the development and prototype project phases.

An integrated systems approach was taken by United Technologies Corporation in developing thick ceramic coatings for abradable seal applications in aircraft gas turbines (Ref.1) and for diesel engine thermal barriers (Ref.2). This paper will discuss the relationship between thermal spray processing (including powder characteristics) and resultant coating properties, both as-sprayed and after thermal exposure. Steps required to adequately control the fabrication process to enable production of high quality parts at high manufacturing yield will also be described.

PROCESS-PROPERTY RELATIONSHIPS

In developing ceramic coatings for TBC or abradable seal applications, it is necessary to understand the thermal and mechanical properties of the coatings in order to apply the necessary design criteria. This can be done for thermal spray coatings by fabricating samples of sufficient thickness, removing the coatings from the substrates, then machining and testing samples in the appropriate manner. In developing the abradable seal, a large data base of basic mechanical and thermal properties was generated on yttria stabilized zirconia in the as-sprayed condition following this method.

Initial work was focused on strength properties of fully stabilized zirconia (fsz) with 20% yttria in the starting powder. In order to determine the potential for the coating to meet the design criteria under the intended conditions, a statistically designed experiment was established in which process parameters were varied over a wide range. The strength of the coatings was measured in four point bend tests at room temperature.

The results of the tests are provided in Figure 1 in which the strength is shown as a function of a parameter related to particle heating and velocity during the deposition process. This heating and velocity parameter, which combines the basic process variables of arc gas flow, gun-substrate distance, power, and relative speed, was formulated based on a model which hypothesized that strength of the coating is controlled primarily by mechanical interlocking of molten splats with some intersplat bonding possible at higher particle temperatures. The photomicrographs in the figure show that the higher strength coatings had a more tightly fitting, lower porosity structure than those with lower strength.

This matrix of tests provided clear documentation of a strong relationship between one critical coating property (strength) and the thermal spray process. From the designer's view this was desirable since it offered flexibility in optimizing coating behavior. From the manufacturer's view it highlighted the need for process control in order to reliably achieve the desired qualities in the coating.

As might be expected, the implications of this initial work were wide-ranging. Indeed it was found that nearly all critical coating properties were closely tied to processing conditions. An example is shown in Figure 2 which presents the relationship between solid particle erosion behavior at 1315°C and the room temperature strength of the fsz coating. The strength of these coatings was varied by changing the process parameters in the same manner as in obtaining the data in Figure 1.

The erosion results show a threshold of coating strength, above which the erosion rate is low and independent of strength. In this regime the erosion mechanism involves "plowing" of the erodent in the well-bonded coating which caused a relatively low amount of removal. At strengths below the threshold of approximately 14 MPa, entire splats were removed by the erodent, and the erosion rate was strongly dependent on the interparticle bonding in the coating. Therefore the erosion behavior, which is critical to the durability of many thermal barrier coatings, is very closely related to the process and how well it is controlled.

THERMAL EXPOSURE EFFECTS

The next step in the overall property-process assessment was to determine the effect of environmental exposure on the coating behavior. Following the same procedures for producing samples as used for as-sprayed coatings, test coupons of fsz were exposed to various time - temperature conditions then tested at room temperature. Preliminary results, summarized in Figure 3 showed a significant effect of the thermal exposure on mechanical and thermal properties of the material. Later, more detailed work on thermal conductivity (Ref 3) showed that the behavior could be predicted with reasonable accuracy over a wide range of exposure times and temperatures (Figure 4). Most importantly, the effect of elevated temperature exposure was very large, with increases of a factor of 4 or greater over as-sprayed conductivity or for exposure conditions greater than approximately 980^{o}C. This fact has a critical impact on the intended primary use of the coatings (thermal barriers) as environments of advanced engines become hotter and the desired coating and component lives are longer.

The cause of this behavior was attributed to sintering of the coating. The conclusion was reached following experiments in which coatings were placed in a dilatometer and maintained at a temperature of 1510^{o}C for 24 hours. Changes in length were recorded over the exposure time

and are presented in Figure 5 along with SEM photos of coating fracture surfaces before and after the exposure. The measured shrinkage was caused by the sintering which is evident in the SEM photos. The photos show that all evidence of the splat structure and directional solidification within the splats was removed by the exposure. The result is a relatively uniform sintered ceramic with strings of porosity at former splat boundaries.

Further investigation of this behavior demonstrated that processing variables again played a major role as was the case for the as-sprayed properties. The first of these variables was the chemistry of the starting powder. A series of samples was fabricated from the standard fsz powder which was found to contain 0.7% silica as an impurity. As shown in the left portion of Figure 6, exposures over a range of temperatures for 24 hours produced length reduction (shrinkage) in a predictable manner, closely following the form of the thermal conductivity results.

It is important to note that this shrinkage is also a source of stress in the coating during service. Since the coatings in these tests were free standing bodies, the shrinkage did not induce any distortion or stress in the coatings. In fact it is likely that the exposure tended to relieve internal stresses caused by the rapid solidification of the molten droplets during coating fabrication. In service, however, the coating is adhered to a bond coat, and the shrinkage will cause a combination of tension in the coating and shear at the interface. These can lead to the frequently observed mud flat cracks and/or delamination when combined with other stresses present.

Transmission microscopy of the exposed samples showed the presence of glassy aluminum-silicon phases at the grain boundaries (Fig. 7). These phases, apparently due to chemical interaction and/or simple melting of impurities, were postulated to act as a liquid phase sintering agent, causing the zirconia to sinter at relatively low temperatures compared with its melting point.

Based on these findings, additional thermal exposure tests were conducted on coatings fabricated from powder in which the silica content was intentionally varied. The graph on the right side of Figure 6 presents linear shrinkage of samples exposed at 1425°C for 24 hours with four different silica contents. The results clearly point out the role that impurities such as silica can play in the properties and behavior of thermally sprayed zirconia.

The final set of experiments which ties the process/properties/exposure relationship together is summarized in Figure 8. FSZ samples were fabricated at different power levels, all with approximately the same porosity which was controlled by using a fugitive polymer in the powder. Free standing coatings were then isothermally aged for 24 hours at 1510°C and their change in lateral dimensions was measured. When plotted against the gun power used in fabrication, a strong linear relationship was obtained. These results, in combination with previous findings, indicate that process (including starting materials), properties, and environmentally-induced effects are all interrelated and must be understood and controlled in a fully successful application.

PROCESS CONTROL

In view of the demonstrated dependency of the behavior of the TBC coatings on the process, it is necessary to provide the proper controls in order to assure consistent quality during production manufacturing. This is best done during the process rather than through typical coating microscopic quality assurance performed "after the fact." In-process controls can be imposed on every part made, not just on a statistical sample. Deviations can be corrected in real time rather than letting many parts be processed incorrectly before being detected. Through in-process controls, costly rework of TBC's can largely be eliminated.

The heart of an in-process control system is the ability to monitor critical process parameters in real time, and to judge the process variation against known allowable standards. This enables the

operator to easily detect when one of the parameters is out of control, and to take necessary corrective action.

A typical screen from a plasma spray control console using proprietary software is shown in Figure 9. Individual parameters are listed and their real time value is presented as horizontal bars in a field of acceptable, caution, and stop colors. The key is to define these limits of acceptability for valid statistical process control. This requires a knowledge of the relationship of these parameters to the properties they influence, both as-sprayed and environmentally exposed, as presented in the previous portions of this paper. Once initial limits have been established, there should be continuous feedback from the field to determine if tighter controls are needed in order to meet performance goals, or if looser controls can be tolerated with consequent cost reduction.

CONCLUSIONS

Thermally sprayed thermal barrier coatings demonstrate a strong interrelationship among the raw materials, process conditions, coating properties, and environmental response. In order to best employ these coatings in existing and future applications, these relationships must be understood and imbedded in engineering design systems and manufacturing process control methodologies in order to achieve the most cost effective coatings.

References

(1) Novak, Richard C. "Processing Aspects of Plasma Sprayed Ceramic Coatings" ASME Paper 88-GT-289 June, 1988

(2) Matarese, A.P. "Thermal Barrier Coatings for Diesel Engines," Coatings for Advanced Heat Engines Workshop, Castine Maine, July 1987

(3) Eaton, H.E., Linsey, J.R., Dinwiddie, R.B. "The Effect of Thermal Aging on the Thermal Conductivity of Plasma Sprayed Fully Stabilized Zirconia," Thermal Conductivity 22 T. Tong editor, 1994

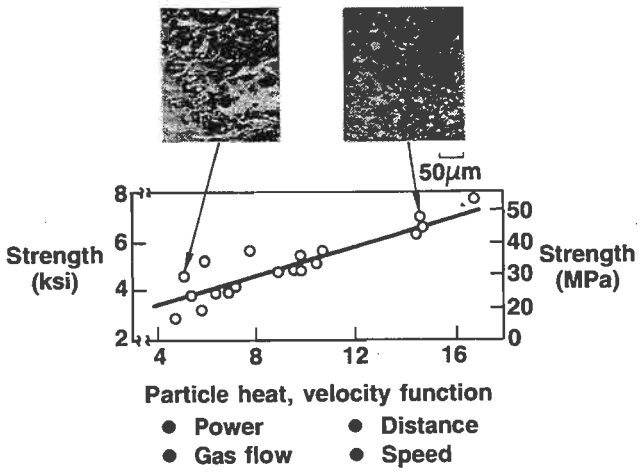

Figure 1. Coating strength depends on process parameters

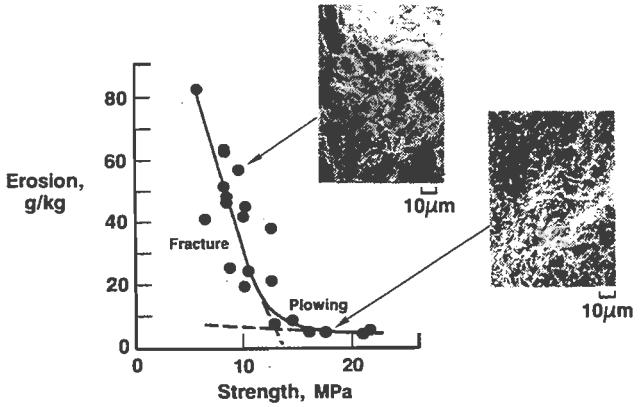

Figure 2. Ceramic erosion controlled by strength

80% dense ZrO_2	R. T. normalized properties			
	$\frac{\sigma}{\sigma_o}$	$\frac{E}{E_o}$	Thermal conductivity	$\frac{\epsilon_f}{\epsilon_{fo}}$
As sprayed	1.00	1.00	1.00	1.00
5 hrs at 1095°C	1.19	1.12	-	-
36 hrs at 1095°C	1.42	1.32	-	-
24 hrs at 1290°C	2.80	4.70	-	0.25
1 hr at 1425°C	3.50	3.10	-	-
5 hrs at 1595°C	3.61	4.10	-	0.20
36 hrs at 1595°C	3.68	4.17	2.53	0.20

Figure 3. Thermal aging affects sprayed $Zr0_2$ properties

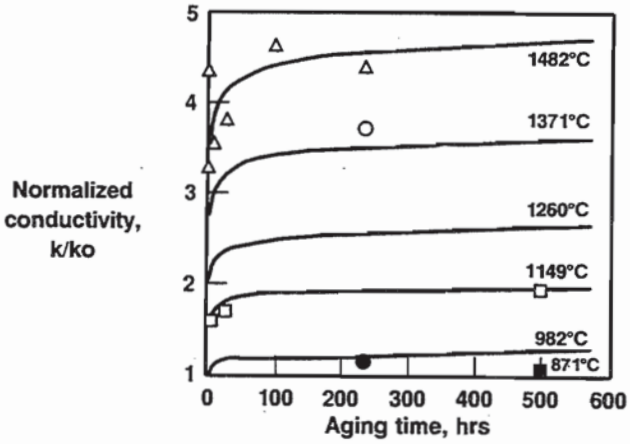

Figure 4. Thermal conductivity changes are caused by time-temperature effects

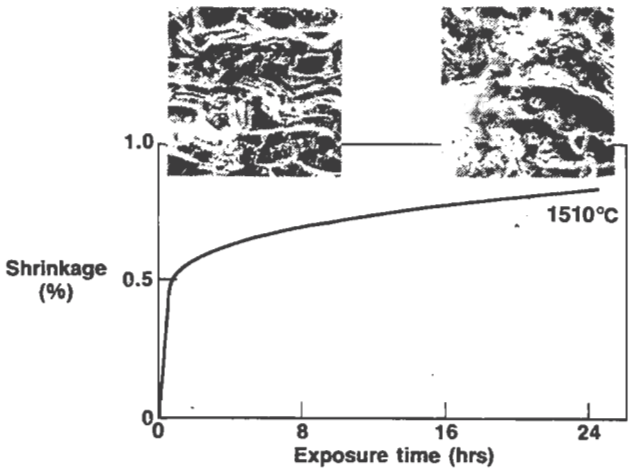

Figure 5. Thermal exposure causes shrinkage

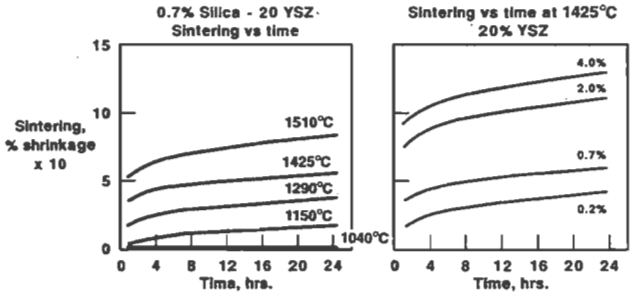

Figure 6. Shrinkage is due to time, temperature, and impurity level

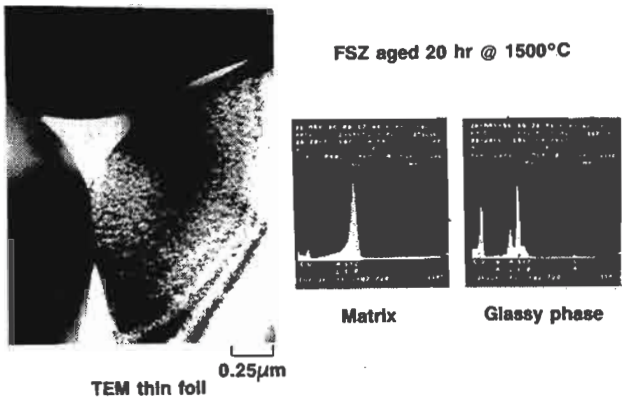

Figure 7. Silicon and aluminum rich phase at grain boundaries

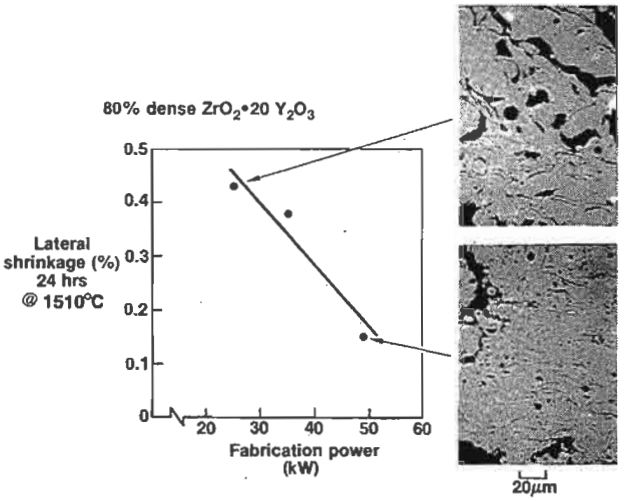

Figure 8. Fabrication power affects shrinkage

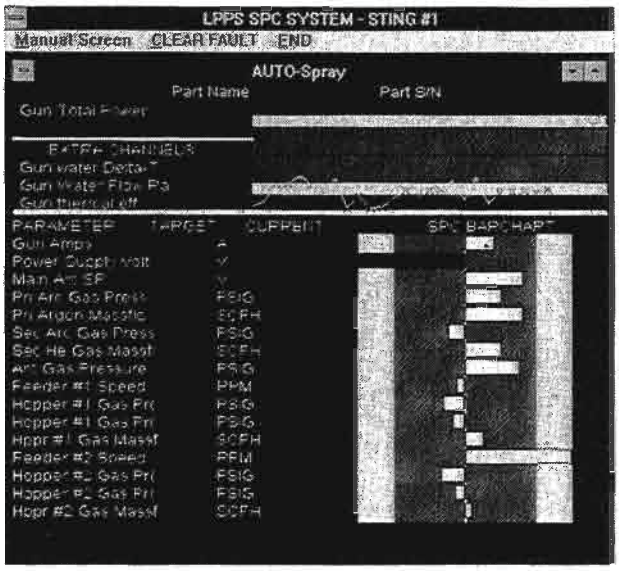

Figure 9. Real time process monitoring

THERMAL CONDUCTIVITY OF ZIRCONIA THERMAL BARRIER COATINGS

R.B. Dinwiddie and S.C. Beecher
Oak Ridge National Laboratory
Oak Ridge, Tennessee

and

B.A. Nagaraj and C.S. Moore
GE Aircraft Engines
Cincinnati, Ohio

Thermal barrier coatings (TBCs) applied to the hot gas components of turbine engines lead to enhanced fuel efficiency and component reliability. Understanding the mechanisms which control the thermal transport behavior of the TBCs is of primary importance. Physical vapor deposition (PVD) and plasma spraying (PS) are the two most commonly used coating techniques. These techniques produce coatings with unique microstructures which control their performance and stability. The PS coatings were applied with either standard powder or hollow sphere particles. The hollow sphere particles yielded a lower density and lower thermal conductivity coating. The thermal conductivity of both fully and partially stabilized zirconia, before and after thermal aging, will be compared. The thermal conductivity of the coatings permanently increases upon exposed to high temperatures. These increases are attributed to microstructural changes within the coatings. Sintering of the as fabricated plasma sprayed lamellar structure is observed by scanning electron microscopy of coatings isothermally heat treated at temperatures greater than 1100°C. During this sintering process the planar porosity between lamella is converted to a series of small spherical pores. The change in pore morphology is the primary reason for the observed increase in thermal conductivity. This increase in thermal conductivity can be modeled using a relationship which depends on both the temperature and time of exposure. Although the PVD coatings are less susceptible to thermal aging effects, preliminary results suggest that they have a higher thermal conductivity than PS coatings, both before and after thermal aging. The increases in thermal conductivity due to thermal aging for partially stabilized plasma sprayed zirconia have been found to be less than for fully stabilized plasma sprayed zirconia coatings. The high temperature thermal diffusivity data indicate that if these coatings reach a temperature above 1100°C during operation, they will begin to lose their effectiveness as a thermal barrier.

MECHANICAL PROPERTIES TESTING AND RESULTS FOR THERMAL BARRIER COATINGS

Thomas A. Cruse and B. P. Johnsen
Vanderbilt University
Nashville, TN 37235

Andrew Nagy
Southwest Research Institute
San Antonio, TX 78228

ABSTRACT

The paper reports on several years of mechanical testing of thermal barrier coatings. The test results were generated to support the development of durability models for the coatings in heat engine applications. The test data that are reviewed include modulus, static strength, and fatigue strength data. The test methods and results are discussed, along with the significant difficulties inherent in mechanical testing of thermal barrier coating materials. The materials include 7%wt. and 8%wt. yttria, partially stabilized zirconia as well as a cermet material. Both low pressure plasma spray and electron-beam, physical vapor deposited coatings were tested. The data indicate the basic trends in the mechanical properties of the coatings over a wide range of isothermal conditions. Some of the trends are correlated with material density.

SYMBOLS

EB-PVD	Electron beam-physical vapor deposited
PSZ	Partially stabilized zirconia
R	Stress ratio
σ	Stress (MPa)
T	Test temperature (C)
TBC	Thermal barrier coating
TMF	Thermomechanical fatigue

BACKGROUND

The goal in mechanical characterization of thermal barrier coating (TBC) systems is to provide sufficient data on material behavior for life prediction of the systems under complex thermomechanical loading environments in heat engines. This goal differs in thrust and approach to what might be called material screening tests which seek to rank-order material durability under a specified test environment. Thus, we seek to characterize the stress-strain-temperature behavior of the TBC systems under conditions that are well-enough controlled that specimen geometry or loading condition uncertainties or influences are minimized. The operating hypothesis is that if we have sufficient mechanical property characterization under

ideal conditions, then we can develop empirical models for correlating fatigue life of the TBC systems under cyclic thermomechanical conditions. Thus, the testing requirements fall between material screening and engine testing.

The mechanical properties of interest include modulus, strength, creep rate, and fatigue strength properties, of course. However, experience has shown that cyclic properties, rate effects, residual stresses *in situ*, and direction and orientation of the TBC material in the testing are very important to correlating thermomechanical life data.

Fatigue life prediction models have been proposed by the principal author of this report for two materials in gas turbine engine applications; a third model for diesel engine applications is under development and is discussed in this paper. Life prediction for turbine engine applications focused on the cyclic thermomechanical strain conditions experienced by critical locations on coated turbine blades and vanes. Diesel engine applications considered isothermal fatigue test conditions. Mechanical testing in these programs therefore considered a wide range of temperature conditions and strain cycles in both tension and compression.[1]

The first turbine engine life model was proposed for a plasma sprayed 7%wt yttria, partially stabilized zirconia (PSZ) material, Ref 1. The life modeling was based on the observation of cyclic thermomechanical fatigue (TMF) microcrack generation and extension. Cyclic hysteresis in the TBC under thermomechanical conditions was modeled using a state variable model of the thermoviscoplastic material. Parameters for the material model were taken from the uniaxial test results that were reported in Ref 2. The testing methodology and results are discussed in this paper as Phase 1 (plasma sprayed PSZ for turbine engines) tests.

The second life prediction model was for the same material but deposited by an electron beam-physical vapor deposition (EB-PVD) process as reported in Ref 3. In this case, the PSZ has a columnar structure which is quite resistant to cracking parallel to the bond coat interface. Mechanical testing of the TBC required significant innovations in test methodology (Ref 4). The test results indicated that the EB-PVD material had substantially higher strain levels of elastic behavior than the plasma sprayed ceramic coating.

Thermomechanical fatigue failures of the TBC occurred within the oxide layer buildup on the bondcoat. The best life correlations were achieved by a fatigue model of the oxide layer in the bondcoat itself, Ref 5. In order to make these predictions, the elastic properties of alumina had to be used to model the thermally-grown oxide on the bond coat. The testing methodology and results are discussed in this paper as Phase 2 (EB-PVD coating for turbine engines) tests.

---

[1] The mechanical tests were developed under the direction of the principal author; Phase 1 and Phase 2 testing was performed by Mr. Nagy, while that of Phase 3 was performed by Mr. Johnsen. The Phase 1 and Phase 2 tests were performed for Pratt & Whitney Aircraft under NASA sponsorship, while that of Phase 3 was performed directly for NASA.

The recent testing of TBC materials reported in this paper seeks to provide insight into the high-cycle fatigue (HCF) behavior ceramic coatings for diesel engine application. The diesel application is characterized by compressive surface stress cycles superimposed on a steady compressive stress background and is associated with the effect of the individual cylinder combustion cycles superimposed on a steady-state engine power condition. Spallation of the TBC was observed to progress from the outer surface, growing over time, and is illustrated in a fatigue specimen failure mode in Ref 6. Mechanical testing in this program therefore concentrated on isothermal fatigue and compressive strength testing at room temperature and temperature levels experienced under steady-state engine operation.

The diesel engine HCF life prediction model requires basic thermoelastic properties for the TBC together with compressive fatigue testing at various levels of compressive stress cycling and stress ratios ($R = \sigma_{max}/\sigma_{min}$). The Phase 1 tensile fatigue testing on a plasma sprayed 7%wt. PSZ resulted in isothermal fatigue strengths approaching the ultimate strength of the material (Ref 7, Ref 8). Further isothermal fatigue test results, life modeling, and physical interpretations of the fatigue failures are given in the current paper. The testing methodology and results are discussed in this paper as Phase 3 (plasma sprayed PSZ and cermet materials for diesel engines) tests.

SPECIMEN SELECTIONS AND TESTS

The various test methods reported in this section are all non-standard tests. The reasons for the use of non-standard tests are the following:

1. Limited thickness of the TBC material as deposited by the standard coating processes.
2. Deposition process itself which requires the use of a substrate material for solidification or deposition.
3. Unique mechanical characteristics of the various TBC materials and the inherent lack of significant tensile strength.
4. Need to achieve states of stress that are uniform tension or compression for the entire specimen cross-section.

The Phase 1 and 2 test programs each required both tensile and compressive load tests. All testing was done isothermally at a range of test temperatures from room temperature to 2200°F (1300°C). All specimens were designed such that the primary (or only) applied stress was oriented parallel to the coating-substrate interface. In the case of the plasma sprayed materials, the loading was parallel to the splat structure of the coating; in the case of the EB-PVD material, the loading was transverse to the columnar growth structure of the coating.

Phase I tensile testing used a "bow-tie" tensile bar and the "Brazil" wafer specimen, which has the appearance of a large aspirin tablet; both were machined from TBC that was deposited on a flat surface. The two specimens are shown in Figure 1. The test apparatus was a standard computer controlled test machine. In the case of the tension test, a highly

flexible load train was used to minimize bending strains on the specimen, which was mounted in the gripping fixture shown. The wafer test is performed in compression by placing the specimen between two anvils; the normal stress on a plane connecting the load points is a nearly uniform tensile stress, as justified in Ref 9.

The bowtie tensile specimen was analyzed to determine the stress concentration factor at the end of the gage section, as the lower temperature tests failed at this location. The K_t was found to be 1.15, a value which brought the tensile strength results for the two tensile specimens together. The two sets of tensile are data reported in the next section. The major problem in both specimens is the inability to provide axial strain measures to be used in making accurate modulus measurements. The bowtie tensile test strains were calculated by a room temperature calibration test of a strain-gaged specimen; the elevated temperature testing was assumed to have the same load system flexibility. The digitized strain data was then subtracted from the load system deflections to obtain stress-strain curves for each tensile test.

The bowtie specimen was also used for tensile creep strain rate data at the higher test temperatures. The specimen failures shifted to the gage section in the creep tests showing that the material lost its notch sensitivity under these conditions.

The lack of good strain measures is a continuing problem for many of the reported tests. Extensometers are generally too heavy for testing unsupported TBC coating specimens. Laser strain measurement methods appear to be the only possible solution to the problem but these are expensive and require special test setups.

The Phase I compression testing used solid cylindrical specimens which were ground from the TTBC which had been previously deposited on a substrate. The specimens were 3.12 mm in diameter and 6.35 mm long. Again, the test direction was aligned parallel to the splats. The specimens were compressively loaded between two anvils. The details of the test results are contained in a sub-contractor report whose contents were reproduced in Ref. 3.

The compression testing was generally successful in that the failures generally appeared to originate in the central regions of the test specimen and not near the ends. High temperature lubricant was used to minimize end-restraint during the compression testing. The alignment was provided by shims of the compression anvils based on the testing a ductile metallic test bar of the same size as the ceramic test pieces.

The compression stress-strain curve data was achieved by running each test temperature to the full ceramic specimen loads, but with no specimen between the anvils. The digitized load-deflection curves were stored for each temperature and then were subtracted from the appropriate test data of load system deflection versus load.

Phase 2 testing was performed on EB-PVD TBC material. The material was deposited on single crystal, nickel superalloy tubes. The EB-PVD TBC material was assumed to have negligible tensile strength and the decision was made to test the TBC/metal system as a

composite system. The metal bar dimensions were selected with different strategies for tension and compression. In the case of compression, the tube geometry was selected to meet the following estimated constraints:

1. Wall buckling of the metal tube defined a relation between the thickness and radius of the metal substrate
2. Wall thickness of the metal substrate was set to assure that the TBC section stiffness was comparable to or greater than that of the substrate section
3. Wall thickness of the TBC was as great as production would permit

The compression specimen thickness was selected on the basis of the plasma-sprayed TBC compression modulus. The substrate inner diameter was about 18 mm and the specimen length was about 22 mm. The substrate wall thickness was selected as about 2.2 mm. Compressive axial strains were measured by an Instron capacitive strain transducer.

In the case of tension testing, the TBC was again deposited on a superalloy tube. However, the tube inner surface was then machined to a wall thickness of about 0.36 mm with a TBC thickness of about 4.6 mm. The specimen substrate cross-section was reduced in the region of the TBC; TBC adherence to the ends of the substrate gage-reduction zone was desired in order to minimize inter-material shear as the loading mechanism. The entire test specimen was sized for the use of an internal extensometer and is shown in Figure 2.

The axial strains were measured by an internally mounted biaxial extensometer developed by Southwest Research Institute (see Ref. 4). The extensometer was developed for measuring both axial and torsional deformations but was used in these tests in the axial mode. The extensometer measured the axial strains over the length of the coating on the tubular specimen. Attempts were made to correlate the internal strain measure on the substrate to axial strains on the TBC coating. This was done by applying foil-type strain gages to the EB-PVD coating; failure of the adhesive caused this approach to be abandoned. A second extensometer was developed for external attachment in a room temperature test. The external clip gage measured coating strains that are about a factor of two lower than those measured internally after a strain of about 0.5%.

The strain data for the composite specimens was obtained by developing a composite load-deflection model for the material system of the TBC and the substrate. The compression specimens were seen to exhibit elastic-perfectly plastic behavior in the substrate. Some of the substrates even showed that only single slip systems were activated (the substrate was a single crystal). The elastic-plastic properties were measured in tests of the substrate material. Poisson's ratios were assumed but found not to have a major effect on the stress-strain algorithm that was reported in Ref. 4. An algorithm for subtracting out the TBC stress strain response from the load-displacement curve is given in the same reference.

The tensile test behavior is quite different in that the TBC has very limited tensile ductility. The substrate, on the other hand, remains elastic at the appropriate load levels. The

analysis was usable only to the point of significant damage to the ceramic coating. However, as discussed below, the tension tests did offer good insight in the tensile behavior of the EB-PVD ceramic coating.

Phase 3 testing has been reported in Ref. 8 and will only be summarized herein. All of the testing in Phase 3 has been in compression. the primary focus of the testing has been to establish the isothermal fatigue strength of the plasma sprayed TBC's under pure compression loading. However, the testing has produced some data of compressive strength, modulus, and cyclic stress-strain behavior as well.

The compression testing used two cylindrical test geometries. Both geometries were fabricated initially by spraying the TBC on iron substrates. The substrates were removed by acid etching processes with mixed results. The compression loading was again parallel to the splat structures of the materials. Considerable attention was given to specimen alignments as these specimens were much bigger than the compressive specimens in Phase 1 and lacked to metal substrate during test that was used in Phase 2. The specimen geometries for Phase 2 are shown in Figure 3.

The modulus measurements in the Phase 3 testing have been made from load-deflection data. The digitized data were obtained from sampling at relatively few bins of displacement data ranges. The digitized curves were then fitted by hand to obtain modulus data.

MODULUS AND STRENGTH RESULTS

The Phase 1 test program showed that the tensile behavior of the plasma sprayed TBC material is nonlinear over the entire range of strain to failure (Ref. 2). The nonlinear behavior may be attributed to the generation and extension of a distributed network of microcracks inherent to this system. The Phase 2 tension testing indicated somewhat more linear behavior up to about 0.04% strain, followed by nonlinear behavior to fracture (Ref. 3). The change in behavior at 0.04% strain is indicative of a residual stress effect, as the material is probably going from initial compression to tension. Compression testing on the other hand showed results that had distinctly linear portions up to temperatures around 1200°C. This indicates that compression loading of the TBC material is not generating and extending the microcracks to the extent that the specimen compliance is affected for significant levels of applied stress.

The modulus data versus test temperatures are plotted together in Figure 4 for all three test phases. The data includes both tension (initial slope) and compression data from Phase 1 and Phase 2. The Phase 3 data is all compressive. For reference, the beam bending data by Brink of Caterpillar (Ref. 6) indicates a modulus value of 44 GPa for a 7.5%wt. yttria PSZ at 400°C.

There are two populations of data with more tensile data in the upper population and more compressive data in the lower population, especially at the higher temperatures. The tensile data are associated with strains less that 0.1% to 0.2%, while that for compression is taken with strains generally exceeding 1%. The tensile moduli are generally taken as initial slopes to strain softening stress-strain curves and is much more subject to error. The bulk compressive specimens for the range of TBC materials tested have reasonably consistent modulus results. These results show that the compressive moduli are below those of the tensile data and the reported data for flexure specimens. Further, the modulus values decrease in a steady manner between room temperature and 1200°C, to values that are about half of the room temperature values.

To further understand the scatter in the modulus data, Figure 5 plots the data versus the measured density of the Phase 3 specimens, as discussed in Ref. 8; the cumulative distribution functions of the density data for the three Phase 3 materials are shown in Figure 6. The scatter in the Phase 3 modulus data shown in the previous figure shows a systematic variation in modulus with density of the 7%wt. PSZ material tested at room temperature. However, the 8%wt. PSZ and the cermet specimens, which have comparable variations in specimen densities, do not seem to exhibit the same systematic variation of modulus with density at room temperature (a) and at 700°C (b). Nonetheless, some of the scatter in the modulus data in Figure 4 may be attributed to variations in specimen density.

The ultimate tensile strength data are plotted in Figure 7. The Phase 1 tensile strength results from Ref. 2 are for the wafer and the bowtie specimens. The Phase 1 data might be seen to indicate a slight downward trend with temperature except for the 1094°C data set. All tensile failures in the bowtie specimen configuration were at the stress concentration at the end of the gage section. Given the difficulty in machining these specimens, the variation in the tensile data is taken to be scatter and not a temperature effect. Creep testing of single specimen at 538°C followed by loading to fracture resulted in a failure in the gage section at a UTS value of 18 MPa. While no longer notch sensitive, the UTS is consistent with that for the non-creep testing. The average of the bowtie tensile data was 19 MPa.

The wafer data in Figure 7 contains three static (non-fatigue) data points. The UTS at 538°C was 23.4 MPa; two static failures were also obtained at 871°C and the strengths were 22.0 and 22.7 MPa. These tensile data suggest that there is no significant temperature difference over that temperature range, an observation that is consistent with the bowtie data for the same temperatures. While the wafer specimens failed in the center of the specimen transverse to the compressive load, as expected for a tensile failure mode, the stress in the mid-portion of this specimen is biaxial. The average of the three data (22.6 MPa) divided by the stress concentration of 1.15 is 19.8 MPa. The data seems to suggest that biaxiality is not an issue but that the stress concentration factor is. If this is true, then the plasma sprayed PSZ tensile strength is insensitive to temperature over a wide range of temperatures.

Phase 2 composite specimen tension results indicated that the EB-PVD material does have a tensile strength capacity, with fracture of the interfaces between the material columns as the

tensile fracture mode. The tensile strength value for the EB-PVD material appears to be on the order of one-half of the strength of the Phase 1 data above about 700°C. The ambient data and some of the higher scatter values suggest tensile strengths approaching 40-50 MPa, values which are consistent with the 400°C tensile strengths reported by Brink, Ref. 6. There is no Phase 3 tensile data. The ambient temperature values of the tensile strength are very dependent on the computed modulus of the material; residual stresses in the TBC were indicated in the tests which affect the modulus calculations. We therefore discount the Phase 2 values of the tensile strength of the TBC at ambient temperature.

Few, if any, of the specimens show linear tensile stress-strain behavior. The Phase 2 tensile data is especially vulnerable to errors in the assumed linear behavior and the derived modulus. Further, the role of substrate is critical as is the role of bending strains. The fracture of a simple bowtie specimen of TBC is quite unlike that of the TBC when it is supported on a metal substrate as in the Phase 2 testing. In terms of component design, the benefits of support are likely to be real in giving a higher effective tensile strength as well as the possibility of beneficial residual stresses away from the ends of the TBC.

The compressive strength data are shown in Figure 8. The Phase 1 cylinder data suggests that the compressive strength shows a stronger temperature effect than that for the tensile data, although no ambient testing was performed. The Phase 2 composite specimen and the Phase 3 8%wt. yttria PSZ materials have higher indicated compressive strengths than the Phase 1 and Phase 2 7%wt. yttria PSZ. The Phase 3 cermet material compressive strengths appear to be about 13% higher than the 8%wt. yttria PSZ material.

The Phase 3 7%wt. yttria PSZ is to be discounted, unfortunately, as the specimens were found to have "mud-flat" cracks. The cracks were widely distributed on the surface and were probably due to swelling of the interface between the ceramic and the substrate during an acid removal of the substrate. The compressive failure origins appeared to be at 45 degrees to the load axis and were at mudflat cracks indicating a surface shear fracture due to the mudflat cracks. The Brink data in Ref. 6, obtained using a composite bend specimen, indicated that PSZ and cermet strengths were in excess of 500 MPa at 400°C, indicating a possible trend to higher strengths at lower temperatures than the data reported herein. More recently, Ref 10 has given data for the 8%wt. yttria PSZ which shows compressive strengths of 450 MPa (805°C), 490 MPa and 520 MPa at room temperature. This data appears most comparable to ours and strongly suggest a lack of temperature influence on compressive strength over this lower temperature range.

Figure 9 plots the Phase 3 compressive strength data for the three materials in terms of the measured specimen density values. In this case, all three data sets show a consistent trend of strength with density. These specimens appear to have failed in an axial splitting mode. Limited scanning electron microscopy (SEM) of the failure surfaces in the 8%wt. yttria PSZ and cermet specimens indicates that the failures cannot be associated with any material or structural abnormality. The investigation concludes that the intrinsic structure of the plasma

sprayed materials is the likely source of the specimen fractures in the absence of mudflat cracks.

Given the density trend similarities in the compressive strength data and the differences in the nature of the failure origins, we conclude that flaw sensitivity of the plasma sprayed TBC's in all three depends on material density. However, since material density and flaw sites are complementary (the flaws primarily being voids between splats), the trend would likely relate to a decrease in the statistical flaw size of the TBC with increasing material density. This would also explain the much lower strengths of the specimens with mudflat cracks only in that the mudflat cracks act as stress risers on the intrinsic material defects.

FATIGUE RESULTS

Phase 1 and Phase 2 testing focused on thermomechanical fatigue (TMF) for gas turbine applications. The TMF testing in both programs was part of the Pratt & Whitney test program and the test data has been reported in Ref. 2 and Ref. 3. Phase 3 testing focused on compressive stress isothermal fatigue for diesel cycle engines.

Limited tensile fatigue testing of the 7%wt. PSZ was performed using the wafer test as reported in Ref. 2. The testing was done at a stress ratio ($R = \sigma_{min}/\sigma_{max}$) of 0.1. The testing was done at stress levels that were about 90% of the tensile strenght of the specimens. The fatigue lives of the specimens were only hundreds of cycles, as plotted in Figure 10, but a specimen runout was obtained at slightly less stress amplitude.

Compressive fatigue testing was done on the Phase 3 program for all three materials. The 7%wt. yttria PSZ material was tested at several stress levels at 700°C. A number of runouts occurred at lower initial cyclic stresses, but there was one successful fatigue failure at a cyclic stress range of 203 (MPa compression) with a life of 2400 cycles. Based on the compressive strength testing results for that material, the cyclic stress range was about 86% of the material compressive strength.

The 8%wt. yttria PSZ material was initially tested in fatigue at 700°C with no failures to a runout of $2x10^6$ cycles and at cyclic stresses on the order of 50% ($R = 0.6$). The maximum compressive stress was selected to be about 90% of the compressive strength of the materials. The same cyclic stress conditions were then applied at room temperature and fatigue lives were in the expected range for both the 8%wt. yttria PSZ and the cermet materials. Figure 10 shows the cyclic stress amplitude applied to the various fatigue specimens for the Phase 1, Phase 3, and two test points from Ref. 10. One run-out (21 million cycles) test point for the 8% yttria PSZ is also shown; the test temperature was 400°C.

The current test program and that reported in Ref. 10 were performed on comparable materials, all prepared by Caterpillar Inc. However, the referenced work was for a stress ratio of 0.1 while ours was for 0.6. The plot in Figure 10 shows that the two very different

mean stress conditions produced quite comparable fatigue lives. Our data peak stress is about 90% of the material compressive ultimate, while that from the reference is about one-half the material ultimate.

The compressive fatigue failure mechanism appears to behave like a tensile fracture mechanics crack growth mode. Cyclic crack growth under tensile stresses has been found to be independent of the value of the stress ratio (R), but to depend solely on the cyclic stress magnitude. This suggests to us that the compressive fatigue mechanism is one of sub-critical crack growth in the TBC materials from the intrinsic defect structures in plasma sprayed systems.

The transverse stresses on the intrinsic defects in the plasma sprayed materials (Phase 1 and Phase 3) are tensile for applied compressive axial stresses. The same stress mechanism seems to be the failure mechanism at compressive ultimate load conditions. The fatigue lives of the 8%wt. yttria PSZ and the cermet materials from the Phase 3 are plotted against the measured specimen material densities in Figure 11. Once again, the data suggests a positive correlation of fatigue life with increasing density, which is a statistically decreasing population of intrinsic defects.

The design implications of this are important at the lower operating temperatures (apparently below 700°C). The fatigue failure behavior found on two of the many test specimens that were generated for the Brink paper (Ref. 6) by Southwest Research Institute included two spallation failures, one of which is shown in that paper. The spallation failure was seen to be quite like the spallation failure of a TBC in an engine test at Caterpillar. The transverse fracture mechanics mechanism that is now postulated would lead on flat surfaces to the type of spallation event seen in the Brink paper.

The design goal then is to keep the cyclic stresses below about 150 MPa compressive at for operating conditions below 700°C. The data in Ref. 10 as well as the current work show, however, that the behavior of these materials above these temperatures suggests an active strengthening mechanism which effectively raises the fatigue limit for the material. While the mechanisms are not yet fully resolved, the data discussed in the next section sheds light on the cyclic strengthening process.

CYCLIC STRESS-STRAIN RESULTS

The original high temperature work in Phase 1 found that there was significant creep behavior of the TBC material at and above 871°C (Ref. 2). The data was measured in the supporting Southwest Research Institute program using the same tensile and compressive specimens used for modulus and strength data, as reported herein. The tests were run under static applied stress conditions and the steady creep strain rate was taken experimentally. Creep tests could not be performed in the Phase 2 tests.

The Phase 3 fatigue test program found that the cyclic-loaded specimens were getting significantly shorter at the suspension of fatigue testing. The length reductions were on the order of 0.5 to 1.0 mm. The length reductions were found for tests run at room temperature as well as at elevated temperatures. The length reductions were subsequently found to be associated with a transient process of cyclic ratchetting of the compressive strains.

The sampled-test records of head displacement and time for three of the fatigue specimens previously reported are shown in Figure 12. The data is for two tests at room temperature (5-2 and 3-3). These fatigue tests were at the same maximum (400 MPa) and cyclic (160 MPa) stresses. The first failed at about 708,000 cycles and the second at about 91,000 cycles. Also plotted is a run-out test at 400°C with a maximum stress of 379 MPa and a cyclic stress of 152 MPa. The room temperature tests were run at 25 hz while the elevated temperature test was run at a cyclic frequency of 60 hz.

Clearly, there is no correlation indicated between these test conditions and the cyclic ratchetting process. It seems that the mechanism of the ratchetting is independent of the failure mechanism, the stress level, and the cyclic frequency. In order to better define the cyclic ratchetting phenomenon, several "four-cycle" tests were performed in Phase 3.

Four-cycle data was obtained by loading each specimen to successively higher loads. A constant preload of about 450 N was maintained on the specimens for all four load cycles. The additional loading was applied at a constant stroke rate over a 20-30 second time interval; the entire four-cycle loading took about 3 minutes. Specimen length was measured prior to and after the tests on five of the eight specimens. Modulus data was recorded for each load cycle and is shown for the first and last of the cycles in Table 1.

Table 1: Four-Cycle Modulus Data

Material	Specimen ID	ΔL (mm)	Density (g/cc)	1st cycle E (GPa)	4th cycle E (GPa)	Modulus Change (GPa)
8% PSZ	1-3	not msrd	5.171	14.2	24.4	10.2
	3-3	not msrd	5.198	14.3	24.0	9.7
	5-2	0.051	5.275	16.0	28.7	12.7
	7-4	0.038	5.284	15.0	24.9	9.9
Cermet	15-2	not msrd	5.384	18.7	28.6	9.9
	15-4	0.064	5.323	17.1	25.7	8.6
	18-1	0.051	5.415	19.8	28.1	8.4
	11-1b	0.051	5.366	19.3	29.5	10.2

The four-cycle modulus data show that the cyclic response of the material not only causes the specimen length to be reduced, but shows that significant changes occur in the measured specimen moduli. The same basic phenomenon was cited also in Ref. 10. Compressive strength testing of the specimens after fatigue testing, during which this cyclic ratchetting was occurring, shows that the compressive fracture strength is significantly elevated as well as the material modulus.

The fatigue test data suggests that the cyclic hardening process occurs at temperatures above 400°C at a high enough rate that the fatigue cracking process is greatly forestalled, if not eliminated. Very limited fatigue testing at increasing levels of applied stress has shown that stresses much higher than the original material strength has failed to cause fatigue failures in very high numbers of total cycles. The phenomenon was observed in one Phase 1 wafer test as well as several Phase 3 7%wt. and 8%wt. yttria PSZ tests.

Such cyclic hardening and the known creep behavior of the material at high temperatures clearly show that a more advanced material constitutive model is required in order to make sensible life predictions under cyclic stress conditions over a range of temperatures. It is hoped that such work will be possible in the future.

SUMMARY

Mechanical test data from several different phases of experimental work with ceramic coatings has been reported. The data on compressive modulus and strength of the ceramic specimens has resulted in a reasonably consistent understanding of these property levels. Material density and cycling have been shown to influence these properties. Compressive failure is most likely caused by the splitting of intrinsic defects in the material, for both static loading and fatigue loading. The fatigue damage process is likely one of sub-critical crack extension from these intrinsic defects and is somewhat mitigated by higher material density.

Tensile testing data contains much more scatter than that for the compressive tests. The tensile behavior of TBC's is generally nonlinear, probably due to the creation and extension of multiple microcracks in the material. As expected, the material is notch sensitive over a wide range of temperatures, but has been found to become notch insensitive in the creep regime. Tensile fractures are likely to be caused by the same defect structures in the ceramics as those for the compressive stress, but are obviously triggered at much lower levels of applied stress.

The material has been found to have very complex cyclic behavior at all temperature ranges. The use of elastic stress analysis models for design work is not likely to be appropriate due to the cyclic ratchetting and creep process effects on the stress state of the material through a redistribution of the material strains. More work is needed to properly model the behavior of these materials in engine operating conditions.

Acknowledgements: We wish to gratefully acknowledge the significant support given to this effort by Dr. Robert A. Miller at the NASA Lewis Research Center, to J. T. DeMasi, K. Sheffler, S. M. Meier, M. Ortiz, and D. M. Nissley of Pratt & Whitney, and to B. Beardsley of Caterpillar, Inc. The work has been financially supported through a series of cooperative agreements with the NASA Lewis Research Center and by Pratt & Whitney.

REFERENCES

1. T. A. Cruse, S. E. Stewart, and M. Ortiz, Thermal barrier coating life prediction model development, *J. Eng. Gas Turb. Power*, Vol. 110, 1988, p. 610-616.

2. J. T. DeMasi, K. D. Sheffler, and M. Ortiz, Thermal Barrier Coating Life Prediction Model Development, NASA Contractor Report 182230, 1989.

3. S. M. Meier, D. M. Nissley, and K. D. Sheffler, Thermal Barrier Coating Life Prediction Model Development, NASA Contractor Report 189111, 1991.

4. T. A. Cruse, A. Nagy, and C. F. Popelar, Mechanical Testing of Advanced Coating System, Final Report, NASA Cooperative Agreement NCC3-89, Southwest Research Institute, San Antonio, Texas, 1990.

5. S. M. Meier, D. M. Nissley, K. D. Sheffler, and T. A. Cruse, Thermal barrier coating life prediction model development, *J. Eng. Gas Turb. Power*, Vol. 114, 1992, p. 258-263.

6. R. C. Brink, Material property evaluation of thick thermal barrier coating systems, American Society of Mechanical Engineers paper 89-ICE-13, Energy-Sources Technology Conference, 1989.

7. T. A. Cruse, B. P. Johnsen, R. A. Miller, and W. J. Brindley, Compressive fatigue behavior of a PSZ TBC -- Status Report, *Proceedings of the 1992 Coatings for Advanced Heat Engines Workshop*, p. II 41- II 47, 1992.

8. B. P. Johnsen, T. A. Cruse, R. A. Miller, and W. J. Brindley, Compressive fatigue of a plasma sprayed ZrO2-8%wt Y2O3 and ZrO2-10%wt NiCrAlCoY TTBC, *J. Eng. Matls. Tech.*, in press.

9. M. C. Shaw, P. M. Braiden, and G. J. DeSalvo, The disk test for brittle materials, *J. Eng. Indus.*, Vol. 97, 1975, p. 77-87.

10. K. F. Wesling, D. F. Socie, and B. Beardsley, Fatigue of thick thermal barrier coatings, submitted for publication.

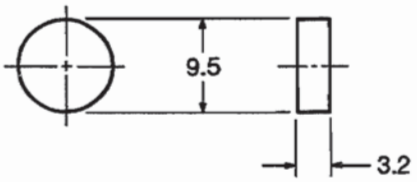

(a) Wafer Specimen

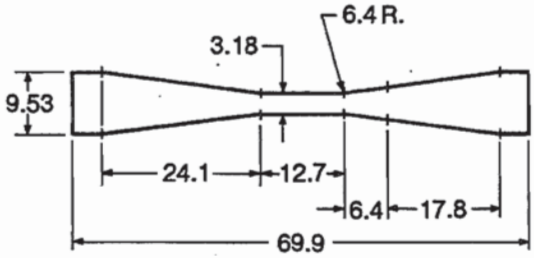

(b) Bowtie Specimen

Note:
Dimensions in Millimeters

Figure 1: Phase 1 tensile specimens

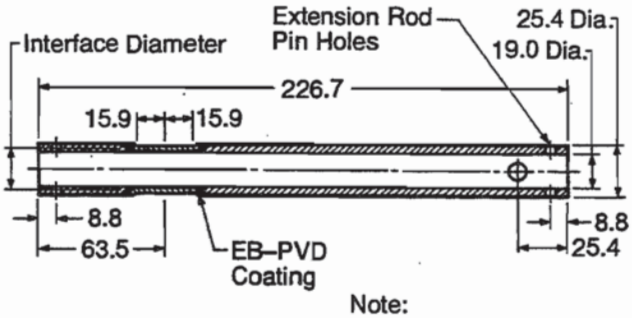

Note:
Dimensions in Millimeters

Figure 2: Phase 2 tensile specimen

Figure 2: Phase 2 Tensile Specimens

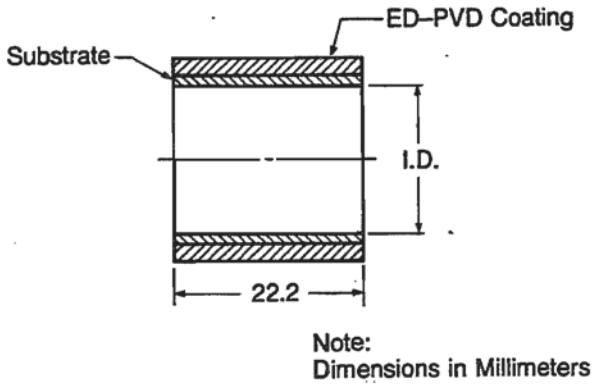

Figure 3: Phase 2 compression specimen

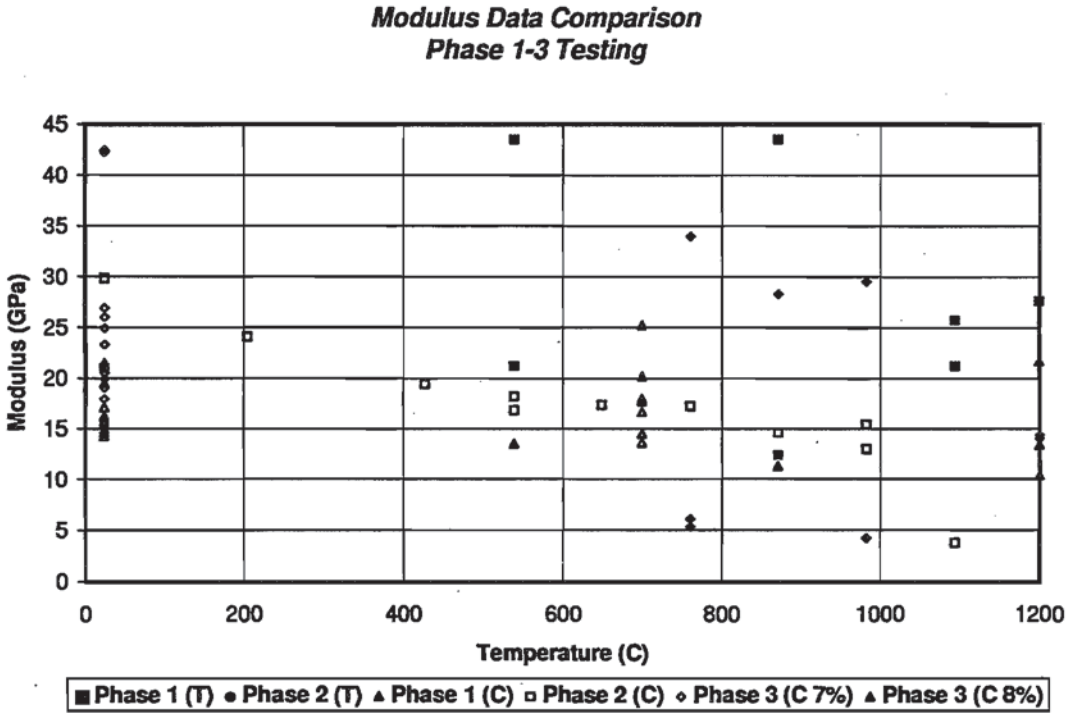

Figure 4: Modulus data vs. temperature

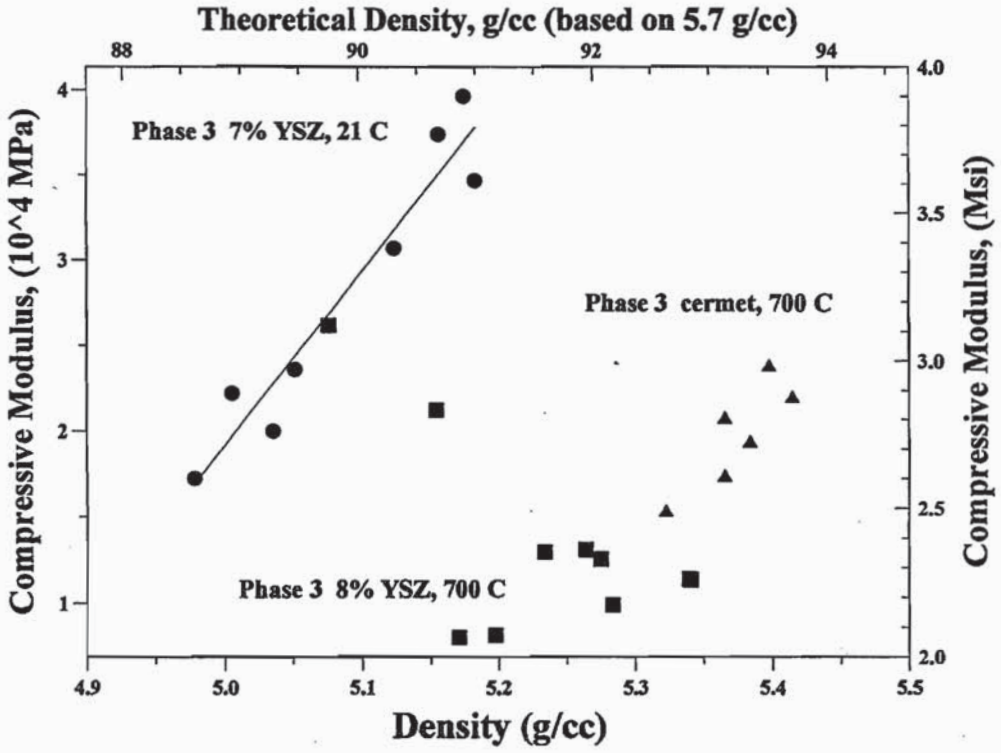

Figure 5: Modulus data vs. density

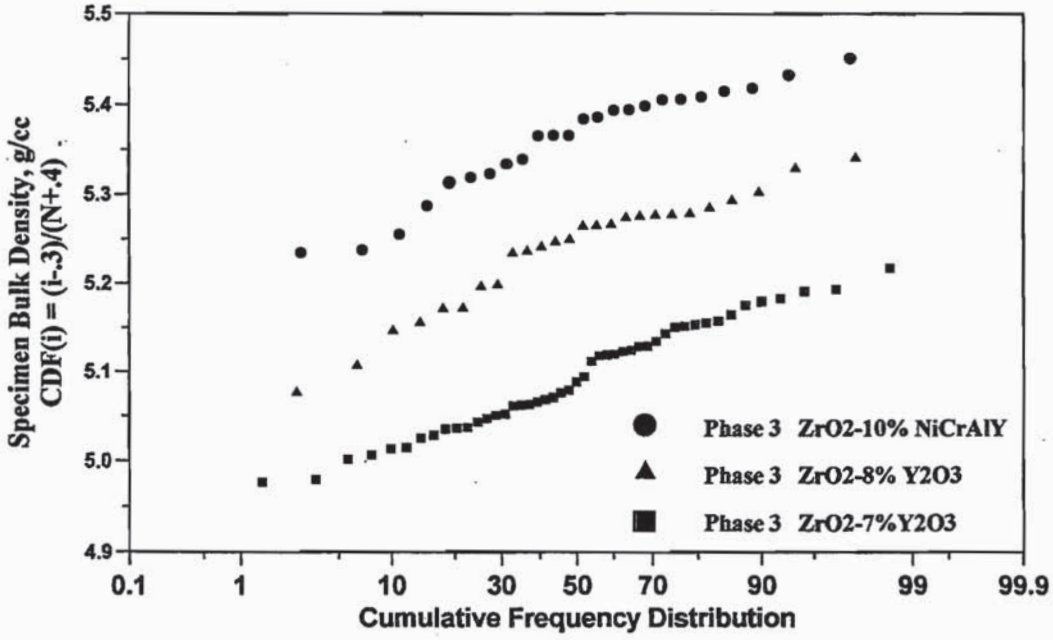

Figure 6: Phase 3 density distributions

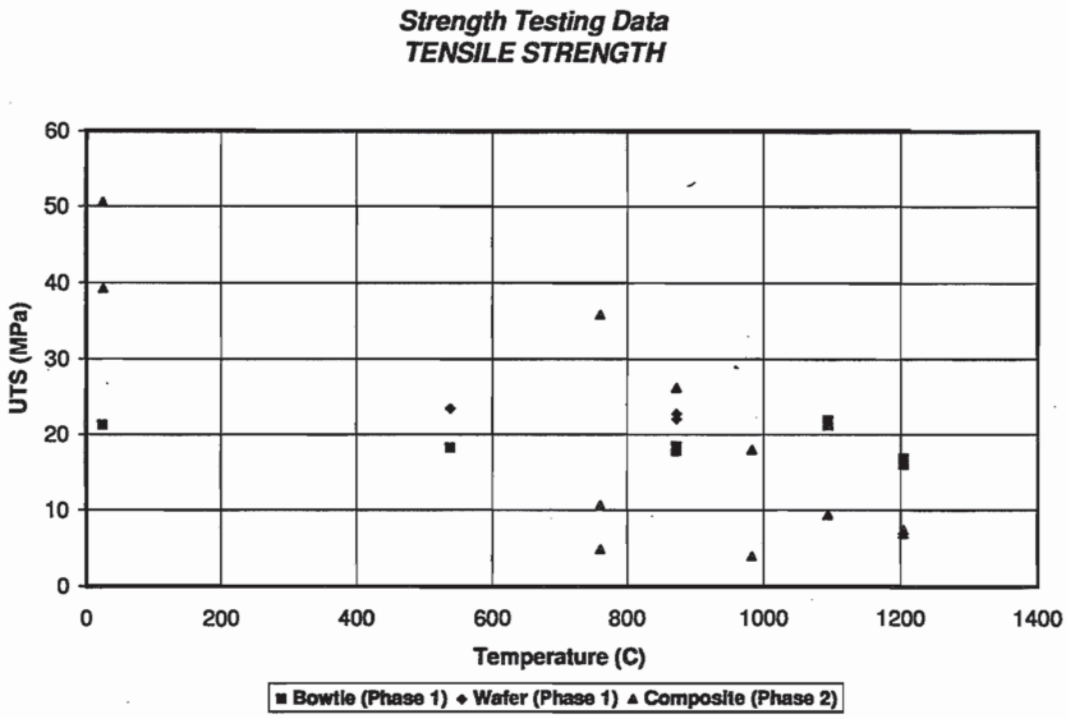

Figure 7: Tensile strength data

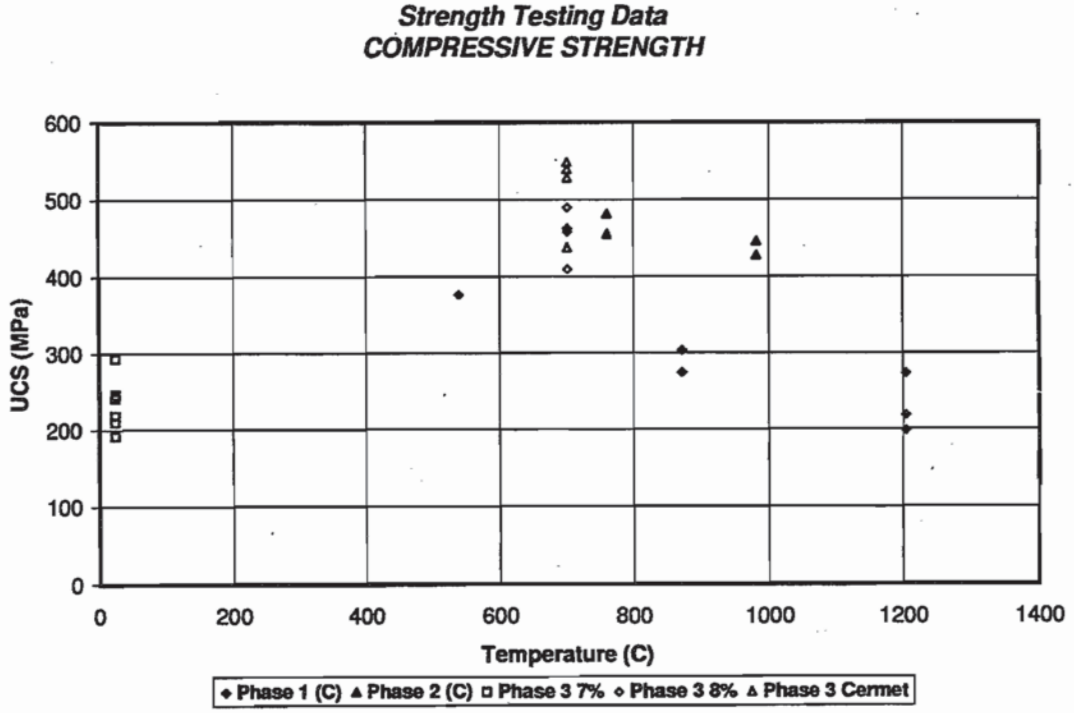

Figure 8: Compressive strength data

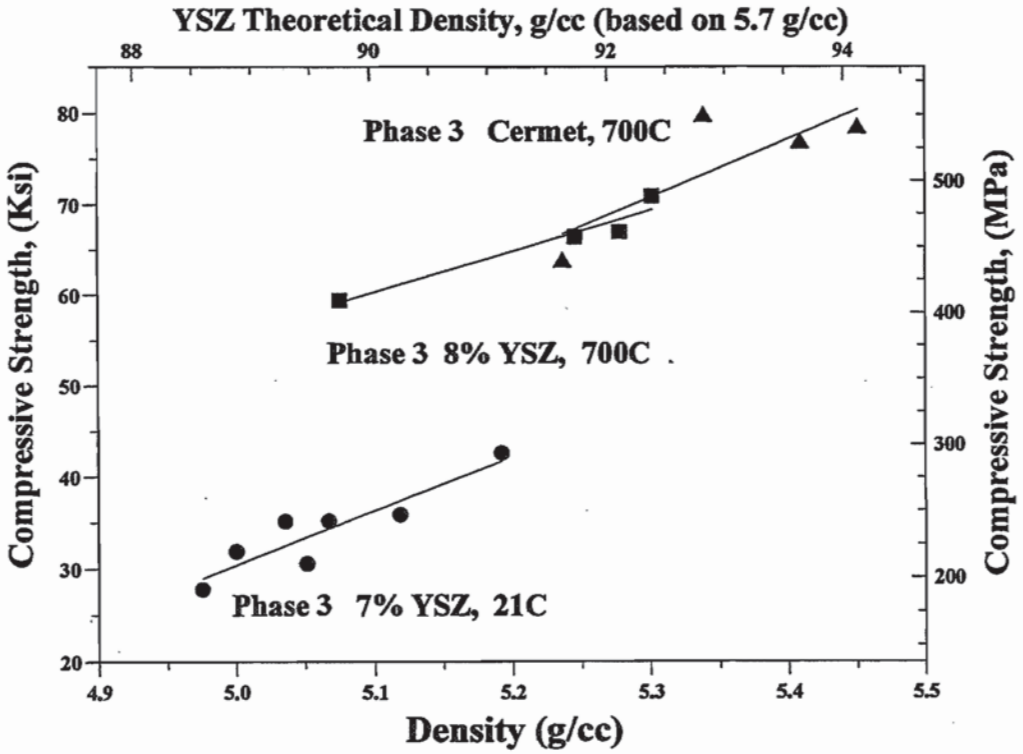

Figure 9: Compressive strength vs. density

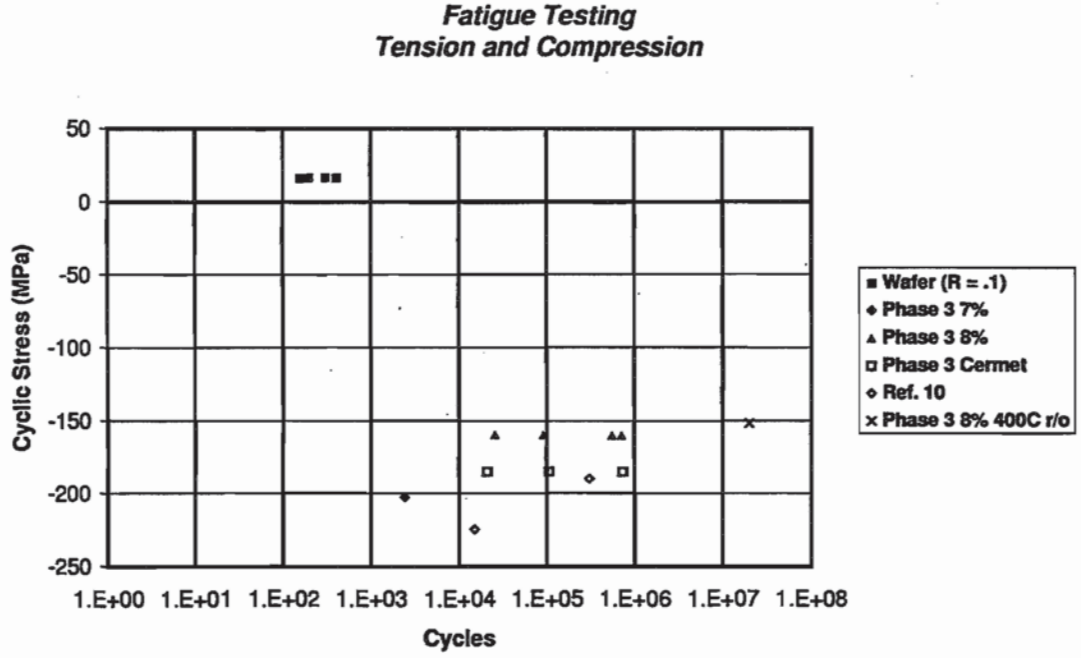

Figure 10: Isothermal fatigue results

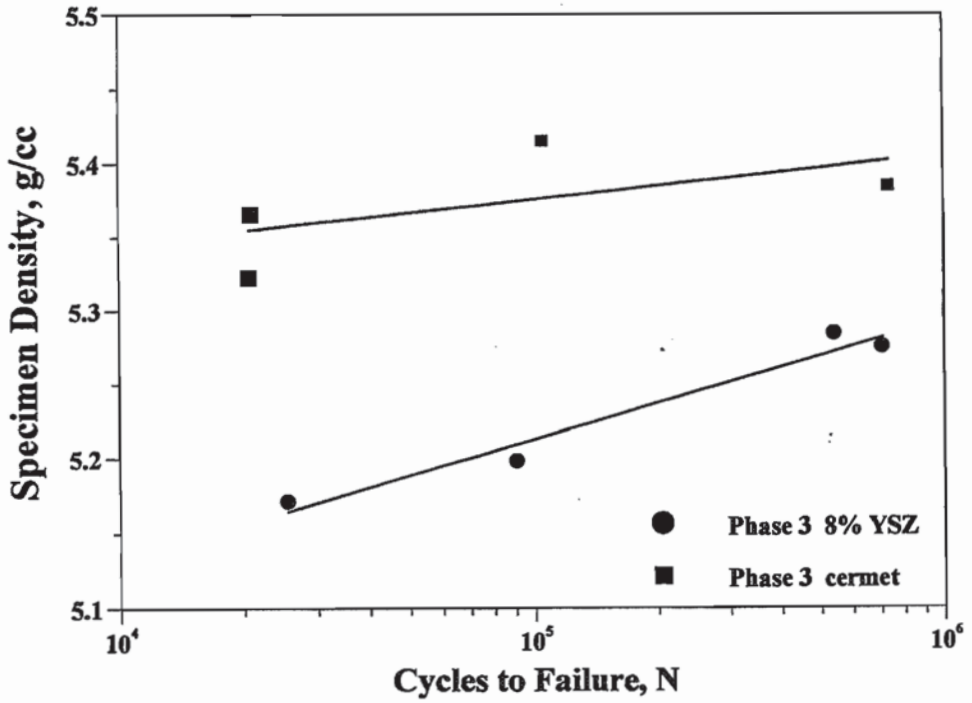

Figure 11: Compressive fatigue vs. density

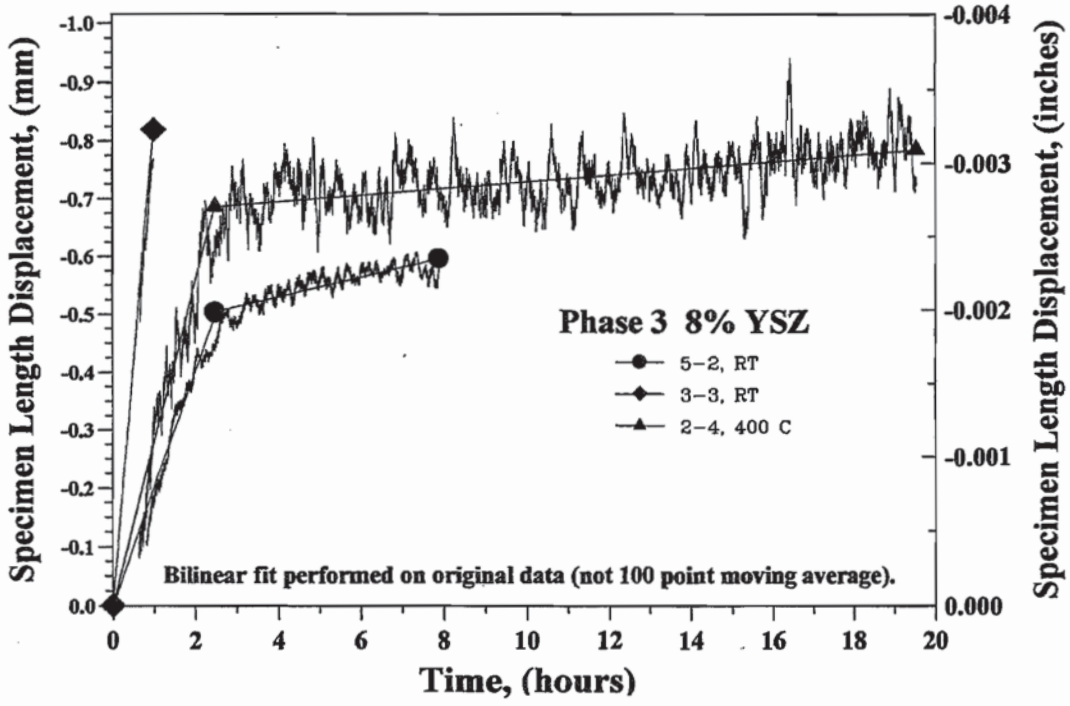

Figure 12: Cyclic ratchetting sampled data

Properties of Plasma Sprayed Bond Coats

W.J. Brindley
NASA Lewis Research Center
Cleveland, Ohio

Abstract

Increasing bond coat oxidation resistance has been clearly linked to increasing durability of the ceramic layer of Thermal Barrier Coatings (TBCs). However, recent studies have shown that significant differences in TBC life can be achieved for different bond coats that have little or no difference in oxidation behavior. This data suggests bond coat properties other than oxidation resistance can also influence TBC life. However, these previous studies did not identify which properties are important to TBC life. A determination of which properties affect TBC life and an understanding of how these properties affect TBC life could be valuable in designing new, more durable TBCs. This paper reviews the results of comparative studies of the properties of three bond coat compositions that have similar oxidation behavior but different TBC lives. An analysis of the properties indicates that the thermal cycle residual stress, calculated from the coefficient of thermal expansion and the stress relaxation behavior of the three alloys, is strongly correlated to the observed differences in TBC life.

Introduction

Plasma sprayed thermal barrier coating (TBC) thermal fatigue life has been shown to be related to both oxidation of the bond coat and to thermal expansion mismatch strains [1,2,3]. The thermal expansion mismatch strains that have received the most attention have been the strains between the substrate and the ceramic layer. The relative lack of interest in the bond coat is because the bond coat coefficient of thermal expansion (CTE) has been shown to be relatively unimportant to the overall CTE of the ceramic layer-bond coat-substrate system, an expected result of the greater thickness of the substrate relative to the bond coat [4]. Thus, development of the bond coat has traditionally been directed to higher bond coat oxidation resistance with little attention paid to the other properties. While this approach has yielded significant improvements in bond coat performance [5], the results of recent studies have indicated that other bond coat properties may also influence the thermal cycle life of TBCs. Work on high strength bond coats by Wortman et al. [6] and an oxidation/thermal cycle life study by Brindley and Miller [7] have both shown that bond coats with poorer oxidation resistance can, in some circumstances, provide longer TBC life than bond coats with better oxidation resistance.

Bond coat properties that can reasonably be expected to influence TBC thermal cycle life, in addition to oxidation response, include CTE, creep (stress relaxation) behavior and elastic modulus [6, 8, 9]. The current paper reviews the results of comparative studies on three bond coat compositions to determine which properties of the bond coat influence TBC life [7, 9, 10, 11]. It will be shown that the residual stress developed during thermal cycling, as determined by the bond coat CTE and stress relaxation behavior, shows a strong correlation to TBC life.

Experimental

The three bond coat compositions examined throughout the series of studies were Ni-16Cr-6Al-0.3Y, Ni-18Cr-12Al-0.5Y and Ni-35Cr-6Al-0.95Y. All of the experiments were conducted on low pressure plasma sprayed (LPPS) deposits of the three alloys. The actual chemistries of the starting powders and the LPPS deposits are given in Table I. The alloys will be referenced throughout the paper by their nominal Cr and Al contents as, for example, 16-6 for the Ni-16Cr-6Al-0.3Y alloy. The LPPS parameters for the bond coat alloys were reported previously [7].

Results and Discussion

Thermal Fatigue Life

The most important property of a bond coat is, of course, the thermal fatigue life of the TBC system for that bond coat. The thermal fatigue life of TBCs incorporating identical air plasma sprayed ceramic top coats and the three different LPPS bond coats were measured in a jet fuel fired Mach 0.3 burner rig [7]. Samples were heated in the burner rig flame for six minutes to a steady state temperature of 1150°C followed by forced air cooling for four minutes. The results of the thermal fatigue testing are shown in Figure 1. The data show that the 35-6 composition has a higher mean thermal fatigue life than the 18-12 alloy and a factor of 3 higher mean life than the 16-6 alloy. Student-Newman-Keuls analysis of the data showed that the differences in mean life were significant at the 95% confidence level, giving a life ranking as: 35-6 > 18-12 > 16-6. The mean TBC lives and 95% confidence intervals for the three bond coat alloys are listed in Figure 1.

Oxidation

Based on the dramatic thermal fatigue life differences, and the assumption that the lowest oxidation resistance bond coat should give the poorest TBC life, it was expected that the 16-6 alloy would show significantly higher oxidation weight gains than the 35-6 alloy. This was not the case. Figure 2 shows the specific weight gains of free standing coupons for isothermal oxidation at 1100°C in air. Each of the three compositions were oxidized in three conditions: polished, grit blasted, and grit blasted + thermal barrier coated [7]. The 16-6 alloy had the lowest weight gain (best oxidation resistance) for all three surface conditions while the 18-12 and 35-6 alloys had the highest weight gains. This result contradicts the expected inverse relation of TBC life to bond coat oxidation weight gain. Clearly the answer to this apparent contradiction is that other bond coat properties, besides oxidation, influence TBC life.

It should be noted that the isothermal oxidation rate results were consistent with the trends in oxide thicknesses for the burner rig tested coupons. Furthermore, the oxide species present on all three alloys after isothermal exposure and after burner rig testing were the same. Thus, TBC life differences could not be explained on the basis of the formation of different oxides for differing bond coat compositions or by a change in oxidation mechanism between isothermal and cyclic exposure [7].

Thermal Expansion

The coefficient of thermal expansion (CTE) of free-standing NiCrAlY coupons was measured as a function of temperature from 23 to 1000°C (Figure 3) [9]. The CTE shown is the average CTE from room temperature to the temperature of interest. The 16-6 alloy exhibited a fairly smooth concave curve that had higher CTEs than the other two alloys up to approximately 900°C. Both the 18-12 and 35-6 alloys show dramatic increases in CTE with increasing temperature, starting at about 800°C and both have higher CTE's than the 16-6 alloy at 1000°C. The CTE response measured at other laboratories for a Ni-22Cr-10Al-Y [12, 13] bond coat alloy were quite similar to that found for the 18-12 alloy. The reason for the differences in CTE response among the alloys has been discussed elsewhere [9, 12]. The important features of these curves for the current paper are simply that there are significant differences in the temperature dependent CTEs of the three alloys and that both the 18-12 and 35-6 alloys have higher CTEs than the 16-6 alloy at 1000°C. A more clear understanding of the significance of these differences will be developed in a later section.

Elastic Modulus

The elastic modulus was measured dynamically on free standing coupons of the three LPPS NiCrAlY alloys as a function of temperature from 23 to 1000°C [11]. The results of the measurements are shown in Figure 4.

There were differences in the bond coat elastic modulus, especially notable at temperatures below 500°C. However, it is clear that the bond coat moduli up to 1000°C were quite high as compared to the modulus of plasma sprayed zirconia-yttria, shown as a range from 20 GPa to 60 GPa on Figure 4 [12, 13]. Elastic moduli measured dynamically for plasma sprayed Ni-22Cr-10Al-Y [12, 13] showed similar behavior to that of the 16-6 and 18-12 alloys of reference 11. Since the elastic stress generated in the coating will be dominated by the lower modulus material, it is evident that the ceramic layer modulus will determine the stress in the TBC up to and probably beyond 1000°C. Noting that the bond coat modulus decreases with temperature, it may be that, at the 1150°C steady state temperature of the burner rig test, the bond coat moduli would be low enough to control stress generation if the system remains elastic. However, as is shown in the later section on stress relaxation, all three bond coats creep rapidly at temperatures above 900°C. Therefore, the stresses will be limited by relaxation of the bond coat and not by the bond coat elastic properties.

Stress Relaxation

There has been a limited amount of creep testing reported on plasma sprayed MCrAlY materials [10, 13, 14, 15]. Creep testing, defined as time dependent deformation under a fixed stress (or load), will give a strong indication of how much stress relaxation will occur for a bond coat. However, the actual deformation which occurs during thermal cycling is time dependent, inelastic deformation imposed by a fixed thermal expansion mismatch strain, in other words, stress relaxation. Stress relaxation tests were conducted on the three alloys to develop data that were directly applicable to stress relaxation during thermal cycling.

The stress relaxation tests were conducted at temperatures from 22 to 1000°C by compressing free standing specimens at a constant crosshead velocity until an approximately steady state stress was attained [10]. At this point the crosshead of the test machine was stopped and the load was monitored as a function of time. Figure 5 shows the stress versus time trace for multiple tests on a single sample. Relaxation data as in Figure 5 were reduced to strain versus time curves, as is usual for representing creep. It was found in doing this that the stress relaxation data and the creep data from ancillary constant crosshead velocity tests agreed quite closely [10]. This means that the creep and stress relaxation behavior are history independent.

Following the procedure shown schematically in Figure 5, it was not possible to test the alloys at identical starting stresses. Therefore, it was not possible to directly compare their stress relaxation behavior. However, it was possible to write Euler forward integration equations for each alloy that were very good descriptions of their isothermal stress versus time behavior during stress relaxation [10]. The result of the calculations for a starting stress of 35 MPa and 900°C are shown in Figure 6. It is clear stress relaxation for all three alloys was quite rapid, even for the relatively low starting stresses. In fact, relaxation reduced the 35-6 stress to approximately 30% of the starting stress at times of 60 seconds or less. This time is well within the approximately 240 seconds that the sample was at the 1150°C steady state temperature in the burner rig. Furthermore, relaxation leads to a final stress for the 16-6 alloy that was a factor of three higher than that for the 35-6 alloy. This relaxation behavior at a constant temperature should be similar to relaxation during the steady state portion of a burner rig cycle. To relate relaxation to TBC life, it is necessary to examine the entire thermal cycle.

Stress Relaxation, CTE and TBC Life

Having identified differences in CTE and relaxation behavior between the alloys leads naturally to the next question: how do these properties affect TBC life? This has been investigated by expanding the simple forward integration model of stress relaxation developed above to predict the stresses in the ceramic layer during two burner rig thermal cycles to 1150°C. The development of the model has been discussed in detail elsewhere [9]. The basic assumptions of the model were that 1) the important stresses driving TBC failure for this burner rig test were out-of-plane tensile stresses generated at the peaks of bond coats [16, 17, 18], 2) the residual stress at the beginning of the first cycle was zero, 3) and the oxidation, ceramic layer creep and substrate effects could be ignored since they were the same for all three bond coats. The model also included the temperature dependent properties of the bond coat and realistic temperatures for the bond coat and top coat during a burner rig thermal cycle (Figure 7)[7]. The assumption used to interpret the data was that TBC life decreases with increasing tensile out-of-plane stresses.

The calculated out-of-plane stress versus time curves for the first two burner rig cycles are shown in Figure 8. As a point of reference, a stress versus time curve for a 16-6 alloy assumed to deform only elastically is also shown in Figure 8. The most striking feature of the figure is that there was a dramatic increase in the out-of-plane tensile stress for the bond coats that were allowed to relax as compared to the 16-6 elastic alloy. The conclusion drawn from this data is that bond coats that relax at the use temperature would provide shorter TBC life than a strong alloy that deforms only

elastically during a thermal cycle. This conclusion agrees qualitatively with the findings of Wortman et al. that showed that creep resistant bond coats provided higher ceramic layer thermal cycle lives than did standard bond coats [6]. The result also agrees with the more quantitative Finite Element Model findings of Petrus and Ferguson [18] for a rough bond coat / ceramic layer interface.

The second point from Figure 8 is that the 16-6 bond coat that was allowed to relax had the highest residual tensile stress at the end of the thermal cycles, the 18-12 is next highest and the 35-6 alloy had the lowest calculated residual stress. A prediction of TBC life based on the calculated residual stress alone follows the ranking of life determined in the actual burner rig test (Figure 1) as 35-6 >18-12>16-6.

A more clear indication of the relation of calculated residual stress to cyclic life is shown in Figure 9. The solid line is the regression fit to the cyclic life versus residual stress data and the dashed lines indicate the 95% confidence interval for the data. While other factors cannot be strictly ruled out, there appears to be a strong correlation between the cyclic life of a TBC and the calculated residual stress. There is no other factor that has been found to date, including oxidation behavior, that can account for the observed differences in TBC life for these three bond coat compositions.

Another feature of Figure 8 that should be noted is that the residual stress at the end of the first thermal cycle is the same as that at the end of the second thermal cycle, in spite of the very different starting stresses for the first two cycles. This is related to the high rate of relaxation for these alloys at the steady state temperature. Obviously, the final stress would not stabilize as readily if the bond coats did not relax to near zero stress during the steady state temperature portion of the thermal cycle. A longer time to stabilize the stress may occur for these alloys at lower steady state temperatures or for more creep resistant alloys at the 1150°C steady state temperature used in this study [9].

It is now appropriate to revisit the role of CTE in residual stress. For this illustration, only the 16-6 and 35-6 alloys will be examined. Both alloys relax to near zero stress during steady state at 1150°C. Thus, out-of-plane tensile stress generation for these alloys occurs only during cooling [Figure 8]. Also, the 35-6 alloy had a higher CTE to 1000°C than the 16-6 alloy (Figure 10) and is expected to have a higher average CTE to 1150°C. Finally, the elastic out-of-plane tensile stress is directly related to the product of the difference in CTE between the ceramic and bond coat (ΔCTE) and the change in temperature (ΔT) as: $\sigma \propto \Delta CTE \bullet \Delta T$. When ΔT is the same for two different systems, the residual stress scales directly to the ΔCTE. Therefore, in the absence of relaxation, a TBC incorporating the 35-6 alloy would have higher out-of-plane tensile stresses on cooling than would the 16-6 alloy because the ΔCTE to 1150°C is higher for the 35-6 alloy than for the 16-6 alloy (see Figure 10). However, relaxation has been calculated for the 35-6 alloy to continue to temperatures as low as 800°C on cooling, while very little relaxation occurred for the 16-6 alloy on cooling [9]. The high temperature relaxation during cool down for the 35-6 alloy in effect eliminates the stress generated during the 800 to 1150°C high CTE portion of the CTE versus temperature curve. The stress for the 35-6 alloy in this case results from an effective ΔCTE much lower than for the elastic case and a smaller ΔT over which to generate stresses than

for the 16-6 alloy (see Figure 10). Thus, it is the interaction of stress relaxation with the path of the CTE curve that allows the 35-6 alloy to have lower ceramic layer residual stresses than the 16-6 bond coat, even though the average CTE to 1150°C is higher than for the 16-6 alloy. The point to remember, then, is that if relaxation of the bond coat is occurring, the path of the CTE versus temperature curve may be more important to the residual stresses than is the average CTE to the maximum temperature.

In light of the data, it is much too simple to state that stronger bond coats will provide longer TBC lives. Clearly a very strong bond coat that behaves elastically will give the lowest ceramic layer residual tensile stresses at the end of the thermal cycle (Figure 8). However, the 16-6, which was the strongest of the three bond coats examined, had the highest residual stresses while the weakest bond coat had the lowest residual stresses. It appears from this that there is a minimum in TBC life with increasing bond coat strength, with an absolute maximum at strengths that make the bond coat "creep-proof." Thus, for thermal cycles at temperatures at which all these alloys remain elastic, the lowest overall CTE bond coat may be the best. Thus, the important point for bond coat design is that the thermal conditions, bond coat CTE path and relaxation behavior of the bond coat must all be considered to design an optimal bond coat for a TBC.

While the calculated residual stresses for the three bond coats of this study showed a strong correlation to TBC life, it must be remembered that there are other factors that are or may be important in determining TBC life. These will include oxidation, interdiffusion with the substrate and others. For the special case in this study, where oxidation and other factors were taken into account, it appears that the residual stress, as determined by the stress relaxation and CTE behavior of each alloy, had a significant influence on TBC life.

Summary and Conclusions

The physical and mechanical properties of three low pressure plasma sprayed (LPPS) NiCrAlY bond coats with similar oxidation behavior were reviewed with the intent of determining which of these properties were of most importance to TBC life. While oxidation is still a primary driver of failure, the cyclic life data showed that other factors can have a significant effect on TBC life. Examination of the elastic modulus, CTE and stress relaxation behavior of the three alloys showed significant differences in CTE and stress relaxation for the alloys while the elastic modulus of the alloys was not expected to be important to TBC life. A simple model devised to examine the potential effect of stress relaxation and CTE on TBC life indicated that :

1) Stress relaxation of the bond coat for plasma sprayed coatings is expected to result in significant increases in the out-of-plane residual stresses generated at bond coat peaks as compared to bond coats that do not creep. Since out-of-plane tensile stresses cause delamination of the ceramic layer, stress relaxation of the bond coat is expected to have a deleterious effect on TBC life.

2) The calculated residual stresses due to bond coat creep showed a strong correlation to the measured thermal cycle lives of TBCs deposited on the three bond coats. Thus, residual stresses can account for the difference in TBC life for the three alloys while the factors of

oxidation and elastic modulus cannot.

3) The scenario treated in this paper was for residual stresses under one thermal cycle condition. It is clear, however, that the residual stresses will depend on steady state temperature and cooling rates and may depend on heating rates. Thus, bond coat selection is not simply a matter of selecting the bond coat that gives the lowest calculated residual stress for the 1150°C burner rig cycle of this study. Rather, it requires consideration of the specific thermal cycle for a given application.

TBC failure is complex and involves numerous factors. For the current study, where oxidation and elastic modulus have been ruled out, and secondary factors, such as bond coat roughness and substrate effects have been minimized, there is strong evidence that bond coat stress relaxation and CTE influence TBC failure. In the general case, additional factors that must be considered in selecting a bond coat include oxidation, bond coat roughness, differences in oxide strength and oxide adhesion and possibly others. These factors require further study to determine their effects on TBC life.

Acknowledgments

The author gratefully acknowledges helpful discussions with R.A. Miller and J.G. Goedjen.

References

1. R.A. Miller, Oxidation-Based Model for Thermal Barrier Coating Life, J. Am. Ceram. Soc., 67 [8] 517-521 (1984).
2. W.R. Sevcik and B.L. Stoner, An Analytical Study of Thermal Barrier Coated First Stage Blades in a JT9D Engine, NASA Contractor Report CR 135360 (1978).
3. J.T. DeMasi-Marcin, K.D. Sheffler and S. Bose, Mechanisms of Degradation and Failure in a Plasma Deposited Thermal Barrier Coating, ASME Paper 89-GT-132 (1989).
4. S. Rangaswamy, H. Herman, S. Safai, Thin Solid Films, 73, 43- (1980).
5. M.A. Gedwill, Improved Bond Coatings for use with Thermal Barrier Coatings, NASA Technical Memorandum TM-81567 (1980).
6. D.J. Wortman, E.C. Duderstadt, and W.A. Nelson, Bond Coat Development for Thermal Barrier Coatings, ASME Paper 89-GT-134 (1989).
7. W.J. Brindley and R.A. Miller, Thermal Barrier Coating Life and Isothermal Oxidation of Low-Pressure Plasma-Sprayed Bond Coat alloys, Surf. Coat. Tech., 43-44, 446-457 (1990).
8. R.A. Miller and C.E. Lowell, Failure Mechanisms of Thermal Barrier Coatings Exposed to Elevated Temperatures, Thin Solid Films, 95, 265-273 (1982).
9. W.J. Brindley, Bond Coat Stress Relaxation and Thermal Barrier Coating Life, submitted to Mat. Sci. Eng.
10. W.J. Brindley and J.D. Whittenberger, Stress Relaxation of Low Pressure Plasma Sprayed NiCrAlY Alloys, Mat. Sci. Eng., A163, 33-41 (1993).
11. L.S. Cook, A. Wolfenden and W.J. Brindley, Temperature Dependence of Dynamic Young's Modulus and Internal Friction in LPPS NiCrAlY, J. Mat. Sci., 29, 5104-5108 (1994).
12. P.A. Siemers and R.L. Mehan, Mechanical and Physical Properties of Plasma-Sprayed

Stabilized Zirconia, Cer. Eng. Sci. Proc., 4 [9/10] 828-840 (1983).
13. R.V. Hillery, B.H. Pilsner, R.L. McKnight, T.S. Cook, and M.S. Hartle, Thermal Barrier Coating Life Prediction Model Development, NASA Contractor Report 180807 (1988).
14. M.G. Hebsur and R.V. Miner, Stress Rupture and Creep Behavior of a Low Pressure Plasma-Sprayed NiCoCrAlY Coating Alloy in Air and Vacuum, Thin Solid Films, 147, 143-152 (1987).
15. J.M. Veys, A. Riviere and R. Mevrel, Mechanical Properties of LPPS NiCoCrAlYTa, in H. Eschnauer, P. Huber, A.R. Nicoll and S. Sandmeier (eds.), Proc. First Plasma Technik Symp., Vol. 2, Plasma Technik AG, Wohlen, Switzerland, 1988, pp. 115-124.
16. A.G. Evans, G.B. Crumley and R.E. Demaray, On the Mechanical Behavior of Brittle Coatings and Layers, Oxid. Metals, 20 [5/6] 193-216 (1983).
17. W. Phucharoen, Development of An Analytical-Experimental Methodology for Predicting the Life and Mechanical Behavior of Thermal Barrier Coatings, Ph.D. Dissertation, Cleveland State University (1990).
18. G. Petrus and B.L. Ferguson, A Software Tool to Design Thermal Barrier Coatings, Proc. of the Thermal Barrier Coating Workshop (1994).

	16-6 POWDER	16-6 DEPOSIT	18-12 POWDER	18-12 DEPOSIT	35-6 POWDER	35-6 DEPOSIT
Ni	BALANCE	BALANCE	BALANCE	BALANCE	BALANCE	BALANCE
Cr	16.5	15.6	18.5	17.2	35.0	33.0
Al	5.8	5.2	12.2	11.6	6.0	6.2
Y	0.30	0.20	0.45	0.98	1.08	0.95
C	0.008	0.01	0.017	0.011	0.014	0.014
O	0.015	0.022	0.025	0.030	0.019	0.039
Fe	0.032	0.4	0.038	0.3	0.18	0.4
Co	0.074	<1PPM	0.038	<1PPM	0.038	<1PPM
Si	0.15	0.5	0.021	0.5	0.065	0.5

Table 1. Chemical analyses of the starting powders and the heat-treated plasma spray deposits.

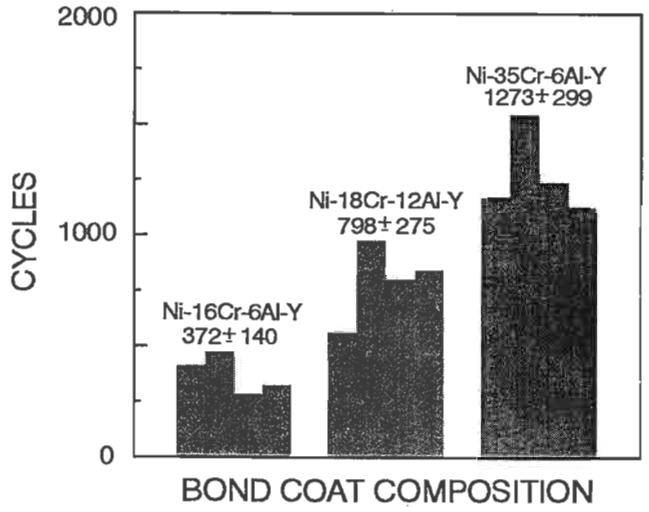

Figure 1. Thermal cycle lives of two layer TBCs, with 16-6, 18-12 and 35-6 bond coats, tested in a JP-5 fueled burner rig [7]. The thermal cycle was 6 minutes in the flame, effectively 4 minutes at 1150°C, followed by 4 minutes of forced air cooling to 30°C. The mean life and 95% confidence interval are indicated for each composition.

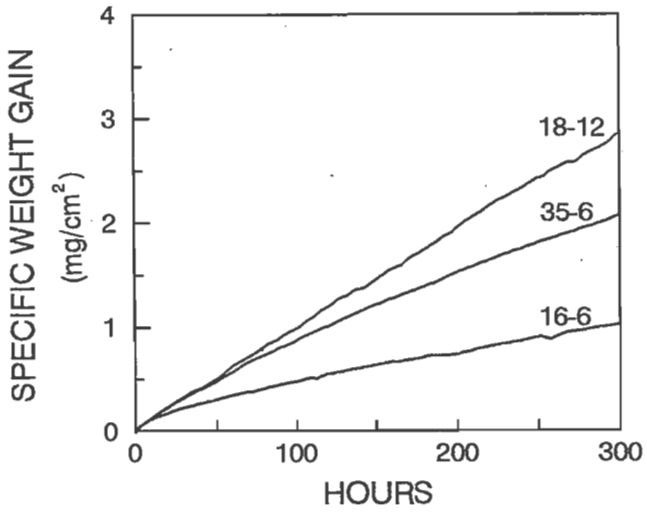

Figure 2. Oxidative weight gains of the 16-6, 18-12 and 35-6 alloys during isothermal oxidation at 1100°C [7]. Curves are representative of six samples for each composition.

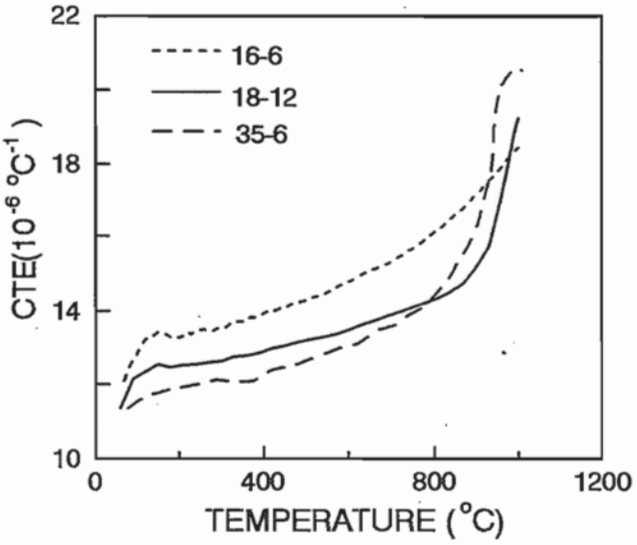

Figure 3. Average CTE from 22°C to the plotted temperature for the 16-6, 18-12 and 35-6 alloys [9]. The plotted data were obtained during cooling.

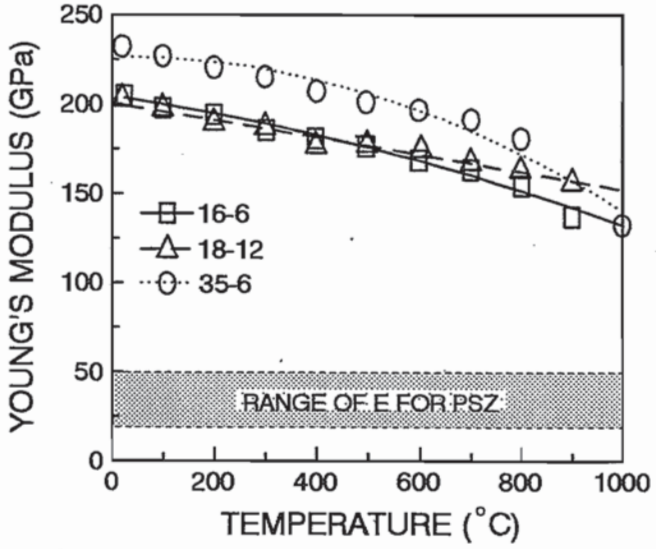

Figure 4. Dynamic Young's modulus as a function of temperature for the 16-6, 18-12 and 35-6 alloys [11].

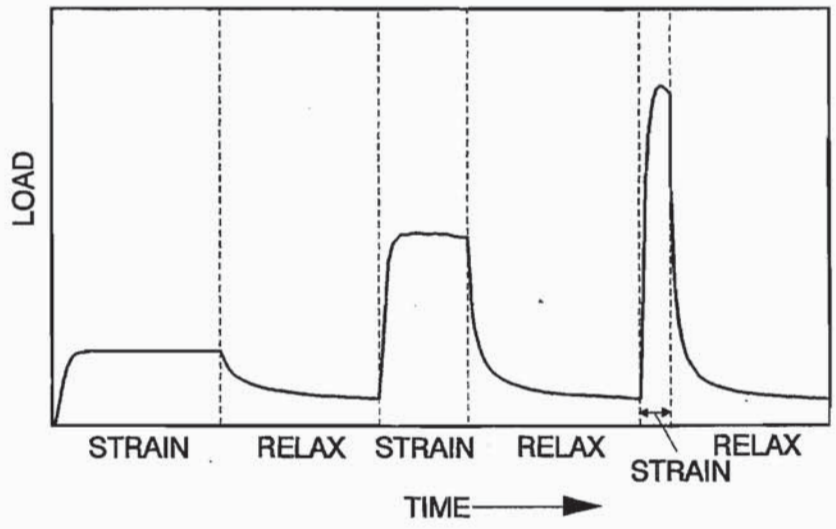

Figure 5. Schematic of the loading and stress relaxation test sequence used to determine relaxation behavior for multiple starting stresses for a single sample [10].

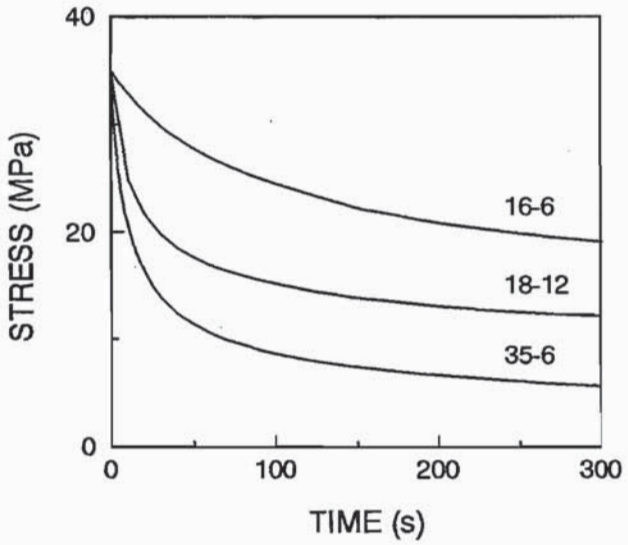

Figure 6. The calculated 900°C isothermal stress relaxation curves for 16-6, 18-12 and 35-6 alloys for a starting stress of 35 MPa [10].

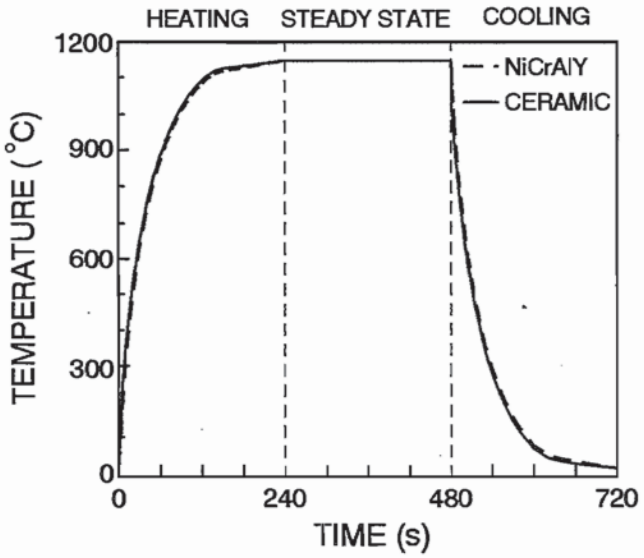

Figure 7. The temperature versus time profiles for the ceramic and bond coat layers during a burner rig thermal cycle to 1150°C. The plotted values are average layer temperatures [9].

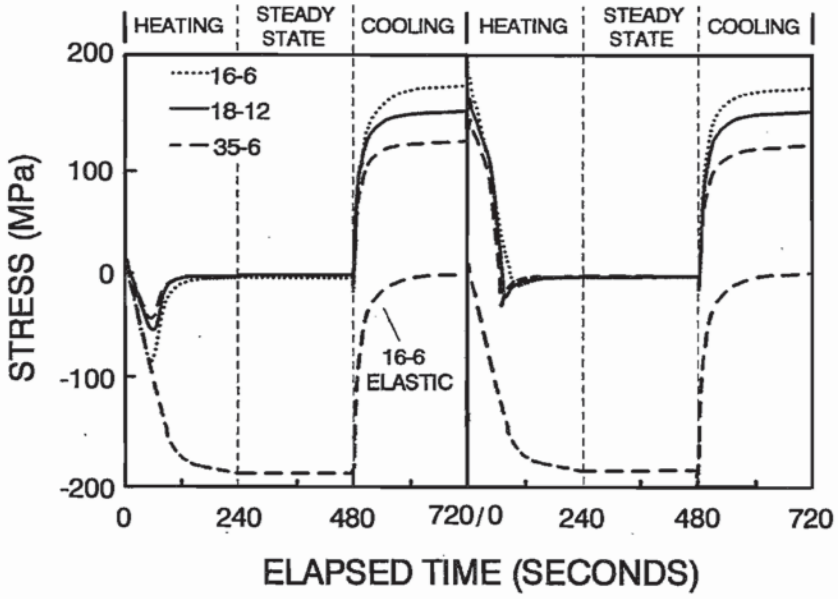

Figure 8. The calculated ceramic layer out-of-plane stress generated during the first two thermal cycles as a function of time for the 16-6, 18-12 and 35-6 alloys. The lowest curve is for an alloy assumed to have the properties of the 16-6 alloy except that it was not allowed to relax [9].

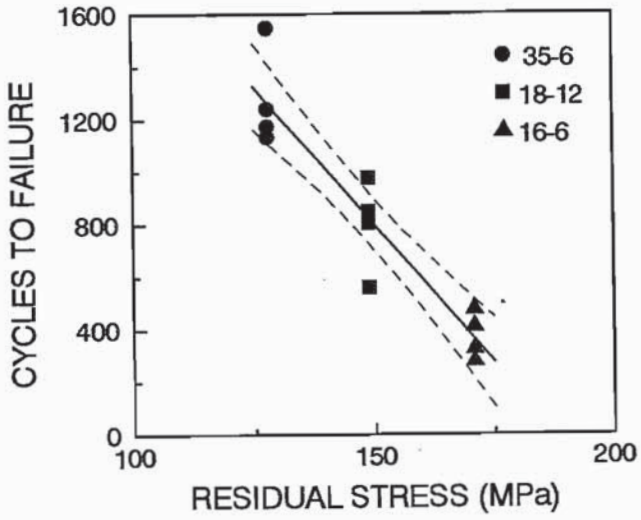

Figure 9. Measured burner rig thermal cycle life versus the calculated residual stress at the end of a cooling cycle. The solid line shows the regression fit to the data and the dashed lines indicate the 95% confidence interval for the line [9].

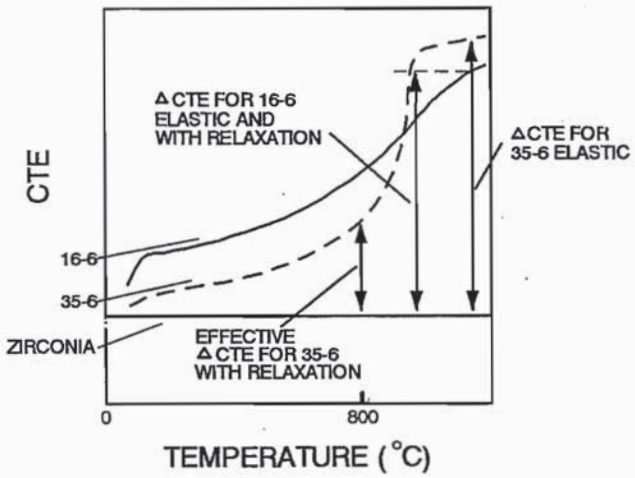

Figure 10.Schematic of CTE versus temperature comparing the ΔCTE for the 16-6 elastic and with relaxation, 35-6 elastic, and the effective ΔCTE of the 35-6 as modified by stress relaxation. ΔCTE is the difference in CTE between the bond coat and the zirconia ceramic layer and is directly related to residual stress generation.

THICK THERMAL BARRIER COATINGS FOR DIESEL ENGINES

M. Brad Beardsley
Caterpillar Inc.
Peoria, IL 61656-1875

ABSTRACT

Caterpillar's approach to applying thick thermal barrier coatings (TTBCs) to diesel engine combustion chambers has been to use advanced modeling techniques to predict engine conditions and combine this information with fundamental property evaluation of TTBC systems to predict engine performance and TTBC stress states. Engine testing has been used to verify the predicted performance of the TTBC systems and provide information on failure mechanisms.

The objective Caterpillar's program to date has been to advance the fundamental understanding of thick thermal barrier coating systems. Previous reviews of thermal barrier coating technology concluded that the current level of understanding of coating system behavior is inadequate and the lack of fundamental understanding may impeded the application of TTBC's to diesel engines. (Ref. 1)

Areas of TTBC technology being examined in this program include powder characteristics and chemistry; bond coat composition; coating design, microstructure, and thickness as they affect properties, durability, and reliability; and TTBC "aging" effects (microstructural and property changes) under diesel engine operating conditions. Methods to evaluate the reliability and durability of TTBCs have been developed that attempt to understand the fundamental strength of TTBCs for particular stress states.

INTRODUCTION

Fifteen TTBC ceramic powders have been evaluated. These powders were selected to investigate the effects of different chemistries, different manufacturing methods, lot-to-lot variations, different suppliers and varying impurity levels, Table 1. The results of the powder characterization for chemistry, particle size distribution, surface area, crystallographic phases, apparent density and Hall flow are shown in Tables 2 to 6. In the chemical analysis, it was found that the three spray dried and sintered materials to be used in the impurity study (lots 34850, 34992, and 34993) range from low levels of alumina and silica (34992), low alumina and mid-level silica (34850), to high alumina and silica (34993), Table 2. The chemistries of the powders produced by different manufacturing methods (HOSP proprietary Metco process, spray dried, spray dried and sintered, fused and crushed, and sol gel materials) also show slightly differing ranges of impurities reflecting the different manufacturing methods.

The particle size distributions of the fifteen materials showed small variations in the mean and size ranges, Table 3. The surface areas of the powders do show a wide range even for similarly manufactured powders (lots 34850, 34992, 34993 and lots 34243, 34302, 34547), Table 4. The crystallographic phases were as expected for the powder processing methods being

investigated, Table 5. The hall flow and apparent density of the materials did not have significant meaning to the results found, particularly the Hall flow which indicated flow problems with several powders which did not occur in use, Table 6.

SPRAY PROCESSING AND THERMAL CONDUCTIVITY

Each of the fifteen materials has been sprayed using 36 parameters selected by a design of experiments to determine the effects of primary gas (Ar and N2), primary gas flow rate, voltage, arc current, powder feed rate, carrier gas flow rate, and spraying distance. The deposition efficiency, density, and thermal conductivity of the resulting coatings were measured. A coating with a high deposition efficiency and low thermal conductivity is desired from an economic standpoint. A general trend for all fifteen materials was an increasing thermal conductivity with higher deposition efficiency as shown in Figure 1. An optimum combination of thermal conductivity and deposition efficiency was found for each lot of powder in follow-on experiments and deposition parameters were chosen for full characterization.

The resulting thermal conductivity and deposition efficiency for each of the powders sprayed with optimized parameters have been determined and are compared to the baseline coating (lot 34547, 8% yttria-zirconia, HOSP) in Figure 2. Several of the powders exhibit a lower thermal conductivity than the baseline coating with the 20% yttria-zirconia and spray dried 8% yttria-zirconia having both lower thermal conductivity and higher deposition efficiency. The higher thermal conductivity of materials such as the calcium titanate may be balanced by its higher deposition efficiency. Whether the higher deposition efficiency balances the higher thermal conductivity (which results in needing a thicker coating to achieve similar thermal conductance) is a component design question.

STRENGTH TESTING

Strengths of the optimized coatings were determined using 4-point bending specimens. The tensile strength was determined using free standing coatings made by spraying onto mild steel substrates which were subsequently removed by chemical etching. The compressive strengths of the coatings were determined using composite specimens of ceramic coated onto stainless steel substrates, tested with the coating in compression and the steel in tension. The compressive strength of the coating was determined from an elastic bi-material analysis of the resulting failure of the coating. The strengths of the coatings compared to the baseline coating are shown in Figure 3.

Although initial comparison of the materials would appear to be straight forward from these results, aging tests of the materials will be necessary to insure that these trends in properties remain after long term exposure to a diesel environment. Some comparisons can be made, such as the comparison between for lot-to-lot variation.

The three lots of 8% yttria-zirconia HOSP materials have similar thermal conductivity, deposition efficiency, and strengths for the parameters selected (all three lots were sprayed with

the same parameters). In order to achieve this, the parameters were selected for robustness. The three lots of material were sprayed with three sets of parameters and the thermal conductivity and deposition efficiency measured. In two of the three sets, the deposition of the lots 34302 and 34143 were approximately one third of the deposition of the baseline material (lot 34547), Table 7. The spray parameters for any given chemistry and specified particle size should be chosen based on the robustness of the parameters over a range of lots rather than on the results from one or two lots of the material.

FATIGUE TESTING

An axial fatigue test to determine the high cycle fatigue behavior of TTBCs has been developed at the University of Illinois (Ref. 4). A fatigue test apparatus has been designed and initial test work performed which demonstrates the ability to provide a routine method of axial testing of coatings. The test fixture replaces the normal load frame and fixtures used to transmit the hydraulic oil loading to the sample with the TTBC specimen itself.

The TTBC specimen is a composite metal/coating with stainless steel ends, Figure 4. The coating is sprayed onto a mild steel center tube section onto which the stainless steel ends are press fit. The specimen is then machined. After machining, the specimen is placed in an acid bath which etches the mild steel away leaving the TTBC attached to the stainless steel ends. Plugs are then installed in the ends and the composite specimen is loaded in the test fixture where the hydraulic oil pressurizes each end to apply the load. Since oil transmits the load, bending loads are minimized. This test fixture as been modified to allow piston ends to be attached to the specimen which allows tensile loading as well as compressive loading of the specimen.

A TTBC coating previously tested at room temperature in compression using this method resulted in a stress-life curve as shown in Figure 5. This data matches previous fatigue data for this material obtained in 4-point bending, but long life data was obtained with this test method (Ref. 3). Tensile data for this coating has also been generated using the modified axial test fixture resulting in a stress-life curve as shown in Figure 6.

In addition to the room temperature data, specimens have recently been tested at 800 C with surprising results. At high temperature, the TTBC exhibits much higher fatigue strength, Figure 7. This behavior is currently thought to be due to sintering of the splat structure of the TTBC at the high temperature (Ref. 4).

Testing of the TTBC using tension/compression cycling has been conducted using the modified test fixture. The goal of this work was to investigate the failure mechanisms of the coating and to determine if tensile and compressive fatigue damage would interact to influence the resulting life of the coating. Coating samples were run with various mean compressive loads and constant tensile loading approximately equal to 90% of the tensile strength of the coating. As shown in Figure 8, there is no interaction of the tensile and compressive load. The material fails in tension at the life predicted by the tensile curve. This indicates that there are two differing failure mechanisms for the TTBC in tension and compression.

AGING EFFECTS

The change in the fatigue strength of the 8% yttria-zirconia at high temperature indicates that the properties of the TTBC materials are not stable at high temperature. In order to further investigate the change in the material properties with exposure at high temperature, a furnace aging test was developed which uses a simulated diesel exhaust environment. This test exposes the specimens to 800 C for 500 hours with no stress applied to the specimens. The resulting change in compressive strength and modulus of aged specimens for six of the fifteen materials is compared to the change in modulus with applied load in Figure 9. The load applied was 40% of the compressive strength prior to aging. As can be seen from Figure 9, the aging with no load at long times has a smaller effect than the stressed condition.

In addition to the static compressive strength and modulus measurements, fatigue studies of the furnace aged materials were also performed. As shown in Figures 10 and 11, the fatigue strength of the aged specimens (500 hour, 800 C, no load) increased for all of the materials tested. The increase in the fatigue strength was not as large as for the specimens held under load, but even the high purity materials exhibited an increase in strength. A more detailed study of the stress-temperature-time affects is needed to fully understand this phenomena.

ACKNOWLEDGMENTS

Research sponsored by the U.S. Department of Energy, Assistant Secretary for Conservation and Renewable Energy, Office of Transportation Technologies, as part of the Ceramic Technology Project of the Materials Development Program, under contract DE-AC05-840R21400 with Martin Marietta Energy Systems, Inc.

REFERENCES

1. R. A. Miller, "Assessment of Fundamental Materials Needs for Thick Thermal Barrier Coatings (TTBC's) for Truck Diesel Engines", DOE/NASA/21749-1, NASA TM-103130, May 1990.
2. M. B. Beardsley, "Thick Thermal Barrier Coatings", Proceedings of the Annual Automotive Technology Development Contractors' Coordination Meeting 1993, pg. 213.
3. R. C. Brink, "Material Property Evaluation of Thick Thermal Barrier Coating Systems", 89-ICD-13, The American Society of Mechanical Engineers, 1989.
4. K. F. Wesling, D. F. Socie, and M. B. Beardsley, "Fatigue of Thick Thermal Barrier Coatings", J. Am. Ceram. Soc., 77[7], 1994, pg. 1863-1868.

Table 1. Powders selected for evaluation to investigate the effects of different chemistries, different manufacturing methods, lot-to-lot variations, different suppliers and varying impurity levels.

MATERIAL	MFG METHOD	SUPPLIER	LOT NO.
8% Yttria-Zirconia	HOSP	Metco	L34547
20% Yttria-Zirconia	Spray Dried	Metco	L34108
24% Ceria-Zirconia	HOSP	Metco	L34209
Calcium Titanate	Spray Dried	Metco	L34849
Mullite	Fused & Crushed	Metco	L34542
DIFFERENT MANUFACTURING METHODS			
8% Yttria-Zirconia	Sprayed Dried	Metco	L32678
8% Yttria-Zirconia	Spray Dried & Sintered	Metco	L34850
8% Yttria-Zirconia	Fused & Crushed	Norton	L281
8% Yttria-Zirconia	Sol Gel	Metco	L34440
DIFFERENT SUPPLIERS			
8% Yttria-Zirconia	Sprayed/Compacted/Sintered	Zircoa	L39073
8% Yttria-Zirconia	Spray Dried & Sintered	Met Tech	L1081
LOT-TO-LOT VARIATIONS			
8% Yttria-Zirconia	HOSP	Metco	L34143
8% Yttria-Zirconia	HOSP	Metco	L34302
IMPURITIES			
8% Yttria-Zirconia	Spray Dried & Sintered	Metco	L34992
8% Yttria-Zirconia	Spray Dried & Sintered	Metco	L34992

Table 2. Chemistries of the fifteen selected materials.

Material	Lot #	Al_2O_3	CaO	Fe_2O_3	HfO_2	MgO	SiO_2	TiO_2	Th+U	Y_2O_3	CeO_2	ZrO_2	Na_2O
8% YSZ-HOSP	L34547	<.01	<.01	<.01	1.73	<.01	<.01	0.09	<.01	7.98	<.01	90.21	0.27
20% YSZ-S/D	L34108	0.06	0.03	<.01	1.51	<.01	0.16	0.07	0.03	19.34	<.01	77.4	0.08
24% CSZ-HOSP	L34209	<.01	0.07	0.02	1.27	0.04	0.04	0.08	<.01	2.42	25.12	70.84	0.15
CaTiO5	L34849	0.21	40.9	0.06		0.23	0.43	57.54	<.01	<.01	<.01	0.09	0.18
Mullite	L34542	74.34	0.03	0.01		<.01	25.32	<.01	<.01	<.01	<.01	0.01	0.37
8% YSZ-S/D	L32678	0.27	0.13	0.06	1.79	<.01	0.72	0.1	0.05	7.34	<.01	89.44	0.1
8% YSZ-S/D-S	L34850	0.01	0.01	0.01	1.74	<.01	0.18	0.04	<.01	7.8	<.01	90.21	0.29
8% YSZ-F/C	L281	0.03	0.04	<.01	1.64	<.01	<.01	0.2	<.01	7.46	<.01	90.63	0.08
8% YSZ-SOLGEL	L34440	<.01	<.01	<.01	1.58	<.01	<.01	0.06	<.01	7.37	<.01	90.99	0.18
8% YSZ-S/C-S	L39073	0.08	0.18	0.11	1.81	<.01	<.01	<.01	0.04	7.5	<.01	90.28	0.03
8% YSZ-S/D-S	L1081	0.01	<.01	0.02	1.84	<.01	0.22	0.08	0.01	7.47	0.01	90.35	0.16
8% YSZ-HOSP	L34143	<.01	<.01	0.04	1.67	<.01	<.01	0.1	<.01	7.77	<.01	90.42	0.11
8% YSZ-HOSP	L34302	<.01	<.01	<.01	1.63	0.03	0.03	0.13	<.01	7.58	<.01	90.51	0.22
8% YSZ-S/D-S	L34992	<.01	<.01	0.03	1.65	<.01	<.01	0.14	<.01	7.2	<.01	90.98	0.22
8% YSZ-S/D-S	L34993	0.26	0.13	0.05	1.76	<.01	0.69	0.1	0.01	7.01	0.01	89.99	0.24

Table 3. Particle size distribution and mean particle size of the fifteen selected materials.

Material	Lot #	Percentile (micron)			Mean Size, micron
		10%	50%	90%	
8% YSZ-HOSP	L34547	20.37	50.87	103.78	56.76
20% YSZ-S/D	L34108	30.16	66.36	124.11	74.15
24% CSZ-HOSP	L34209	22.12	50.92	103.15	56.92
CaTiO5	L34849	39.23	67.09	119.88	75.61
Mullite	L34542	52.32	94.38	147.48	96.22
8% YSZ-S/D	L32678	29.41	60.67	113.99	67
8% YSZ-S/D-S	L34850	27.95	56.54	108.7	62.82
8% YSZ-F/C	L281	32.07	64.08	117.48	70.01
8% YSZ-SOLGEL	L34440	33.62	57.22	101.93	62.59
8% YSZ-S/C-S	L39073	34.74	63.82	110.45	68.3
8% YSZ-S/D-S	L1081	29.01	54.95	102.47	60.42
8% YSZ-HOSP	L34143	25.23	54.08	105.31	59.9
8% YSZ-HOSP	L34302	22.85	49.65	102.46	56.32
8% YSZ-S/D-S	L34992	26.08	53.84	104.87	59.91
8% YSZ-S/D-S	L34993	26.5	55.08	104.66	60.67

Table 4. Surface areas of the fifteen selected materials.

MATERIAL	LOT NO.	Single Point, m^2/g	BET, m^2/g
8% YSZ-HOSP	L34547	0.3346	0.3461
20% YSZ-S/D	L34108	1.9386	2.0047
24% CSZ-HOSP	L34209	0.2994	0.3031
CaTiO5	L34849	2.2343	2.3069
Mullite	L34542	0.1833	0.1440
8% YSZ-S/D	L32678	3.6373	3.7554
8% YSZ-S/D-S	L34850	1.0337	1.0640
8% YSZ-F/C	L281	0.0623	0.0442
8% YSZ-SOLGEL	L34440	4.1542	4.2505
8% YSZ-S/C-S	L39073	0.1715	0.1307
8% YSZ-S/D-S	L1081	0.3071	0.3155
8% YSZ-HOSP	L34143	0.2559	0.2664
8% YSZ-HOSP	L34302	0.2671	0.2790
8% YSZ-S/D-S	L34992	0.7742	0.7970
8% YSZ-S/D-S	L34993	0.2544	0.2706

Table 5. Crystallographic phases for the fifteen powders selected. (ND - Not detected)

MATERIAL	LOT NO.	Stabilized Phases & Tetragonal Zirconia	Monoclinic Zirconia	Yttria
8% YSZ-HOSP	L34547	91.1	8.9	ND
20% YSZ-S/D	L34108		82-80	18-20
24% CSZ-HOSP	L34209	93.8	6.2	ND
CaTiO5	L34849	100% Calic	um Titanate	
Mullite	L34542	100% Mull	ite	
8% YSZ-S/D	L32678		92-93	7-8
8% YSZ-S/D-S	L34850	63.5	36.5	ND
8% YSZ-F/C	L281	100	ND	ND
8% YSZ-SOLGEL	L34440	100	0	ND
8% YSZ-S/C-S	L39073	85.7	14.3	ND
8% YSZ-S/D-S	L1081	62.5	37.5	ND
8% YSZ-HOSP	L34143	93.0	7.0	ND
8% YSZ-HOSP	L34302	91.1	8.9	ND
8% YSZ-S/D-S	L34992	73.5	26.5	ND
8% YSZ-S/D-S	L34993	70.1	29.9	ND

Table 6. Hall flow and apparent density for the fifteen selected materials.

Material	Lot #	Hall Flow, sec	Apparent Density, g/cc
8% YSZ-HOSP	L34547	77.9	2.27
20% YSZ-S/D	L34108	47.3	1.52
24% CSZ-HOSP	L34209	34.1	2.4
CaTiO5	L34849	117.4	1.05
Mullite	L34542	71.6	1.16
8% YSZ-S/D	L32678	52.2	1.44
8% YSZ-S/D-S	L34850	*	1.1
8% YSZ-F/C	L281	45.1	2.55
8% YSZ-SOLGEL	L34440	39.2	1.72
8% YSZ-S/C-S	L39073	*	1.84
8% YSZ-S/D-S	L1081	40.3	2
8% YSZ-HOSP	L34143	51.3	2.27
8% YSZ-HOSP	L34302	81.7	2.26
8% YSZ-S/D-S	L34992	*	2.26
8% YSZ-S/D-S	L34993	46.3	1.76

* material did not flow

Table 7. Thermal conductivity and deposition efficiency for three lots of HOSP, 8% yttria-zirconia showing variations when sprayed with three different sets of parameters.

	Thermal Conductivity, W/m-K			Deposition Efficiency, %		
Parameter Set	Lot 34547	Lot 34302	Lot 34143	Lot 34547	Lot 34302	Lot 34143
1	0.79	0.94	0.94	30	26	22
2	0.91	1.07	1.07	48	37	38
3	1.20	1.25	1.29	65	58	60

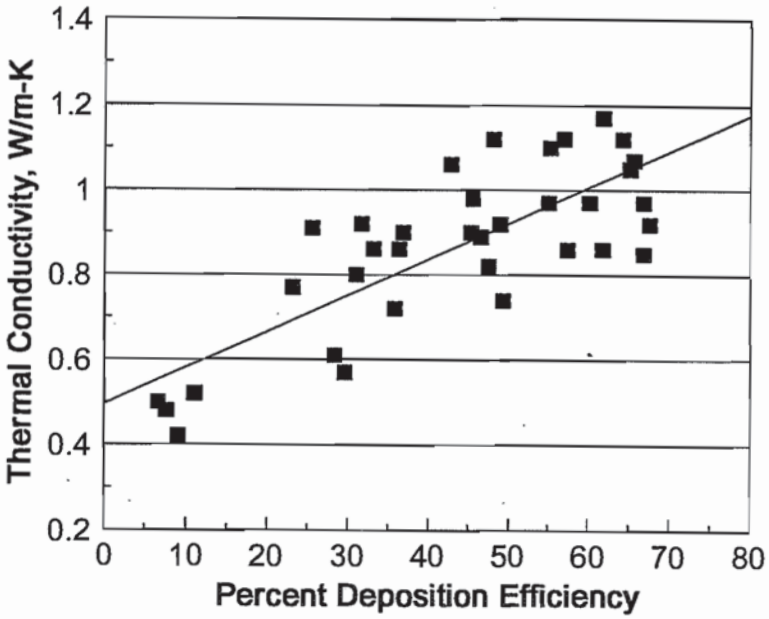

Figure 1. Thermal conductivity verses deposition efficiency for the 36 spray parameters used to spray the baseline 8% yttria-zirconia (HOSP, lot 34547).

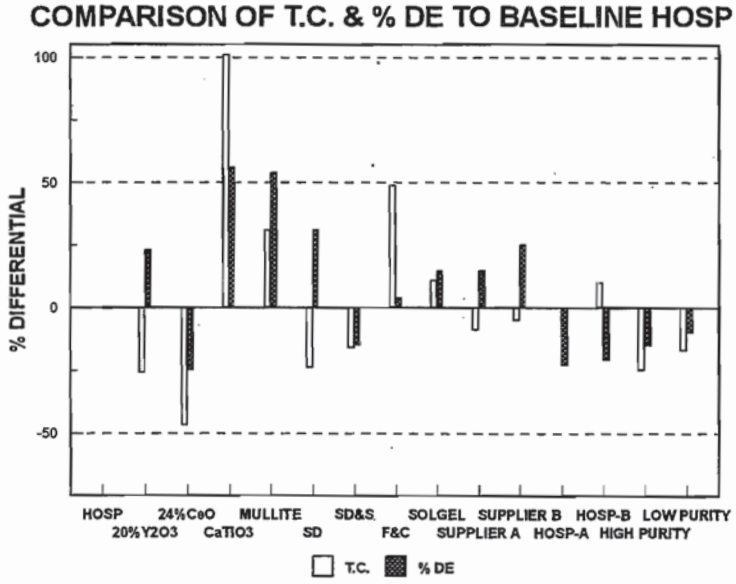

Figure 2. Optimized thermal conductivity and deposition efficiency for each material compared to the 8% yttria-zirconia baseline (HOSP, lot 34547).

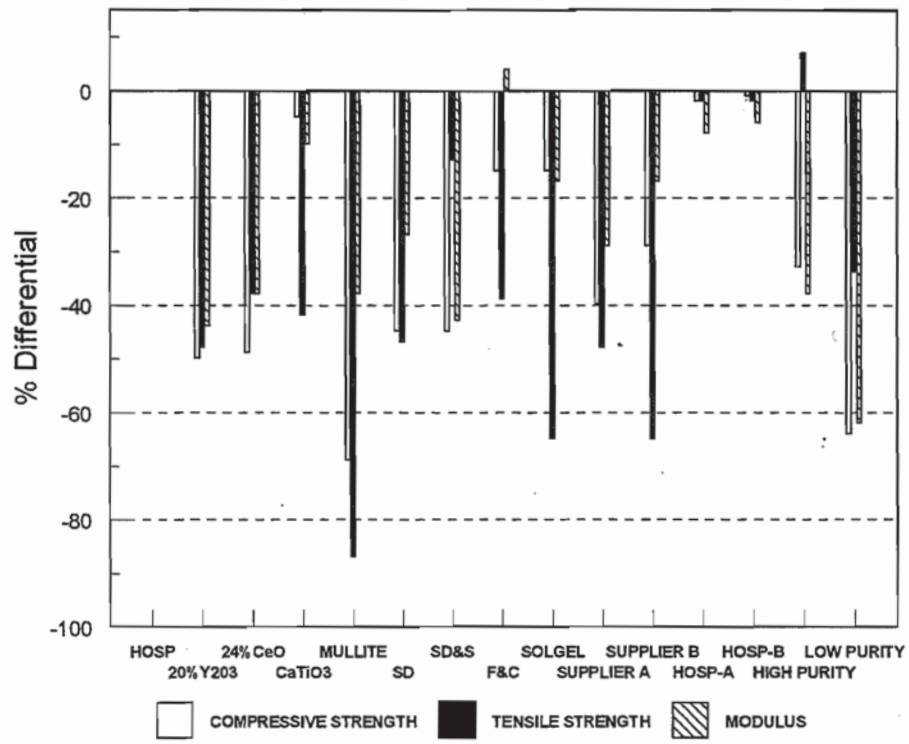

Figure 3. Tensile and compressive strengths and compressive elastic modulus of the fifteen materials compared to the baseline 8% yttria-zirconia (HOSP, lot 34547)

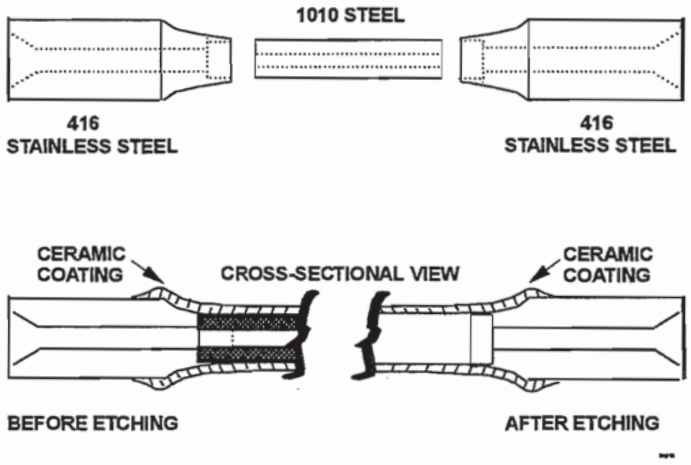

Figure 4. Composite metal/coating specimen used to obtain axial fatigue strength of selected coating materials.

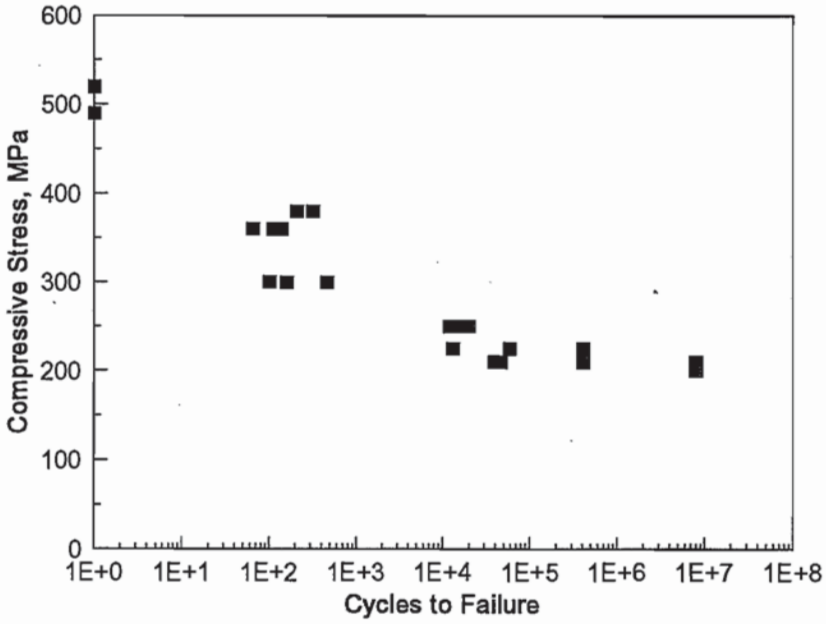

Figure 5. Compressive fatigue strength of an 8% yttria-zirconia TTBC at room temperature as determined using the composite metal/ceramic axial test specimen. (stress ratio = 0.07)

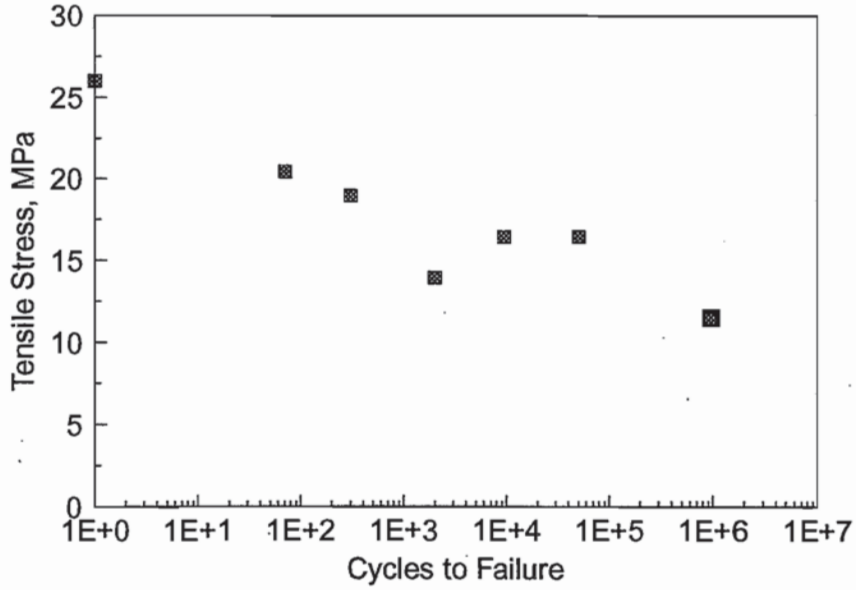

Figure 6. Tensile fatigue data generated using the modified axial test fixture. (stress ratio = 0)

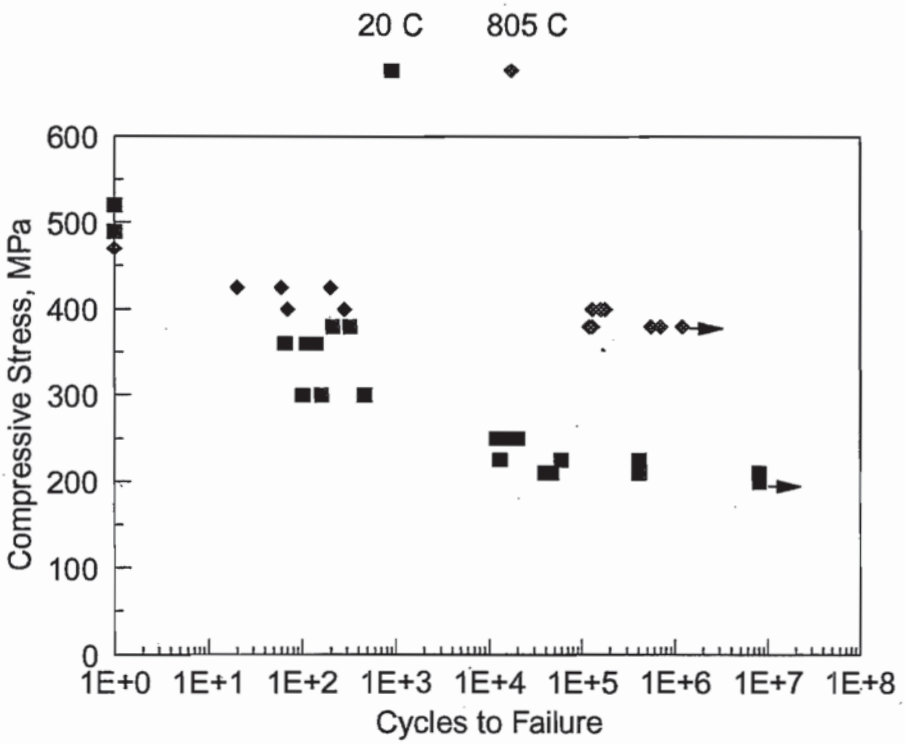

Figure 7. Comparison of room temperature and 800 C test results for compressive fatigue strength of 8% yttria-zirconia showing the increased strength at high temperature thought to be caused by sintering of the splat structure of the TTBC.
Figure 8.

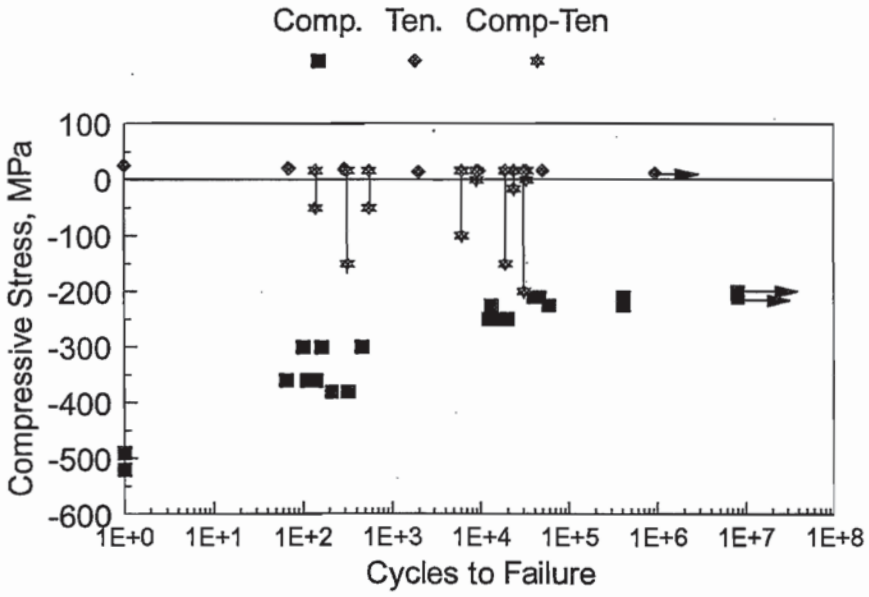

Figure 8. Comparison of the compressive, tensile and combined compressive-tensile testing of an 8% yttria-zirconia TTBC showing no interaction between the failure in tension and compression.

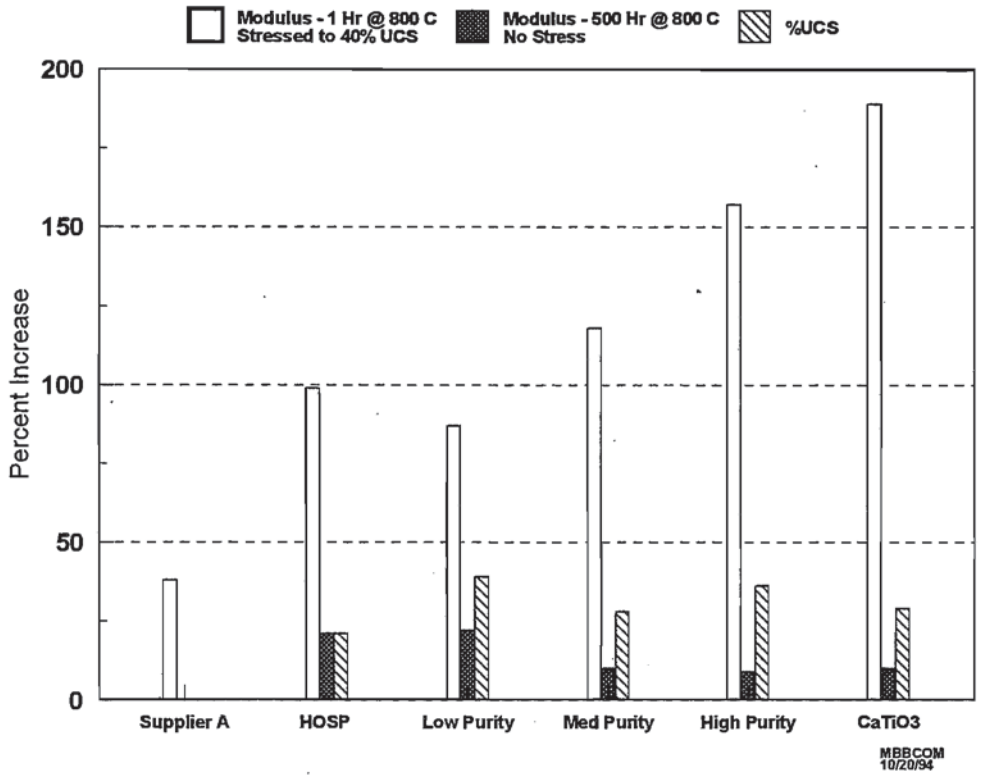

Figure 9. Increases in the elastic modulus and compressive strength of six of the materials in the aged condition (500 hours, 800 C, no load).

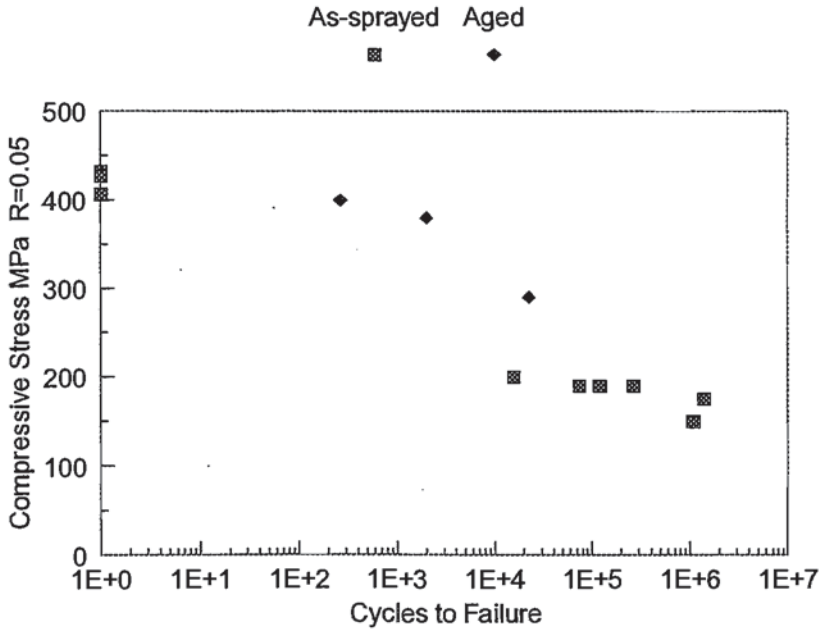

Figure 10. The fatigue strength of aged specimens (500 hour, 800 C, no load) increased slightly for the 8% yttria-zirconia baseline material (HOSP, lot 34547).

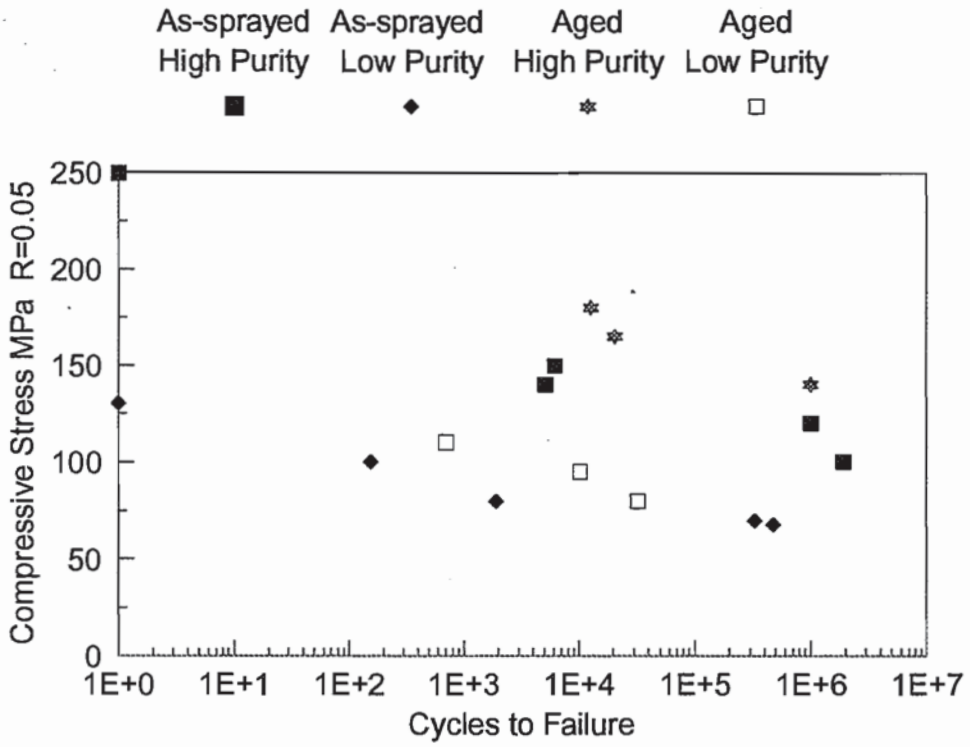

Figure 11. The fatigue strength of aged specimens (500 hour, 800 C, no load) for the high purity (lot 34992) and low purity (lot 34993) 8% yttria-zirconias showing similar fatigue strength increases in the aged condition.

SOME ASPECTS OF THE HOT CORROSION OF THERMAL BARRIER COATINGS

Robert L. Jones
Code 6170, Chemistry Division
Naval Research Laboratory
Washington, DC 20375-5342

ABSTRACT

This paper provides a pro tem review of the hot corrosion of zirconia-based thermal barrier coatings for engine applications. Emphasis is placed on trying to understand the chemical reactions, and such other mechanisms as can be identified, that cause corrosive degradation of the thermal barrier coating. The various approaches taken in attempts to improve the hot corrosion resistance of thermal barrier coatings are also briefly described and critiqued.

INTRODUCTION

Because of the improved engine efficiency and component life that they promise, we may in the future see substantial use of thermal barrier coatings (TBCs) in industrial gas turbine or diesel engines burning low quality fuel, or operating in corrosive environments. Thermal barrier coatings are envisioned also for military land or sea engines which must be capable of surviving low quality fuel and corrosive environments in wartime emergency. Therefore we clearly need to better understand the potential effects of hot corrosion on thermal barrier coatings.

The majority of present-day engine TBCs are of the Y_2O_3(8wgt%)-stabilized ZrO_2 type. This material has been developed over many years, and is currently thought to give the best TBC performance, especially in aviation gas turbines. Yttria-stabilized zirconia (YSZ) thermal barrier coatings are normally applied either by atmospheric plasma spraying (APS) or electron beam-physical vapor deposition (EB-PVD) over bond coats that are usually MCrAlY's (where M = Ni, Co or Ni,Co), but may also be aluminides or various combinations. Schematic representations of APS and EB-PVD thermal barrier coatings are given in Figs. 1 and 2.

The details of thermal barrier coating production by APS have been described by Miller (1), and those of TBC production by EB-PVD by Strangman (2). In APS, the zirconia layer is built up of "splatted down" molten droplets, and contains a certain amount of porosity. This porosity is highly critical in determining the thermal cycle life of APS thermal barrier coatings (1). In contrast, the EB-PVD zirconia layer consists of columnar particles which are "strain-tolerant" and therefore thought to give increased thermal cycle life. Studies suggest that whereas APS coatings generally fail in the zirconia phase just at the bond coat-zirconia layer interface, perhaps because of strains introduced by oxidation of the bond coat (3), EB-PVD coatings fail within the bond coat oxide that is thermally grown on the bond coat during service life (4).

As recounted by Miller (1), many factors are crucial in obtaining satisfactory Y_2O_3-ZrO_2 thermal barrier coating performance. These include the APS powder (5) and EB-PVD ingot

themselves, the exact operating parameters used in the coating process, the composition and structure of the bond coat, and the physical and crystal structure of the zirconia layer. The achievement and maintenance of the so-called "nontransformable" tetragonal *t'* phase structure, as first identified by Scott (6), appears particularly important. If ZrO_2 containing about 8 wgt% (4.5 mol%) Y_2O_3 is heated into the cubic or molten phase regions of the Y_2O_3-ZrO_2 phase diagram (Fig. 3) and then quenched rapidly (as in APS or EB-PVD processing), the tetragonal *t'* phase is produced (7,8). Evidence suggests that this phase is the major reason for the superior TBC performance of Y_2O_3(8wgt%)-ZrO_2, both in that it has a microcracked structure that may alleviate thermal stress (1), and that it avoids the catastrophic (because it involves a 4-5% volume change) transformation between the tetragonal *t* phase and monoclinic phase that normally occurs with thermal cycling of zirconia. However, the *t'* phase is metastable, and it undergoes phase separation into the low Y_2O_3-content "transformable" tetragonal *t* phase and high Y_2O_3-content cubic phase if isothermally aged at 1200°C and above (7,8). The resultant tetragonal *t* phase transforms as normal to the monoclinic phase at low temperature, which promotes physical disintegration of the coating.

The phase transformations of the Y_2O_3-ZrO_2 system, especially cubic (*c*) → metastable tetragonal (*t'*) and tetragonal (*t*) → monoclinic (*m*), are of high interest in ceramic science, and have been reviewed and compared by Heuer et al (9). Recently, Sheu et al (10) studied the *c* → *t'* transformation for the ZrO_2-$MO_{1.5}$ systems where M = Sc, In, Y and rare earths (R). They concluded, among other points, that the *t'* and *t* phases are fundamentally the same tetragonal polymorph and differ only in their range of composition. Other important papers concerning the tetragonal *t'* phase are by Noma et al (11) who show that apparent stability of the *t'* phase up to 1700°C can be obtained by certain processing, and by Virkar and Matsumoto (12) who propose that the *t'* phase is toughened by a ferroelastic domain switching mechanism as opposed to *t* → *m* transformation toughening for the tetragonal *t* phase. Of interest to the TBC coating field are the results of Taylor et al (13) which indicate that CeO_2(25wgt%)-ZrO_2 retains a tetragonal structure even after 100 h at 1600°C, and that CeO_2(25wgt%)-ZrO_2 might therefore be preferable to Y_2O_3(8wgt%)-ZrO_2 for ultra high temperature TBC applications.

One would intuitively expect that reactions with molten deposits could affect these critical phase transformations and thereby the performance of zirconia TBCs. However, this is difficult to demonstrate explicitly, since quantitative x-ray analysis for the various ZrO_2 phases is difficult (8,14), and would be even more so in the presence of co-mixed salt phases. Little evidence therefore can be found in the literature (except in the limited context discussed below) to show the effect of molten salts in driving the various zirconia transformations.

Modes of Hot Corrosion by Molten Deposits

Hot corrosion of TBCs by molten deposits can be categorized into at least four different modes, these being attack by chemical reaction, by "mineralization", by corrosion of the bond coat, or by physical damage by molten phases penetrating into the TBC intragranular voids.

Chemical reaction. -- Attack by chemical reaction is characterized by the presence of an identifiable reaction product, and usually the ability to postulate a specific reaction. It is subject to the laws of stoichiometry and thermodynamics, and the conditions under which attack by

chemical reaction will occur (or can be avoided) should be predictable, provided that the requisite thermodynamic data and a knowledge of the solution chemistry of the involved species are available. The latter can be a particular problem. For example, Y_2O_3(8wgt%)-ZrO_2 contains 4.5 mol% Y_2O_3, and the Y_2O_3 activity would therefore be 0.045 if Y_2O_3 followed ideal solid solution behavior in ZrO_2. Activity coefficients of about 0.1 and 0.01 have been found, however, for Y_2O_3 and Sc_2O_3, respectively, in 5 mol% solid solution in ZrO_2 at 2300-2500°C (15,16). At lower temperatures, these activity coefficients would likely be even smaller (since systems tend to move away from ideal behavior as the temperature decreases), giving a Y_2O_3 activity in, say, Y_2O_3(8wgt%)-ZrO_2 at 1000°C of perhaps 4.5×10^{-4} or lower. The solution chemistry of the various components of the vanadate-sulfate corrosive melts may tend also to exhibit negative deviation from ideal behavior, as has been shown for V_2O_5 in equilibrated SO_3-$NaVO_3$ melts at 800°C (17).

Mineralization. -- Mineralization is defined as an action, usually involving a liquid phase, which tends to move a stressed or nonequilibrium phase toward equilibrium. The mechanism is generally undefined, although it may involve dissolution and reprecipitation. Mineralization has been used extensively in obtaining equilibrium in silica systems, and also in certain zirconia systems. An example where molten $NaVO_3$ may have acted to mineralize CeO_2(20wgt%)-ZrO_2 is cited below.

Bond Coat Corrosion. -- Although we are concerned with hot corrosion of zirconia TBCs, even yttria-stabilized zirconia often appears superior to the MCrAlY or aluminide bond coat in resisting hot corrosion. In his review of TBCs for electric utility gas turbines, Miller (18) cites three references reporting instances where the thin residue of zirconia left after spalling of the zirconia layer protected the underlying bond coat from hot corrosion. While slight corrosion of the bond coat is sometimes found in burner rig tests, heavy corrosion of the bond coat under the zirconia layer has been rarely reported. This may be because, as the bond coat corrosion becomes more severe, the buildup of corrosion product at the ceramic-bond coat interface causes spalling of the zirconia layer, especially for APS coatings. One then finds a "bond coat corrosion at a spall site" morphology, but it is difficult to be certain whether the majority of corrosion occurred before or after spalling of the zirconia.

Physical Damage by Molten Salt Penetration. -- This has been a continuing concern for TBCs used in deposit-producing high temperature environments, and now gains new attention because of the possibility of melt penetration between the columnar grains of TBC coatings produced by EB-PVD. Miller discusses the conditions under which molten deposit penetration into the zirconia layer of TBCs may occur (18). Molten deposits contract on solidification (unlike ice), but the presence of melt phases within the voids or columnar grain boundaries of the TBC zirconia is nonetheless likely to reduce its tolerance to thermal or physical stresses.

It should be appreciated that there may also be penetration of corrosive gases into, and through, the zirconia layer. For example, experience from the field of metallic hot corrosion suggests that reaction of engine gas SO_3 with transient molten NaCl deposits on the TBC could produce HCl or Cl_2 that would penetrate to the zirconia/bond coat interface and cause accelerated, nonprotective Al_2O_3 growth (which would promote zirconia phase spalling) upon the bond coat surface.

PAST EXPERIENCE IN TBC HOT CORROSION

The majority of research on the hot corrosion of TBCs occurred in the fuel-crisis 1970s and, at least in the USA, mostly under the sponsorship of the US Dept. of Energy. This work has been reported in DOE Conferences of 1979, 1982 and 1987. Other TBC hot corrosion studies relating to electric utility gas turbines have been summarized by Miller (18). One of the first workers in the field of TBC hot corrosion was I. Kvernes, who has published numerous papers including a 1986 review which describes many of his results, as well as other TBC corrosion studies in Europe (19). The present paper draws heavily from these sources.

Experience to date indicates that the principal corrosive fuel impurities capable of causing TBC hot corrosion are sodium, sulfur, vanadium, and possibly also lead and phosphorus. Molten silicates from ingested desert sands are now also considered a hot corrosion threat for TBCs at very high temperatures (20). During combustion, the fuel impurities are oxidized to form oxides which have strong acid or base properties, and which undergo reactions such as

$$Na_2O \text{ (base)} + SO_3 \text{ (acid)} \rightleftarrows Na_2SO_4 \text{ (salt)} \quad [1]$$

$$Na_2O \text{ (base)} + V_2O_5 \text{ (acid)} \rightleftarrows 2\ NaVO_3 \text{ (salt)} \quad [2]$$

Solid inorganic oxides also have innate Lewis acid-base natures, and by studying the high temperature reactions of compounds such as Na_3VO_4 ($3Na_2O \cdot V_2O_5$), $NaVO_3$ ($Na_2O \bullet V_2O_5$) and V_2O_5 itself with TBC (and other) oxides, one can demonstrate (Fig. 4) the potential importance of acid-base interactions in the hot corrosion of TBCs. Note in Fig. 4 that acids react with bases, and vice versa, but no reaction occurs between compounds of comparable acid-base strength. Note also that $NaVO_3$ acts as an acid toward basic Y_2O_3, but as a base toward acidic GeO_2 or Ta_2O_5.

Against this background, we now briefly review reported TBC hot corrosion results. This review is not exhaustive, but rather touches only on those works that serve to illustrate the general TBC hot corrosion experience. McKee et al (21) examined the hot corrosion of APS Y_2O_3-ZrO_2 thermal barrier coatings by deposits typical of Na, S, Pb and V fuel impurities, as well as in burner rig tests burning NaCl and S doped fuel. After 1600°F (871°C) burner rig tests, Na_2SO_4 was found in the pores of the zirconia layer, but X-ray showed no destabilization of the YSZ crystal structure. However, sulfide formation was detected at the substrate IN-738 superalloy/bond coat interface, indicating penetration of the molten sulfate (or possibly a gaseous S_2 phase) through both the zirconia layer and APS NiCrAlY bond coat. Crucible tests with molten vanadates resulted in YVO_4 formation, and cracking and spalling of the YSZ zirconia. Molten $PbSO_4$-Na_2SO_4 in crucible tests gave no discernible destabilization or reaction of the YSZ ceramic, but there was corrosion of the NiCrAlY bond coat with $PbCrO_4$ being formed (presumably by reaction of PbO (base) with Cr_2O_3 (acid)).

In 800°C burner rig tests using GT No. 2 fuel doped with various levels of Na, V, P, Ca, Fe, Mg and S, Bratton et al (22,23) found that MgO-stabilized ZrO_2 is attacked and destabilized according to

$$ZrO_2(MgO) + SO_3\ (g) \rightarrow ZrO_2\ (monoclinic) + MgSO_4 \qquad [3]$$

For fuels containing no Mg, destabilization of MgO-stabilized ZrO_2 occurs also by reactions of the type

$$ZrO_2(MgO) + V_2O_5\ (l) \rightarrow ZrO_2\ (monoclinic) + Mg_3V_2O_8 \qquad [4]$$

When both V_2O_5 and SO_3 are present, they compete for reaction with the MgO stabilizer, much as the case when MgO inhibitors are used with V- and S-containing fuels (24), and destabilization may occur by either $MgSO_4$ or $Mg_3V_2O_8$ formation depending upon the specific activities of SO_3 and V_2O_5 in the corrodent melt.

For Y_2O_3-stabilized ZrO_2 TBCs, Bratton et al concluded that, when both Mg and V are present in the fuel and react to form $Mg_3V_2O_8$, the destabilization reaction is

$$ZrO_2(Y_2O_3) + Mg_3V_2O_8 \rightarrow ZrO_2\ (monoclinic) + 2\ YVO_4 + 3\ MgO \qquad [5]$$

In the absence of Mg in the fuel, the destabilization reaction as determined by Kvernes (25), Hamilton and Nagelberg (26) and others is simply

$$ZrO_2(Y_2O_3) + V_2O_5 \rightarrow ZrO_2\ (monoclinic) + 2\ YVO_4 \qquad [6]$$

Details of the specific course of reaction of V_2O_5 with YSZ, as well as the diffusion behavior of V and Y within the YSZ matrix, are given by Hertl (27). The crystallographic aspects of the reaction of V_2O_5 with Y_2O_3-stabilized ZrO_2 have also been examined by transmission electron microscopy by Susnitzky et al (28).

Note that reactions [5] and [6] indicate Y_2O_3 to be a stronger base than MgO; that is, the stronger base, Y_2O_3, displaces the weaker base, MgO, from reaction with acidic V_2O_5 by

$$Mg_3V_2O_8 + Y_2O_3 \rightarrow 2\ YVO_4 + 3\ MgO \qquad [7]$$

If the fuel contains no V but has high S, YSZ may be destabilized by the reaction of Y_2O_3 with SO_3 in the presence of Na_2SO_4, as shown by Pettit and Barkalow (29), according to

$$ZrO_2(Y_2O_3) + 3\ SO_3\ (+\ Na_2SO_4) \rightarrow Y_2(SO_4)_3\ (in\ Na_2SO_4\ soln) \qquad [8]$$

The reaction occurred more readily at low temperature (704°C) than at high temperature (982°C), and required SO_3 partial pressures of the order of 10^{-4} atm at 704°C and 10^{-3} atm at 982°C for significant reaction to take place. In general, yttria-stabilized zirconia TBCs may thus tend to resist sulfur degradation but be susceptible to vanadium degradation. On the other hand, magnesia-stabilized zirconia is more susceptible to sulfur degradation (18), but could possibly be superior to YSZ in resistance to attack by V_2O_5, as indicated by reactions 5-7.

No chemical reaction of the ZrO_2 matrix itself with V_2O_5 or SO_3-Na_2SO_4 is normally detected in the hot corrosion of TBCs. However, Bratton et al (22) found that reaction of ZrO_2

may occur when phosphorus is present as a fuel contaminant. (Petroleum fuels tend to contain little phosphorus, but phosphorus may be found in alternative fuels such as derived by coal liquefaction). Destabilization of YSZ by P_2O_5 occurs by the reaction

$$ZrO_2(Y_2O_3) + P_2O_5 \rightarrow ZrO_2 \text{ (monoclinic)} + 2\ YPO_4 \qquad [9]$$

When sodium is present, Bratton et al report that there can also be reaction of the ZrO_2 by

$$8\ ZrO_2 + 4\ Na + O_2 + 6\ P_2O_5\ (g) \rightarrow 4\ NaZr_2(PO_4)_3 \qquad [10]$$

while Jones (30) has shown that ZrO_2 reacts readily with P_2O_5 according to

$$ZrO_2 + P_2O_5\ (l) \rightarrow ZrP_2O_7 \qquad [11]$$

Silica in the form of silicates derived from desert sand has recently come into concern as a threat to aircraft engines using TBCs at very high temperatures (> 1200°C). Stott et al (20) have studied the attack of various desert sand melts and silicate glasses at 1400-1600°C on specimens of both APS and EB-PVD Y_2O_3(8wgt%)-ZrO_2. Two mechanisms of attack were identified, depending primarily on the amount of CaO in the melt. While both ZrO_2 and Y_2O_3 were extracted from the YSZ by low-CaO melts, proportionately more Y_2O_3 was extracted, and the YSZ became partially monoclinic because of Y_2O_3 depletion. In the high-CaO melts, less Y_2O_3 was extracted, and there was diffusion of CaO into the ZrO_2 matrix, with the net effect being that the YSZ tended to remain in the tetragonal crystal structure. Substantial damage to the YSZ ceramic resulted in each case, however. The deleterious effect of silica as a materials impurity on the thermal cycle life of Y_2O_3(7wgt%)-ZrO_2 TBCs has also been recently established by Miller et al (31).

Finally, although not directly relevant to TBC hot corrosion, there have been tests by Mitamura et al (32) of ZrO_2 partially stabilized by 3 mol% (5.4 wgt%) Y_2O_3 in alkaline halide melts at 850-1050°C that are of interest. No $t \rightarrow m$ transformation was observed in Na_2CO_3, NaCl + KCl, Na_2SO_4 + NaCl, or K_2SO_4; however, when Na_2SiF_6 was added, there was extensive and rapid $t \rightarrow m$ transformation. No yttria reaction products were detected in the salt, and electron microprobe analysis indicated that Y_2O_3 remained in the ZrO_2 ceramic, but that F, Si, and Na had diffused into the ceramic also, and therefore presumably were the cause of the rapid $t \rightarrow m$ transformation. In contrast, tests with molten PbF_2 resulted in very vigorous corrosion of the Y_2O_3(3mol%)-ZrO_2, but no $t \rightarrow m$ transformation. The authors concluded that the tetragonal phase remained stable because of a strong (physical?) restriction on the *t*-phase particles by the Pb element that had permeated into the sintered zirconia body. These "fluoride effects" are useful in reminding us that there could yet be important interactions between hot corrosion melts and stabilized zirconia TBCs that have not been identified.

APPROACHES TO IMPROVEMENT OF TBC HOT CORROSION RESISTANCE

Generally speaking, the approaches to developing hot corrosion-tolerant thermal barrier coatings have been either 1) to go to a different material than zirconia, 2) to change the Y_2O_3

content, 3) to provide "laser-glazing" or seal coats to prevent salt penetration into the YSZ, or 4) to seek new corrosion-resistant stabilizers for ZrO_2, since the stabilizing oxide has appeared to be the weak point in zirconia TBC corrosion performance.

Different TBC Materials. -- In the past, several different materials such as $CaTiO_3$, $ZrSiO_4$, $ZrTiO_4$ and Ca_2SiO_4 have been proposed for corrosion-resistant "thermal barrier" use. These materials have not come into widespread application. They suffer from not offering the high thermal insulation of zirconia, and commonly have a lower (less desirable) coefficient of thermal expansion. They may also have their own corrosion problems; for instance, Ca_2SiO_4 was found (23) to be extremely susceptible to reaction with SO_3 in the burner rig gas by

$$Ca_2SiO_4 + 2\ SO_3\ (g) \rightarrow 2\ CaSO_4 + SiO_2 \qquad [12]$$

Another proposal (33) has been to add Al_2O_3 and SiO_2 to Y_2O_3-ZrO_2 so as to, upon sintering, envelope the $ZrO_2(Y_2O_3)$ crystallites by zirconium and aluminum silicates which then protect the YSZ crystallites from Y_2O_3 depletion during V_2O_5 hot corrosion. However, given the recent findings of Miller et al as to the harmful effect of silica in YSZ coatings (31), one would expect that the thermal cycle life of such coatings would be reduced, at least in aircraft applications. A new high temperature thermal barrier material, $(Ca_{1-x},Mg_x)Zr_4(PO_4)_6$, has recently been developed which is said to have lower thermal conductivity than zirconia, as well as a coefficient of thermal expansion of near zero (34). It is not certain, however, whether this material would be suitable for TBC usage, or whether it has been tested for hot corrosion resistance. Now the champion of several decades standing, stabilized zirconia is likely to be difficult to dethrone, especially for aircraft use, when all of the necessary properties for successful TBCs are considered.

Higher Y_2O_3 Content. -- One might postulate that increasing the Y_2O_3 content of YSZ could improve its hot corrosion resistance, both by providing "excess" Y_2O_3 to allow for a certain amount of Y_2O_3 depletion without (hopefully) TBC degradation, or by moving into the cubic structure stability region and thereby avoiding the troublesome $t \rightarrow m$ transformation altogether. This idea has been addressed by Miller (18) who, after reviewing the literature, points out that the thermomechanical performance of Y_2O_3(6-8wgt%)-ZrO_2 is so superior to that of higher Y_2O_3 compositions that any benefit gained by increasing Y_2O_3 content would likely be minimal at best.

Sealing of TBC Surface. -- Over the years there have been, and still continue to be, efforts to close the surface of zirconia TBCs by laser-glazing or various "seal coats" to prevent penetration of molten deposits into the zirconia voids. Miller (18) describes some of the early work in this area. None of these procedures have yet come into common usage, perhaps because there have been few applications of TBCs in engines or other applications where heavy surface deposits are developed. The question of salt penetration also needs to be further explored. Nagaraj et al (35) note that, in addition to the Y_2O_3(8wgt%)-ZrO_2 not being destabilized, there was no penetration of salt into the TBC, nor corrosion of the underlying bond coat, in burner rig tests of APS and EB-PVD yttria-stabilized zirconia TBCs at 704°C (2 wgt% S, 10 ppm sea salt) or 927°C (0.4 wgt% S, 5 ppm sea salt). This was true even for EB-PVD coatings which had been feared to be possibly prone to salt infiltration down the intra-columnar

porosity. Similarly, in aircraft engine tests of YSZ thermal barrier coatings, no infiltration of salt through the TBC (although Na_2SO_4 was found on the TBC surface) nor bond coat corrosion was detected despite engine gas pressures of approximately 10 atms, and corrosion conditions aggressive enough to significantly hot corrode aluminide coatings on adjacent 2nd stage HP vanes (36). The extent of TBC penetration could depend, however, on the composition and wetting properties of the specific deposit, with V_2O_5-containing melts known to be particularly wetting.

Corrosion-Resistant Stabilizers. -- While ZrO_2 itself is resistant to reaction with either SO_3-Na_2SO_4 (37) or V_2O_5-containing melts (38), the commonly used CaO, MgO or Y_2O_3 stabilizers for zirconia react readily with these corrodents, forming either the corresponding sulfate or vanadate. Therefore corrosion-resistant stabilizers for ZrO_2 have been sought, with CeO_2, Sc_2O_3 and possibly In_2O_3 being so far the stabilizers that have been proposed for improving TBC corrosion resistance.

Ceria: Ceria was patented as improving TBC hot corrosion performance in 1982 (39). Subsequent laboratory tests confirmed that CeO_2 (presumably because of its greater Lewis acidity) is more resistant to chemical reaction with SO_3-Na_2SO_4 (37) and sodium vanadates (38) than Y_2O_3. However, other laboratory tests (40) indicated that sintered CeO_2(20wgt-%)-ZrO_2 (CSZ) was as rapidly destabilized as sintered Y_2O_3(8wgt%)-ZrO_2 by molten $NaVO_3$, even though pure ZrO_2 and CeO_2 separately did not react chemically with $NaVO_3$.

The destabilization of CSZ by molten $NaVO_3$ appears to be a "mineralization" effect. When CSZ is destabilized by V_2O_5, the product is monoclinic ZrO_2 with surface crystals of $CeVO_4$ (40). However, when CSZ is destabilized by $NaVO_3$, the product is monoclinic ZrO_2 with surface crystals of CeO_2 (containing some Zr), and not $CeVO_4$. Thus there is no evidence of chemical reaction between CSZ and $NaVO_3$; one only "gets back" the original CeO_2 stabilizer. The CeO_2-ZrO_2 system is well known as being difficult to bring to equilibrium, especially at temperatures below 1400°C. However, by using a hydrothermal technique in which 15 wgt% LiCl was added as a mineralizer to the aqueous mixture, Tani et al (41) obtained the CeO_2-ZrO_2 phase relationships depicted in Fig. 5. They propose the equilibrium phases at 900°C to be monoclinic ZrO_2 containing 1-2 mol% CeO_2 which is in equilibrium with cubic CeO_2 containing ~5 mol% ZrO_2. These are the same phases that we detected in the destabilization of CSZ by molten $NaVO_3$. It is probable therefore that, although $NaVO_3$ does not have a high enough V_2O_5 activity to react chemically with CSZ to form $CeVO_4$, $NaVO_3$ may nonetheless destabilize CSZ by a mineralizing effect that allows the metastable tetragonal CSZ to transform at 900°C into its equilibrium monoclinic ZrO_2 and cubic CeO_2(ZrO_2) phases.

A more realistic (in terms of engine service) evaluation of the corrosion behavior of CSZ thermal barrier coatings has been made by Nagaraj and Wortman (42) in burner rig tests using vanadium-doped fuels. The tests compared the performance of CSZ TBCs with that of YSZ and MSZ (MgO-stabilized ZrO_2) TBCs at 704° and 899°C using contaminant levels of 29.6 ppm of sea salt in air, and 1.93 vol% S and 32 ppm V in fuel. Both APS and EB-PVD prepared coatings were tested, as well as EB-PVD coatings which had sputtered "seal" coats of HfO_2 (45 microns), Al_2O_3 (7.5 microns), or Pt (7.5 microns).

The MSZ thermal barrier coating suffered the most hot corrosion, with major amounts of $MgSO_4$ and minor amounts of Mg vanadate forming at both temperatures (although no spalling was observed within the 200 h test period). More moderate hot corrosion was shown by the YSZ and CSZ TBCs. The Y_2O_3-stabilized ZrO_2 coatings, both APS and EB-PVD, survived 400 h at 899°C and 200 h at 704°C without spalling or bond coat corrosion. However, there was extensive YVO_4 formation on the YSZ surface at both temperatures, with an additional blocky crystal phase containing yttrium sulfate being found at 704°C. The APS and EB-PVD CeO_2-stabilized ZrO_2 coatings also survived 400 h at 899°C, but APS CSZ spalled within 200 h at 704°C. Only $CeVO_4$ and "free" CeO_2 were found on the 899°C CSZ surface, while the 704°C CSZ surface exhibited mostly cerium sulfate, with minor amounts of $CeVO_4$. Chemical reaction with V_2O_5 therefore occurred with both YSZ and CSZ in these burner rig tests, and it was difficult to ascertain whether CSZ or YSZ was "better". This reflects the problem of obtaining discriminating corrosion tests; if the corrodent level (V in this case) is too low, both coatings look good, if it is too high, both coatings fail. One needs to obtain an intermediate corrodent level that is discriminating, i.e., where the good coating passes and the poor coating fails. However, one can view the burner rig tests here as defining a level of contaminants at which it is known that CSZ (as well as YSZ) will suffer hot corrosion by chemical attack. Moreover, the authors point out that vanadium is the major problem, since in essentially equivalent tests where V was absent, YSZ coatings survived in excess of 1000 h of 927°C cyclic burner rig testing. Another result of these tests was to show that, while the Al_2O_3 , HfO_2 or Pt sputtered seal coats did not suffer chemical reaction, they were not impervious to salt penetration and did not protect the underlying zirconia phase, as evidenced by the corrosion found at the sealant/zirconia interface in each case.

Scandia and india: Sc_2O_3 and In_2O_3 have been identified, primarily from laboratory studies at NRL, as possible new corrosion-resistant stabilizers for ZrO_2 TBCs. These oxides were first selected as being more acidic than Y_2O_3, and therefore less likely to react with acidic vanadate melts than Y_2O_3 (38). Chemical studies confirmed that, as the pure oxide, both Sc_2O_3 (43) and In_2O_3 (44) are more resistant to reaction with molten vanadates or SO_3-Na_2SO_4 than Y_2O_3. In subsequent thermogravimetric (TGA)/SO_3 equilibrium experiments, a semi-quantitative ranking of the resistance of MgO, Y_2O_3, Sc_2O_3, and In_2O_3 (45), as well as CeO_2 (17), to reaction with molten vanadate-sulfate melts was established, with the order of resistance being In_2O_3 > Sc_2O_3,CeO_2 > Y_2O_3,MgO.

However, in addition to corrosion resistance, the candidate oxides must have good "stabilizing ability", and this is not yet fully verified for Sc_2O_3 and especially In_2O_3. Sasaki et al (46), for example, have sought to quantify the stabilizing efficiency of the various oxides, and rank $ScO_{1.5}$ and $InO_{1.5}$ as being significantly less effective (at least for the $t \rightarrow m$ transformation) in stabilization than $YO_{1.5}$. There is also the conclusion by Sheu et al (10) that the stabilizing effect of Sc_2O_3 and In_2O_3 is different from that of Y_2O_3 and the other rare earth oxides. On the other hand, laboratory tests at NRL have indicated the stabilizing ability of Sc_2O_3 in APS ZrO_2 thermal barrier coatings to be on par with that of Y_2O_3, while confirming that the vanadate resistance of Sc_2O_3-ZrO_2 (SSZ) is unequivocally better than that of YSZ (47). India-stabilized zirconia (ISZ) appears more questionable as a high temperature, corrosion-resistant stabilizer. ISZ lost In_2O_3 (by volatilization) during plasma spraying (48), and ISZ has also been found to be destabilized (probably by mineralization as with CeO_2) by molten sodium vanadate (44). The

properties of ISZ might conceivably be improved by better processing, however, since Sasaki et al (46), who have recently studied the In_2O_3-ZrO_2 system in depth, were able to prepare ZrO_2-$InO_{1.5}$ ceramics which allowed equilibrium studies at temperatures up to 1700°C. Burner rig tests and engine trials are presently being sought to give a final, critical evaluation of the potential of scandia- and india-stabilized zirconia for TBC use in corrosive engine environments.

Ytterbia: Ytterbia has been reported bu Stecura (49) as being an effective stabilizer for ZrO_2. Ytterbia is one of the more acidic of the rare earth oxides, and if Lewis acid-base interactions are in fact important in TBC hot corrosion, it might be that Yb_2O_3-stabilized ZrO_2 could prove at least somewhat superior to YSZ as a hot corrosion resistant TBC material.

CLOSURE

Results to the present time suggest that yttria-stabilized zirconia may be adequate for TBC applications where the corrodents are only Na and S (i.e., Na_2SO_4-SO_3), and the SO_3 partial pressure is not extraordinarily high. Damaging penetration of Na_2SO_4 into the YSZ ceramic has not been reported for either plasma-sprayed or EB-PVD produced TBCs, at least for aircraft type operations. Seal coating or laser-glazing of the upper YSZ surface generally has not been found to be significantly effective. Although not reviewed here (since little work has been reported), the bond coat composition and structure may have an effect on TBC cycle life under corrosive conditions, with one recent paper, for example, reporting an improvement in TBC corrosion life by the use of a dual-layer bond coat (50).

Because of the strong reaction between Y_2O_3 and V_2O_5, YSZ is unlikely to be a suitable TBC material in engine environments containing appreciable vanadium. Scandia-stabilized zirconia currently appears to be the most promising TBC ceramic for improved vanadate hot corrosion resistance. However, burner rig and engine tests are needed to verify that SSZ has the thermomechanical and other properties necessary for engine TBC use. How much improvement in hot corrosion resistance would result from the use of SSZ rather YSZ, and whether this would justify the additional cost of Sc_2O_3, remains also to be demonstrated.

ACKNOWLEDGEMENTS

Much of the NRL research reported in this paper was performed under the sponsorship of the Office of Naval Research, with Dr. A. J. Sedriks as the Scientific Officer. The support is gratefully acknowledged.

REFERENCES

1. R. A. Miller, Current Status of Thermal Barrier Coatings -- An Overview, Surface and Coatings Technol., Vol. 30, 1987, p 1-11

2. T. E. Strangman, Thermal Barrier Coatings for Turbine Airfoils, Thin Solid Films, Vol. 127, 1985, p 93-105

3. G. C. Chang, W. Phucharoen and R. A. Miller, Behavior of Thermal Barrier Coatings for Advanced Gas Turbine Blades, Surface and Coatings Technol., Vol. 30, 1987, p 13-28

4. S. M. Meier, D. M. Nissley and K. D. Sheffler, Thermal Barrier Coating Life Prediction Model Development, Phase II - Final Report, NASA CR-189111, July 1991, Pub. NASA-LeRC, Cleveland, OH, USA

5. D. V. Rigney, T. E. Mantkowski and M. J. Froning, Influence of Raw Materials on the Performance Characteristics of Ceramic Coatings, in Proc. of the 1987 Coatings for Advanced Heat Engines Workshop, CONF 870762, Pub. U.S. Dept. of Energy, Washington, DC, USA, 1987, p V-45 to V-60

6. H. G. Scott, Phase Relationships in the Zirconia-Yttria System, J. Matls. Sci., Vol. 10, 1975, 1527-1535

7. R. A. Miller, R. G. Garlick and J. L. Smialek, Phase Distributions in Plasma-Sprayed Zirconia-Yttria, Ceramic Bulletin, Vol. 62, No. 12, 1983, p 1355-1358

8. R. A. Miller, J. L. Smialek and R. G. Garlick, Phase stability in Plasma-Sprayed, Partially Stabilized Zirconia-Yttria, in Advances in Ceramics, Vol. 3, Science and Technology of Zirconia, Pub. The American Ceramic Society, Columbus, OH, USA, 1981, p 241-252

9. A. H. Heuer, R. Chaim and V. Lanteri, Review: Phase Transformations and Microstructural Characterization of Alloys in the System Y_2O_3-ZrO_2, in Advances in Ceramics, Vol. 24A, Science and Technology of Zirconia III, Pub. The American Ceramic Society, Columbus, OH, USA, 1988, p 3-20

10. T.-S. Sheu, T.-Y. Tien and I-W. Chen, Cubic-to-Tetragonal (t') Transformation in Zirconia-Containing Systems, J. Am. Ceram. Soc., Vol. 75, No. 5, 1992, p 1108-1116

11. T. Noma, M. Yoshimura and S. Somiya, Stability of Diffusionlessly Transformed Tetragonal Phases in Rapidly Quenched ZrO_2-Y_2O_3, in Advances in Ceramics, Vol. 24A, Science and Technology of Zirconia III, Pub. The American Ceramic Society, Columbus, OH, USA, 1988, p 377-384

12. A. V. Virkar and R. L. K. Matsumoto, Ferroelastic Domain Switching as a Toughening Mechanism in Tetragonal Zirconia, J. Am. Ceram. Soc., Vol. 69, No. 10, 1986 p C-224 to C-226

13. R. Taylor, J. R. Brandon and P. Morrell, Microstructure, Composition and Property Relationships of Plasma-Sprayed Thermal Barrier Coatings, Surface and Coatings Technol., Vol. 50, 1992, p 141-149

14. J. R. Brandon and R. Taylor, Phase Stability of Zirconia-Based Thermal Barrier Coatings, Part I. Zirconia-Yttria Alloys, Surface and Coatings Technol., Vol. 46, 1991, p 75-90

15. A. N. Belov and G. A. Semenov, Thermodynamics of Binary Solid Solutions of Zirconium, Hafnium and Yttrium Oxides from High-Temperature Mass Spectrometry Data, Russ. J. Phys. Chem., Vol 59, No. 3, 1985, p 342-344

16. A. N. Belov, G. A. Semenov, G. A. Teterin and T. M. Shkol'nikova, Evaporation and Thermodynamic Properties of Sc_2O_3 and of ZrO_2-Sc_2O_3 Binary Solid Solutions Accordingto High-temperature Mass Spectrometry Data. II. Calculations, ibid., Vol 61, No. 4, 1987, p 468-470

17. R. F. Reidy and R. L. Jones, Thermogravimetric Analysis of the Reaction of CeO_2 with the $NaVO_3$-SO_3 System, in press, J. Electrochem. Soc., 1995

18. R. A. Miller, Ceramic Thermal Barrier Coatings for Electric Utility Gas Turbine Engines, NASA TM 87288, 1987, Pub. NASA-LeRC, Cleveland, OH, USA

19. R. Burgel and I. Kvernes, Thermal Barrier Coatings, in High Temperature Alloys for Gas Turbines and Other Applications 1986, Pub. D. Reidel Publishing Co., Boston, MA, USA, 1986, p 327-356

20. F. H. Stott, D. J. de Wet and R. Taylor, Degradation of Thermal-Barrier Coatings at Very High Temperatures, MRS Bulletin, October 1994, p 46-49

21. D. W. McKee, K. L. Luthra, P. Siemers and J. E. Palko, Resistance of Thermal Barrier Ceramic Coatings to Hot Salt Corrosion, in Proc. of 1st Conf. on Advanced Materials for Alternative Fuel Capable Directly Fired Heat Engines, CONF-790749, Pub. US Dept. of Energy, Washington, DC, USA, 1979, p 258-269

22. S. C. Singhal and R. J. Bratton, Stability of a $ZrO_2(Y_2O_3)$ Thermal Barrier Coating in Turbine Fuel with Contaminants, Trans. ASME, J. Engr. for Power, Vol. 102, 1980, p 770-775

23. R. J. Bratton, S. K. Lau, C. A. Andersson and S. Y. Lee, Studies of Thermal Barrier Coatings for Heat Engines, in Proc. of the Second Conf. on Advanced Materials for Alternative-Fuel-Capable Heat Engines, EPRI RD-2369-SR, Pub. Electric Power Research Inst., Stanford, CA, USA, 1982, p 6-72 to 6-101

24. T. N. Rhys-Jones, J. R. Nicholls and P. Hancock, Effects of SO_2/SO_3 on the Efficiency with Which MgO Inhibits Vanadic Corrosion in Residual Fuel Fired Gas Turbines, Corrosion Sci. Vol. 23, No. 2, 1983, p 139-149

25. I. Kvernes, J. K. Solberg and K. P. Lillerud, Ceramic Coatings on Diesel Engine Components, in Proc. of 1st Conf. on Advanced Materials for Alternative Fuel Capable Directly Fired Heat Engines, CONF-790749, Pub. US Dept. of Energy, Washington, DC, USA, 1979, p 233-257

26. J. C. Hamilton and A. S. Nagelberg, In Situ Raman Spectroscopic Study of Yttria-Stabilized Zirconia Attack by Molten Sodium Vanadate, J. Am. Ceram. Soc., Vol. 67, No. 10, 1984, p 686-690

27. W. Hertl, Vanadia Reactions with Yttria Stabilized Zirconia, J. Appl. Phys., Vol. 63, No. 11, 1988, p 5514-5520

28. D. W. Susnitzky, W. Hertl and C. B. Carter, Destabilization of Zirconia Thermal Barriers in the Presence of V_2O_5, J. Am. Ceram. Soc., Vol. 71, No. 11, 1988, p 992-1004

29. R. H. Barkalow and F. S. Pettit, Mechanisms of Hot Corrosion Attack of Ceramic Coating Materials, in Proc. of 1st Conf. on Advanced Materials for Alternative Fuel Capable Directly Fired Heat Engines, CONF-790749, Pub. US Dept. of Energy, Washington, DC, USA, 1979, p 704-714

30. R. L. Jones, The Development of Hot-Corrosion-Resistant Zirconia Thermal Barrier Coatings, Matls. at High Temperatures, Vol. 9, No. 4, 1991, p 228-236

31. R. A. Miller, W. J. Brindley, J. G. Goedjen, R. Tiwari and D. Mess, The Effect of Silica on the Cyclic Life of a Zirconia-Yttria Thermal Barrier Coating, in Proc. of 7th Natl. Thermal Spray Conf., Pub. ASM International, Metals Park, OH, USA, 1994, p 49-54

32. T. Mitamura, E. Kogure, F. Noguchi, T. Iida, T. Mori, and Y. Matsumoto, Stability of Tetragonal Zirconia in Molten Fluoride Salts, in Advances in Ceramics, Vol. 24A, Science and Technology of Zirconia III, Pub. The American Ceramic Society, Columbus, OH, USA, 1988, p 109-118

33. W.-F. Chu and F. J. Rohr, Corrosion-Resistant Thermal Barrier Coatings, Advanced Ceramic Materials, Vol. 3, No. 3, 1988, p 222-224

34. D. A. Hirschfeld, D. M. Liu and J. J. Brown, CMZP - A New High Temperature Thermal Barrier Materials, in 4th Intl. Symp. on Ceramic Materials and Components for Engines, Pub. Elsevier Applied Science, London, UK, 1992, p 372 - 380

35. B. A. Nagaraj, A. F. Marichocchi, D. J. Wortman, J. S. Patton and R. L. Clarke, Hot Corrosion Resistance of Thermal Barrier Coatings, 92-GT-44, Pub. The American Society of Mechanical Engineers, New York, NY, USA, 1992, p 1-4

36. D. J. Wortman, B. A. Nagaraj and E. C. Duderstadt, Thermal Barrier Coatings for Gas Turbine Use, Materials Sci. and Engr., Vol. A121, 1989, p 433-440

37. R. L. Jones, S. R. Jones and C. E. Williams, Sulfation of CeO_2 and ZrO_2 Relating to Hot Corrosion, J. Electrochem. Soc., Vol. 132, No. 6, 1985, p 1498-1501

38. R. L. Jones, C. E. Williams and S. R. Jones, Reaction of Vanadium Compounds with Ceramic Oxides, J. Electrochem. Soc., Vol. 133, No. 1, 1986, p 227-230

39. P. A. Siemers and D. W. McKee, Method of Coating a Superalloy Substrate, Coating Compositions, and Composites Therefrom, U.S. Patent No. 4,328,285, 1982

40. R. L. Jones and C. E. Williams, Hot Corrosion Studies of Zirconia Ceramics, Surface and Coatings Technol., Vol. 32, 1987, p 349-358

41. E. Tani, M. Yoshimura and S. Somiya, Revised Phase Diagram of the System ZrO_2-CeO_2 Below 1400°C, J. Amer. Ceram. Soc., Vol. 66, No. 7, 1983, p 506-510

42. B. A. Nagaraj and D. J. Wortman, Burner Rig Evaluation of Ceramic Coatings with Vanadium-Contaminated Fuels, Trans. ASME, J. Engr. for Gas Turbines and Power, Vol. 112, 1990, p 536-542

43. R. L. Jones, Scandia-Stabilized Zirconia for Resistance to Molten Vanadate-Sulfate Corrosion, Surface and Coatings Technol., Vol. 39/40, 1989, p 89-96

44. R. L. Jones and D. Mess, India as a Hot Corrosion-Resistant Stabilizer for Zirconia, J. Am. Ceram. Soc., Vol. 75, No. 7, 1992, p 1818-1821

45. R. L. Jones, Thermogravimetric Study of the 800°C Reaction of Zirconia Stabilizing Oxides with SO_3-$NaVO_3$, J. Electrochem. Soc., Vol. 139, No. 10, 1992, p 2794-2799

46. K. Sasaki, P. Bohac and L. J. Gauckler, Phase Equilibria in the System ZrO_2-$InO_{1.5}$, J. Am. Ceram. Soc., Vol. 76, No. 3, 1993, p 689-698

47. R. L. Jones, Hot Corrosion Resistance of Scandia Stabilized Zirconia Coatings, in Corrosion and Corrosive Degradation of Ceramics, Ceramics Trans. Vol. 10, Pub. The American Ceramic Society, Westerville, OH, USA, 1990, p 291-308

48. R. L. Jones, D. Mess and H. Herman, 1991, unpublished research

49. S. Stecura, New ZrO_2-Yb_2O_3 Plasma-Sprayed Coatings for Thermal Barrier Applications, Thin Solid Films, Vol. 150, 1987 p 15-40

50. B. A. Movchan, I. S. Malashenko, K. Yu. Yakovchuk, A. I. Rybnikov and A. A. Tchizhik, Two- and Three-Layer Coatings Produced by Deposition in Vacuum for Gas Turbine Blade Protection, Surface and Coatings Technol., Vol. 67, 1994, p 55-63

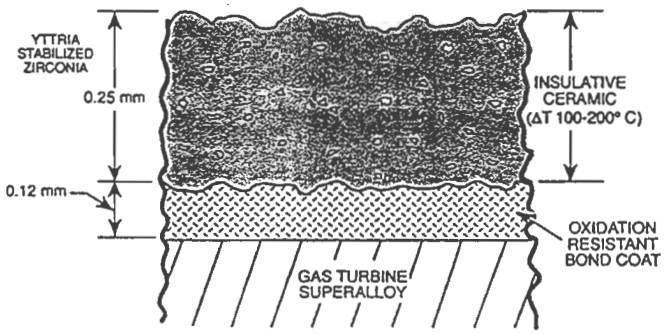

Fig. 1 Schematic representation of the cross-section of a thermal barrier coating produced by atmospheric plasma spraying (APS).

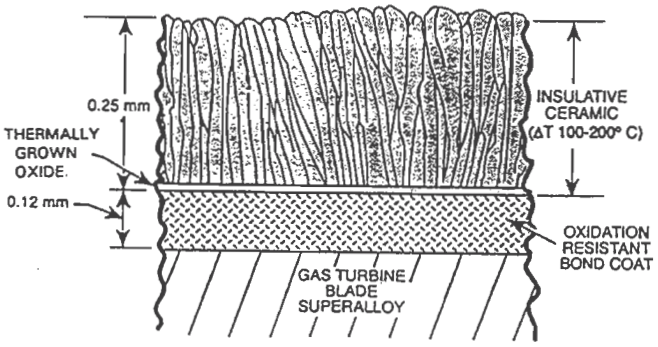

Fig. 2 Schematic representation of the cross-section of a thermal barrier coating produced by electron beam-physical vapor deposition (EB-PVD).

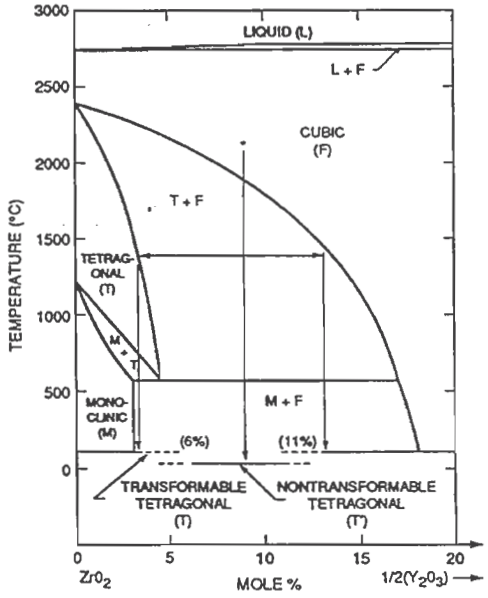

Fig. 3 Phase diagram of the Y_2O_3-ZrO_2 system illustrating phase reactions involving the tetragonal (t') phase. Adapted from Fig. 2 of Ref. 8.

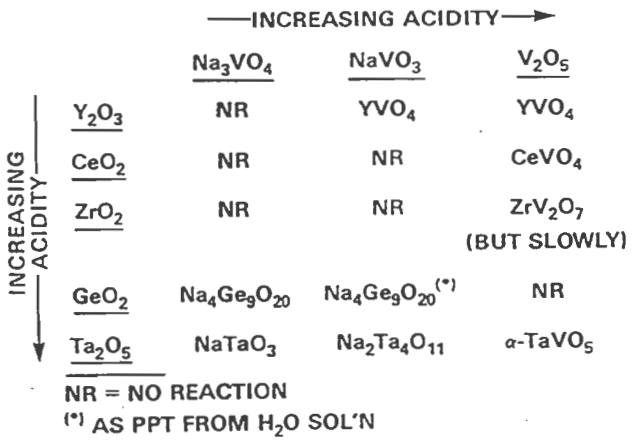

Fig. 4 Reaction behavior of ceramic oxides with vanadium oxide compounds of varying acidity.

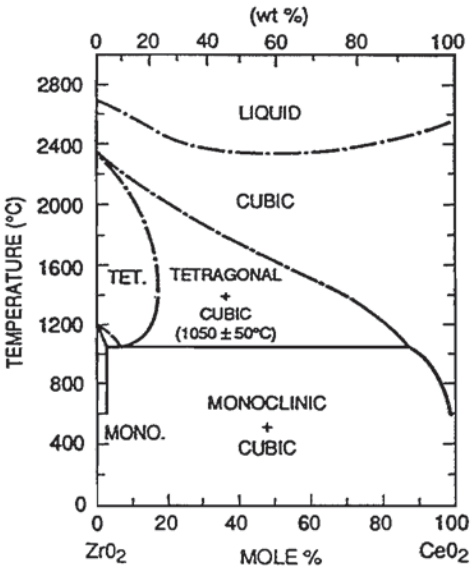

Fig. 5 Phase diagram of the CeO_2-ZrO_2 system according to Tani et al. Adapted from Fig. 4 of Ref. 41.

THERMAL FRACTURE MECHANISMS IN CERAMIC THERMAL BARRIER COATINGS

Klod Kokini, Brian D. Choules, Yoshimi R. Takeuchi
Purdue University
School of Mechanical Engineering
West Lafayette, IN 47907

ABSTRACT

Ceramic thermal barrier coatings represent an attractive method of increasing the high temperature limits for systems such as diesel engines, gas turbines and aircraft engines. However, the dissimilarities between ceramics and metal, as well as the severe temperature gradients applied in such systems cause thermal stresses which can lead to cracking and ultimately spalling of the coating. This paper reviews the research which considers initiation of surface cracks, interfacial edge cracks and the effect of a transient thermal load on interface cracks. The results of controlled experiments together with analytical models are presented. The implications of these findings to the differences between diesel engines and gas turbines are discussed. The importance of such work for determining the proper design criteria for thermal barrier coatings is underlined.

INTRODUCTION

High temperature systems such as diesel engines, gas turbines, jet engines need the development, design and use of materials which can make it feasible to leap to the temperature requirements of the next generation systems. Ceramic thermal barrier coatings offer an attractive means of protecting the current metallic components. On the other hand, the significant differences in properties between ceramic and metal, as well as the severe environments that these materials have to survive present a challenging scientific problems, since under these circumstances, these systems tend to delaminate and spall. There have been many studies which have considered the time to spalling under different conditions (Ref. 1-3). One significant contributor to such spalling was identified as oxidation of the bond coat in conditions which simulate jet engine applications (Ref. 4-5). However, even in diesel engines where the conditions do not lead to oxidation, spalling has been found to be a result limiting the use of thermal barrier coatings (Ref. 6). Consequently, there has been a more concentrated effort, in recent years, to study the mechanisms of crack initiation and propagation in thermal barrier coatings under controlled experimental conditions. In this paper, such efforts by the present authors are reviewed and the results obtained with respect to surface crack initiation, the implications for using functionally graded materials systems are presented. The differences between diesel engines and gas turbines/jet engines from the perspective of thermal barrier coating design are shown. The results for edge crack initiation are also reviewed with similar conclusions.

INITIATION OF SURFACE CRACKS

The objective of this work was to identify the mechanisms by which the first crack initiated on the surface of a multilayer, graded ceramic thermal barrier coating. The experimental conditions were designed to simulate thermal loadings which are encountered in the combustion chamber of a diesel engine. The materials system used was also one that was experimented with on the surface of a piston. The beam specimens shown in Figure 1 were subjected to a concentrated line heat flux at the surface (Ref. 7). The specimen was made of a steel substrate with a bond coat (CoCrAlY), a layer of 40% zirconia with 60% bond coat, followed by 85% zirconia/15% bond coat and, at the surface, a layer of 100% zirconia.

The experimental set-up consisted of two high-intensity infra-red focused lamps that projected a line heat flux at the center of the specimen. The bottom of the steel substrate was cooled by connecting a water cooled copper plate. The experimental conditions are shown in Figure 2.

The experimental procedure consisted of subjecting the surface to the heat flux until steady-state, keeping it at steady-state for two hours and then allowing it to cool to room temperature. The temperature distribution caused by this thermal loading history is shown in Figure 3. All such experiments resulted in a crack forming at the surface, in the region where the heat flux was concentrated (Ref. 7). The stress distribution at the different stages are shown in Figure 4. It can be noted that the surface is under some residual compression due to an assumed uniform cooling from a manufacturing temperature of 590°C. The heat flux causes increased compression. However, this compressive stress is relaxed after two hours and when the specimen is cooled back to room temperature a tensile stress is generated which is believed to initiate the crack. This mechanism was also confirmed by measuring the variation of strain at the bottom of the substrate in a different specimen configuration (Ref. 8).

INITIATION OF EDGE CRACKS

In order to study the effect of a transient thermal load on the initiation of edge cracks in thermal barrier coatings, the experiment described above was modified by allowing the line heat flux to be applied over the *length* of the specimen. This is shown in Figure 5. Also, in order to significantly decrease the effect of stress relaxation, the coating was made of multi-layers of mullite instead of zirconia (see Figure 6). Besides its reduced stress relaxation behavior, mullite also exhibits a lower thermal expansion coefficient than zirconia. As a result, when water cooling was applied at the bottom of the substrate, it was not possible to obtain any cracking. Thus, the experimental procedure was modified by removing the water cooling and allowing the substrate to be exposed to still air. The control of the thermal loading (and therefore of the stresses was then provided by 1) controlling the time of heating 2) applying surface cooling with the help of an air jet. A typical example of the temperature-time history for the surface and substrate is shown in Figure 7. The corresponding stress vs time at the surface of the cooling is shown in Figure 8.

It can be noted that at the end of the heating process, the surface is under a small tensile stress. When the air jet cooling is activated a significantly larger transient maximum tensile stress is obtained. It can also be noted that if further heating was allowed, the stresses would

have reached the same level of tension without the cooling. This is caused by the fact that as the temperature in the specimen becomes more uniform with time, the substrate starts to expand more than the surface, thus causing a tensile stress to develop. This transient peak stress during cooling is plotted in Figure 9 as a function of the temperature difference between the coating surface (T_c) and the substrate (T_s) for different values of T_c. This shows that as T_c increases the surface stress increases. Similarly, as (T_c–T_s) decreases, the stress also increases. Therefore, for applications such as diesel engines where the surface temperature is relatively low and the temperature difference (T_c–T_s) is relatively large due to aggressive cooling, mullite is an excellent alternative to zirconia in terms of durability. However, for a jet engine application where T_c is large and (T_c–T_s) is small, the same material would result in significant surface cracking.

The behavior of the edge of the interface is impossible to quantify in terms of stresses since these become singular at the edge (Ref. 9). Consequently, these stresses are expressed in terms of quasi-stress intensity factors K_1 (opening mode) and K_2 (shearing mode) as

$$\sigma_{yy} = K_1 \, r^{-\beta} \tag{1}$$

$$\sigma_{xy} = K_2 \, r^{-\beta} \tag{2}$$

where σ_{yy} and σ_{xy} are respectively the stress component normal to the interface and the shear stress component. r represents the distance from the free edge, while β is an exponent which quantifies the strength of the singularity. β is dependent on the Young's moduli, the Poisson's ratios of the two materials as well as on the geometry of the edge of the interface. The details of the calculations related to determining K_1 and K_2 when subjected to a transient thermal load are presented elsewhere (Ref. 10). In general, the time dependent behaviors of K_1 and K_2 are similar to that of the surface stress when subjected to the transient thermal load. Therefore, in Figures 10a and 10b the values of the maximum K_1 and K_2, respectively, at the edge of interface 3 are plotted vs. (T_c–T_s) for different values of T_c. It is shown that for both quantities the magnitudes are largest when T_c is large and (T_c–T_s) is small.

In Figure 10, the values of K_1 and K_2 at interface 3 are given because the experiments performed showed that crack initiation always occurred at this interface (60/40 - bond coat interface). This is also the interface that experiences the largest magnitude of K_1. In general, it can be said that reducing the magnitudes of K_1 and K_2 should reduce crack initiation at the edge. Figure 10 shows again, that thermal loading conditions encountered in an aircraft engine would be detrimental to the edge as compared to conditions in a diesel engine.

INTERFACE CRACKS

One of the most interesting aspects of thermal fracture mechanisms of thermal barrier coatings is cracking of one of the interfaces between any of two layers in a multilayer material system. The question of which interface is most likely to exhibit crack initiation and how to predict it is a challenging one. In order to develop some understanding of the mechanics of such processes, a model was used which considered the presence of an interface crack of length a = 0.3175 mm between the top two layers (c.f. Figure 11). The cases of a zirconia as well as a mullite coating were considered.

The model was used to simulate the effect of applying a transient thermal load at the surfaces due to a heat flux generated by 1) the high intensity infra-red lamps 2) a high power (1.5 kW) CO_2 laser. The distribution of the heat flux on the surface due to each method of heating is shown in Figure 12.

The model assumed the crack to be insulated. The finite element method was used to determine the transient temperature distribution as well as the transient opening (Δv) and shearing deformations (Δu) near the crack tip. This information was then used to calculate the transient strain energy release rate due to the thermal load. The equations used for calculating G have been presented elsewhere and will not be repeated here (Ref. 11-12).

The surface temperature for both zirconia and mullite specimens are shown in Figure 13. The temperature distribution around the crack, immediately before cooling is initiated is presented for each case in Figure 14. It is clear that the assumption of an insulated crack results in a large temperature change across the crack.

The resulting crack openings Δv near the crack tip at a distance of $r = 7.94 \times 10^{-6}$ mm are presented in Figure 15. The largest crack opening occurs for the mullite interface subjected to laser heating. Clearly the zirconia experiences a larger crack tip opening under laser heating than under the heat lamps. On the other hand, the largest crack tip shearing deformation shown in Figure 16 is experienced by the zirconia interface subjected to laser heating. The resulting transient strain energy release rates shown in Figure 17 indicate that the largest G is experienced by the zirconia coating subjected to laser heating followed by cooling. In particular, the laser heating should result in a significantly facilitated interface crack propagation process as compared to the infra-red lamp heating. If it is therefore assumed that the laser heating simulates conditions similar to ones encountered in a gas turbine/aircraft engine, delamination of the interface is expected to occur sooner in this system rather than in a diesel engine. On the other hand, it is possible that mullite could be more resistant than zirconia to such delamination. At this stage of the research, these predictions have not been verified experimentally and are the subject of on going investigations.

CONCLUDING REMARKS

Ceramic thermal barrier coatings are subjected to various transient thermo-mechanical loads, during their use, which result in different potential crack initiation and propagation mechanisms. The results presented above consider three of these mechanisms which consist of surface cracking, free-edge cracking and interface cracking.

The surface cracking is shown to initiate, in the case of zirconia coatings, from stress relaxation at high temperature which decreases the compressive stresses due to heating over time and results in tensile stresses upon cooling. The use of a material such as mullite which does not relax as much, was shown to result in at least an order of magnitude increase in the life of the coating (Ref. 13-14). It was also shown that, while the mullite is an excellent substitute for zirconia in a diesel engine, the same would not be true for a gas turbine, because of the significantly different thermal loading conditions.

In the case of the edge crack initiation, the results showed that the singular nature of the stresses does not allow a stress criterion to be used. The edge does experience both opening and

shearing modes of stress intensity factors, which similar to the surface stresses, behave considerably differently in diesel engine and gas turbine environments.

The interface cracks subjected to different transient thermal loading conditions experience significantly different opening and shearing deformations, as well as total strain energy release rates G. The significance of each of these quantitative measures to crack propagation needs to be determined by experimental work which is under progress.

It is clear, however, that the *design* of a thermal barrier coating is a complex process which has to consider the thermal loading and other conditions which can be vastly different from one application to the other. In each case, the design process needs to establish criteria for acceptability from the point of view of delaying crack initiation and propagation processes. On the other hand, since the function of a thermal barrier coating is to protect metallic substrates from high temperatures, the thermal resistance of the coating is also an important consideration.

The worldwide research efforts, in the recent years, related to functionally graded material systems offer additional design opportunities, while at the same time, complicating the design equation (Ref. 15-16). It was shown by the present authors, however, that a functionally graded coating *can* be designed which would resist surface cracking as well as a very thin coating, but with an increased thermal resistance (Ref. 17).

ACKNOWLEDGEMENTS

Support of this research by Cummins Engine Company and the National Science Foundation through Grant No. MSS 9301265 is gratefully acknowledged.

REFERENCES

1. R.A. Miller and C.C. Berndt, Performance of Thermal Barrier coatings in High Heat Flux Environments, *Thin Solid Films*, Vol. 119, 1984, p. 195-202.

2. C.H. Leibert and R.A. Miller, Ceramic Thermal Barrier Coatings, *I&EC Product Research and Development*, Vol. 12, 1984, p. 334-349.

3. J.T. DeMasi, K.D. Sheffler and M. Ortiz, Thermal Barrier Coating Life Prediction Model Development, NASA CR 182230, December 1989.

4. R.A. Miller and C.E. Lowell, Failure Mechanisms of Thermal Barrier Coatings Exposed to Elevated Temperatures, *Thin Solid Films*, Vol. 95, 1982, p. 265-273.

5. W.J. Brindley and R.A. Miller, Thermal Barrier Coating Life and Isothermal Oxidation of Low-pressure Plasma-Sprayed Bond Coat Alloys, *Surface and Coating Technology*, Vol. 43-44, 1990, p. 446-457.

6. T.M. Yonushonis, K.L. Hoag, P. Huston, A.P. Matarese, R.C. Novak and D.P. Roehling, Thick Thermal Barrier Coatings for Diesel Engines, *Proc. 25th Automotive Tech. Dev. Contract. Coord. Mtg.*, SAE Publication P2009, 1987.

7. K. Kokini and Y.R. Takeuchi, Initiation of Surface Cracks in Multilayer Ceramic Thermal Barrier Coatings Under Thermal Loads, *Material Science and Engineering A*, Vol. 189, 1994, p. 301-309.

8. Y.R. Takeuchi and K. Kokini, Thermal Fracture of Multilayer Ceramic Thermal Barrier Coatings, *ASME Transactions, Journal of Engineering for Gas Turbines and Power*, Vol. 116, 1994, p. 266-271.

9. D.B. Bogy, Two Edge-Bonded Elastic Wedges of Different Materials and Wedge Angles Under Surface Tractions, *J. Applied Mechanics*, Vol. 38, 1971, pp. 377-386.

10. M. Case and K. Kokini, Thermally Induced Initiation of Interface Edge Cracks in Multilayer Ceramic Thermal Barrier Coatings, *Proceedings of the Symposium on Ceramic Coatings*, K. Kokini, Ed, ASME MD-Vol. 44, 1993, p. 149-162.

11. R.R. Reynolds and K. Kokini, Transient Thermoelastic Fracture of Interface Cracks: Effect of Bending Restraints, *International Journal of Fracture*, Vol. 54, 1992, p. 185-195.

12. K. Kokini and Y.R. Takeuchi, Transient Thermal Fracture of an Interface Crack in the Presence of a Surface Crack, *Journal of Thermal Stresses*, Vol. 17, 1994, p. 63-74.

13. Y.R. Takeuchi, K. Kokini and T.M. Yonushonis, Thermal Barrier Coating Development for Pistons, *Proc. of the 1992 Coatings for Advanced Heat Engines Workshop*, U.S. Department of Engrg, 1992, p. II 31-40.

14. P.M. Pierz, Thermal Barrier Coating Development for Diesel Engine Aluminum Pistons *Surface and Coatings Technology*, Vol 61 1993, p. 60-66.

15. M. Yamanouchi, M. Koizumi, T. Hirai and I. Shiota, *Proceedings of the First International Symposium on Functionally Gradient Materials*, FGM Forum, Japan, 1990.

16. J.B. Holt, M. Koizumi, T. Hirai and Z.A. Munir, *Functionally Gradient Materials*, Ceramic Transactions, Vol. 34, American Ceramic Society, 1993.

17. B.D. Choules and K. Kokini, Multilayer Ceramic Coating Architecture Against Surface Thermal Fracture, *Proceedings of the Symposium on Ceramic Coatings*, K. Kokini, Ed., ASME MD-Vol. 44, 1993, p. 73-86.

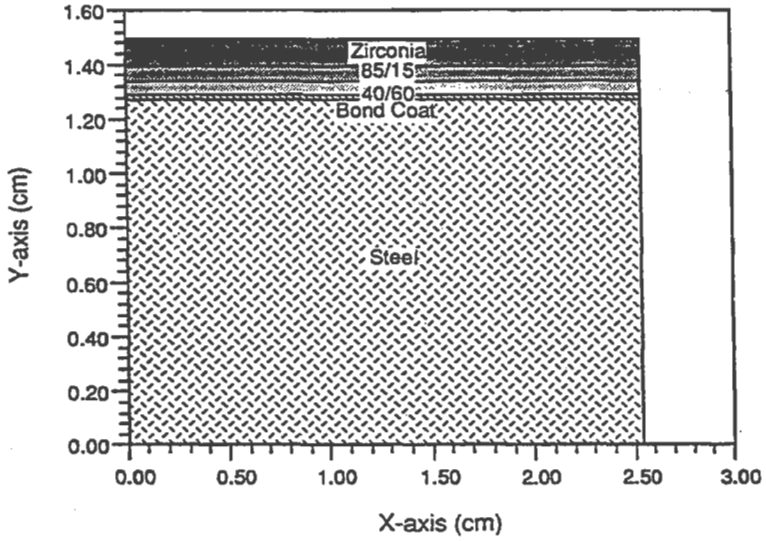

Figure 1. **Specimen used for surface crack initiation studies.**

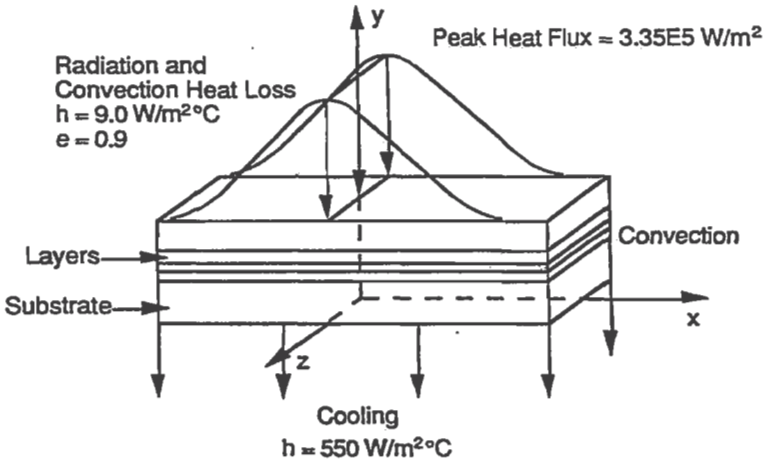

Figure 2. **Boundary conditions representing the thermal loading under the heat lamps.**

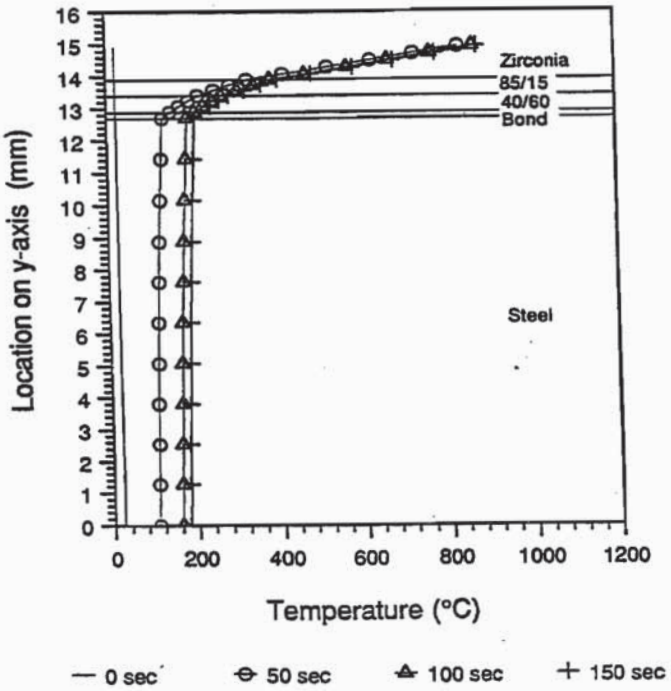

Figure 3. Temperature distribution in the specimen at different times.

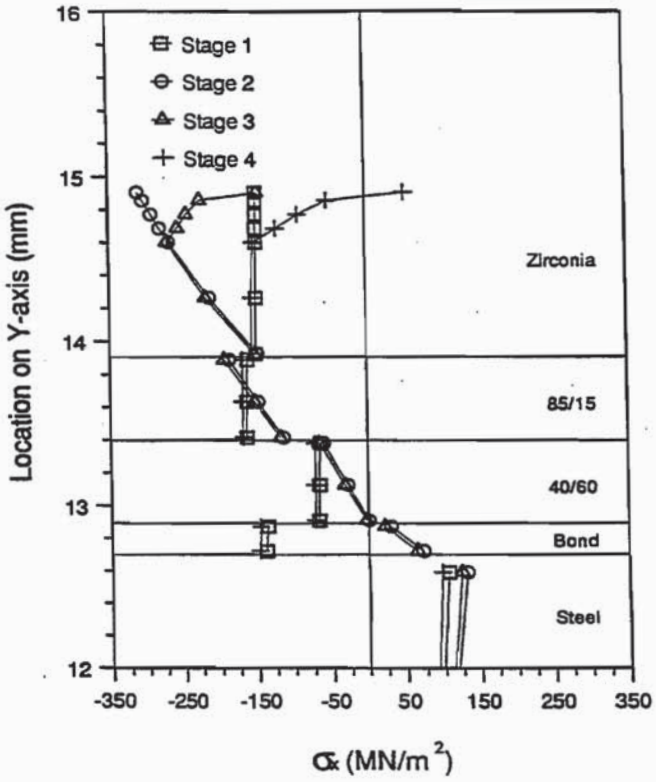

Figure 4. Stress distribution in the coating.
Stage 1: Residual stress
Stage 2: Steady-state heating
Stage 3: Stress relaxation for two hours
Stage 4: Uniform cooling to room temperature.

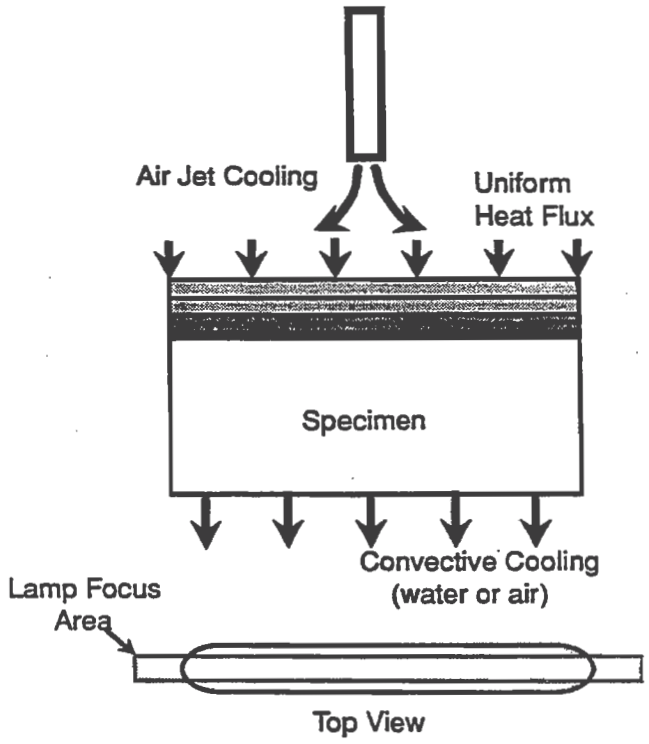

Figure 5. Thermal loading for edge crack initiation experiments.

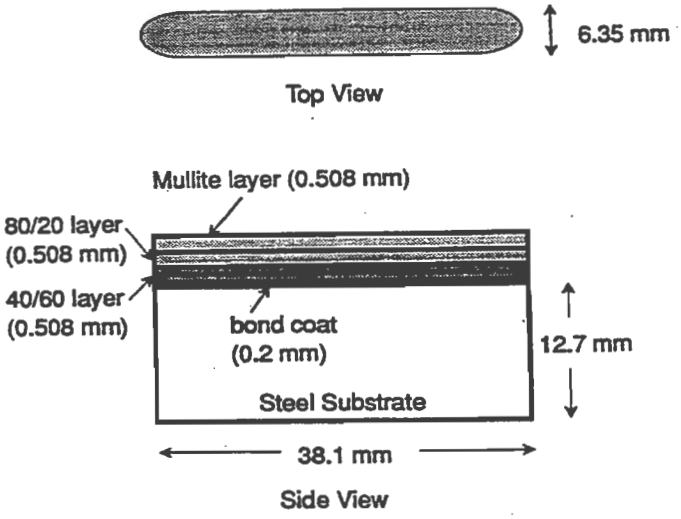

Figure 6. Specimen used for edge crack initiation studies.

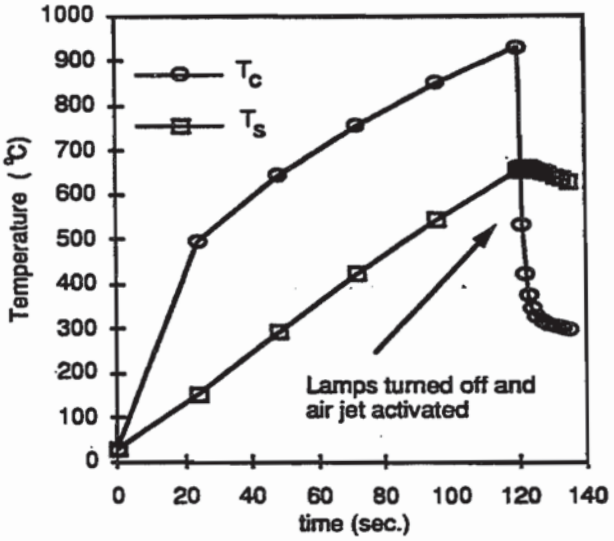

Figure 7. Temperature vs time for coating surface and substrate.

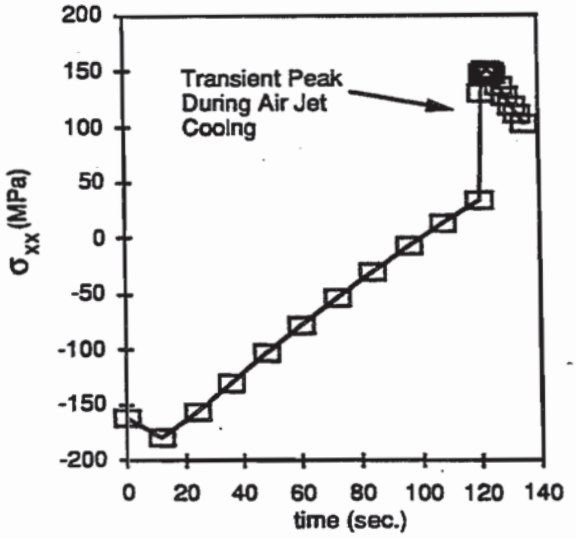

Figure 8. Surface stress vs time.

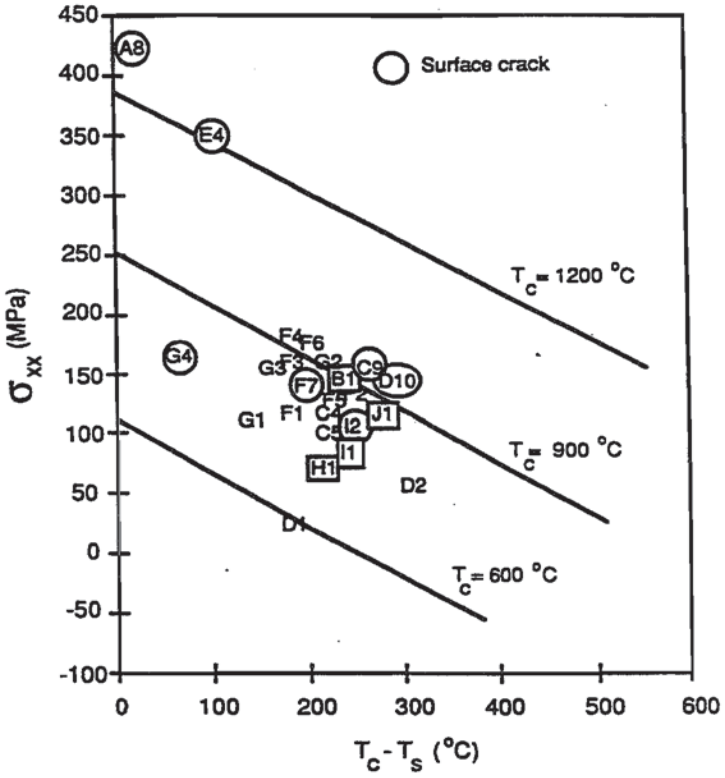

Figure 9. Maximum surface stress vs (T_C–T_S) for the specimen studied.

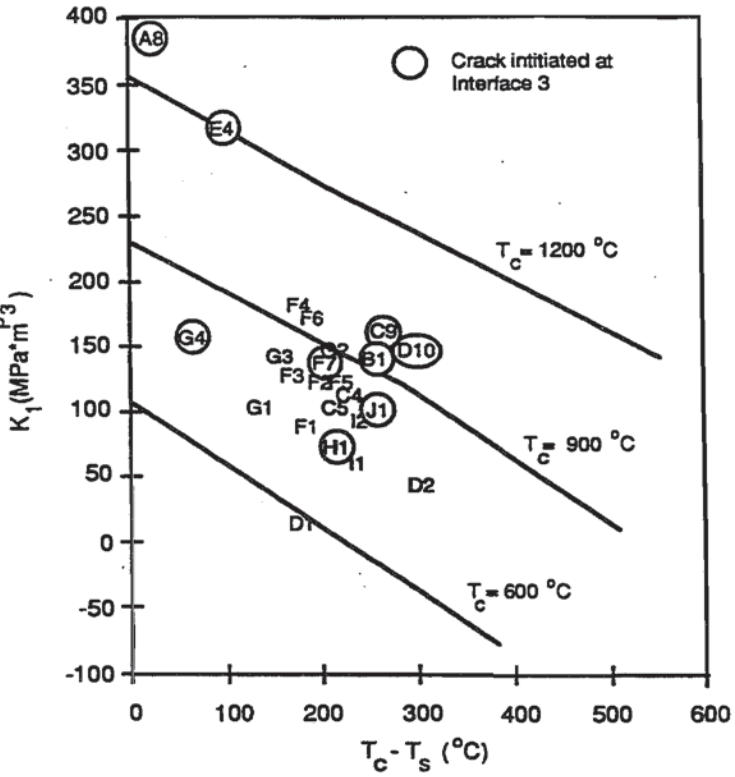

Figure 10a. Maximum K_1 vs. (T_C–T_S) for interface 3 of specimen studied (β_3 = 0.0049).

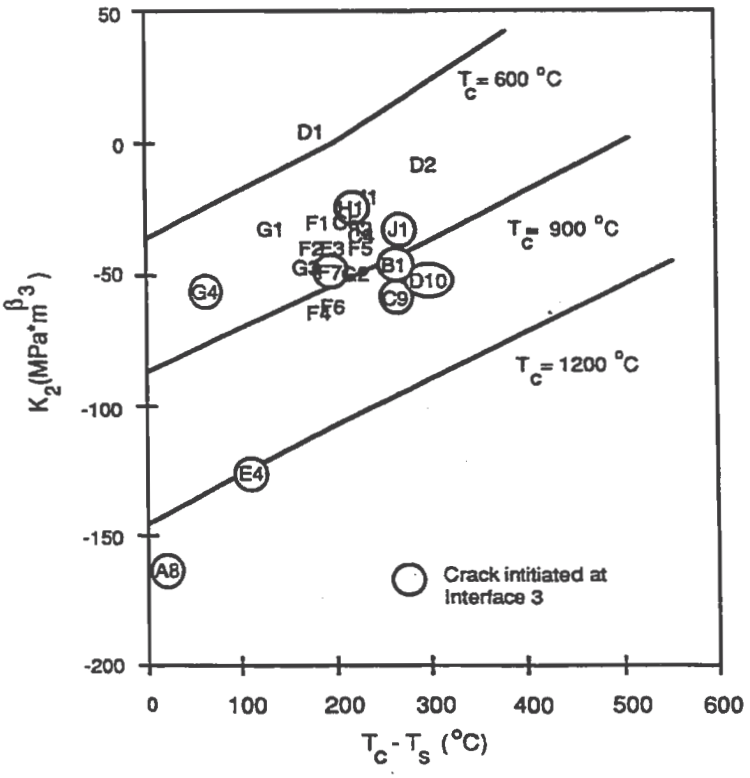

Figure 10b. Maximum K_2 vs. (T_C–T_S) for interface 3 of specimen studied (β_3 = 0.0049).

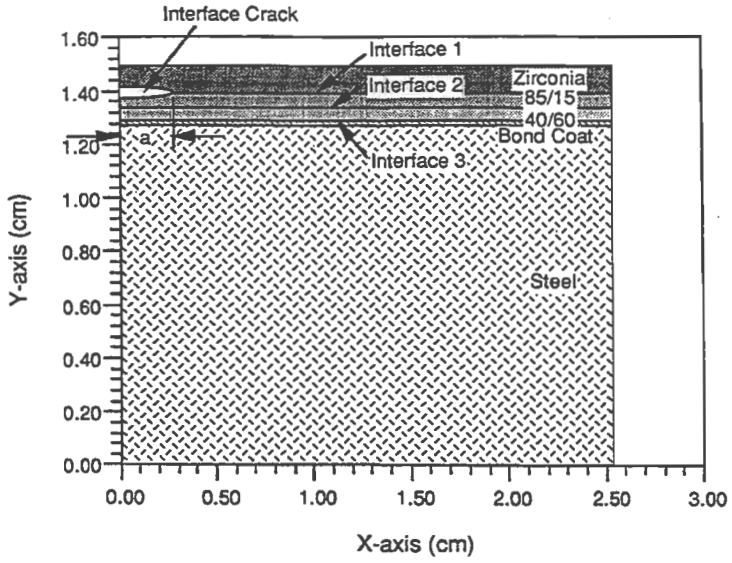

Figure 11. Model used to study the behavior of an interface crack.

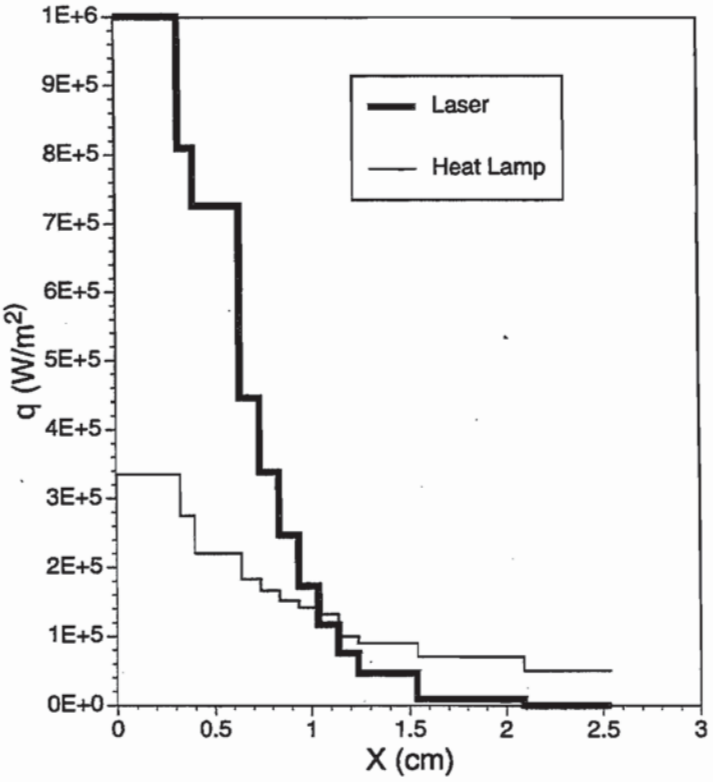

Figure 12. Distribution of heat flux applied on the surface.

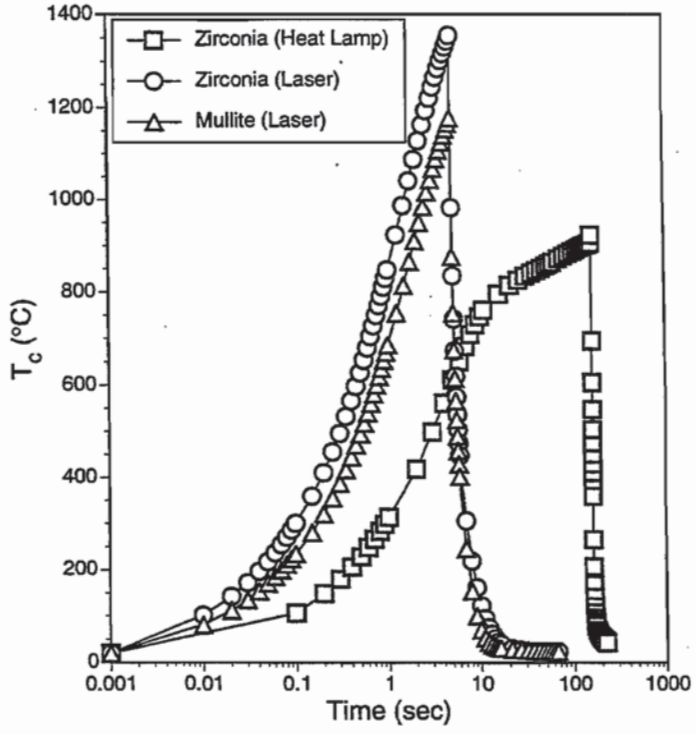

Figure 13. Surface temperature vs time for the different loadings.

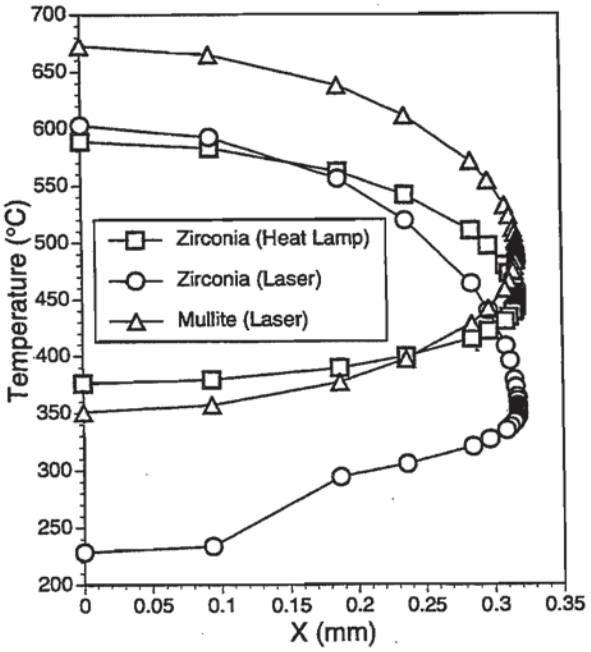

Figure 14. Temperature distribution around the crack at the time of maximum surface temperature.

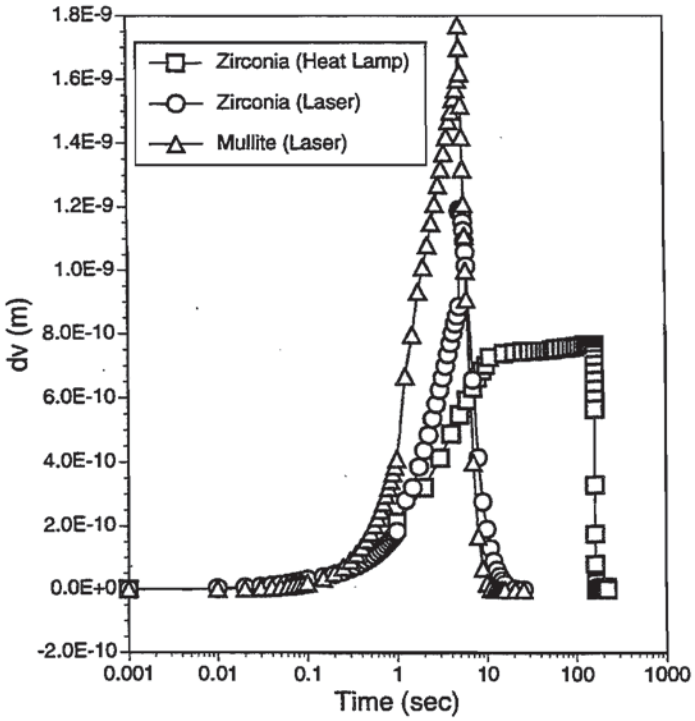

Figure 15. Crack tip opening vs time at $r = 7.94 \times 10^{-6}$ mm from the crack tip.

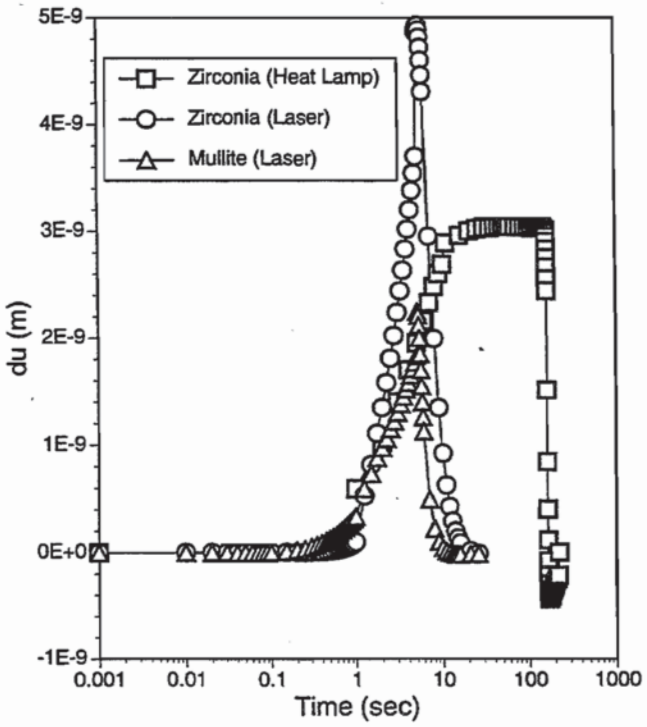

Figure 16. Crack tip sliding vs. time at $r = 7.94 \times 10^{-6}$ mm from the crack tip.

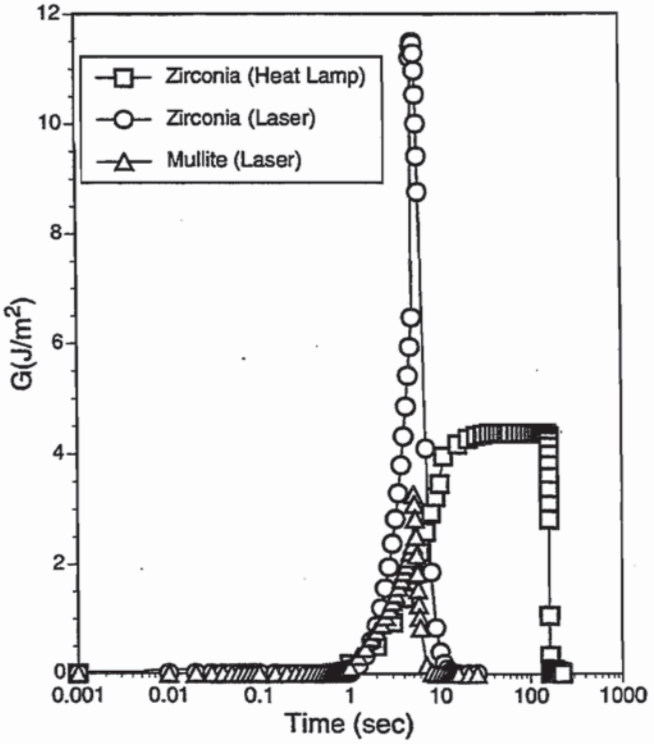

Figure 17. Strain energy release rate vs. time.

A SOFTWARE TOOL TO DESIGN THERMAL BARRIER COATINGS

Gregory Petrus and B. Lynn Ferguson
Deformation Control Technology, Inc.
Cleveland, OH 44130

ABSTRACT

This paper summarizes work completed for a NASA Phase I SBIR program which demonstrated the feasibility of developing a software tool to aid in the design of thermal barrier coating (TBC) systems.(Ref 1) Toward this goal, three tasks were undertaken and completed. Task 1 involved the development of a database containing the pertinent thermal and mechanical property data for the top coat, bond coat and substrate materials that comprise a TBC system. Task 2 involved the development of an automated set-up program for generating two dimensional (2D) finite element models of TBC systems. Most importantly, Task 3 involved the generation of a rule base to aid in the design of a TBC system. These rules were based on a factorial design of experiments involving FEM results and were generated using a Yates analysis. A previous study had indicated the suitability and benefit of applying finite element analysis to perform computer based experiments to decrease but not eliminate physical experiments on TBC's.(Ref 2) This program proved feasibility by expanding on these findings by developing a larger knowledgebase and developing a procedure to extract rules to aid in TBC design.

INTRODUCTION

The application of a thermal barrier coating (TBC) provides a method for improving turbine efficiency by allowing the engine to operate at higher temperatures. By coating the surface of a turbine blade with a ceramic material (top coat) having a low thermal conductivity, such as yttria stabilized zirconia, the maximum temperature in the blade can be maintained below a critical level as the combustion temperature is increased. However, direct application of a ceramic to a metallic substrate by plasma spraying does not produce acceptable performance due to mismatch between the Coefficients of Thermal Expansion (CTE's) of the substrate and ceramic, and because the ceramic does not sufficiently protect the substrate from oxidation. Both conditions lead to large stress at the ceramic-substrate interface resulting in delamination and failure due to spalling. The addition of a compliant layer, termed a bond coat, between the substrate and ceramic top coat has been found to greatly improve the operating life of a TBC system.(Ref 3) The properties of the bond coat relative to those of the substrate and the top coat, and the interface roughness which provides mechanical bonding sites for the plasma sprayed top coat determine the TBC system performance.

At this time, the nature of the relative effects of system variables and the interrelations between these variables has not been quantified. TBC system design has therefore progressed by judicious experimentation. Previous studies have investigated the effects of properties and surface geometry on a limited scale by applying the finite element method.(Ref 4) More recently, a study by Ferguson, et al., (Ref 2) has shown that the coefficient of thermal

expansion, cooling rate, the creep rate of the TBC constituents, as well as the roughness of the bond coat have significant effects on the stresses generated at the bond coat - top coat interface of the thermal barrier coating. The trends derived from these FEA simulations of a burner rig cycle have agreed with trends observed from burner rig tests.

Based on the qualitative agreement between FEA results and experimental results from these prior studies, it seems reasonable that computer based experiments could be performed to examine the effects of TBC variables in greater detail. Furthermore, the use of a designed set of experiments coupled with a method of interpreting the results should allow quantitative relationships of the effects of TBC variables on performance criteria to be derived. On these assumptions, a plan for the development of a software tool to aid in the design of TBC systems was formulated, with the purpose of Phase I being to demonstrate the feasibility.

Three main technical tasks were identified to demonstrate the feasibility of this approach to TBC design. First, a material property database was developed to incorporate the properties of selected substrate, bond coat and ceramic materials. Second, an automated set-up program was built to generate 2D models for FEA evaluation. This set-up program would access the database to extract material properties, and it would create a command file used for actual FEA model generation by the FEA preprocessor. Third, a set of rules was constructed based on the results of a designed set of computer simulations. This report documents the performance and results of these tasks.

METHODOLOGY

Task 1: Material Properties Database Development

The functional form and framework of a database needed to support finite element simulation of TBC's was developed. The database structure allows for addition, modification and deletion of material property data. The database was sparsely populated with a couple of known materials to demonstrate that it does function as required. The developed database was designed to be both user friendly and functional. Written in the C-language, most programmers can easily modify the program if necessary. The program itself stores and retrieves various properties for substrates, bond coats and top coats. This helps the user to more quickly and efficiently locate the appropriate material properties. The program also outputs the data in the correct form so that the property data can be directly included into the input file for computer simulation.

Task 2: Development of a FEA Set-Up Utility

Since the finite element method will be used extensively for computer based experiments, the user will need an easy method of generating model geometry and building analysis input files. Since the analysis code to be used in this study has a preprocessor, MAZE, that generates input files, the function of the set-up utility was defined to generate MAZE command files.(Ref 5) A set of generic geometries that is common for TBC test geometries was defined. These configurations included a cylinder and a flat, circular disk. These shapes can be defined by a dimensional set, namely radius, length, bond coat thickness, top coat thickness and interface roughness. Materials can be linked to each TBC component to add the necessary material

property data to the command file.

Using the programming language Pascal, a PC-based set-up program for 2-d model development was written. The user selects the geometry type, cylinder or disk in this limited case, and then enters the radius, length, bond coat thickness, top coat thickness, and interface roughness. After these selections have been made, the set-up program writes the proper MAZE command file and terminates.

The MAZE command file is an ASCII text file which is a list of commands that drives the preprocessor MAZE which is then used to generate a complete NIKE2D input file.(Ref 6) The MAZE command file defines the model geometry, the mesh for each component, the nature of the interface between components, the material properties, and the model boundary conditions. Once the input files have been written, they are ready for execution by NIKE2D without modification. While NIKE2D was the finite element code of choice for this program, this set-up tool can be expanded to include other codes. As in Task 1, the developed set-up utility is a user feature that an industrial user would want to have available to speed model development.

Task 3: Rule Base Methodology and Development

A burner rig test is a common test for evaluating the performance of turbine engine components, and it has been widely used to examine TBC behavior.(Ref 7 and Ref 8) A typical burner rig test sample and a typical temperature vs. time cycle provide a sound framework for developing and testing TBC systems. Because of the large experience base for this test, it also provides a sound framework for developing a methodology for rule base development. Therefore, the burner rig cycle test was chosen for all the simulation work completed in this study.

Figure 1 shows the burner rig cycle that was used as the basis for a set of computer simulations of TBC response. Also shown in Figure 1 is a modified cycle with a more rapid cooling rate which was also simulated. The burner rig cycle time can be subdivided into three regions: heat-up, steady state (at operating temperature), and cool down, as indicated in Figure 1. In performing these simulations, a factorial experimental design was followed to allow the effects of several material properties and TBC system features to be examined. The details of the computer model, the experimental design and the variables follow.

Model Geometry

Modeling was performed on a 486 class PC workstation using a steady state creep model to examine the time dependent effects of the thermal cycle on stress and deformation in the TBC System. A thin axisymmetric slice of a typical burner rig test bar was selected as the geometry to model. The bond coat and ceramic outer coat were applied to the outer surface of the bar. Since axisymmetry was assumed by this geometry, a single radial cross section was used to develop the finite element mesh. The basic radial dimensions for the various cross sections were:

- superalloy bar radius: 0.0127 m (0.5 in)
- average bond coat thickness: 130 μm (5.1 mils)
- average ceramic coat thickness: 250 μm (9.8 mils)

The coating thicknesses correspond to typical TBC system thicknesses.

The geometry of the bond coat - ceramic interface was modeled as a sine wave to simulate surface roughness axially along the test bar. In simulating roughness, the effect of increasing the amplitude is to increase the surface roughness. The effect of decreasing the wavelength (increasing the frequency) is to reduce the roughness spacing. The model geometry is shown in Figures 2 and 3 for low and high roughness materials respectively. Included in these figures are the element numbers corresponding to the peak, the valley and the mid-height of the sine waves. The stresses at these elements as a function of burner rig cycle time were used to develop functional relationships. In this geometry, a peak is defined to be a peak in the bond coat.

Model Boundary Conditions

The thermal profile of Figure 1 was imposed uniformly on the entire body for each of the models in this study. In Phase II, a transient heat transfer model will be implemented and actual time-temperature histories for each node will be computed.

Steady State Creep Model

A power law creep model resident in the NIKE2D code was used. The basic relationship in this creep model is summarized by equation (1):

$$\epsilon = A \cdot (\sigma_{effective})^B \qquad \text{eq. (1)}$$

where A is the creep coefficient, and
B is the power law creep exponent.

As implemented, A and B are functions of temperature. This model is discussed in more detail in Ref 9 and Ref 2.

2^5 Factorial Experiment

A factorial analysis is a means of designing experiments whose factors or variables can be discreetly separated into a high value and a low value, a middle value, or even a multiple set of values. This type of experimental design provides an opportunity to determine the effects of each of the factors or variables, as well as the interactions between them on a desired property or performance indicator. In addition, an analysis of variance (ANOVA) table can easily be constructed from the results in order to rank the significance of the factors and their interactions. In this task, a 2 level - 5 variable factorial experiment was conducted resulting in 32 finite element models being executed. The maximum and minimum stresses in the three regions of the burner rig cycle were documented.

Parameters for the Factorial Experiment

The parameters used in this experiment as well as their values are presented in detail in Ref 1 and are too detailed to include here. These tables contain all of the material property data used in the various simulations. The ceramic top coat material data was for yttria stabilized zirconia, ZrO_2 - 8%Y_2O_3. Bond coat properties are similar for Ni-35%Cr-6%Al-0.95%Y bond coat materials. The superalloy base material property was that for a typical Ni-based superalloy.

The low and high values were somewhat arbitrarily selected to demonstrate the feasibility of rule development.

1. Bond Coat Creep

The bond coat creep resistance was studied primarily because the TBC will be subjected to high temperatures at the operating regime of turbines. It was reported in previous studies that the bond coat creep rate or the bond coat creep strength is a significant variable in TBC failures.(Ref 8 and Ref 2) The values used for "low" and "high" refer to **resistance** to creep, so the numerical values for the power law creep coefficient A are higher for low creep resistance than they are for high creep resistance. The creep coefficient values in the "low" creep resistance bond coat are for a Ni-35%Cr-6%Al-0.95%Y bond coat material; this material is known to have low resistance to creep. The numerical values in the "high" column of creep coefficient were taken as an order of magnitude less than those in the "low" column.

2. Bond Coat Coefficient of Thermal Expansion (CTE).

The functional correlation between CTE and temperature was assumed to be a linear relationship. The CTE's used in this experiment have the same intercept at 0°C (12.0E-6/°C) but have different slopes. The slopes for the high CTE material and the low CTE material are 8.0E-9/°C^2 and 2.0E-9/°C^2 respectively. The graph of the two CTE lines are shown in Figure 4.

3. Bond Coat Roughness.

In order to promote a mechanical bond between the top coat and the bond coat, a certain degree of roughness is necessary as chemical bonding between the materials is minimal. However, a rough interface provides stress concentration sites at the interface between materials. A smooth interface would have no stress concentration sites, but bonding of the top coat to the bond coat would be poor due to the lack of mechanical bonding sites and poor chemical interaction. It is desirable to be able to define an optimum roughness that minimizes interfacial stress while adequately providing for mechanical bonding.

The interface is assumed for simplicity to be a sine wave which has a defined amplitude and wavelength. In this experiment, the low and high roughness geometries are taken as 1/2 and 2X the normal roughness, where the normal roughness is defined as that having an amplitude of 10 microns and a wavelength of 50 microns. Thus the low roughness would have an amplitude and wavelength of 5 and 25 microns respectively while the high roughness would have an amplitude and wavelength of 20 and 100 microns respectively. Refer to Figures 2 and 3 to compare the profiles for the low and high roughness configurations. To represent roughness as a single factor calculated as:

$$\text{roughness} = \frac{\text{amplitude}^{1.5}}{\text{wavelength}}$$

4. Top Coat Creep.

In the previous report by Ferguson, et al. (Ref 2), it was observed that the top coat stress decreases slightly during the operating temperature regime while the bond coat stress is nearly zero. This indicates that the top coat creeps somewhat during the operating temperature regime. If so, the creep of the top coat can relieve stresses due to CTE mismatch at higher temperatures, thus prolonging or preventing failure. On the other hand, creep can also weaken the top coat to such an extent that failure occurs. In this experiment, a knowledge of how much the creep strength affects the failure characteristics of TBC's will aid in the design and materials choice for a top coat.

5. Burner Rig Test Cooling Rate.

The cool down portion of the burner rig cycle has been shown to promote TBC failure. A rapid cooling rate promotes a high thermal stress rate due to CTE mismatch, as well as differential cooling rate in materials. A slow cooling rate results in lower stress rate, and this could allow rate sensitive relaxation mechanisms to be active, depending on the time at elevated temperatures. A finite element simulation that included creep behavior, as this one does, can predict stress development during the cool down region of the burner rig cycle. Figure 1 shows the different cooling rates used in these models.

THE YATES ANALYSIS

The Yates analysis is a means of computing the effects of the independent variables used in a factorial analysis on the dependent variables. This analysis method also determines the amount of interaction between the variables. The result is a response surface which amounts to a mathematical curve fit of the five independent variables and any output of choice from the simulations i.e. radial stress in the top coat at the interface peak. In addition, from the response surface, an analysis of variance (ANOVA) table can also be constructed. The ANOVA can be used to examine the main effects to determine the significance of a factor and its interaction with other factors.

The response surface (equation) generated by the Yates analysis can be used to determine how much each of the factors should be changed in order to reach the maximum stress as quickly as possible, or conversely, how to maintain minimum stress. The method used to analyze the response surface is called the path of steepest ascent.

RESULTS AND DISCUSSION

The superalloy substrate controls the global stress state of these models due to its mass dominance. The roughness of the interface between the bond coat and top coat, however, plays a dominant role in establishing the local stress state. Failure of the TBC system has been associated with the interface region, and for this reason the interface has been a focal point of

attention. Because the role of the bond coat is to provide compliance between the substrate and the ceramic, the properties of the bond coat have been shown to be critical in enhancing TBC life. The direct effect of the bond coat mechanical behavior on TBC performance can be seen by examining the stresses at the bond coat / top coat interface.

A typical simulation result is shown in Figure 5 for radial stress as a function of time at bond coat and top coat peak and valley interface locations. The three regions of the burner rig cycle are indicated in the figure. Notice that during heating, radial stress builds in both the top coat and bond coat, but in opposite senses. Before heating is completed, relaxation occurs and stresses drop toward zero. During the operating or steady state region, the bond coat radial stress is nearly zero, and the top coat stress continues to decrease toward zero. Creep of the top coat is most likely responsible for this radial stress reduction. Upon entering the cool down region, radial stress builds very quickly; interestingly, the interface roughness effect can be seen by the difference in the sign of the stress at the peak and valley in the top coat. Interpretation of these and similar results allows a sense of what may be happening in this simulated test. However, it can get to be very confusing in terms of comparing results to determine effects of variables simply because of the volume of data to be evaluated.

During the operating temperature regime, the temperature is held constant, the bond coat creeps and stresses relax to nearly zero, while the top coat shows a stress decreasing more slowly with time. During cool down, both the bond coat and the top coat experience a stress opposite in sign to that experienced during heat-up. The stresses at the end of cool down are generally larger on the cool down portion of the cycle than on the heat up. The creep mechanism in the materials is responsible for this. On heat up, stresses are induced due to CTE mismatch between materials. However, as temperature rises, creep mechanisms are activated to relax the stresses induced by the CTE mismatch. Thus, at the end of heat up, a large portion of the thermally induced stress may be relieved, depending on the magnitude of the CTE mismatch and the creep resistance of the bond coat and top coat materials. After a sustained time at operating temperature, the TBC nearly settles to a new equilibrium stress state due to relaxation at the high temperature hold. Upon cool down, both factors of CTE mismatch and creep resistance work against the TBC in terms of minimizing stress. On cool down, thermal stresses (opposite in sign now) begin to again be imposed. In this case, the temperature is decreasing and, as the thermal stresses increase, creep (or stress relaxation) mechanisms are no longer active due to the cooler temperatures. Compounding this difference between heat up and cool down is the level of stress in the TBC while the material is at temperatures where creep is active. During cooling the stresses in the TBC are low while creep is active. The bulk of the cooling regime occurs when creep is not active and as a result stress can only be relieved by plasticity or by fracture. During heating, the stresses are high when creep becomes activated due to the large temperature change from ambient to the operating temperature. The combination of high stress and high temperature drives stress relaxation.

The top coat radial stress generally shows an initial compressive stress at the peak of the interface while the valley has a tensile stress during the heat up cycle. During the end of heat up where bond coat stress relaxation begins and during operating temperature where bond coat stress moves toward zero, the top coat stresses tend to reverse. Once the stress in the bond coat is nearly relaxed the top coat stresses slowly move to zero due to creep although more slowly

than the bond coat. At the cool down, the stresses reverse themselves from the heat up cycle and end up in tension for the peak, and compression at the valley. This may be a significant factor as the top coat is relatively weak in tension.

Increased roughness is shown to result in higher stresses during heat-up and cool down, and it was shown to be the second most significant factor by the ANOVA. It is also interesting to note that there is a relatively high level of radial tension in the top coat at the end of the cool down time period caused by stress concentrations of the rough interface in some of the simulations. Radial tension is thought to contribute significantly to cracking near the interface.

By using the Yates analysis, the relative dominance or importance of each of the five parameters tested in this experiment could be determined. In the analysis, the variable values are normalized between -1 (low) and +1 (high), and the resulting coefficients are for the normalized values. The Yates analysis shows bond coat coefficient of thermal expansion, which causes the thermal expansion mismatch between the top coat and the bond coat, is the largest contributor in generating stress and is the most significant factor. This is evident in the majority of the experimental simulations where the CTE ranked first and second. Interface roughness was the second most significant factor.

Bond coat and top coat creep strength are of roughly equal significance and rank third for these simulations, but at a much lower level of significance than CTE or roughness. From previous work, the bond coat creep strength was shown to be significant, especially during cool down.(Ref 2) A purely elastic response of the TBC system (no creep effects) to the burner rig cycle would be to return to the initial stress-free state upon cool down. The fact that a different stress state results after burner rig cycling for simulations that include creep effects indicates the significant effect that creep does have on TBC response. The significance of this effect was washed out for these simulations because creep during the operating hold time relaxed stress to nearly a zero level for both high and low bond coat creep levels. If some of the simulations had not had this behavior, the significance of the creep effect would have been more prominent.

To determine the conditions that result in the desired maxima or minima stresses, an analysis to determine the change in variable values can be performed. For efficiency, the path of steepest ascent or descent offers the fastest method of determining conditions that generate maxima or minima.

This simulation provides an excellent means by which results can be generated in a cost effective manner in the least amount of time. In addition, new developments of materials for TBC's can be tested immediately and quickly, and without significant expenditure of resources. The complexity of the response surface equations can be increased as more variables are included or as higher order effects are included. The assumptions used in these analyses included linearity of response. Additional FEA simulations can be performed to augment the results, and nonlinear effects can be investigated. Also, sensitivity studies can be conducted to identify the variables that have the most significant effect on TBC life. These process-property relationships can be used to produce TBC's with improved life.

SUMMARY AND CONCLUSIONS

This Phase I SBIR effort has demonstrated the feasibility of developing a software system to aid in the design of TBC systems. Of primary significance was the development of a set of equations that form a rule set to be used to avoid aggravating stress conditions through specification of bond coat - top coat interface roughness, bond coat CTE, bond coat creep strength, and top coat creep strength. This development relied on the use of the finite element method to perform computer simulations in place of or in addition to physical experiments. By following an experimental design such as a full or fractional factorial design, standard statistical methods can be applied to determine these equation sets. In this case, Yates analysis was successfully used on a 2^5 factorial design to generate a response surface to the five variables investigated. For more complex analysis, other methods are available if needed. This methodology represents a portion of the framework that is needed to build complex relationships between the process used to produce the TBC system, the materials that make-up the TBC, and the predicted life.

These developments demonstrate the feasibility of this approach to TBC design. The methodology will be extended in Phase II by expanding and enhancing the rule base through further finite element simulations. These will include: the transient effects of thermal gradients generated during heating, operation and cooling; the effects of multiple burner rig cycles; the use of a wider range of system variables to examine nonlinear effects as well as other possible critical variables; the incorporation of top coat fracture and crushing; and additional harmful stress at the interface due to bond coat oxidation. Thus, the simulations will account for more factors that would force the simulation to more closely approximate actual conditions to which TBC's are exposed.

REFERENCES

1) B.L. Ferguson, G.J. Petrus and M. Ordillas,"A Software Tool to Design Thermal Barrier Coatings", NASA Phase I Final Report Project no. 93-1-04.23-8477, 1994.

2) B.L. Ferguson, G.J. Petrus and T.M. Krauss,"Modeling of Thermal Barrier Coatings", NASA Contractor Report NAS3-26664, November 12, 1992.

3) W.J. Brindley and R.A. Miller, "TBC's for Better Engine Efficiency", Advanced Materials and Processes, pp 29-33, August 1989.

4) W. Phucharoen, "Development of an Analytical-Experimental Methodology for Predicting the Life and Mechanical Behavior of Thermal Barrier Coatings", Ph.D. Thesis, Cleveland State University, Aug. 1990.

5) J.O. Hallquist,"MAZE - An Interactive Input Generator for DYNA2D and NIKE2D",UCID-19029, Rev. 2, 1983.

6) B. Engelmann and J.O. Hallquist,"NIKE2D A Nonlinear, Implicit, Two-Dimensional Finite Element Code for Solid Mechanics - User Manual", Lawrence Livermore National Labs. Report UCRL-MA-105413, April 1991.

7) J.T. DeMasi, et al., "Thermal Barrier Coating Life Prediction Model Development: Phase 1 Final Report", NASA Contract Report 182230, December 1989.

8) R.V. Hillery, et al., "Thermal Barrier Coating Life Prediction Model Development", NASA Contract Report 180807, Nov. 1988.

9) R.D. Krieg, "Numerical Integration of Some New Unified Plasticity-Creep Formulations", SMiRT-4, M6/4, 1977.

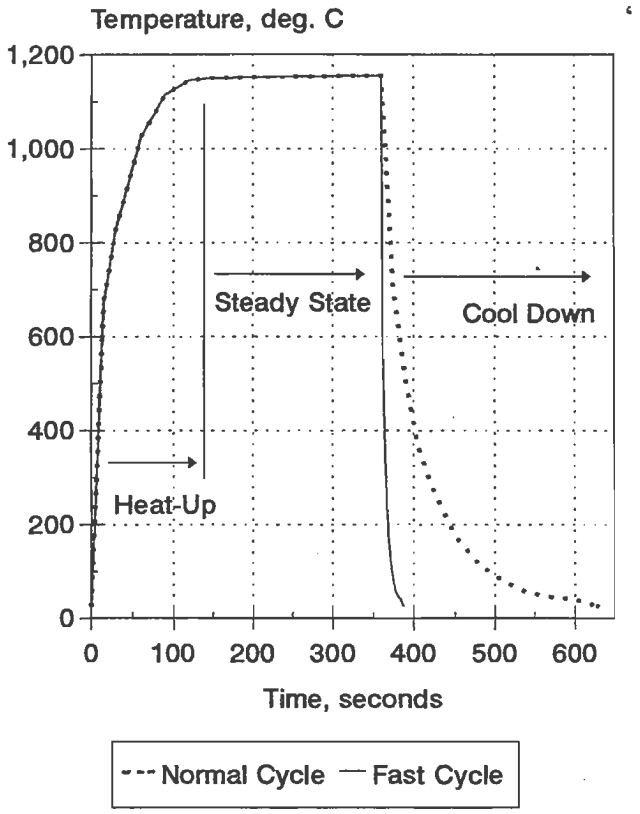

Figure 1. Burner Rig Test Cycle

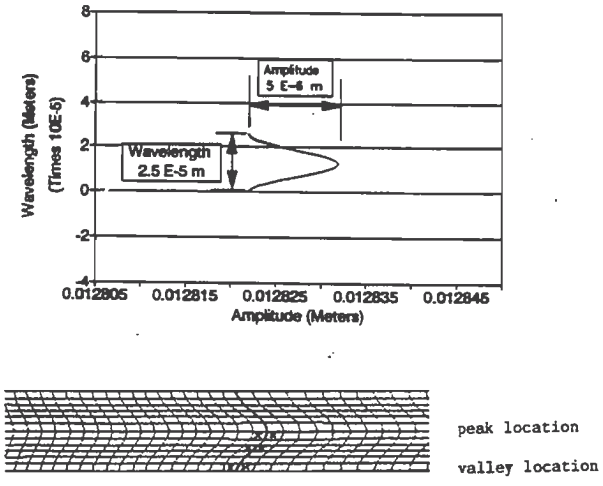

Figure 2. Low Roughness Profile of Bond Coat

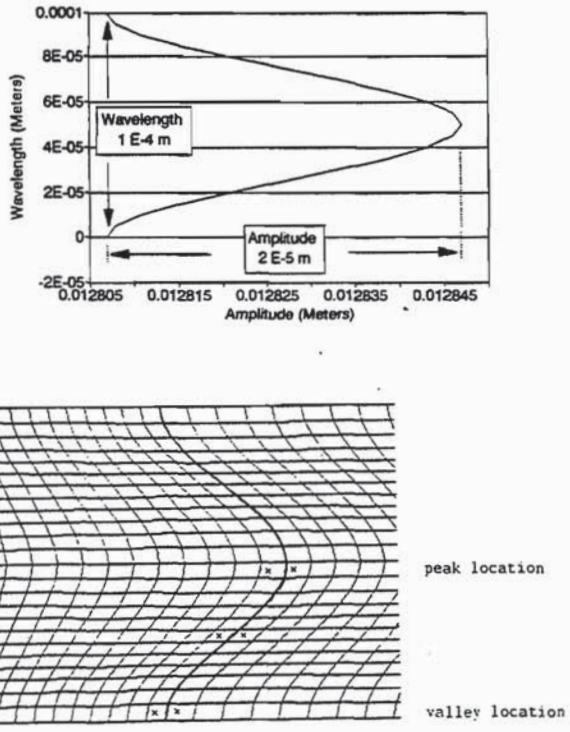

Figure 3. High Roughness Profile of Bond Coat

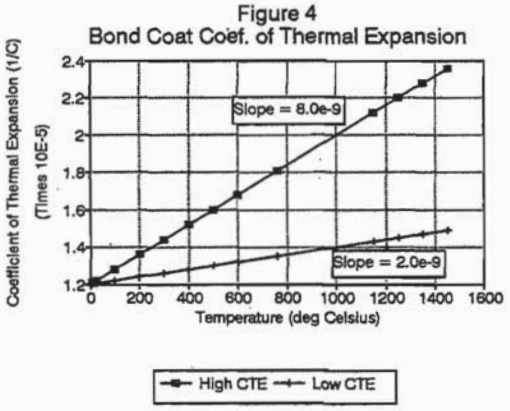

Figure 4. Bond Coat Coefficient of Thermal Expansion (CTE)

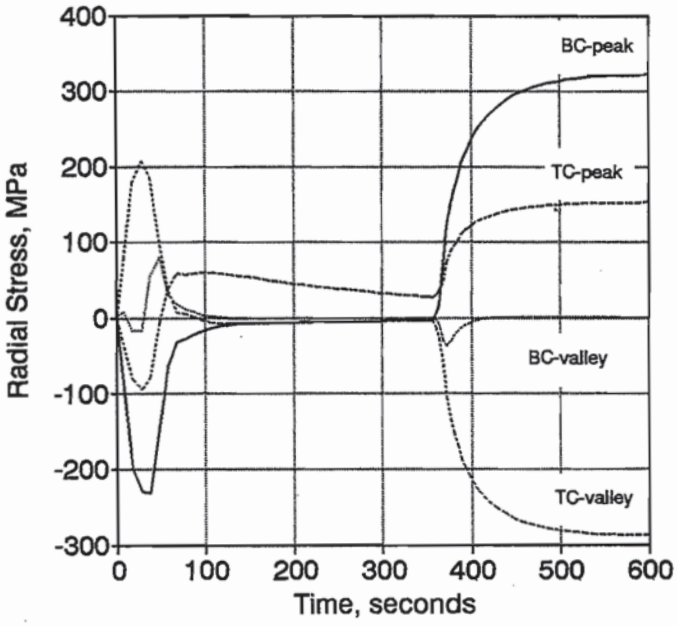

Figure 5. Typical Stress vs. Burner Rig Time Plot (Model RLON5)

THERMAL BARRIER COATING LIFE MODELING IN AIRCRAFT GAS TURBINE ENGINES

David M. Nissley
United Technologies Corporation
Pratt & Whitney
400 Main Street
East Hartford, Connecticut 06108

ABSTRACT

Analytical models for predicting ceramic thermal barrier coating (TBC) spalling life in aircraft gas turbine engines are presented. Electron beam–physical vapor deposited (EB–PVD) and plasma sprayed TBC systems are discussed. An overview of the following TBC spalling mechanisms is presented: metal oxidation at the ceramic–metal interface, ceramic–metal interface stress singularities at edges and corners, ceramic–metal interface stresses caused by radius of curvature and interface roughness, material properties and mechanical behavior, temperature gradients, component design features and object impact damage. TBC spalling life analytical models are proposed based on observations of TBC spalling and plausible failure theories. TBC spalling was assumed to occur when the imposed stresses exceed the material strength (at or near the ceramic–metal interface). TBC failure knowledge gaps caused by lack of experimental evidence and analytical understanding are noted. The analytical models are considered initial engineering approaches that capture observed TBC failure trends.

INTRODUCTION

Since the 1950's the rotor inlet temperature of aircraft gas turbines has risen at a rate of about 40°F (22°C) per year (Ref 1). This rise in operating temperature has been accommodated by improved cooling methods and superalloys such as nickel–based single crystals. However, as cost effective cooling and superalloy advancements become exhausted, TBC insulation is required to shield the turbine superalloy components from the increasingly severe temperature environment.

Thermal barrier coatings are a powerful cooling method. Each 0.001 inch (0.025 mm) of TBC thickness provides up to 30–60°F (17–33°C) temperature reduction depending on the TBC ceramic structure and level of convective cooling (Ref 2). Unfortunately, TBC delamination and spalling in hot section components may occur before reaching the component design life requirement. Local TBC spalling introduces a hot spot condition in the substrate which aggravates substrate thermomechanical fatigue (TMF) crack initiation (e.g., Ref 3). As a result, the full TBC cooling benefit can not be realized. Cooling air is needed to counteract the effect of hot regions in components caused by local TBC failure. Accurate TBC life prediction models are needed to optimize cooling flows, reduce component design and development costs and create avenues for TBC material and/or processing improvements.

TBC systems used in aircraft gas turbines are fabricated by plasma spray or EB–PVD. These TBC systems nominally consist of a 0.005 in. (0.127 mm) MCrAlY bond coat and a 0.010 in. (0.254 mm) ceramic top coat. The bond coat is needed to prevent oxidation of the substrate material and provide a good ceramic–metal bond. Yttria partially stabilized zirconia (nominally 7wt% Y) is typically used for the ceramic top coat. Plasma sprayed TBC is a bulk coating in which the ceramic contains pre–existing micro–defects. Plasma sprayed TBC failure occurs just above the metallic bond coating in the ceramic material. Ceramic delamination cracks initiate very near (or at) peaks in the rough bond coating and propagate along the interface in the ceramic layer. An EB–PVD ceramic has a columnar structure as a result of the vapor deposition process. EB–PVD TBC failure occurs in the thermally grown oxide (TGO) layer adjacent to the metallic bond coating. The TGO in EB–PVD TBC remains adherent to and is lost with the ceramic during a spall event. The typical structure of plasma sprayed and EB–PVD TBC coatings is presented in Figure 1. In general, the TBC ceramic layer is in considerable residual compressive in–plane stress at room temperature. Crack growth and spalling (far from edges and corners) is predominantly associated with coating buckling (Refs 4,5).

Initial engineering TBC spalling life correlations were accomplished by charting the observed TBC life vs. temperature. TGO formation was considered the primary TBC delamination cracking mechanism. Temperature was used as an indirect measurement of TGO formation at the ceramic–metal interface. By the end of the 1980's, more sophisticated TBC spalling life prediction models were developed (Refs 6–8). These improved models captured TBC spalling life by combining a structural analysis of the TBC (i.e., substrate, bond coat and ceramic) with the accumulated TGO thickness. However, further investigation of TBC spalling mechanisms and modifications to the Reference 6–8 TBC life models are needed to adequately capture TBC spalling life. Areas of investigation and model modifications are suggested herein.

OVERVIEW OF TBC SPALLING MECHANISMS

Metal Oxidation (TGO formation)

TGO formation due to metal bond coat oxidation is a volumetric expansion process that occurs during high temperature exposure. The volume change is constrained in the plane of the interface because the stiffness of the TGO is insignificant relative to the stiffness of the substrate. As a result, the TGO forms with a residual compressive stress. Upon cooling to ambient conditions, the TGO is forced further into compression. It is speculated that TGO formation creates (or increases) the normal stress perpendicular to the ceramic–metal interface at defect sites in either the ceramic or TGO layer. However, based on static furnace tests, it is known that TGO formation by itself is insufficient to cause TBC spalling. No TBC failures were observed in static furnace oxidation tests so long as the specimens remained in the furnace. The TBC spalled when the specimens were removed from the furnace and cooled to ambient conditions (Refs 6–8).

Radius of Curvature

The local radius of curvature directly affects the normal stress perpendicular to the interface, σ_n (Refs 4,5). Consistent with the observation that TBC spalling is a buckling phenomena, the in–plane hoop stress, σ_Θ, is compressive. Then, on concave surfaces, such as on the pressure surface of airfoils, σ_n is compressive, and on convex surfaces, such as airfoil suction surfaces, σ_n is tensile. In general, a finite element analysis is used to determine σ_n, but isothermal conditions can be modeled by using a thin wall pressure vessel formula.

$$\sigma_n = \varrho \; t \; \sigma_\Theta \qquad . \tag{1}$$

where ϱ is the local radius of curvature and t is the coating thickness.

Interface Roughness

Interface roughness (or waviness) is considered a stress concentration that affects the local level of σ_n. For plasma sprayed TBC a residual σ_n develops that is tensile at the bond coat peaks and compressive at the bond coat valleys (Ref 4). The ceramic–metal interface of an EB–PVD TBC is smooth relative to a plasma sprayed TBC. Thus, the contribution of interface roughness to the residual σ_n in an EB–PVD coating is considered small. As an initial approach, Evans, Crumley and Demaray (Ref 4) proposed the solution of an isolated cylindrical inclusion:

$$\sigma_n \approx \frac{[\Delta\alpha\Delta T][1/\varkappa + E_c(1 + \nu_c)(R\varrho)] \sin(2\pi y/\lambda)}{1 + R/t} \tag{2}$$

$$\varkappa = (1 + \nu_c)/2E_c + (1 - 2\nu_s)/E_s \tag{3}$$

where $\Delta\alpha\Delta T$ is the ceramic–metal thermal mismatch strain, R and λ are the amplitude and wavelength of the wavy interface, E_c, ν_c, E_s and ν_s are the coating and substrate modulus and Poisson's ratio and y is the distance along the interface. The interface roughness effect is presented in Figure 2. Equation (2) generates stress trends in qualitative agreement with the finite element results of Chang, Phucharoen and Miller (Ref 9).

Ceramic Sintering

As–deposited ceramics can sinter rapidly when exposed to temperatures above 2000°F (1093°C). The sintering process causes significant volumetric and material property changes. Sintering shrinks the ceramic and introduces in–plane tensile strain that can cause cracks perpendicular to the interface (i.e., mudflat cracks). Typically, the ceramic becomes stiffer and more linearly elastic with a commensurate decrease in ductility. Thermal conductivity generally increases. The effects of sintering on a plasma sprayed zirconia ceramic is presented in Table 1. In EB–PVD coatings, the columnar structure can be destroyed by sintering. The long term effect of ceramic sintering on TBC spalling needs further experimental and analytical investigation.

TABLE 1
Sintering Affects Sprayed Zirconia Properties

Sintering Condition	Room Temperature Normalized Properties			
	$\frac{\sigma_f}{\sigma_{fo}}$	$\frac{E}{E_o}$	$\frac{k}{k_o}$	$\frac{\varepsilon_f}{\varepsilon_{fo}}$
As Sprayed	1.00	1.00	1.00	1.00
5 hrs at 2000F (1093C)	1.19	1.12	–	–
36 hrs at 2000F (1093C)	1.42	1.32	–	–
24 hrs at 2350F (1288C)	2.80	4.70	–	0.25
1 hr at 2600F (1427C)	3.50	3.10	–	–
5 hrs at 2900F (1593C)	3.61	4.10	–	0.20
36 hrs at 2900F (1593C)	3.68	4.17	2.53	0.20

σ_f = Failure Strength E = Elastic Modulus k = Thermal Conductivity ε_f = Failure Strain

Material Constitutive Behavior

Ceramic – Ceramics are often considered elastic materials; however, it is known that TBC ceramics behave in an inelastic fashion as well (Refs 6–8). Tensile inelastic deformation and stress relaxation can increase the residual in–plane compressive stress that contributes to TBC spallation by buckling.

Unified viscoplastic models can be modified to capture the first order inelastic behavior of TBC ceramics (Refs 6–8). As an example, a transient heat transfer and nonlinear structural analysis was performed on a TBC coated flat plate using an enhanced version of the LAYER finite element program (Ref 10). Substrate and TBC heat transfer boundary conditions are presented in Figure 3. A total of three consecutive thermal cycles were analyzed. The substrate was 0.090 in. (2.29 mm) MAR–M509 with 0.005 in. (0.127 mm) MCrAlY bond coat and 0.010 in. (0.254 mm) ceramic top coat. Structural analysis results are presented in Figures 4 and 5. In turbine applications, plasma sprayed ceramics exhibit cyclic inelasticity; however, EB–PVD ceramics are virtually elastic in the normal temperature usage range. The EB–PVD columnar structure, unlike a plasma sprayed ceramic, is considered incapable of holding significant tensile stress (Refs 7,8). The EB–PVD constitutive model captures tensile straining by assuming that the ceramic columns break apart when subjected to tensile stress. Then, upon reverse loading, the ceramic columns are brought together before compressive stress is imposed.

TGO – TGO constitutive behavior has not been determined experimentally as yet. TGO behavior is typically assumed to be elastic with material properties equal to Al_2O_3 (Refs 7,8).

Bond Coat – The bond coat is an oxidation resistant metallic coating, usually of the MCrAlY family, that is plasma sprayed onto the substrate. Such coatings are highly viscoplastic above about 1200°F (650°C) and very strong below about 800°F (427°C) (Ref 11). As a result, substantial inelastic deformation occurs in the bond coating during thermal cycling. Bond coat non-

linear structural analysis results are presented in Figures 4 and 5. Chang, Phucharoen and Miller (Ref 9) suggest that the effect of bond coat inelasticity is small, however, further investigation across the entire anticipated usage temperature envelope is needed.

Substrate – Understanding the inelastic behavior of the substrate is important because the substrate controls the deflections imposed on the TBC (assuming insignificant TBC stiffness). For example, hot spot component locations can stress relax quickly and influence the local strain field of the TBC. Many viscoplastic models are currently available for predicting substrate inelastic deformation (e.g., Refs 11–13).

Local Component Geometric Design Details

Normally, no shear stress exists at a smooth ceramic–metal interface unless an interface crack is present (Ref 4). However, some component design details introduce shear stress into the interface by imparting a "punch" load. This situation is similar to an end supported beam that is loaded at its middle (i.e., three–point bending). Such loading can introduce significant (i.e., >10% of fracture strength) transverse shear stress at the interface. Usually, transverse shear stress occurs at local features such as at airfoil pedestal trailing edges and combustor liner welded lap joints.

Thermal Gradients

The maximum in–plane stress occurs during transient operating conditions. Whereas the outer ceramic layer responds rapidly to transient thermal conditions, the substrate does not because of the ceramic insulation. The substrate constrains the TBC until enough heat is conducted through the ceramic such that the substrate thermal growth overtakes the ceramic thermal growth. For steady state constant heat flux conditions, Andersson (Ref 5) estimates σ_n for cylindrical geometries by combining Equation (1) with the following formula for hoop stress:

$$\sigma_\Theta = -\frac{\alpha_c E_c}{(1-\nu_c)} \frac{Q\ t}{A\ k_c} \tag{4}$$

where α_c and k_c are the ceramic coating thermal expansion coefficient and thermal conductivity, respectively, and Q/A is the heat flux per unit area. For a given TBC system, Equation (4) infers that spalling life is reduced as heat flux and ceramic thickness are increased. This is consistent with TBC spalling observations (Ref 6).

Stress Singularities at Edges and Corners

Frequently, TBC spalls originate at component edges or corners such as at drilled film cooling holes or flowpath endwalls. Stress singularities exist at such locations because of dissimilar material properties. As shown in Figure 6, the edge condition can not be solved by conventional finite element analysis because asymmetrical shear violates the theory of elasticity in the element along the edge. As a result, stress singularities are introduced near the edge to satisfy the edge boundary conditions (e.g., Refs 14,15). Recent numerical modeling trends indicate that stress

intensity can be used to model the edge condition. One such approach (Ref 15) involves a hybrid technique that combines the results of finite element and surface integral analyses to calculate the mode I and mode II stress intensities along the interface. Typical edge stress singularity results are presented in Figure 7. The relationship between the edge stress intensities and TBC spalling life must be determined experimentally.

Impact Damage

TBC spalling due to object damage can occur when material particles impinge on the ceramic layer (Ref 3). Impact damage assessment of TBC is done by observing engine tested components. For simplistic understanding purposes, impact damage can be considered contact between a sphere (the particle) and a surface (Ref 16). Assuming that the particle momentum is wholly converted to normal force, contact normal and shear stresses introduced in the TBC are sufficient to cause spalling.

SPALLING LIFE MODELING APPROACH

It is assumed that TBC spalling follows the weakest link theory (i.e., spalling occurs when the imposed stress exceeds the material strength) regardless of the TBC structure. TBC spalling occurs as a result of either monotonic (an overload/thermal rupture situation) or cyclic thermal loads. The typical failure mode is ceramic layer buckling due to compressive in–plane stresses. The life models focus on the material layer in which failure occurs. Specifically, the stresses at the TBC failure location are assessed and used to correlate TBC spalling life. Empirical TBC spalling life models are developed based on a combination of failure mode observations, TBC spalling life data and stress analyses.

LIFE MODELING

Plasma Sprayed TBC

Life modeling of plasma sprayed TBC was based on a combination of metal oxidation and ceramic cyclic inelasticity (Ref 6). The life model followed a power law relationship:

$$N_f = A\Delta\varepsilon^{-b} \tag{5}$$

$$\Delta\varepsilon = [\ (\ \Delta\varepsilon_{ff}\ /\ \Delta\varepsilon_{in}\ )\ (\ 1 - \delta/\delta_c\ )^c + (\ \delta/\delta_c\ )^c\ ] \tag{6}$$

where $\Delta\varepsilon_{ff}$ is the ceramic failure in–plane normal inelastic strain range in the absence of oxidation, $\Delta\varepsilon_{in}$ is the ceramic in–plane normal inelastic strain range, δ is the metal oxide thickness and δ_c is the "critical" oxide thickness that causes TBC spalling in one cycle. A correlation of burner rig data from Reference 6 is presented in Figure 8. The burner rig data consists of three generic test cycles: strain emphasis, oxide emphasis and mixed mode. A strain emphasis cycle consists of a 2 minute heating to maximum temperature and a 4 minute cooling to about 100°F (38°C). An oxide emphasis test consists of a 1.5 minute heating from about 1000°F (538°C) to maximum temperature, a several minute dwell at maximum temperature and then a 0.5 minute

cooling back to 1000°F (538°C). Finally, the mixed mode cycle is a combination of strain emphasis heating and cooling transients and oxide emphasis dwell at maximum temperature. A modified Walker's unified viscoplastic constitutive model was used to determine the ceramic inelastic strain range in the Reference 6 program. The observed TBC spalling life from cyclic burner rig tests was correlated within about $\pm 3X$ which is considered inadequate for TBC coated component design application.

Of all the failure mechanisms, the stress introduced by interface roughness is considered the dominant mechanism that controls plasma sprayed TBC delamination crack initiation. Detailed micrographic data (Ref 6) shows that delamination cracks initiate at (or very near) the peaks of the rough interface where the tensile stress normal to the interface is highest. Even in the absence of significant TGO buildup (specimen furnace exposure in argon), TBC delamination cracks were observed emanating adjacent to the bond coat peaks (Ref 6). Also, flat plate and small diameter rig specimen data indicate that the rough interface overwhelms any radius of curvature effect (Ref 6). Initial investigation of a wavy interface stress field is provided in References 4 and 9. In general, however, the stress field along the rough interface may change dramatically as the interface morphology evolves by diffusion processes (e.g., ceramic sintering and TGO formation). Understanding the effects of such processes is necessary prior to making TBC life model modifications.

EB–PVD TBC

Life modeling of EB–PVD TBC was based on a combination of metal oxidation (TGO formation) and TGO tensile strain (Refs 7,8). The life model followed the power law relationship of Equations (5) and (6). A correlation of burner rig data from the Reference 7 program is presented in Figure 9. The correlation capability is within about $\pm 2X$ which is considered acceptable for TBC coated component design purposes.

However, the notion that the TGO is in tension is suspect. A review of the TGO displacement calculation in the Reference 7 program indicates that the calculated TGO tensile strain is an artifact of the assumed stress free temperature of the substrate–bond coat–ceramic composite. The stress free temperature was assumed to occur at elevated temperature during the TBC fabrication process. As mentioned previously, TGO formation is a volumetric expansion process that is constrained by the stiffness of the substrate. As a result, the TGO is initially in in–plane compression which is contrary to the Reference 7 model. Cooling to ambient conditions increases the TGO compression due to thermal expansion mismatch strains. Thus, the TGO in–plane strain is entirely compressive.

Based on the above argument and a review of EB–PVD ceramic microstructures and spalling data from the Reference 7 program, the following conceptual EB–PVD TBC spalling life prediction model is proposed. Since the TGO is in compression regardless of the cycle type, the TGO mechanical strain range is used as a starting point. TGO strain range vs. life for the Reference 7 data is presented in Figure 10. Notice that TGO strain range and thickness (thermal exposure time) qualitatively correlates the strain emphasis and mixed mode tests (i.e., mixed mode

cycle equals strain emphasis cycle plus dwell at maximum temperature). However, for equivalent TGO thicknesses, the oxide emphasis tests spalled much sooner than the mixed mode tests. The shorter oxide emphasis lives can be explained by including the effects of ceramic structure sintering. Ceramic microstructures of the strain emphasis and mixed mode tests are similar. Cycling to near room temperature tended to break any bonds between ceramic columns caused by sintering. The oxide emphasis test minimum temperature was about 1000°F (538°C). Sintering bonds were left relatively intact in the oxide emphasis tests (Ref 7). Thus, the ceramic columnar structure is somewhat destroyed and the residual compressive stress is greater (which makes TBC buckling more likely) than either of the other two cycle types. The apparent effect of sintering on ceramic behavior is presented in Figure 11.

CONCLUSIONS

Further experimental and analytical investigation of plasma sprayed and EB–PVD TBC is needed to quantify the dominant TBC delamination crack and spalling mechanisms. Available rig data indicates that TBC spalling typically occurs as a result of ceramic layer buckling. Existing TBC spalling life models (Refs 6–8) do not capture the TBC buckling failure mode. Development of an accurate plasma sprayed TBC spalling life model requires a more thorough understanding of the rough interface stress field. An improved EB–PVD spalling life model is suggested based on a combination of TGO formation and ceramic sintering. The proposed EB–PVD model qualitatively captures the observed spalling life trends and is consistent with the TBC buckling failure mode.

REFERENCES

1) B. L. Koff, Spanning the Globe with Jet Propulsion, AIAA paper 2987, AIAA 1991 Annual Meeting and Exhibit, April 30– May 2, 1991 Arlington, VA.

2) K. D. Sheffler and D. K. Gupta, Current Status and Future Trends in Turbine Application of Thermal Barrier Coatings, Journal of Engineering for Gas Turbines and Power, Vol. 110, October 1988, pp. 605–609.

3) P.A. Siemens and W. B. Hillig, Thermal–Barrier–Coated Turbine Blade Study, NASA CR–165351, Aug. 1981.

4) A. G. Evans, G. B. Crumley and R. E. Demaray, On the Mechanical Behavior of Brittle Coatings and Layers, Oxidation of Metals, Vol. 20, No. 5–6, Dec. 1983, pp. 193–216.

5) C. A. Andersson, Thermal Stress Fracture of Ceramic Coatings, Proceedings of the 3rd International Symposium on the Fracture Mechanics of Ceramics, Fracture Mechanics of Ceramics, Vol. 6, 1983, pp. 497–509.

6) J. T. DeMasci, K. D. Sheffler and M. Ortiz, Thermal Barrier Coating Life Prediction Model Development, Phase I – Final Report, NASA CR–182230, Dec. 1989.

7) S. M. Meier, D. M. Nissley and K. D. Sheffler, Thermal Barrier Coating Life Prediction Model Development, Phase II – Final Report, NASA CR–189111, July 1991.

8) S. M. Meier, D. M. Nissley, K. D. Sheffler and T. A. Cruse, Thermal barrier Coating Life Prediction Model Development, Journal of Engineering for Gas Turbines and Power, Vol. 114, April 1992, pp. 258–263.

9) G. C. Chang, W. Phucharoen and R. A. Miller, Thermal Expansion Mismatch and Plasticity in Thermal Barrier Coating, NASA CP–2493, October, 1987, pp. 357–368.

10) D. M. Nissley, Layer User and Programmer Manual, NASA CR–187038, October, 1990.

11) D. M. Nissley, T. G. Meyer and K. P. Walker, Life Prediction and Constitutive Models for Engine Hot Section Anisotropic Materials Program – Final Report, NASA CR–189223, September, 1992.

12) K. S. Chan, U. S. Lindholm and S. R. Bodner, Constitutive Modeling for Isotropic Materials (HOST) – Final Report, NASA CR–182132, June, 1988.

13) A. D. Freed and K. P. Walker, Refinements in a Viscoplastic Model, NASA TM–102338, December, 1989.

14) An–Yu Kuo, Thermal Stresses at the Edge of a Bimetallic Thermostat, Journal of Applied Mechanics, Vol. 56, September 1989, pp. 585–589.

15) M. Bak and H. A. Koenig, Prediction of Edge Stresses in Layered Media using the Surface Integral–Finite Element Technique, Engineering Fracture Mechanics, Vol. 48, No. 4, 1994, pp. 583–593.

16) R. J. Roark and W. C. Young, Formulas for Stress and Strain, Fifth Edition, McGraw–Hill Book Company, 1982, p. 516.

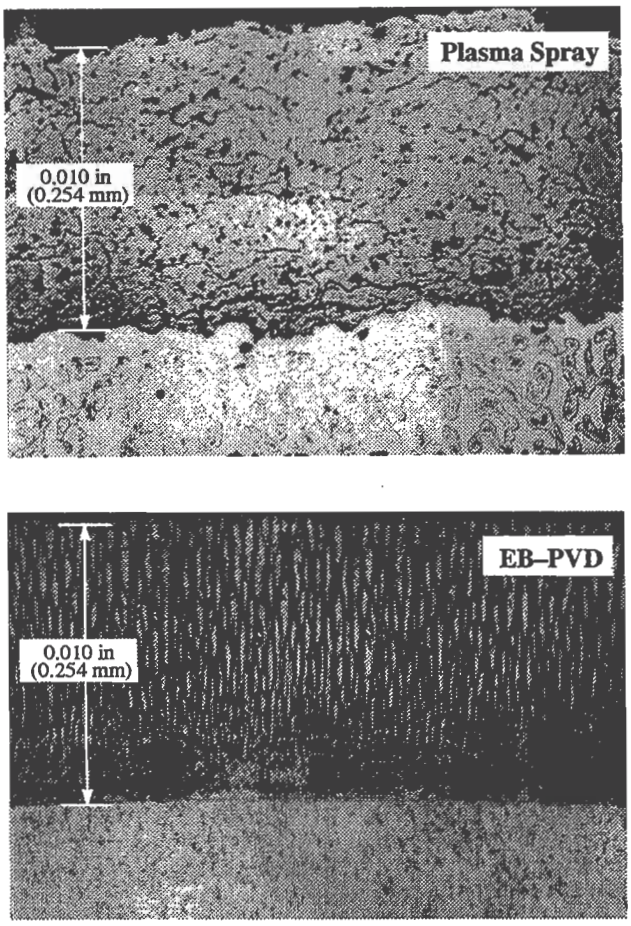

Figure 1: Typical Microstructures of TBC Coatings

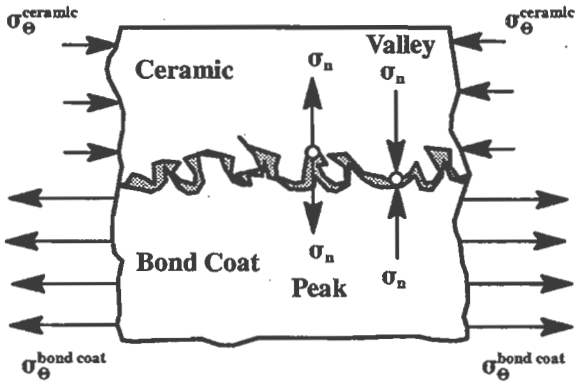

Figure 2: Interface Roughness Effect on the Local Residual Stress Field (Based on Ref 4)

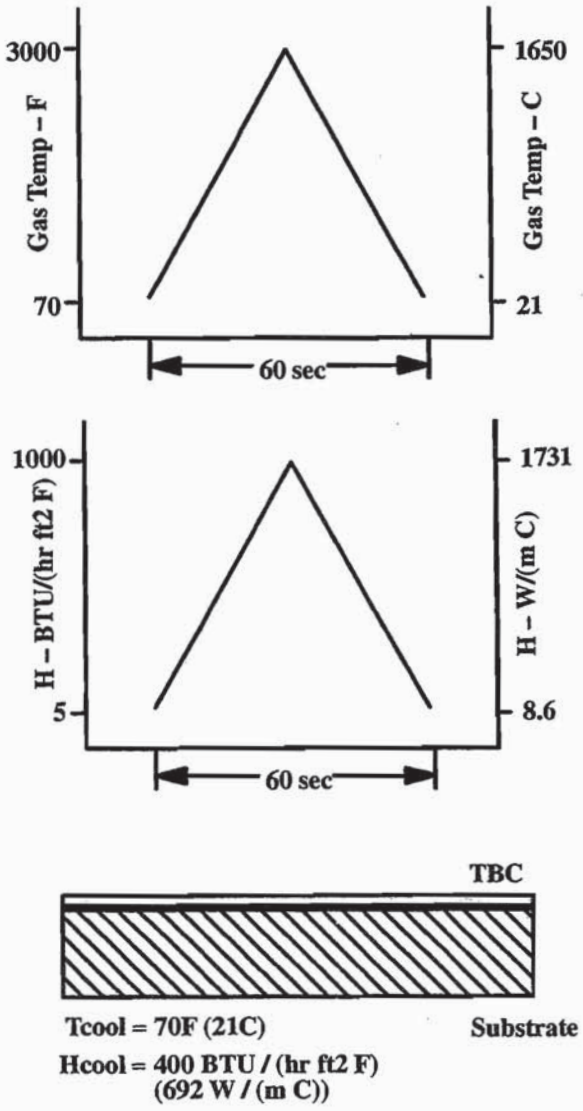

Figure 3: Boundary Conditions Used for Heat Transfer and Structural Analysis of TBC

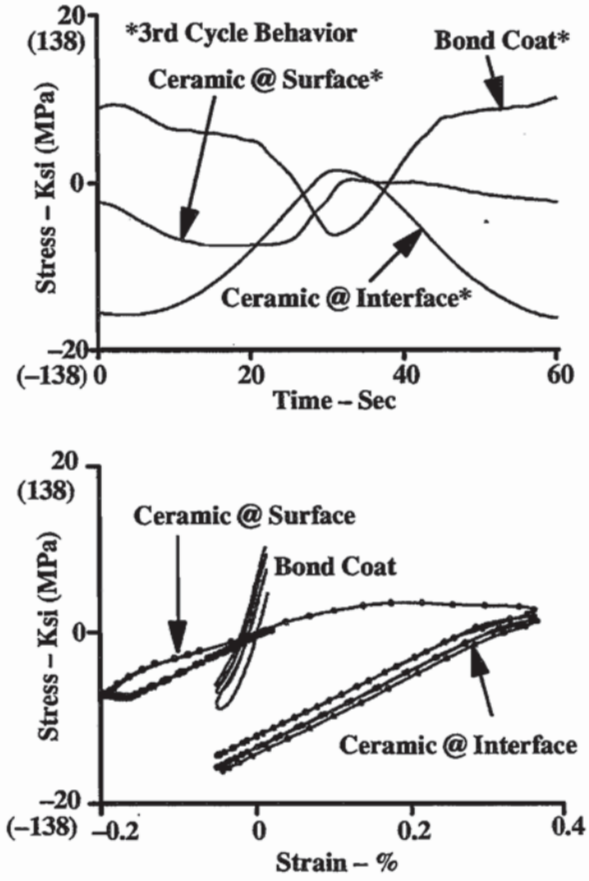

Figure 4: Constitutive Behavior of a Plasma Sprayed Thermal Barrier Coating

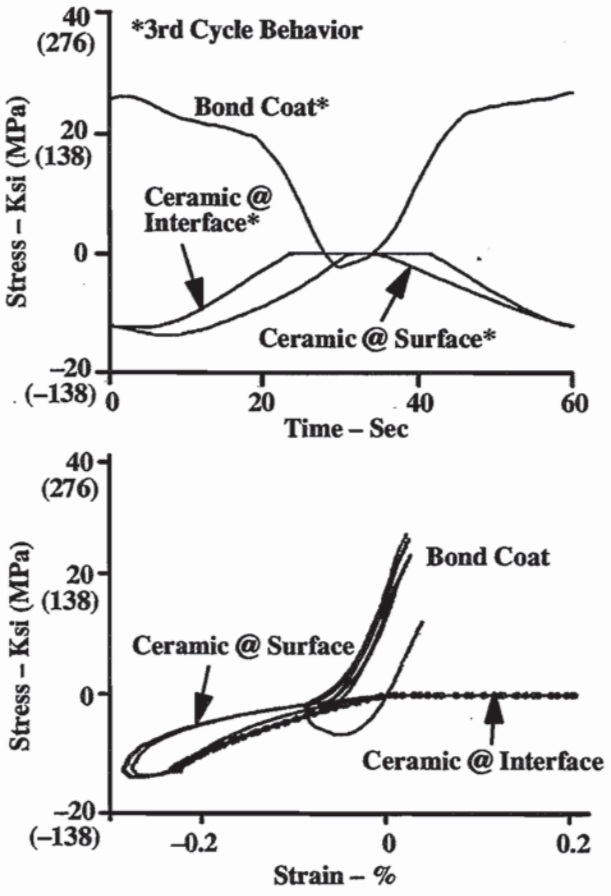

Figure 5: Constitutive Behavior of an EB–PVD Thermal Barrier Coating

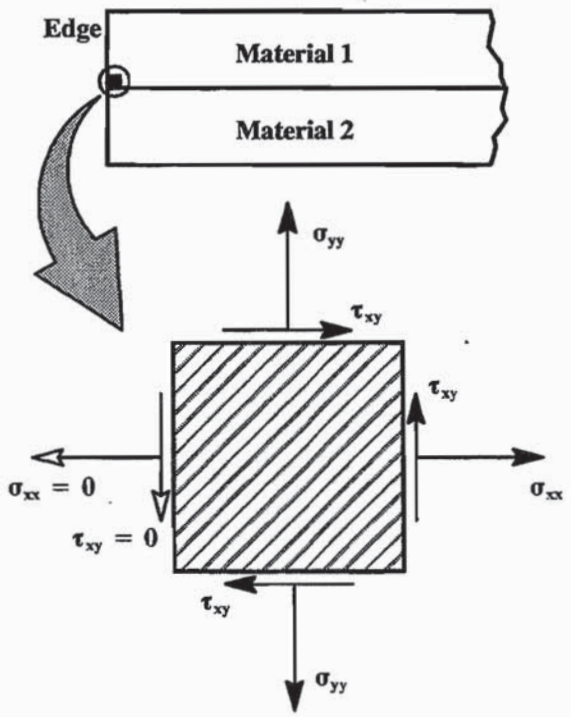

Figure 6: The Edge Condition at the Interface Between Two Dissimilar Materials

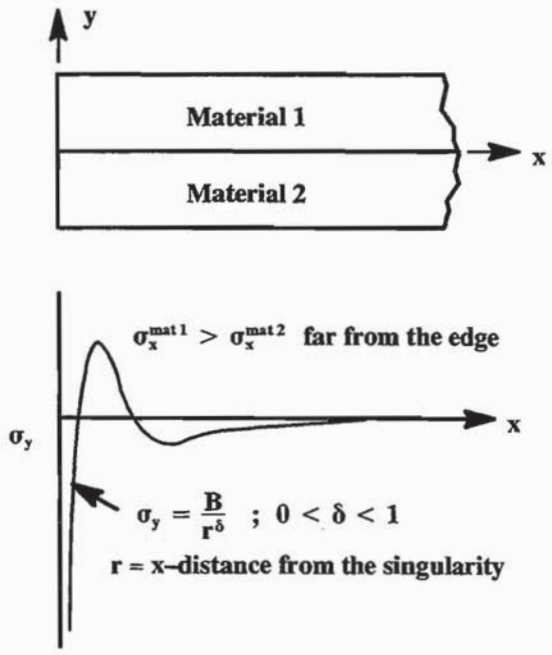

Figure 7: General Shape of the Normal Stress Singularity Along the Interface

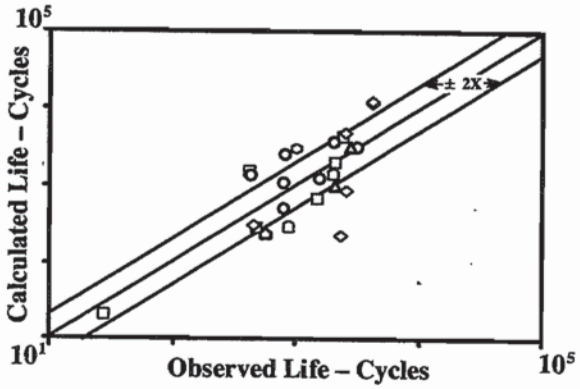

Figure 8: Plasma Sprayed TBC Spalling Life Correlation from Reference 6

- o Oxide Emphasis
- □ Strain Emphasis
- ◇ Mixed Mode
- △ Strain Emphasis – Small Diameter Bars
- □ Mixed Mode – Block Thermal Loading
- △ Strain Emphasis – Flat Plate
- o Oxide Emphasis – Flat Plate

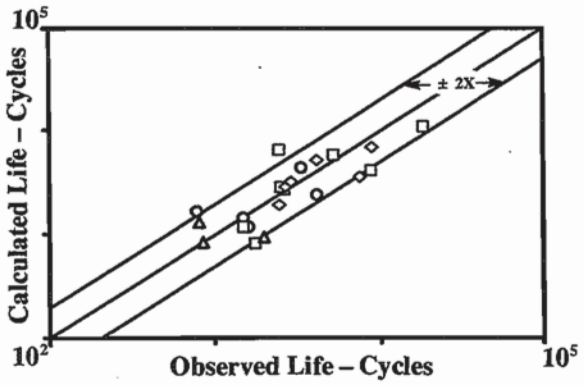

Figure 9: EB–PVD TBC Spalling Life Correlation from Reference 7

- o Oxide Emphasis
- □ Strain Emphasis
- ◇ Mixed Mode
- △ Verification Tests

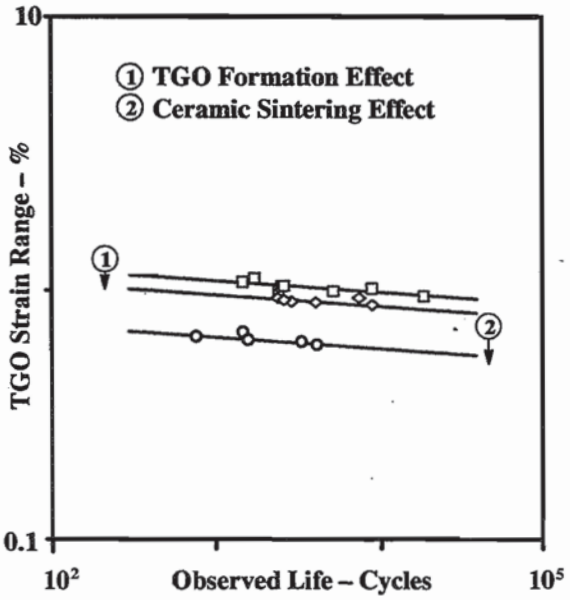

Figure 10: EB–PVD TBC Spalling Life Correlation Using TGO Strain Range

- ○ Oxide Emphasis
- □ Strain Emphasis
- ◇ Mixed Mode

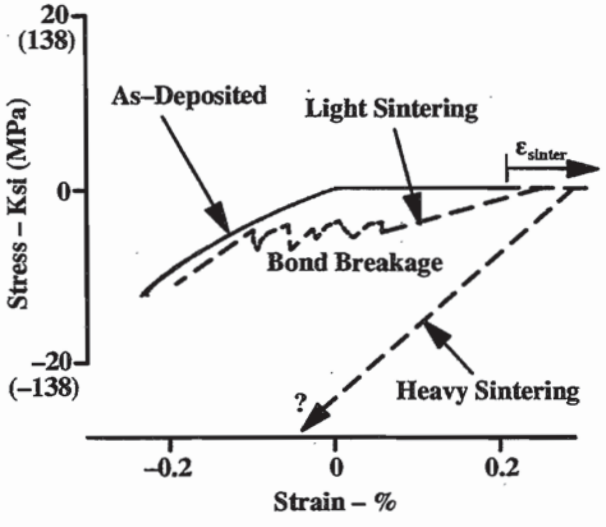

Figure 11: Effects of Sintering on EB–PVD Ceramic In–Plane Stress

REPORT DOCUMENTATION PAGE

Form Approved
OMB No. 0704-0188

1. AGENCY USE ONLY (*Leave blank*)	2. REPORT DATE	3. REPORT TYPE AND DATES COVERED
	October 1995	Conference Publication

4. TITLE AND SUBTITLE

Thermal Barrier Coating Workshop

5. FUNDING NUMBERS

WU-505-63-52

6. AUTHOR(S)

W.J. Brindley, compiler

7. PERFORMING ORGANIZATION NAME(S) AND ADDRESS(ES)

National Aeronautics and Space Administration
Lewis Research Center
Cleveland, Ohio 44135-3191

8. PERFORMING ORGANIZATION REPORT NUMBER

E-9871

9. SPONSORING/MONITORING AGENCY NAME(S) AND ADDRESS(ES)

National Aeronautics and Space Administration
Washington, D.C. 20546-0001

10. SPONSORING/MONITORING AGENCY REPORT NUMBER

NASA CP-3312

11. SUPPLEMENTARY NOTES

Responsible person, W.J. Brindley, Materials Division, NASA Lewis Research Center, organization code 5160, (216) 433-3274.

12a. DISTRIBUTION/AVAILABILITY STATEMENT

Unclassified - Unlimited
Subject Categories 26 and 27

This publication is available from the NASA Center for Aerospace Information, (301) 621-0390.

12b. DISTRIBUTION CODE

13. ABSTRACT (*Maximum 200 words*)

This document contains papers for the Thermal Barrier Coating Workshop sponsored by NASA Lewis Research Center and cosponsored by DOE and NIST. The workshop was held in Westlake, Ohio, March 27-29, 1995. The workshop covered thermal barrier coating (TBC) issues related to applications, processing, properties, and modeling. The intent of the workshop was to highlight the state of knowledge on TBC's and to identify critical gaps in knowledge that may hinder TBC use in advanced applications. The workshop goals were achieved through presentations by 22 speakers representing industry, academia, and government as well as through extensive discussion periods.

14. SUBJECT TERMS

Thermal barrier coating; TBC; Engine experience; Properties; Modeling; Processing; Aircraft engines; Land-based turbines; Gas turbine engines; Diesel engines

15. NUMBER OF PAGES
287

16. PRICE CODE
A13

17. SECURITY CLASSIFICATION OF REPORT	18. SECURITY CLASSIFICATION OF THIS PAGE	19. SECURITY CLASSIFICATION OF ABSTRACT	20. LIMITATION OF ABSTRACT
Unclassified	Unclassified	Unclassified	